The effects of innate lymphocyte derived cytokines on spinal bone and entheses derived mesenchymal stem cells

Tobias James Wallace Russell

Submitted in accordance with the requirements for the degree of
Doctor of Philosophy

The University of Leeds

School of Medicine

May 2021

The candidate confirms that the work submitted is his own, except where work which has formed part of jointly authored publications has been included. The contribution of the candidate and the other authors to this work has been explicitly indicated below. The candidate confirms that appropriate credit has been given within the thesis where reference has been made to the work of others.

Jointly authored publications:

IL-17A and TNF Modulate Normal Human Spinal Entheseal Bone and Soft Tissue Mesenchymal Stem Cell Osteogenesis, Adipogenesis, and Stromal Function (Sections in Chapters 3, 4 and 5).

Tobias Russell, Abdulla Watad, Charlie Bridgewood, Hannah Rowe, Almas Khan, Abhay Rao, Peter Loughenbury, Peter Millner, Robert Dunsmuir, Richard Cuthbert, Ala Altaie, Elena Jones and Dennis McGonagle

Cells. 2021, 10(2), p.341

Worked attributed to Tobias Russell: study conception and design, manuscript preparation and final draft, performing the experiments, acquisition, analysis and interpretation of data, composition of figures, response to reviewers and revisions following peer review.

Work attributed to others: A.W., C.B., R.C., A.A., E.J. and D.M. contributed to the study planning and design. A.W., C.B., H.R., R.C., A.A., E.J. and D.M. contributed to acquisition, analysis, or interpretation of data and critical revision of the manuscript. A.W., C.B., H.R., A.K., A.R., P.L., P.M., R.D., R.C., A.A., E.J. and D.M. contributed to the acquisition of data and drafting of the manuscript

Acknowledgements

Abstract

Spondyloarthropathies (SpA) are intimately linked to new bone formation in response to tissue damage via the Interleukin-17A (IL-17A) and tumour necrosis factor (TNF) pathways. Mesenchymal stem cells (MSCs) are known to play a role in tissue repair due to their ability to differentiate into a range of tissue types which can be enhanced or suppressed by IL-17A or TNF. This study investigated MSCs from the spinal peri-entheseal bone (PEB) and entheseal soft tissue (EST) responses to IL-17A and/or TNF including their osteogenic, adipogenic, stromal supportive and ability to support lymphocyte recruitment.

Normal spinal PEB and EST were characterised for MSCs by immunophenotypic, osteogenic, adipogenic and chondrogenic criteria. Functional and gene transcriptome analysis was carried out on undifferentiated, adipo-differentiated, and osteo-differentiated MSCs. Histology staining was carried out to identify the tissue morphology, alongside lymphocyte chemoattractant expression from MSCs.

Cultured MSCs from both PEB and EST displayed a tri-lineage differentiation ability. EST MSCs exhibited 4.9-fold greater adipogenesis ($p<0.001$) and a 3-fold lower osteogenic capacity ($p<0.05$). IL-17A stimulation moderately elevated osteogenesis in both PEB MSCs and EST MSCs, with early elevations of *alkaline phosphatase*. IL-17A suppressed adipogenic differentiation, with a significant decrease in fatty acid-binding protein 4 (*FAPBP4*). IL-17A significantly increased the *CCL20* transcript ($p<0.01$) and protein expression ($p<0.001$) in MSCs supporting a role in type 17 lymphocyte recruitment. Histology of the spinous process showed discontinuations in the cortical bone, EST and PEB MSCs showed increased migration molecules after TNF stimulation.

Normal spinal enthesis harbours resident MSCs with different *in vitro* functionalities in bone and soft tissue, especially in response to IL-17A, which enhanced osteogenesis and CCL20 production and reduced adipogenesis compared to unstimulated MSCs. This MSC-stromal-enthesis immune system may be a hitherto unappreciated mechanism of "fine tuning" tissue repair

responses at the enthesis in health and could be relevant for SpA under-
standing.

Table of Contents

List of Tables

List of Figures

List of Abbreviations

Abbreviation:	Definition:
7-AAD	7-Aminoactinomycin D
ADIPOQ	Adiponectin
ALP	Alkaline phosphatase
AM	Adipogenic media
AS	Ankylosing spondylitis
BASDAI	Bath Ankylosing Spondylitis Disease Activity Index
BMP	Bone morphogenetic protein
CCL	C-C Motif chemokine ligand
CCR6	C-C Chemokine receptor type 6
CD	Cluster of differentiation
cDNA	Complementary deoxyribonucleic acid
CEBP	CCAAT/enhancer-binding protein
CIDEC	Cell death inducing DFFA like effector C
CM	Chondrogenic media
COX	Cylooxygenase
CT	Cycle threshold
CXCL12	C-X-C Motif chemokine ligand 12
DKK	Dickkopf
DNA	Deoxyribonucleic acid
EDTA	Ethylenediaminetetraacetic acid
ER	Endoplasmic reticulum

ERAP1	Endoplasmic reticulum aminopeptidase 1
EST	Entheseal soft tissue
FABP4	Fatty acid binding protein 4
FACS	Fluorescence-activated cell sorting
FCS	Foetal calf serum
FITC	Fluorescein isothiocyanate
FSC	Forward scatter
GAG	Glycosaminoglycan
GWAS	Genome wide association studies
H&E	Haematoxylin and Eosin
HLA-B27	Human leukocyte antigen B27
HLA-DR	Human leukocyte antigen – DR isotype
HPRT1	Hypoxanthine phosphoribosyltransferase 1
IBD	Inflammatory bowel disease
ICAM-1	Intercellular adhesion molecule 1
IFC	Integrated fluid circuits
IFN	Interferon
IL	Interleukin
ILC3	Type 3 innate lymphoid cells
ISCT	International Society for Cellular Therapy
ITS	Insulin–transferrin–selenium
JAK	Janus kinase

LNGFR	Low-affinity nerve growth factor receptor
MFI	Median fluorescent intensity
MHC-I	Major histocompatibility complex-I
MRI	Magnetic resonance imaging
MSC	Mesenchymal stem cell
NK	Natural killer
nrAxSpA	Non-radiographic axial SpA
NSAIDs	Non-steroidal anti-inflammatory drugs
OM	Osteogenic media
OMD	Osteomodulin
OPG	Osteoprotegerin
P	Passage
PA	Pre-amplification
PBS	Phosphate buffered saline
PCR	Polymerase chain reaction
PDs	Photodiodes
PEB	Peri-entheseal bone
PLIN1	Perilipin 1
PMTs	Photomultiplier tubes
PPARγ	Peroxisome proliferator-activated receptor γ
PsA	Psoriatic arthritis
qPCR	Quantitative polymerase chain reaction
RA	Rheumatoid arthritis

RNA	Ribonucleic acid
rpm	Rotations per minute
RT	Room temperature
RUNX2	Runt-related transcription factor 2
RUNX3	Runt-related transcription factor 3
sGAG	Sulphated glycosaminoglycan
SNP	Single nucleotide polymorphism
SpA	Spondyloarthropathies
SSC	Side scatter
STAT	Signal transducer and activator of transcription
TE	Tris-ethylenediaminetetraacetic acid
TNF	Tumour necrosis factor
VCAM-1	Vascular cell adhesion molecule 1
nrAxSpA	Non-radiographic axial SpA
RA	Rheumatoid arthritis
HLA-B27	Human leukocyte antigen B27
GWAS	Genome wide association studies
SNP	Single nucleotide polymorphism
ERAP1	Endoplasmic reticulum aminopeptidase 1
RUNX3	Runt-related transcription factor 3
CD	Cluster of differentiation
MHC-I	Major histocompatibility complex-I
ER	Endoplasmic reticulum
MRI	Magnetic resonance imaging

COX	Cylooxygenase
PsA	Psoriatic arthritis
NSAIDs	Non-steroidal anti-inflammatory drugs
IBD	Inflammatory bowel disease
DKK	Dickkopf
OPG	Osteoprotegerin

Chapter 1 – Introduction

1.1 – Spondyloarthritis

The seronegative spondyloarthropathies (SpA) including ankylosing spondylitis (AS) and non-radiographic axial SpA (nrAxSpA) are a group of diseases associated with post-inflammatory excessive tissue repair responses that manifests as new bone formation (1). These diseases were first classified together due to their shared clinical and immunological features by Moll *et al.* in the 1970's (2). This family of diseases contains AS, psoriatic arthritis (PsA), inflammatory bowel disease (IBD) associated with arthropathy, including Crohn's disease and ulcerative colitis, enterogenic and urethrogenic reactive arthritis and anterior uveitis (3, 4). Typically, SpA diseases present with post-inflammatory excessive tissue repair in response to damage (1, 5). This is in contradistinction to other inflammatory diseases such as rheumatoid arthritis (RA), where inflammation leads to predictable bone and cartilage destruction (6). The prevalence of SpA varies between ethnicities, ranging from 0.2% in South-East Asia to 1.61% in Northern Arctic communities (7). These diseases all share common themes of axial inflammation or low back pain at the sacroiliac joint, peripheral lower limb oligoarthritis, potential enthesitis, evidence of infection or intestinal dysfunction and negativity for rheumatoid factor (1, 5).

An interesting parallel to axial disease in SpA is psoriasis, a disease characterised by an excessive tissue repair response with marked epidermal hyperplasia (8, 9). Likewise, the most common intestinal manifestation of AS is subclinical Crohn's disease of the terminal ileum and right side of the colon (10). In its fully-fledged form, the inflammation of Crohn's disease is associated with excessive repair responses manifesting as intestinal structuring and obstruction (11); 2.6% ulcerative colitis and 6% of Crohn's disease patients present with AS, a figure which rises to 20% and 26% when considering all SpA diseases (12).

The discovery of the association of human leukocyte antigen B27 (HLA-B27) with AS, PsA axial disease, IBD related axial arthritis, anterior uveitis and reactive arthritis further supported the idea proposed by Moll *et al.* (2, 13-16). Subsequent genome-wide association studies (GWAS) have also implicated a strong link for the IL-23 pathway and related cytokines (Figure 1.1) genetic polymorphisms in the whole spectrum of SpA diseases (17-20).
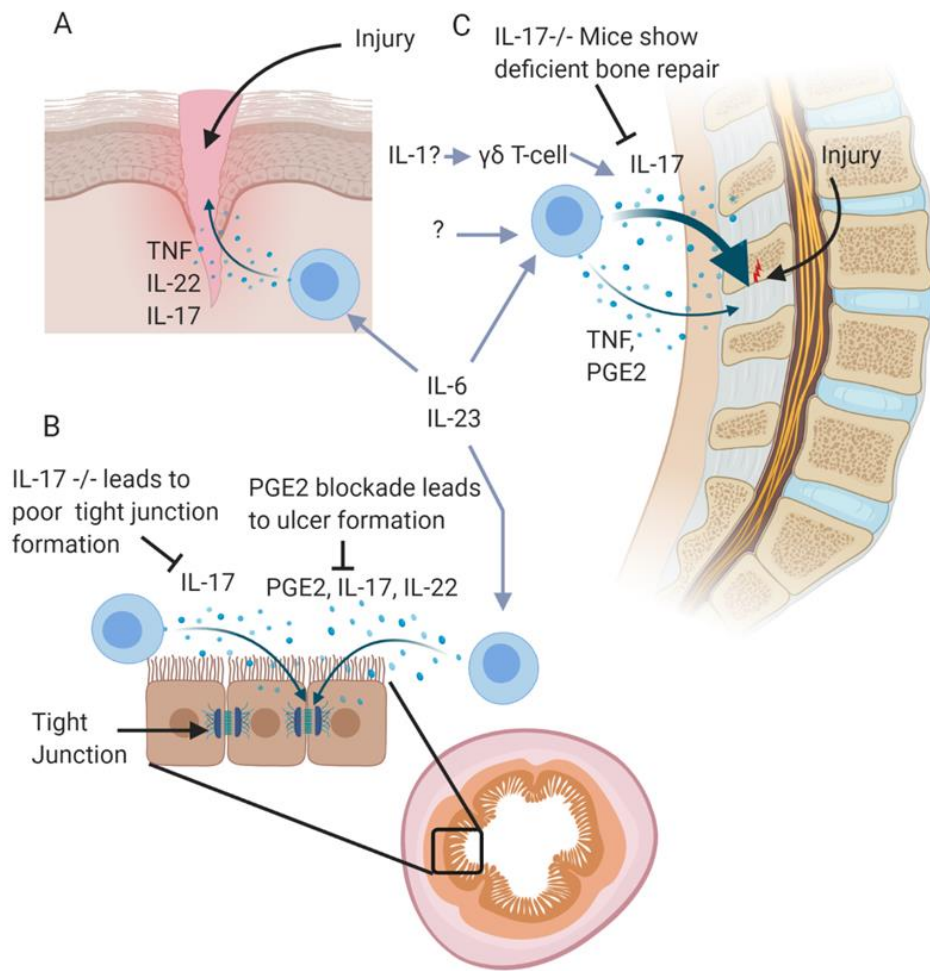
Figure 1.1: IL-23 pathway involvement in SpA related tissues

The spondyloarthropathy target tissues beyond the spine - including the gut and the skin - have a well-established understanding whereby the immune system plays a key role in physiological tissue repair. A) Damage to the skin leads to a rapid influx of immune cells producing cytokines including TNF, IL-17 and IL-22 which are involved in keratinocyte proliferation and extracellular matrix deposition. B) The evidence for microdamage to the spinal enthesis and how this regulates IL-17A, TNF and PGE2 at entheses and tendons is discussed in the text. Mouse knockouts for IL-17A show impaired fracture healing responses which are rescued by IL-17A supplementation. C) The hostile enzymatic and microbial normal gut environment is associated with tissue microdamage. IL-23, IL-22, IL-17A, IL-22 or PGE2 play key roles in gut homeostasis in experimental models. IL-17A plays a pivotal role in the tight junction formation between cells that are damaged resulting in leaky gut

1.1.1 – Ankylosing Spondylitis

Clinically ankylosing spondylitis can have a severe impact on a patient's quality of life. The early phases of AS remain largely enigmatic, with only the recent characterisation of oedemas seen at the vertebral body corners being confirmed as new fat cells replacing the destroyed bone induced by inflammation (21). The major clinical features associated with AS are inflammatory back pain caused by sacroiliitis and inflammation at other regions of the axial skeleton (22). The inflammation and structural changes of the axial spine lead to spinal stiffness and is associated with a subsequent reduction in spinal mobility (23). The early structural changes seen in AS patients are known to precede the formation of new bone at the entheseal attachment sites, these syndesmophytes further reduce patients quality of life and in severe cases can lead to complete ossification of the ligamentous tissue between the vertebral bodies (24). Patients are also at an elevated risk of vertebral fractures (25, 26), which may add to the hyperkyphosis seen in AS patients further reducing their quality of life and the disease burden (22).

Due to the manner in which AS manifests in patients, methods of quantifying disease activity and the impacts on the patient are self-reported by patients. The Bath Ankylosing Spondylitis Disease Activity Index (BASDAI) is widely used by both clinicians and clinical trials to assess disease activity (27-31). The scoring system was first published in 1994 by Garret *et al.* (32). BASDAI looks at 6 patient-reported outcomes: back pain, fatigue, peripheral joint pain and swelling, localised tenderness, and the duration and severity of morning stiffness. These outcomes are scored on a scale of 0-10, with the average of the questions being used to characterise disease activity. An average score above 4 is used to define active disease, with 10 being maximal disease activity and 0 being no disease activity (33-35). However, BASDAI does not contain any objective markers that may relate to disease activity. Further, due to the nature of self-reporting test scores are dependent on what a patient perceives to be related to their AS, with no clinician's perspective.

As with SpA, the prevalence of AS varies between ethnic groups, ranging from 0.02% in Sub-Saharan Africa to 0.35% in North Arctic communities (7). The

pathogenesis of AS is not completely understood as it likely involves interplay between genetic predispositions, risk factors and environmental factors.

1.1.1.1 – Genetic risk factors

Since it was first identified in 1973, HLA-B27 has remained the major genetic risk factor associated with AS (13), with over 90% of AS patients having an HLA-B27 polymorphism (15, 36). Though this percentage does vary with ethnicities the risk associated with HLA-B27 is still present (37-39). Whilst other major histocompatibility complex class I (MHC-I) antigens have been linked to AS, notably HLA-B40 (19), up to 167 variants of HLA-B27 have been reported to be involved in AS, and those which aren't usually have structural changes within the amino acid peptide-binding groove (16). However, less than 5% of individuals positive for HLA-B27 will go on to develop AS, which suggests that other pathways and genes that must be involved in AS pathogenesis (40).

GWAS have identified single nucleotide polymorphisms (SNP) in proteins involved in the interleukin (IL)-23 signalling pathway as well as those belonging to the M1 family of zinc metallopeptidases such as the endoplasmic reticulum aminopeptidase 1 (ERAP1) which, with its interactions with HLA-B40 is involved with peptide trimming for T cell presentation (19, 41). Other non-HLA genes associated with AS, include *CARD9 (19), IL1R1 (42, 43), ILR2 (42, 43), IL6R (19), IL12B (44), IL27 (19), PTGER4 (19), RUNX3 (40, 45, 46), TYK2 (19), ZMIZ1 (19).* Many of these genes are associated with type 3 immunity, which is mediated by innate and adaptive immune effector cells that produce IL-17 family cytokines.

The SNP of runt-related transcription factor 3 (RUNX3), which when combined with the epigenetic regulation of RUNX3 locus in cluster of differentiation (CD)8+ T cells affects their differentiation in AS (45, 47). This combined with the roles that ERAP1 and other MHC-I proteins play in antigen presentation and adaptive CD8+ T cell responses strongly implicates them in disease pathogenesis.

However, despite all of this, a classical adaptive immune response in early AS has yet to be defined. As a result, other mechanisms have been investigated,

with CD4+ T cells being a target as they are capable of binding to and recognising misfolded HLA-B27 (48). This forms part of the unfolded protein response mechanism. The misfolded HLA-B27 protein leads to endoplasmic reticulum (ER) stress, which induces macrophage activation with the associated interleukin (IL)-23 induction (49). The problem is that whilst AS HLA-B27+ blood-derived macrophages have been shown to secret elevated levels of IL-23 compared to healthy controls, this is thought to be independent of ER stress (50).

1.1.1.2 – Pathological changes at the bone and enthesis in AS

The archetypal enthesis organ is the Achilles tendon, where the tendons insertion into the bone leads to the formation of deep fibrocartilage in both the tendon and into the adjacent calcaneal bone (51). However, these entheseal attachment sites - and indeed the synovial-entheseal complex - are seen in the spine (52). It is recognised that the spinal enthesis is the site of high mechanical stress and loading, areas of high stress around the bone develop microcracks or micro-damage (53).

During healthy fracture or damage repair, multiple processes occur including the initial formation of a blood clot at the injury site, inflammation, callus generation, primary bone formation and secondary bone remodelling (54). The damaged bone needs to be removed, it is well established that T cells infiltrate damaged sites and stimulate an increase in osteoclastogenesis which is associated with bone degradation (55, 56). However, excessive inflammation is known to alter the normal balance and activity between osteoblasts and osteoclasts (57). It can either drive excessive destruction of the bone (as seen in RA) or, as is the case in AS leads to an initial bone loss which is gradually replaced with excessive over-repair and new bone formation at the enthesis (6, 58). These changes in the outcomes of normal bone repair are driven by populations of immune cells at these sites secreting an array of cytokines, notably IL-17A and TNF both of which are not only implicated in normal fracture repair but also show heavy involvement in AS pathogenesis (59-61).

The initial radiographic damage seen in early AS is associated with increased osteoclast activity, which is driven the acute inflammatory phase in response

to microdamage of the enthesis (62). The excessive cortical bone loss, which presents as oedema or 'shiny corners' (63), is seen clearly on magnetic resonance imaging (MRI) and is now identified as newly formed fat cells filling the joint space (Figure 1.2) where the cortical bone has been destroyed by inflammation (21). This early fatty disposition is a strong marker for subsequent new bone formation, which over time replaces the fat where increased osteoblast activity is seen in the chronic inflammatory phase at these sites (64, 65). During this chronic inflammatory period in AS, two key events occur which lead to the formation of syndesmophytes at the enthesis. Mesenchymal stem cells have an enhanced differentiation potential (66, 67) and osteoblasts ossify more of the subchondral granulation tissue leading to the formation of the syndesmophytes (68, 69). In more extreme cases the formation of syndesmophytes can lead to complete ossification of the ligamentous tissue between the vertebrae inducing 'bamboo spine' where a patient has significantly reduced quality of life (24).

1.1.2 – Therapeutic targeting

Given the heavy implication of the IL-23 pathway in AS pathogenesis, there was a strong rationale for IL-23 inhibition as a therapeutic intervention for AS. However, two separate IL-23 antibodies (risankizumab and ustekinumab) failed at phase II and phase III trials respectively in treating AS (70, 71), yet in peripheral PsA there is evidence of responses to anti-IL-12/23 or anti-p19 IL-23 blockers (72). Experimental models in HLA-B27/Huβ2m transgenic rats which spontaneously develop SpA showed that IL-23 was needed for the initiation of SpA but not for its continuation once onset had started (73, 74). How this relates to humans is unclear, given that the nuances involved in comparing this rat model with the human phenotype are not entirely understood (1, 75). This supports the idea for IL-17A production independent of IL-23.

The use of anti-TNF blockers has proven to be highly successful in slowing the new osteogenesis and formation of syndesmophytes in AS (30, 76, 77). Despite these strong results, there is a potential for some patients to either lose remission or have subsequent disease flare-ups whilst on anti-TNF therapy (78). An alternate target is IL-17A and as long-term results are still

outstanding for its efficacy in AS, the current studies show promising results in slowing bone formation in active AS patients (79-82). However, despite these promising results there is growing evidence of IL-17F having similar osteogenic enhancing potential as IL-17A. When dual neutralising both IL-17A and IL-17F *in vitro* there was a greater decrease in osteogenesis than when inhibiting either alone (83).

Outside of anti-cytokine targeting, AS has shown good responses to cyclooxygenase (COX) enzyme inhibition (84). The non-steroidal anti-inflammatory drugs (NSAIDs) are remarkably effective for the therapy of human AS with many patients demonstrating good and sustained responses with inflammation and sub-fibrocartilage neo-vascularisation abrogation as shown in the imaging (85). That collectively inhibition of some of these pathways (COX and IL-17 axis) is so effective in AS but not RA empirically shows that they are central to the pathology of axial SpA. Inhibition of other pathways including TNF and JAK, also appears to be pivotal in SpA whilst also showing strong efficacy in RA, thereby indicating shared inflammatory mechanisms in these situations.
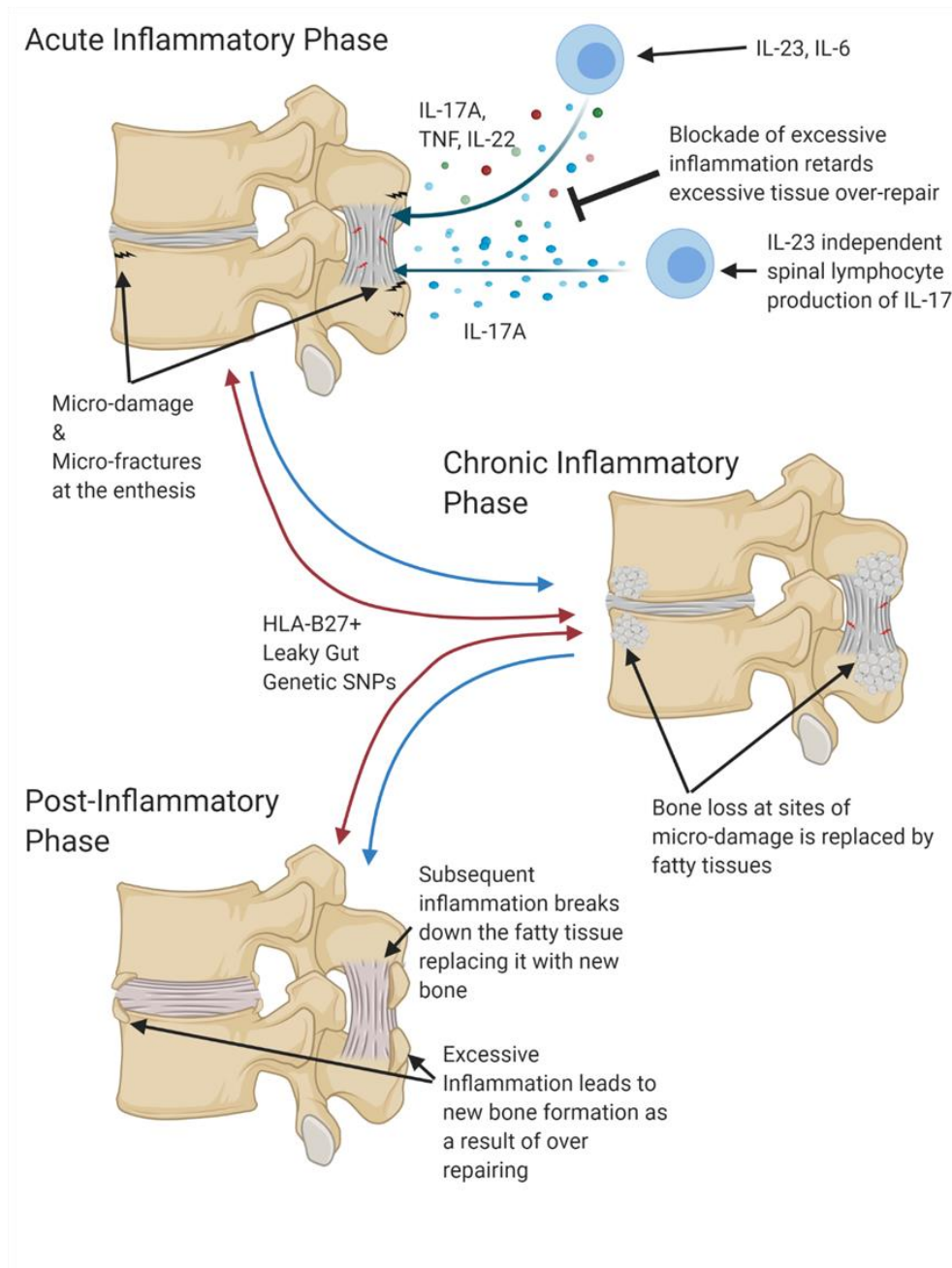
Figure 1.2: Immune system overactivation in AS

Overactivation of the immune system in tissue damage and excessive bone repair responses in ankylosing spondylitis. SNPs in PGE2 and IL-23/17 axis cytokines and others are linked to spinal inflammation and post-inflammation repair. It is proposed that the initial microdamage to the spinal enthesis as shown leads to inflammation and an immune driven tissue repair response. The same cytokine TNF and IL-23/17 pathways are responsible for both inflammation and also contributing to excessive repair responses. The dysregulation of homeostatic fine tuning of tissue repair thus results in the characteristic post inflammation disease phenotype.

1.2 – Linking immunity and SpA associated tissue repair

Genome-wide association studies of AS have implicated several immune pathways which usually play a role in healthy tissue repair, of particular interest are those of the IL-23/ IL-17 pathway (Figure 1.3), control of NF-KB and other genes regulating CD4+ and CD8+ T cell subsets (17, 18, 47). The healthy human enthesis harbours resident populations of type 3 ILC's (innate lymphoid cells) (86), natural killer (NK) cells (87), γδ T cells (88), conventional CD4+ and CD8+ T cells (89) and populations of myeloid cells shown to be the main secreters of IL-23 (90). These cell populations are all capable of IL-17A secretion (Figure 1.3) and with myeloid cells IL-23 secretion supports the GWAS findings. Importantly these AS related cytokines, tumour necrosis factor (TNF) and IL-17A are shown in experimental models to drive primary enthesitis which can spread to the adjacent tissues (91-93).

The focus on the idea of tissue repair after mechanical damage or stimulus in SpA does not preclude other pathogenic mechanisms exacerbating the condition and being involved in disease progression. Reactive arthritis is a sterile arthritis typically appearing after a gastrointestinal infection with *Salmonella Yersinia, Shigella, Chlamydia trachomatis, Campylobacter* and *Escherichia coli* all known to trigger reactive arthritis (94-97).

Following infection and subsequent immune challenge, there is an increase in cytokines associated with host-pathogen defence such as IL-17A and TNF (98-100). With the increases in cytokines and the well-characterised repertoire of immune cells at the enthesis and joints, there is the potential to develop reactive arthritis. Indeed, reactive arthritis patients show increased circulation of Th17 cells in both the peripheral blood and synovial fluid (101-104). Both IL-17A and TNF not only play a role in reactive arthritis and host-pathogen defence but are heavily implicated in AS development. Patients with AS after a gastrointestinal infection saw a disturbed permeability of the gut wall allowing for pathogens to enter circulation (105, 106). The circulating pathogens were seen to induce joint and tendon inflammation, resulting in AS disease flare-ups and likely an active disease state as defined by BASDAI (105). HLA-B27 positivity in infected patients also saw a significant increase in joint paint when compared to HLA-B27 negative patients further supporting

a link for immune challenge leading to disease flare-ups in AS or SpA patients due to an increase in circulation of disease-relevant cytokines (96, 103, 104).
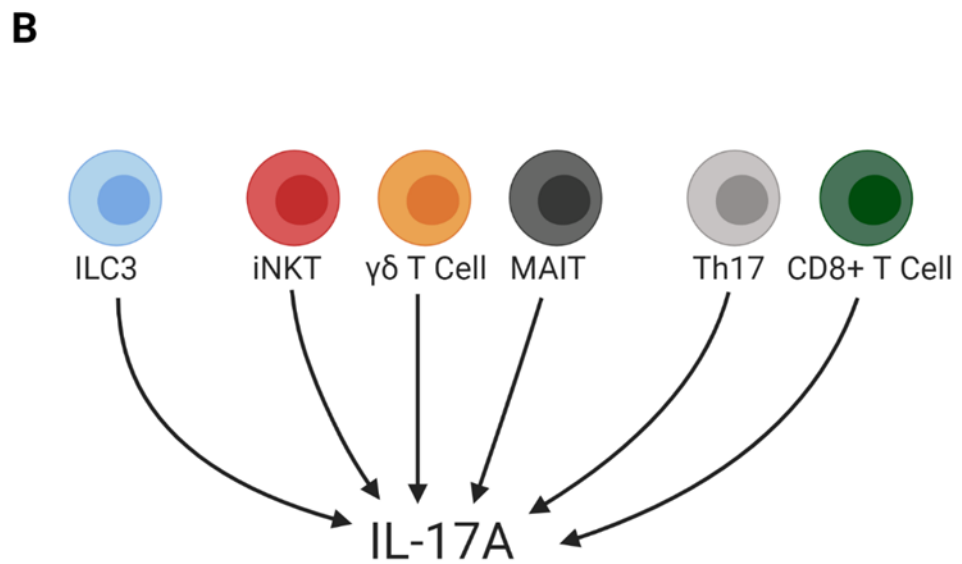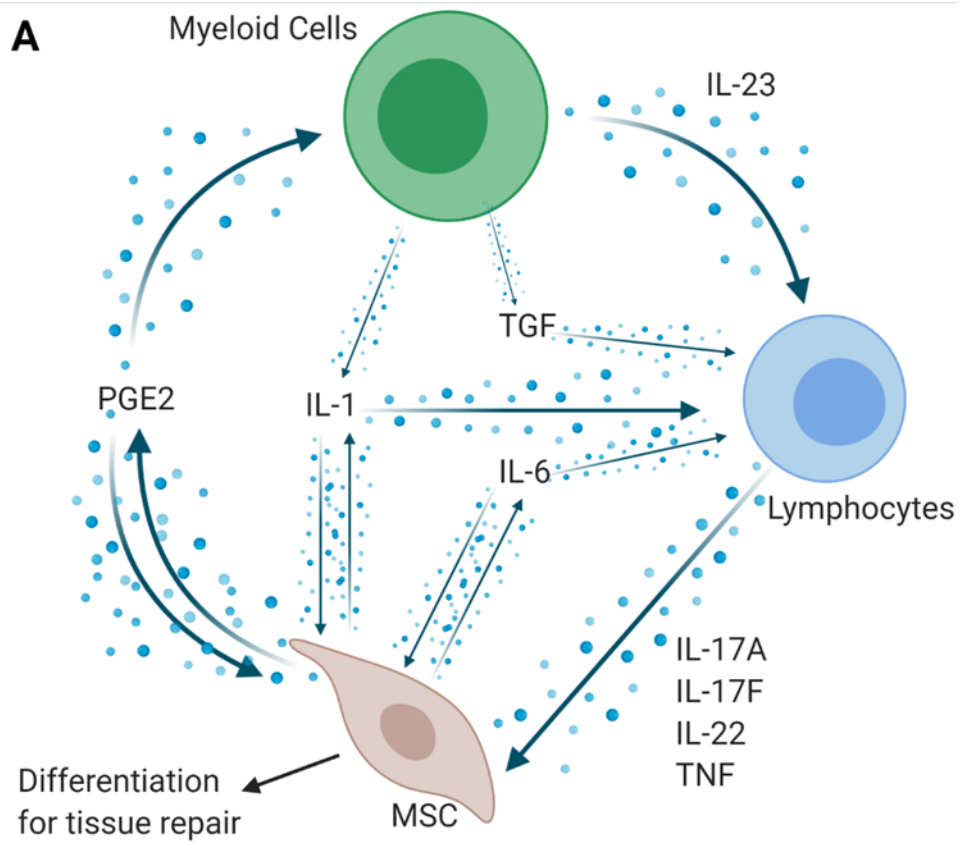
Figure 1.3: The IL-17/IL-23 axis

A) Outside of IL-17A and TNF other cytokines are indirectly involved in the IL-17/IL-23 axis, cytokines such as IL-1, IL-6, TGF-beta all independently impact the IL-17 pathway and/or MSCs directly. B) A wide range of cells from the immune system are all capable of IL-17A secretion from both the innate and adaptive immune system

1.2.1 – TNF in tissue repair in SpA prone sites

TNF forms a homotrimeric cytokine, which asserts its effects through two different receptors; TNFR1/p55 and TNFR2/p75 (107). TNFR1 is expressed ubiquitously and constitutively, whilst TNFR2 is only expressed on immune, endothelial, and neuronal cells. TNF is mainly produced by myeloid cells such as macrophages, but other immune such as CD4+ and CD+ T cells (89) and stromal cells are capable of secretion (108). Pharmacological targeting of TNF has proved highly successful in the treatment of AS (30, 76), psoriasis (109, 110), and inflammatory bowel diseases (IBD) (111, 112).

The most compelling data on the role of TNF in tissue repair comes from experimental models of skin injury or wound healing. TNF expression sources vary as wound healing moves through each phase. In early wound healing, stromal cells are the main expressers of TNF, though during the inflammatory phase macrophages and neutrophils become the primary expressers of TNF (113). The release of TNF increases the expression of cell adhesion molecules such as vascular cell adhesion molecule (VCAM)-1 and intercellular adhesion molecule (ICAM)-1, thus aiding further immune cell recruitment (114-116).

The initial experimental wound repair TNF knockout demonstrated reductions in neo-vascularisation of the wound, and reduced re-epithelialisation and fibroblast proliferation (117-119). These actions of TNF can occur either directly or indirectly.

TNF directs the localisation of RORγ$^+$ Group 3 innate lymphoid cells (ILC3s) in a Notch1 dependent fashion. Mice deficient for RORγ$^+$ ILC3 display a poor wound healing response arising from delays in epidermal proliferation and macrophage recruitment via a CCL-3 dependent process. Addition of TNF to wounds showed significant increases in the number of RORγ$^+$ ILC3 cells at day 2 with greater associated wound closure by day 5 when compared to wounds exposed to anti-TNF therapies (116). Group 3 ILCs are known to be potent producers of the IL-17 family particularly IL-17F which also plays a role in wound repair, and is covered later on (116).

However, despite the beneficial role TNF plays in normal wound healing, when dysregulated it is shown to be a potential cause of chronic wound states. Mouse chronic wound models involving the knockout of a secretory leukocyte protease inhibitor (SLPI) caused an increase in levels of TNF in wounds (120). SLPI inhibits macrophage production of TNF, possibly through the inhibition of activation of the NF-κB complex (121). This build-up of TNF causes a significant reduction in the amount of Col1A1 expression at day 5 post wound when compared to a wild type wound (120). Via TNF's activation of NF-κB, Col1A1 expression is suppressed (122-124). With the downregulation of Col1A1 matrix deposition becomes impaired leading to delayed wound healing as seen in chronic wound states. The addition of anti-TNF was shown to noticeably accelerate wound healing in SLPI-null mice and in wild type mice, though in wild type mice the change was to a much lesser extent (120). In septic disease states the increase in systemic TNF leads to a reduction in the amount of TNF present at the wound site in the early inflammatory stage, causing a significant delay in the wound closure (119). A translationally relevant parallel to the differing effects of TNFi in wound repair may be the fact that active inflammation in the spine may suppress tissue repair which is re-established with cytokine suppression and then post inflammation new bone formation.

In TNFR1 knockout mice macroscopic wound healing was shown to be faster than wild type mice. Additionally, the TNFR1 knockout mice had significantly less macrophage and neutrophil influx. The knockouts also displayed increases in angiogenesis, collagen content and re-epithelialisation associated with upregulation of gene expression of TGF-β1, connective tissue growth factor, vascular endothelial growth factor (125). Collectively these findings suggest the TNF is beneficial in the epidermis when a wound is infected but may be counter-productive in normal tissue repair in a non-infected environment.

1.2.1.1 – Bone healing and TNF

TNF is shown to play a role in normal fracture repair with murine knockouts of TNFR1 and TNFR2 resulting in a delay of MSC migration and subsequent postponement in the formation of endochondral tissue. The knockout of the

TNFR1 and TNFR2 did not prevent the eventual formation of endochondral tissue and its resorption, it only delayed the time at which this occurred (126). Conversely, supplementation of a mouse fracture with TNF resulted in accelerated healing, with greater callus mineralisation at 28 days post-fracture (127, 128).

These premises also hold true in normal human fracture repair which is aided by the presence of TNF at certain time points along its repair pathway. Assuming that correct alignment of the fracture site is present then within 72 hours of fracture there is a significant elevation in peri-fracture TNF, peaking at 24 hours post-fracture and returning to only a slight elevation above baseline levels by 72 hours (129, 130). The early peak in TNF is thought to encourage migration of MSCs to the fracture site, through the upregulation of ICAM-1 and VCAM-1 (131-133).

Protracted elevated TNF expression can be undesirable since normal fracture repair TNF levels are at baseline levels after day 3, if levels of TNF and IL-1β remain elevated after this initial elevation they work in a synergistic fashion resulting in increased chondrocyte apoptosis and impaired chondrocyte proliferation (134, 135).

Between days 7-14 of fracture repair, TNF level expression is low as during this phase the recently formed fracture callus is re-vascularised and at the same time ossification of the cartilage bridge is occurring. TNFR1 and TNFR2 knockout models have shown that TNF plays an important role in the revascularisation of the fracture callus (136). TNF also acts in the ossification of the cartilage bridge by inducing chondrocyte apoptosis and the formation of hypertrophic chondrocytes, via the activation of metalloproteinase (MMP) 9 & 14 (136, 137). After Day 14 the ossified fracture callus is replaced with trabecular bone, TNF is shown to cause the upregulation of certain Wnt (Wnt5a & Wnt10b) pathway proteins in MSCs which is involved in osteoblastic function and subsequent mineralisation (138, 139).

However, in RA TNF in the presence of IL-1β causes a decrease in the expression of RUNX2, which leads to a decrease in collagen expression and consequently diminished bone formation (140-142). This decrease in bone

formation is unable to compensate for the cytokine driven induced bone loss in RA.

Interestingly, TNF stimulates tissue nonspecific alkaline phosphatase and subsequent mineralisation in the presence of collagen, independent of the RUNX2 pathway (141). With the collagen-rich environment at the enthesis, this ectopic mineralisation of the collagen fibrils could be acting as a template for calcium crystal deposition and potentially assisting in the new bone formation at the enthesis.

Elevated levels of TNF are seen to induce persistent elevation of Wnt proteins. Elevation activates NF-κB (p65) and c-Jun N-terminal kinase (JNK)/activator protein 1 signalling pathways leading to bone formation. However, both the canonical and non-canonical pathways are needed to induce bone formation via inflammation with inhibition of either pathway significantly decreasing bone formation (139). However, TNF is shown to elevate levels of Dickopff-1 (DKK-1), this is shown in mouse models to suppress Wnt signalling, allowing for enhanced bone resorption with an increase in osteoclast activator RANKL (143). Inhibition of DKK-1 resulted in increased bone formation via Wnt signalling activation, with subsequent RANKL mediated bone resorption being blocked by osteoprotegerin (OPG) (143).

In AS the role that DKK-1 remains contentious with various studies and meta-analyses showing contrasting results with some showing significant elevation of DKK-1 in AS (144, 145), others showing a significant decrease (146, 147) whilst some showed no significant differences (148, 149). There is some evidence DKK-1 is dysfunctional in AS and a result is capable of abnormal activation of β-catenin independent Wnt signalling by binding less avidly to low-density lipoprotein receptor-related protein 6 (LRP6), a key receptor in the canonical Wnt pathway (150). Nevertheless, with the mixed literature on its potential effects it is impossible to determine if it plays a role in the pathogenesis of AS. The idea that new bone formation occurs in AS via DKK-1 in face of high TNF remains unsubstantiated.

1.2.2 – IL-17 Family

In mammals IL-17 comprises of 6 members IL-17A-F, which signal through 5 receptors A-E (Figure 1.4); though IL-17RD has been identified it is not currently known what signals through it (151). Each member of the IL-17 family behaves differently, with some acting in a pro-inflammatory role whereas others act in a tissue-protective capacity (151). Due to the shared 55% homology IL-17A is capable of forming a heterodimer complex with IL-17F (152).
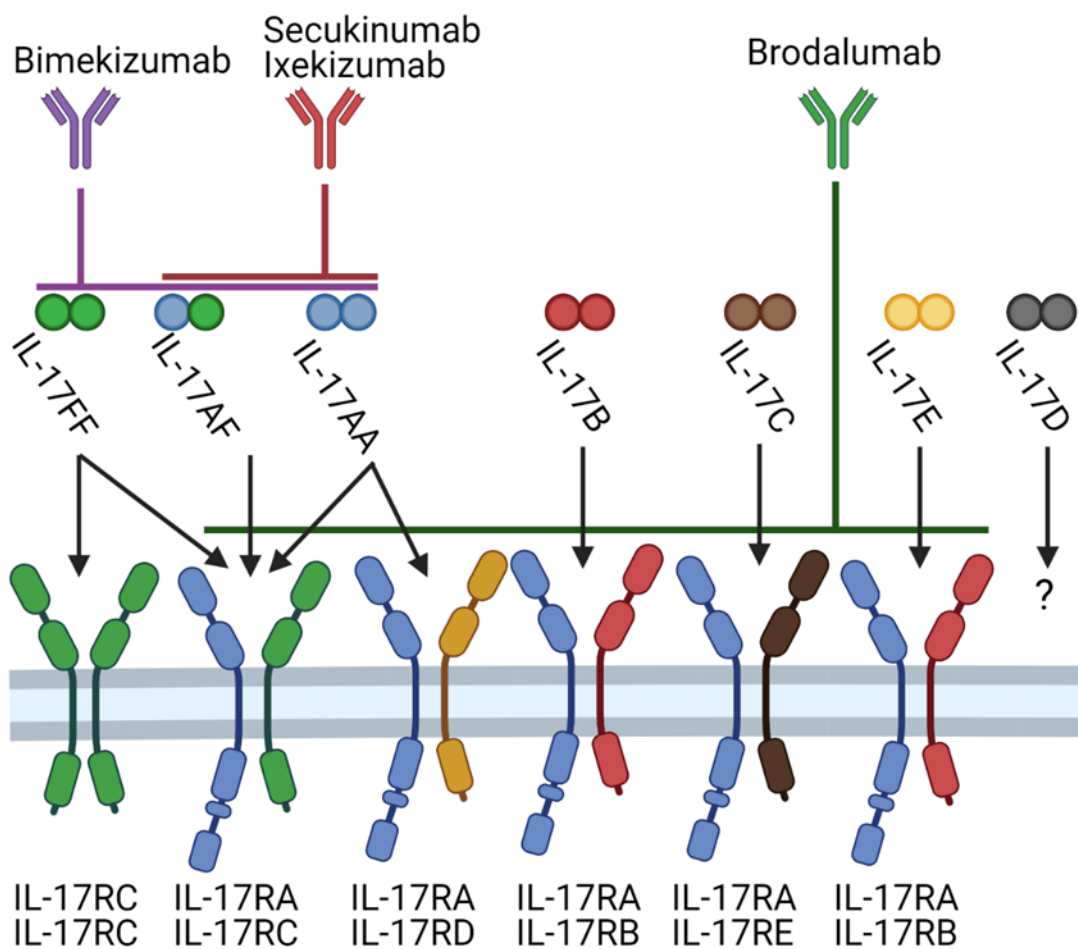
Figure 1.4: IL-17 receptor family

The IL-17 family has an array of receptors with the majority all incorporating IL-17RA as part of the receptor heterodimer, except for IL-17RC which can form a receptor homodimer. IL-17D's receptor remains unknown currently. Therapeutic targeting is broadly separated into IL-17RA antagonists (Brodalumab) and IL-17AF/AA (Secukinumab, Ixekizumab) or IL-17FF (Bimekizumab) proteins binders which inhibit their signalling potential.

1.2.2.1 – IL-17A

IL-17A is expressed from a range of cell populations from both the adaptive and innate immune system including γδ T Cells (60), Th17 Cells (153), CD8+ Cells (89, 154), ILC3 (86, 155), invariant natural killer T cells (156, 157) and mucosal-associated invariant T cells (154, 158). IL-17A binds to its heteromeric receptor complex consisting of IL-17RA and IL-17RC, IL-17F also signals through this receptor complex (159).

During wound healing IL-17A is expressed via stimulation of resident γδ T cells or dendritic T cells in the epidermis in response to an increase in IL-1β (160, 161). The elevation of IL-17A at the site of the wound is known to play a role in protection against potential infections such as *Staphylococcus aureus* (162) via promoting neutrophil migration into the wound site (163). Neutrophils are highly important in early wound repair, they play a role in cleaning up cellular debris, bacteria and any foreign particles in the wound, but have also been associated with delayed wound healing (164). An IL-17A knockout mouse showed improved wound healing times, associated with an attenuation in the number of neutrophils present in the wound (163, 165). The buildup of neutrophils in the wound is associated with an increase in secreted proteases (164). These proteases, such as MMP-2, MMP-8, and MMP-9, can damage extracellular matrices in the wound and perpetuate local inflammatory responses (166).

However, impaired wound healing was also shown in IL-17A knockout mice when γδ T cells - including dendritic epidermal T cells - were absent (167). The differences between these studies could be because of how the wounds are dressed. When comparing between an open and a closed wound model, IL-17A knockout mice showed a delayed wound healing response compared to wild type in an open wound (163).

This suggests that IL-17A's role in skin injury is primarily associated with protection from infections and after a fibrinogen clot has formed, IL-17A should decrease in tandem with neutrophil numbers (164, 166). Though if prolonged elevated levels of IL-17A are present from Vγ4 T Cells, it inhibits the secretion of insulin-like growth factor (IGF)-1 from dendritic epidermal T cells, leading to a delayed wound re-epithelisation (168).

IL-17A clearly drives the pathogenesis of psoriasis as is evidenced by the excellent responses for anti-IL-17A (169). Psoriasis can be viewed as an excessive repair to injury model. Briefly, psoriatic plaques occur due to hyper-proliferation and aberrant terminal differentiation of keratinocytes in response to elevated IL-17A levels (170). The aberrant IL-17A levels cause downregulation of proteins associated with cell adhesion at the epidermis, such as filaggrin which is required for hydration of the stratified corneum (171, 172). This results in a disease state presenting in red, scaly plaques chronically appearing at various sites on the body particularly elbows, knees, and the scalp. Histologically this results from thickened epidermis with marked keratinocyte hyperplasia with increased levels of CD8+ T cells and neutrophils, neo-vascularisation of the papillary dermis - allowing for excessive infiltration of T cells - and dendritic cells in the dermis (173). Pharmacological targeting of IL-17A improves the disease state in patients, highlighting a clear role in disease cause (169).

It has been reported that IL-17A inhibition can increase the risk of infections (174) and exacerbate Crohn's Disease (175). Innate IL-17A production, independent of IL-23, regulates the tight junction protein occludin during epithelial injury limiting excessive permeability and maintaining the gut barrier integrity (176). Deficiency of IL-17A in mice dextran sulphate sodium-induced colitis models show impaired epithelial proliferation and barrier repair (177). This demonstrates the key role in experimental SpA for IL-17A for tissue in the bone, gut and skin and the overarching concept of disease states linked to local tissue perturbations in intrinsic immune responses that fine tune repair.

1.2.2.2 – IL-17 in the bone repair

In the skeleton, IL-17A is seen to be elevated in the early weeks after a bone fracture, with γδ T Cells being the primary source (60). This early elevation relates to the suspected role that elevated levels of IL-17A play in fracture repair shortly after injury (60, 178). The reasoning for this increase is mixed within the literature available, with IL-17A shown to both increase osteogenesis (60) but in rat calvarial cells to decrease osteogenesis (179). The difference in effects IL-17A has on osteogenesis is suggested to be

dependent on the target cells origin. Immature mesenchymal cells such as MSCs are reported to display increased osteogenesis with exposure to IL-17A (59, 67, 180), whereas calvarial pre-osteoblasts are seen to show decreased osteogenesis (179, 181).

Generally, it is thought that the elevation of IL-17A in the aftermath of a bone injury promotes bone regeneration, with murine IL-17A-/- models displaying impaired bone regeneration following drill holes in the femur at 14 & 21 days post-injury compared to wild type mice (60). Elevation of IL-17A activates osteoblasts via JAK2/ signal transducer and activator of transcription (STAT)3 signalling pathway, causing osteogenesis and fracture repair (67). Yet, in human RA, elevated IL-17A is shown to cause joint destruction and bone loss (55, 182).

1.2.2.3 – IL-17F

IL-17F signals through the same receptor complex as IL-17A, which is a complex comprising of IL-17RA/C (159). However, IL-17RC has been reported to form a homodimer through which IL-17F can signal (183). IL-17F is often co-expressed with IL-17A and, due to their location at the same locus this also results in the same cell types expressing IL-17F as well as IL-17A (184). IL-17F is thought to have similar biological effects to IL-17A, though acting as a weaker stimulus (185). IL-17F has a higher affinity for IL-17RC, whilst IL-17A has a higher affinity for IL-17RA (186). IL-17RC is preferentially expressed on nonimmune cells, with IL-17RA more on immune cells (187). IL-17F is required for host protection against pathogens after wound healing or exposure to an infectious agent (187-189), patients with an ACT1 mutation, which is a common adaptor for IL17A and IL-17F signalling, display chronic mucocutaneous candidiasis (190).

Elevated levels of IL-17F are seen in lesional skin of psoriatic patients (191). Interestingly, some mouse models of imiquimod induced psoriasis display a greater disease resistance when they are IL-17F deficient (192). Even though it is thought that IL-17F is a weaker signal inducer than IL-17A, the prevalence of its preferred receptor on keratinocytes could explain why IL-8 and IL-6

production is higher from normal human epidermal keratinocytes than that of IL-17A (193).

IL-17F is expressed after an inflammatory stimulus, it is seen to activate the CCAAT/enhancer-binding protein (C/EBP)-β-mediated osteoblastogenesis seen in early fracture repair (185, 194). This is supported by a mouse tibial fracture model where IL-17F is seen to be elevated three days after the fracture at the fracture callus demonstrating a role in fracture repair (195).

Rag1 knocked-out mice, which prevents the development of mature B and T cells, demonstrated impaired fracture healing compared to wild types and – interestingly - IL-17F was shown to rescue this impaired osteogenesis (195). This increased osteogenesis by IL-17F has not only been reported on MC3T3-E1 cell lines (194) but it also increased human osteoblastic differentiation from human and mouse bone marrow-derived MSCs (59, 195). Clearly, from these experiments, it will be important to ascertain whether IL-17F dysregulation could play a role in AS related inflammation and post inflammation tissue remodelling. Of particular interest was the demonstration of two IL-17F gene polymorphisms (7383A/G & 7488A/G) associated with AS disease in a Turkish patient cohort (196).

1.2.2.4 – IL-17B, IL-17C, IL-17-D and IL-17E

As described IL-17A and IL-17F have clear roles in some SpA target tissue homeostasis but the remaining IL-17 family members are relatively less widely studied, though there is evidence that they are involved in tissue homeostasis. The receptor complexes for some of these family members are still unknown. IL-17B is now known to signal through the receptor complex containing IL-17RA and IL-17RB (197, 198), IL-17C signals through a heterodimeric complex of IL-17RA/E (199), IL-17D's receptor complex is still unidentified (200), and IL-17E, also known as IL-25, signals through the heterodimeric receptor complex IL-17RA/B (197).

During normal wound healing, IL-17C and IL-17E play a role in protection against infection during the early phases of wound healing (201, 202). Though the actions for this appear to be different. The receptor complexes for IL-17C and IL-17E are both found on epithelial cells (199, 203) and keratinocytes

(201), a difference that whilst IL-17E is expressed by lymphocytes (204) and eosinophils (205), IL-17C is not seen on immune cells (206). Mice overexpressing IL-17C show a significant upregulation in anti-microbial transcripts S100A8 and S100S9 (202), with keratinocytes expressing IL-17E leading to M2 macrophage recruitment of neutrophils to the wound site (201). Demonstrating a role in the removal of pathogenic agents from the wound site. There is also evidence that they play a role in re-epithelisation of the wound with both IL-17C and IL-17E capable of inducing epidermal thickening. Intradermal injections of IL-17C led to thickening of the epidermis (206) and IL-17E causing proliferation of murine keratinocytes via STAT3 activation (207).

Despite an apparently beneficial role in wound healing both IL-17C and IL-17E elevation has been identified in psoriatic plaques (202, 208). In particular, IL-17C's ability to potentiate Th17 cell response via the use of the downstream adaptor Act1 induces the expression of IκBζ, inducing a further pro-inflammatory response associated with psoriasis (209, 210). Neutralisation of IL-17C in a murine psoriasis model reduced skin inflammation (211), whilst the use of adalimumab in patients results in a decrease in IL-17C mRNA levels associated with improved disease states (212). This in part is likely due to the autocrine pro-inflammatory signalling cascade in keratinocytes, when stimulated with IL-17C and TNF significant increases in pro-inflammatory genes and cytokines are seen (202, 206). The role that IL-17E plays is still unclear, though single nucleotide polymorphism (RS79877597) in the IL-17E gene is associated with a more severe disease state and increased prevalence of psoriatic arthritis (213). It is likely that IL-17E is involved in the thickening of the epidermis, by inducing excessive proliferation of keratinocytes (207), evidenced as murine knockouts for IL-17E are resistant to imiquimod induced psoriasis (207). There is no known role for either IL-17B or IL-17D in psoriasis, despite the IL-17D being elevated in psoriatic lesional skin (214).

During fracture repair IL-17B is suggested to play a role in the early phases post-fracture. Elevated levels of IL-17RB are seen in the first two weeks post-fracture in rat long bones, with it localised to trabecular bone osteoblasts,

primitive and pre-hypertrophic chondrocytes as well as localised MSCs (215). The exact role it might play is not known or well-studied.

The compelling evidence that these cytokines are involved in SpA like diseases from murine CIA models. The CIA model shows a prominent inflammatory entheseal component, which was previously regarded as an experimental bulwark of RA pathogenesis (91). With both IL-17C and IL-17B mRNA being elevated in the arthritic paws of CIA mice, the disease is ameliorated with the addition of IL-17B antibodies (216). Moreover, IL-17C enhanced the production of TNF from murine peritoneal exudate cells, with IL-17C transduced CD4+ T Cells exacerbating the arthritic destruction (216). Interestingly the addition of IL-17E to a CIA mouse model attenuated the disease state (217). This is associated with IL-17E role in inhibiting the differentiation of Th17 cells from CD4+ T cells, causing a subsequent reduction in pro-inflammatory cytokines associated with arthritis (217-219).

As with IL-17A being important in the gut, IL-17C appears to be important in gut homeostasis and protection though its exact role remains unclear. With murine IL-17C knockouts were displaying exacerbated colitis induced by dextran sulphate sodium when compared to wild types (220). In humans with IBD IL-17C is seen to be elevated, though it's not entirely clear why this is the case (221, 222). In patients with Crohn's disease the use of anti-TNF can result in paradoxical psoriasis associated with elevated IL-17C dependent on a mechanism involving IL-36γ (223).

1.2.3 – IL-22

IL-22 is a distant family member of the IL-10 family and acts through a receptor complex consisting of IL-10Rβ and IL-22Rα (224), though it acts as a soluble receptor complex with IL-22 first binding to IL-22Rα with the complex subsequently binding to IL-10Rβ (225). IL-10Rβ is ubiquitously expressed by both immune and non-immune cells, whilst IL-22Rα is not expressed on immune cells (226) but is expressed on a range of other cell types such as MSCs (227), keratinocytes (228) and epithelial cells (226). As with other IL-10 family members, IL-22 signals through the Jak-STAT signal transduction pathways (224). IL-22 also has an alternate soluble receptor that acts to inhibit

the signalling actions of IL-22, known as IL-22 binding protein (IL-22BP) (229, 230).

IL-22's upstream signaller IL-23 is seen to be upregulated in the days after femoral fracture in mice, this is likely to correlate with an upregulation of IL-22 expression (231). IL-22 drives the migration of MSCs towards a site of injury where elevated levels of IL-22 could be present (227). The location of IL-22Rα restrictions creates a uni-directional signalling pathway, and as a result only immune cells are seen to express IL-22, with CD4+ T cells (232), CD8+ T cells (233, 234), γδ T cells (235) and natural killer T cells (236). In ILC populations RORγt is required to induce IL-22 expression due to the role it plays in IL-23R upregulation (237). Regulation by IL-23 is seen in IL-22 expression with blockades of mTOR in neutrophils showing inhibited IL-22 production (238). IL-23 is also shown to drive T cell activation and subsequent increase in pro-inflammatory cytokines such as IL-22 (91, 239). The use of IL-23 inhibitors in AS patients for a phase two trial showed no meaningful clinical improvements (70), with rat SpA models showing the same results unless anti-IL-23 is used prophylactically when there was suppression of IL-22 (74). This suggests at IL-22 production in a potentially independent manner from IL-23, where IL-23 is needed for disease initiation but not its continuation or progression.

During normal wound healing, IL-22 helps to drive keratinocyte wound epithelialisation (228). Keratinocyte differentiation is inhibited by IL-22, in combination with activation of STAT3 and increase in genes associated with extracellular matrix (ECM) remodelling such as MMP-1 and type I collagen (228, 240) pointing towards an important role for IL-22 in normal wound healing. With mouse IL-22 knockouts in full-thickness wounds displayed major defects in the ECM, manifesting as delayed wound closure and a decrease in ECM gene expression (241). In type 2 diabetic mice with an impaired wound healing response addition of IL-22 appeared to rescue the impaired wound healing response, by inducing re-epithelialisation and genes associated with ECM remodelling (242).

IL-22 also acts in increasing the expression of antimicrobial genes (S100A7, S100A8 & S100A9), with mice IL-22 knockouts display a significantly worse

pathology at the sites of parasitic infections which was associated with a loss of wound healing functions in keratinocytes (228, 243).

Despite its beneficial role in normal wound healing, IL-22 is elevated in psoriatic plaques and serum (244, 245). The exact role that it plays is unknown, though transgenic mice that overexpress IL-22 develop skin that mimics psoriatic skin (246). Potentially with the strong expression of the IL-22Rα on epithelial cells in the skin the overexpression of IL-22, induces abnormal ECM remodelling from the local keratinocytes and fibroblasts.

Osteogenic differentiation from MSC is enhanced by elevated IL-22, subsequently IL-22 activates osteoblast induced bone remodelling via phosphorylation of STAT3 (91, 227). Interestingly, mouse primary osteoblasts display only low levels of the IL-22Rα receptor, though its expression was upregulated when primed with bone morphogenetic protein (BMP)-2 (247). This suggests that it only plays a small role in normal bone remodelling in comparison to the skin where it has greater importance.

Immune cells associated with IL-22 production are seen to be elevated in the peripheral blood, bone marrow, synovial fluid and in the gut of patients with AS (155, 158, 248). Though its role remains mostly unknown, based off the evidence that it can increase osteogenesis in an inflammatory environment it could well play a role in the formation of excessive bone in AS (91, 227).

In the gut IL-22 is seen to act protectively during colitis, where IL-22BP can inhibit its actions (249). The protective actions of IL-22 in the gut, cause increased proliferation of intestinal epithelial cells (IECs) as well as migration of IECSs towards the site of injury (250), at the same time increasing mucus deposition (251). Patients with early-onset inflammatory bowel disease showed a defective IL-10Rβ signalling response, where they did not upregulate the protective transcripts when stimulated by IL-22 (252). However, these same protective proliferative effects are also shown to enhance tumorigenesis in the gut. Colorectal cancer cells are seen to show increased proliferation in response to IL-22 (253)

1.2.4 – PGE2

Prostaglandin E2 can be produced by almost every cell in the human body, it is a lipid mediator that is synthesised from arachidonic acid via COX enzymes (254). Interestingly, PGE2 acts in a homeostatic (255), inflammatory (256) or anti-inflammatory (257) manner in various contexts. Prostaglandin E2 exerts its effects through four different G protein-coupled receptors (EP1-EP4), EP4 is of particular interest for potential roles in AS (44) and normal bone formation (258).

Prostaglandin E2 has long been known to cause an increase in osteogenesis, with immobilized femurs of female rats treated with PGE2 showing increased osteogenesis in these immobilized bones (259). More recently co-culture models of M1 macrophages and MSCs demonstrated enhanced mineralisation compared to MSCs cultured alone (256). The levels of increase in osteogenesis were closely associated with PGE2 secretion by the M1 macrophages in early phases of MSC differentiation, with a significant decrease in mineralisation observed when a COX-2 inhibitor was added to the culture (256). With macrophages being elevated early at fracture sites (260) this suggests a role for PGE2 in normal fracture repair. Knockouts of COX-2 in mice showed a delayed initiation and an impaired endochondral bone repair associated with severe angiogenesis deficiency (261). Agonists for EP4 or EP2 can rescue impaired fracture healing seen in COX-2 knockout mice (261), they can also augment normal fracture repair in rat fracture models (262). This all suggests an early role for PGE2 in fracture healing.

Of considerable interest after a GWAS in AS was a single nucleotide polymorphism (SNP) at chromosome 5p13 (44). The rs10440635 SNP in the prostaglandin E receptor 4 (PTGER4) gene is heavily associated with AS (44). PTGER4 encodes the prostaglandin E2 receptor 4 (EP4), which when activated is seen to amplify CD40 mediated induction of IL-23 p19 expression (263). The evidence that NSAIDs are highly effective at reducing new bone formation linked to PGE2 expression suggests at a potential role (85).

1.3 – Cytokines outside the TNF and IL-23/17 pathway

Aside from the TNF and IL-23/IL-17 pathways, other cytokine signalling pathways have been genetically linked to AS such as IL-1 and IL-6 (18, 42). There is evidence for the limited efficacy of anti-IL-1 (264) in AS but no evidence for the efficacy of anti-IL-6 (265) which appears to place these molecules of much lower clinical translational relevance. Nevertheless, the genetic associations with AS and roles in repair merit some description

1.3.1 – IL-1 Family

The IL-1 pathway has repeatedly been identified in GWAS in AS (42, 43). With IL-17 appearing to be capable of being produced independently from IL-23 (74), and IL-1β being evidence to drive maturation of IL-17 producing T cells (266-268). This supports a role for the IL-1 family in AS especially since IL-23 blockade is ineffective for spinal disease. Deficiency of the IL-1 receptor antagonist in humans, termed DIRA, is associated with new bone formation in the spine (269), indicating that unrestrained IL-1 family activity may lead to new bone formation.

1.3.1.1 – IL-1α

IL-1α is important is in the initiation of an inflammatory response and subsequent tissue repair, or potentially pathological conditions. In wound healing IL-1α knockout mouse models demonstrate that without IL-1α early activation in response to cellular damage, subsequent collagen formation and tissue repair is delayed after damage by ultraviolet light (270). This is achieved by IL-1α upregulation of genes associated with tissue repair such as BMP2 and keratinocyte growth factor whilst also acting as a chemotactic attraction for keratinocytes (270-272). However, just as the removal of IL-1α can delay the wound healing response excessive levels of IL-1α can delay wound healing and potentially lead to a chronic wound state (273, 274).

IL-1α is important in normal bone metabolism and remodelling, with its expression seen in the early and the late phases of fracture repair and subsequent remodelling (275). IL-1α can activate RANK signalling pathways directly, independent of RANKL (276). IL-1α enhances bone resorption by

stimulating osteoclastogenesis, when IL-1α is knocked out in mice they display an increased bone density (276). Interestingly IL-1α is also seen to inhibit differentiation and induce apoptosis of an osteoblast-like cell line (MC3T3-E1). IL-1α inhibits via its activation of the JNK and p38 mitogen-activated protein kinases (MAPK) pathways (277). When taken together this demonstrates why excessive IL-1α in inflammatory diseases causes bone resorption and subsequent joint destruction such as RA (278, 279).

The role of IL-1α in the heart appears to be a much more pathogenic role than the potentially beneficial role seen in other organs. IL-1α elevates rapidly after myocardial infarction, causing an upregulation of proteins associated with clearing of damaged tissues and a progressive further thinning of the myocardial walls associated with subsequent adverse events (280-282).

1.3.1.2 – IL-1β

In normal wound healing IL-1β is expressed immediately after damage by local keratinocytes and fibroblasts. The elevation of IL-1β expression induces upregulation of fibroblast growth factor-2 (FGF2), this then stimulates migration of fibroblasts to commence re-epithelisation of the wound (271, 283). IL-1β has also been suggested to improve the adhesion of fibroblasts to MMP3-degraded fibronectin, following an inflammatory stimulus (284). The role of IL-1β is particularly important during the inflammatory phase of wound healing, where aside from inducing the migration of fibroblasts it also stimulates macrophage recruitment and maturation (285). However, if levels of IL-1β stay elevated then chronic wound states can develop due to over activation of immune cells and production of proteases preventing the normal wound healing pathway (286). This is an issue seen in diabetic patients, who can display impaired wound healing or ulcers. These ulcers and chronic wounds can be reversed and restored to a normal wound healing response by the inhibition of IL-1β highlighting its role in abnormal wound healing (287, 288).

IL-1β expression is seen to be biphasic in fracture repair, with elevation seen in the immediate hours after fracture and the subsequent second increase during the remodelling phase weeks later (275). The early elevated

expression of IL-1β results in an increased number of osteoclasts in a polarised morphology (289), the activation of osteoclastogenesis can be achieved independently of RANKL (276). The increase in polarised osteoclasts induces bone resorption seen in the early stage of fracture repair as well the late phases associated with trabecular bone remodelling (290). IL-1β effects on osteoblasts are conflicted, with one study suggesting that IL-1β stimulates proliferation of osteoblast-like cell lines (MC3T3-E1) and mineralisation of bone matrix (290). IL-1β has also been shown to suppress BMP-2 mediated osteoblast differentiation in MC3T3-E1 cells (291), whilst also inhibiting the migration of osteoblasts towards elevated levels of platelet-derived growth factors at a fracture site (292). In humans genetic diseases such as Muckle-Wells syndrome results in overexpression of IL-1β during times of inflammation (293). In the most severe cases of Muckle-Wells syndrome this overexpression of IL-1β is shown to cause epiphyseal growth plate overgrowth associated with bony overgrowth and ossification of bones in particular the patella (294). These symptoms are seen to be improved with the application of IL-1β receptor antagonists (295).

However, in a rat model with elevated levels of IL-1β, a fracture site haematoma with thinner fibres and a denser clot structure was created, which inhibited migration of stem cell populations towards the fracture site (296). Elevated levels of IL-1β and the associated changes in normal healing can lead to non-union fractures or inflammatory diseases resulting in abnormal bone resorption (297-299).

As IL-1β plays a role in disease states, it is sometimes targeted therapeutically. However, due to the cytokine signalling cascade induced by IL-1β inhibition, it usually serves only to prevent further disease progression rather than completely curing the pathology (160, 300).

IL-1β can induce the expression of other inflammatory cytokines from CD4+ and CD8+ cells, this allows for the initiation of an inflammatory response seen in tissue repair. IL-1β along with IL-23 is capable of inducing the expression of IL-17 from Th17 cells, but IL-1β is also shown to induce the expression of IL-17, IL-21 and IL-22 from γδ T cells due to their expression of the transcription factor RORγt (also seen on Th17 cells) (160). IL-1β is also known

to induce the expression of IL-6 from peripheral blood monocytes and epithelial cells (301, 302).

1.3.2 – IL-6

IL-6 is a pleiotropic cytokine involved in a range of biological processes both inflammatory and anti-inflammatory (303). One such function is that it can assist in priming Th17 cells in conjunction with IL-23 (304). IL-6 has two distinct signalling pathways the classical and the trans-signalling pathway, both of which require glycoprotein (gp) 130 (303, 305). The trans-signalling pathway involves the generation of soluble IL-6 receptor by proteolytic cleaving of the membrane-bound precursor, the two signalling pathways can elicit distinct biological responses which can translate into variations between knockout models (305, 306).

IL-6 is heavily involved in normal wound healing. IL-6 is expressed shortly after wound damage by local keratinocytes and local fibroblasts, macrophages and Langerhans cells peaking at 24 hours (307, 308). The importance of IL-6 in normal wound healing is evidenced by IL-6 knockout mice displaying a significantly delayed wound healing, characterised by impaired re-epithelisation (309, 310). IL-6 induces keratinocyte migration across the wound, whilst also increasing the proliferation of keratinocytes through activation of periostin and STAT3 (311-313). However, overexpression of IL-6 in the skin during wound healing is associated with pathological conditions such as psoriasis (314), systemic lupus erythematosus (315) and scleroderma (316).

IL-6 is expressed by osteoblasts following a fracture, due to the rapid increase in local IL-1β (275, 317). The levels of IL-6 decrease over the course of the fracture repair (318), which is supported by the suspected role IL-6 plays in fracture healing. Knockouts of IL-6 in mice fractures causes a significant reduction in osteoclastogenesis and impaired callus strength, though by 6 weeks post-fracture most of the biomechanical features of the fracture were similar to wild type mice (319). IL-6 also has a chemotactic effect upon resident mesenchymal cells, which migrate towards the site of the fracture (275).

Though just as loss of IL-6 function can have adverse effects certain pro-inflammatory conditions that induce an abnormal and prolonged upregulation of IL-6, such as rheumatoid arthritis, can cause significant bone degradation (320). In murine models elevated levels of IL-6 (among other cytokines discussed) causes an upregulation in STAT3 activation in osteoblasts and local fibroblasts (321). This activation of STAT3 was seen to promote expression of RANKL and subsequent osteoclastogenesis, creating a positive feedback loop resulting in the prolonged inflammation and joint destruction associated with RA (321). Blockading of IL-6 signalling is seen to ameliorate osteoclastogenesis and joint destruction in both animal models (322, 323) as well in the use of tocilizumab for the treatment of rheumatoid arthritis in humans (324, 325). However, due to the redundancy associated with inflammatory responses even when IL-6 is targeted as a therapy it usually only prevents or limits further disease progression (326).

As mentioned prior, gut homeostasis is heavily reliant on the discussed cytokines for homeostasis; this is also true for IL-6, with Paneth cells in the intestinal crypt being activated by STAT3 IL-6 driven signalling, resulting in increased cellular proliferation. Resident stem cell populations also respond to the increased IL-6 and proliferate to aid in barrier repair (327). This signalling pathway is capable of acting in an autocrine signalling manner (327) but intraepithelial lymphocytes also secret IL-6 in response to epithelial damage (328). IL-6 knockout mice display increased paracellular permeability caused by a decrease in the barrier protein claudin-1 (328). Blockading of IL-6 with tocilizumab in RA patients was linked with substantially higher incidences of lower intestinal perforations than TNFi (329). This was also seen in the use of IL-6 blockers in Crohn's Disease, where there were elevated levels of intestinal abscesses when compared to the placebo (330). This highlights that the roles of cytokines can differ greatly depending on tissue or concentration.

As with TNF driving ILC3 recruitment (116), IL-6 is shown to drive the accumulation of Th17 cells in the gastrointestinal tract environment, in this case the oral environment (331). Damage to the gingiva, either through mastication or abrasion in mice models saw a rapid increase in IL-6

expression from a CD45- cell population in the epithelium (331). IL-6 is known to promote Th17 cell differentiation (332, 333) when chimeric mice were generated with IL-6R knockouts gingival Th17 cells had the cellular machinery to produce IL-17A but due to the loss of IL-6 signalling could not (331). However, Th17 cells taken from both gut and the skin of the same chimeric mice were fully capable of producing IL-17A independent of IL-6 signalling, demonstrating that IL-17A production in the gingiva is IL-6 dependent (331). Briefly, the role of the produced gingival IL-17A appears to be for protection against infection from the damaged gingival barrier, but also plays a role in age-related periodontitis and bone loss as seen in both humans (334, 335) and mouse models (331).

1.4 – Emergence of Th2 cytokines

There has recently been a re-evaluation into the role of the traditional Th2 cytokines, and the SpA field. IL-4 and IL-13 are classical Th2 cytokines, with a documented role in atopic dermatitis and asthma (336). As well as driving Th2 differentiation, these cytokines are involved in IgE class switching. The many shared functions of IL-4 and IL-13 is related to signalling through the commonly shared receptor (IL-14Rα). Recent data in atopic dermatitis patients undergoing dupillumab treatment (IL-4 and IL-13 blocker) reported the development of peripheral enthesitis (337). These observations have also been supported by other case reports of enthesitis development following dupilumab therapy (338).

The mechanism surrounding IL-4/IL-13 blocking induced enthesitis is presently unknown but genetic associations of unknown functional significance between IL-13 and psoriatic arthritis have been reported (339-341). It is also of note that the IL-13 genetic associations do not appear to occur in AS, given the many subtle differences between these diseases. It could be hypothesised that IL-4 and IL-13 blockage could change the differentiation of immature T cells from a Th2 phenotype to a Th1/Th17 phenotype with subsequent increased IL-17/IL-22 and TNF production. In support of this, we recently showed that IL-4/IL-13R cells are present in the normal enthesis, and the synovial fluid of PsA patients contains measurable

IL-4 and IL-13 (342). IL-4+ T cells are also present at the normal enthesis, and IL-4/13 reduced Th17 cytokines from stimulated entheseal T cells (342). It has been known for over 20 years that IL-4 has a protective role in cartilage destruction, including that induced by IL-17 (343). In the murine CIA arthritis model, both IL-4 and IL-13, reduced symptoms and bone erosion (343, 344), however this model at a pathological level is far closer to RA than SpA. The role of IL-4 and IL-13 in bone modelling has also been studied with KO models. IL-4 or IL-13 KO mice both present with reduced cortical bone mass (345). In a murine fracture model, net bone formation or mineral deposition was not affected by either IL-4 or IL-13 KO, however, subtle perturbations in associated vascularisation and innervation were noted (346).

1.5 – Relevance of MSCs to SpA

MSCs were first identified in 1970 by Friedenstein *et al.* (347) in the bone marrow of guinea pigs, and since then resident populations of MSCs have been identified in almost every post-natal tissue in humans (348, 349). However, to date they have not been characterised in the human entheseal tissue of the interspinous ligament, likely reflecting the comparatively difficult access of this tissue.

Local populations of MSCs are known to play important roles in the homeostasis of tissues throughout the human body and are also shown to be heavily involved with tissue repair after damage (350-352). The wide range of tissue repair and homeostatic roles is due to MSCs containing the osteoprogenitor pool that is thought to drive the spinal bone formation seen in AS (353). Bone and periosteum-resident MSCs are known to play important roles in healthy skeletal tissue repair after injury, migrate to fracture sites, and differentiate into chondrocytes and osteoblastic cells of the fracture callus (178), as well as adipocytes in the long-bone marrow cavities of the elderly (354). It is also known that adipocytes are present at the normal enthesis and may play an important biological role (51). Moreover, in AS, the intraosseous anchorage sites of the annulus fibrosis are associated with post-inflammatory adipogenic differentiation, which is a harbinger of future new bone formation in the adjacent anterior longitudinal ligament, but the mechanisms of this are

poorly understood (21). Other studies on AS have produced evidence for osteoprogenitors from the facet joints, but whether such cells are derived from bone or entheseal soft tissue has not been clearly defined and it has not been confirmed whether such cells are multipotential and hence represent MSCs (67).

The early phases of AS remain largely unknown, with recent works confirming the presence of fatty depositions at the entheseal attachment sites preceding the neo-osteogenesis seen in AS (21), there is a need to better understand the pathological changes seen in early disease. In particular, there is an absence of work investigating MSCs responses to SpA relevant cytokines in response to adipogenesis, and whether these changes are driven by the entheseal soft tissue or the bone.

In addition to the fact that MSCs are the parent cells for osteoblasts, chondrocytes, and adipocytes, they are also known to be immunomodulatory via the secretion of immune cell mediators, including chemoattractants (355), notably C-C Motif Chemokine Ligand 20 (CCL20), which is a known T cell chemoattractant via its interaction with C-C Motif Chemokine Receptor 6 (CCR6) (356). Importantly, previous studies have identified a range of immune cell populations at the human spinal enthesis, which plays a role in AS pathogenesis (86, 88, 90); notably, populations of CD4+ and CD8+ T cells capable of secreting both IL-17A and TNF (89). Populations of CCR6+ CD4+ and CD8+ T cells have been identified at the human spinal enthesis, helping to provide an insight into how MSCs may help to drive inflammation at the enthesis and how this can impact the differentiation capabilities of MSCs (357). Of interest is how other chemoattractant molecules may be secreted by MSCs at the enthesis and how the use of IL-17A monoclonal antibodies may influence suppressing the secretion of these and the subsequent reduction of inflammation.

It is now firmly established that the normal enthesis including spinal enthesis has a resident immune system including innate lineage myeloid cells and innate and adaptive lymphocytes that can be induced to secrete MSC relevant cytokines including IL-17, TNF and IL-22. This has been well described in other recent publications (88-90). Based on the aforementioned ability of

some cytokines to "fine tune" tissue repair, the central tenet of this thesis is that cytokines derived from these populations in SpA may lead to aberrant tissue repair responses. Therefore, the disease state is ultimately due to subtle perturbations of "cytokine fine tuning" of repair. Given that MSCs are thought to be the key cell for skeletal repair these were investigated with an eye on the known immunopathology of AS.

1.6 – Hypotheses and aims

It was hypothesised that MSCs exist in both the peri-entheseal bone and the entheseal soft tissue fragment of digested spinous processes and intra-spinous ligaments. These MSCs respond in a pro-osteogenic manner when stimulated by pivotal SpA relevant cytokines (IL-17A and TNF), which results in a reciprocal suppression of adipogenesis, something of relevance given that adipogenesis predates osteogenesis in AS. Cytokine cross talk with MSCs may further augment entheseal inflammatory responses.

The aims of this thesis are:

1. To characterise MSCs that meet the ISCT criteria are present in both the peri-entheseal bone and entheseal soft tissue, with CD271+ MSCs being present in the peri-entheseal bone but not the entheseal soft tissue (Chapter 3)
2. To investigate the roles of IL-17A and TNF on the osteogenic and adipogenic potential of MSCs from both the peri-entheseal bone and entheseal soft tissue (Chapter 4)
3. To investigate the role of MSCs from both the peri-entheseal bone and entheseal soft tissue on immunomodulation of resident immune cells. As well as to investigate the potential for MSC migration between the two tissues towards sites of damage seen in AS (Chapter 5).

Chapter 2 – General materials and methods

A full list of reagents, buffers, solutions, and equipment is found in the Appendices.

2.1 – Ethical approval

The investigation was approved by North West-Greater Manchester West Research Ethics Committee (REC: 16/NW/0797). Patients gave informed consent in accordance with the declaration of Helsinki. A full sample list is available in Appendix A.

2.2 – Spinous process and interspinous ligament digestion & preparation

Healthy human peri-entheseal bone (PEB) from the spinous process and entheseal soft tissue (EST) from the interspinous ligament were harvested from healthy patients undergoing operations for either scoliosis correction or spinal decompression of thoracic or lumbar vertebrae at Leeds General Infirmary. Entheseal tissue donors were not known to have any systemic inflammatory conditions, including SpA unless otherwise specified.

Samples were stored overnight in saline at 4°C before being digested as with previous studies (1, 86, 88, 90). Samples were carefully separated using a scalpel into the PEB and EST (Figure 2.1). PEB was further broken down into <5mm^2 fragments using bone cutting forceps. The EST was also minced into similarly sized fragments using a scalpel (Figure 2.1). Broken down samples of PEB and EST were put into independent 50ml Falcon centrifuge tubes, the mass of the samples was then recorded to make a collagenase digestion solution.

For each 1g of sample, 5ml of the collagenase solution was applied. The collagenase digestion solution contained 20% foetal calf serum (FCS), 80% Dulbecco's Modified Eagle Medium (DMEM) and 600U/ml collagenase. Collagenase, as supplied, contained several isoforms of 2 different

collagenases, a sulfhydryl protease, clostripain, a trypsin-like enzyme, and an aminopeptidase.

Samples were incubated at 37ºC in this solution for 3.5 hours with gentle agitation via inversion of the tube every 30-minutes. After digestion, samples were filtered through a 70μm sterile filter and were washed with sterile phosphate-buffered saline (PBS). Any material that could not pass through the filter was discarded.

Samples were centrifuged at 400xg for 10-minutes to pellet the cells, after which they were resuspended in a red blood cell lysis buffer for 5-minutes. After red blood cell lysis, samples were centrifuged again at 400xg for 10-minutes before being in an appropriate volume of DMEM (supplemented with 1% Penicillin-Streptomycin and 10% FCS), and viable cells were counted using a haemocytometer with Trypan blue as a viability stain.

2.2.1 – Cell counting and viability

Trypan blue is not taken up by viable cells as the intact cellular membrane prevents uptake, whereas non-viable cells which have compromised membrane integrity uptake it. Therefore, using the Trypan blue allowed for visual counting of viable cells after enzymatic digestion and discrimination against non-viable cells using an inverted light microscope and haemocytometer.

The cell suspension had 10μl diluted in a 1:1 ratio with Trypan blue and mixed in a 96-well round-bottom plate. From this mixture, 10μl was transferred via capillary action to the haemocytometer and viewed under a bright field microscope at 10x magnification. All viable cells were counted on four separate 1mm^2 squares and were averaged; a minimum of 100 cells was counted to maintain accuracy. Should viable cells be too hard to count either due to excessive numbers or too low numbers, the DMEM solution was either diluted or centrifuged and re-suspended into a more appropriate volume of DMEM.

Once an average for the number of viable cells in one 1mm^2 square was determined, the number of cells/ml of the DMEM cell solution was calculated using the following equation:

$$No. of\ viable\ cells/ml$$
$$= Average\ No. of\ counted\ cells \times dilution\ factor\ \times 10{,}000$$

For the total cell count of the DMEM cell solution, this value is then multiplied by the volume of the solution used.
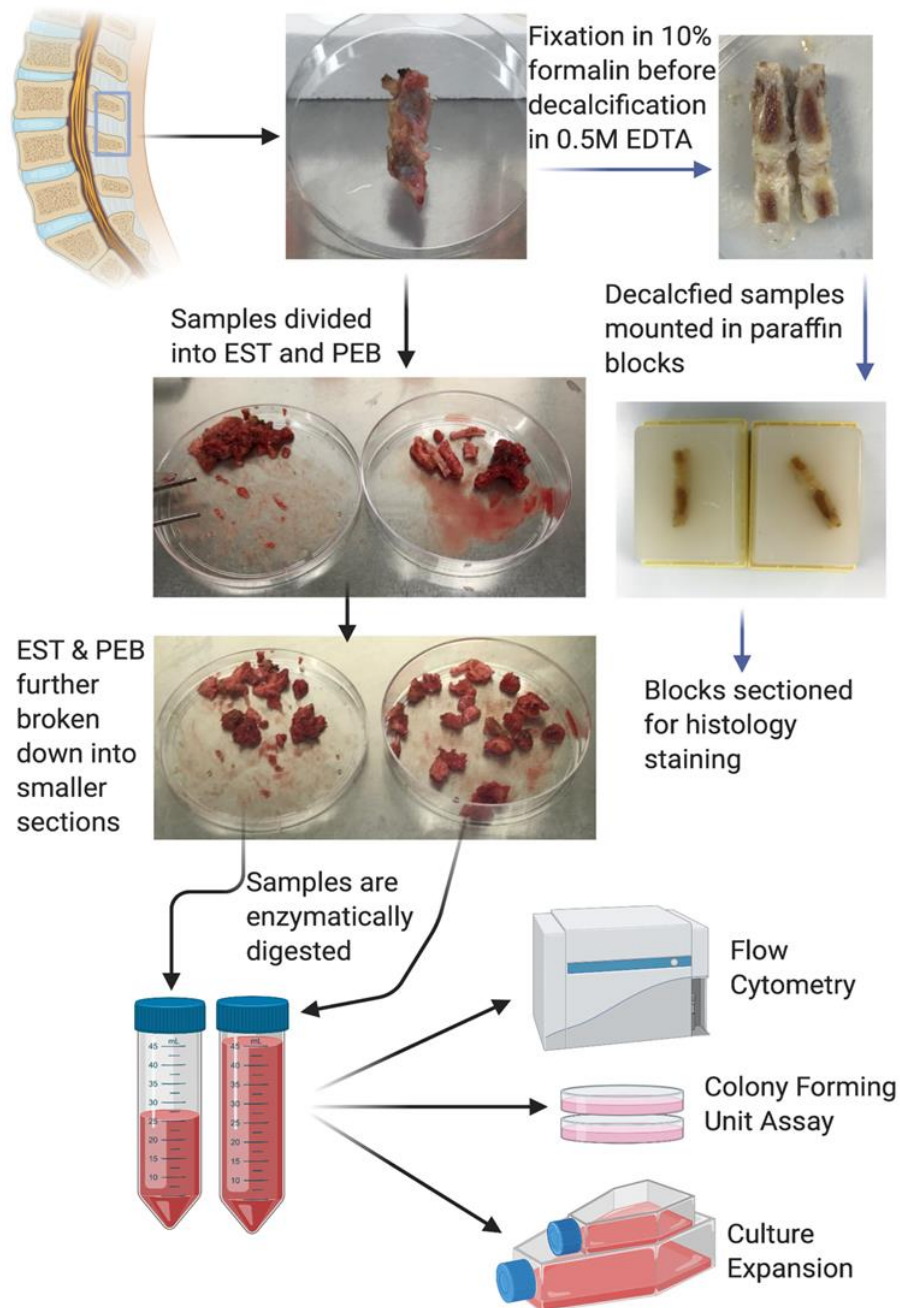
Figure 2.1: Preparation of entheseal tissue for downstream experimental use

Samples consisting of the PEB and EST are enzymatically digested. Where they are separated using scalpels into their constituent parts (PEB & EST) and minced into <5mm² pieces and digested using collagenase solution to free the cells from the extra-cellular matrix. These cells are then either prepared for flow cytometry, colony forming unit assays or culture expansion. Alternatively, samples are wholly fixed using 10% formalin before decalcification in 0.5M EDTA and mounting in paraffin blocks for subsequent sectioning for histology uses.

2.3 – MSC culture expansion and long-term storage

After digestion, depending on the number of viable cells, digests were either culture-expanded or frozen for future expansion or flow cytometry.

2.3.1 – MSC culture expansion

For MSC expansion, cells from both the PEB and EST digests were seeded into culture flasks at 15,000 cells/cm^2 in StemMACS MSC expansion media with 1% Penicillin-Streptomycin**.** After 48-hours, media was removed, and cells were washed twice with PBS to remove any non-adherent cells. Fresh StemMACS media was then applied. Half media changes were subsequently conducted every 3-days until cells reached >70% confluence. Cells were cultured in humidified incubators at 37ºC and 5% CO_2.

When >70% cell confluence was observed, cells were passaged. Complete removal of media from the flasks was then followed by a PBS wash. Cells were then incubated in an appropriate volume of a 0.05% Trypsin-ethylenediaminetetraacetic acid (EDTA) and PBS solution for 5-minutes at 37ºC.

After incubation, the Trypsin-EDTA-PBS solution with cells was transferred into a 50ml falcon tube, the flasks were then washed with DMEM to collect the remaining cells, which was transferred to the same falcon tube. Tubes were centrifuged at 500xg for 5-minutes. Following centrifugation, the supernatant was discarded, and the cells were resuspended in DMEM and counted using a haemocytometer as described previously.

For further cells expansion, new sterile flasks were used, and cells were seeded at 4,500 cells/cm^2; cultures were expanded until either a minimum of 10^6 MSCs for both PEB and EST was counted or until a maximum of passage (P) 2. If MSCs were not immediately used for downstream experiments, they were prepared for long term storage in liquid nitrogen until use.

2.3.2 – Freezing & retrieval of cells from long term storage

Cells to be frozen from fresh digests were counted and then centrifuged at 500xg for 5-minutes. The supernatant was then discarded, and the pellet was

re-suspended in freezing media at a concentration of 10^6 cells/ml. Cells were transferred to 1ml cryovials labelled and then initially stored a CoolCell® at -80ºC overnight before being transferred to liquid nitrogen within 1-week of initial freezing for long term storage. Cells frozen after culture expansion were treated the same as above, except they were frozen at a lower cell concentration of between 1-2x10^6 cells/ml.

Retrieval of cells for future experiments from either frozen digests or culture expanded cells followed the same procedure. Selected vials were defrosted in a water bath at 37ºC, and the thawed cell suspension was then added to a 15ml flacon tube containing 10ml DMEM with 10% FCS and antibiotics. Cells were pelleted by centrifuging at 600xg for 5-minutes at room temperature. The supernatant was discarded, the pellet was then re-suspended in an appropriate volume of DMEM, and cells were counted for use in subsequent downstream uses.

2.4 – Flow cytometry

2.4.1 – Fluorescence

Fluorescence is a key component of how flow cytometry works. In brief, fluorescence occurs when a compound absorbs energy in the form of light; this excites its electrons into a higher energy state. To return to its original state, the excess energy is emitted as a photon, allowing the electron to return to its pre-excitement state. The emitted light is always lower energy than the exciting light, meaning that the wavelength is higher than that of the exciting light. This allows for the separation of wavelengths using filters (358).

2.4.2 – Principles of flow cytometry

Flow cytometry is a technique that uses the principles of fluorescence to label cells and thereby identify specific cell subsets in a heterogeneous cell population or even confirm the presence of MSCs in culture in accordance with the ISCT guidance (358, 359).

Flow cytometers consist mainly of three main components which all play an important role: the fluidic system, the optical system and the signal detection and processing.

The fluidic system is responsible for the transport of the cells from their solution through the instrument and its detectors. This system contains two components: the sheath fluid and pressurised lines. Sheath fluid (commonly PBS) is injected into the flow chamber via pressurised lines. Another pressurised line also injects the suspended cells from the sample tube into the heart of the machine. Due to the relatively higher pressure of the sample fluid compared to the sheath fluid, this creates a coaxial flow based upon the pressure difference (360, 361). The higher pressure of the sample fluid causes the cells to align into single file fashion, allowing for the uniform excitation of the cells by the laser beams (360, 361).

The optical system contains the detectors, filters and the lasers used to excite the electrons into their higher energy orbitals. Lasers will have a specific wavelength that is used to excite specific fluorophores. For example, an argon laser with a wavelength of 488nm excites fluorescein isothiocyanate (FITC), resulting in an emission of a higher wavelength (525nm). The emitted photons pass through a series of mirrors and filters to separate and direct specified wavelengths to appropriate optical detectors (362).

Importantly it is not just the fluorescence produced from the electron excitement that is used to identify cell populations but also the forward scatter (FSC) and side scatter (SSC) are used to help identify (358). FSC is a measure of the size of the cell as a result of diffraction measured along the same axis as the laser beam. SSC is a measure of the granularity of the cell or internal complexity of the cell and is measured via the refraction and reflection of light at ~90⁰ to the laser beam (358). These two measurements allow for the differentiation of cell types in a heterogeneous population, for example, the difference in scatter profiles between granulocytes and lymphocytes (362).

Finally, the generated photons need to be converted to voltages by photodetectors as part of signal detection and processing. Two types of detectors are used depending on the sensitivity required; these are either

photodiodes (PDs) or photomultiplier tubes (PMTs) (362, 363). When photons are detected by either PDs or PMTs the photons are converted into a proportional number of electrons to generate an electrical current. In turn the current travels to an amplifier subsequently converting into a voltage pulse, which peaks when the cells are in the centre of the laser beam before returning to baseline as the cell passes through the beam (363). This generates an analogue signal, which is amplified by two types of amplifier (linear or logarithmic). To generate the histograms and plots on the computer, this analogue signal is converted into a digital output via an analogue to digital converters (363).

2.4.3 – Sample preparation and cell staining for flow cytometry

Flow cytometry was conducted on two different sample types, these being either culture-expanded cells or cells directly after digestion. In both cases, the procedure was the same; each experiment's antibodies will be listed in the appropriate chapter.

For culture-expanded cells, a minimum of 500,000 viable cells/tube were pelleted at 400*xg* for 5 minutes, whilst cells straight from digestion had a minimum of 3,000,000 cells/tube pelleted using the same conditions as culture-expanded cells.

The supernatant was discarded, and cells were then resuspended in 50µl of FACS block and incubated at room temperature for 15 minutes. After this incubation, the appropriate antibodies were added to each tube and subsequently incubated at room temperature in the dark for 15 minutes. At the end of the incubation, cells were washed with 500µl of FACS buffer, before being centrifuged for 5 minutes at 400xg. Cells were resuspended in 500µl of FACS buffer and had 5µl of 7-Aminoactinomycin-D (7-AAD) added. Any tubes that had cells from digestion were then filtered through a 70µm cell strainer to remove any larger non-cellular bodies that might interfere with the cytometer. Tubes were stored on ice in the dark until they were run through a Cytoflex S cytometer (Beckham Coulter).

Intact cellular bodies were selected based upon their forward and side scatter profiles combined with doublet discrimination, with dead cells excluded based

on their uptake of 7-AAD. Data were analysed and compensated on CytExpert V2.3 software package (Beckham Coulter).

2.5 – Gene expression

Genes are the backbone of all genetic information relating to an individual. The measurement of their expression has long been used to identify how different pathways or genes are expressed in relation to disease and cellular processes such as MSC differentiation. To understand which pathways or proteins are expressed over the course of MSC differentiation and how they may be affected by cytokine stimulation, gene expression experiments were carried out.

2.5.1 – Principle

In its simplest form polymerase chain reaction (PCR) is defined as a chain reaction that exponentially increases DNA quantity. This occurs via the use of the enzyme polymerase, primers, DNA template and nucleotides. This technique, however, is only qualitative and has other limitations including, the numbers of samples that can be run at any time and that detection of the amplified product is only seen after all cycles have ended.

A more quantitative development of PCR is quantitative PCR (qPCR), which provides several advantages. Whilst PCR can only be detected at the end of all the cycles, in qPCR the use of fluorescently labelled probes allows for quantification at every step of the reaction. In this thesis, TaqMan probes are used. These probes have a fluorophore that is not active at the beginning of the reaction due to a quencher attachment. The fluorophore is located at the 5' end whilst the quencher is at the 3' end (FAM-MGB respectively). Over the course of the reaction the fluorochrome is separated from the quencher by Taq DNA polymerase. The separation from the quencher activates the fluorophore; this allows for its fluorescence to be tracked in an amplification dependent manner providing the amplification curve. This technique also allows for larger numbers of samples to be run, making qPCR the preferred technique when investigating gene expression (as opposed to normal PCR).

qPCR acts as an indirect measurement of RNA via its conversion to cDNA as required for the procedure.

2.5.2 – Fluidigm and integrated fluid circuits (IFC)

Whilst qPCR is useful when looking for known genes of interest in a targeted pathway, of many of the downstream targets from certain inflammatory stimuli during differentiation are unknown. The use of a methodology that allowed for high quality and consistent outputs for a wide range of genes from potentially small cDNA samples was important. The use of integrated fluid circuits (IFC) chip technology met these requirements. IFC uses the principles of microfluidics and is based on qPCR principles but are further miniaturised whilst also integrating the liquid handling components on a single chip. These chips contain networks of minuscule diameter fluid lines (10^{-6}m), small volume chambers (10^{-9}l) and Nanoflex^{TM} valves that allow the chip to withstand high pressures (175mmHg) (364). Importantly these chips only require small volumes of samples and TaqMan primers to carry out a very high number of reactions.

For this work a 48.48 chip was used, which allowed for up to 2304 reactions to be carried out per chip. These chips allowed 47 genes of interest plus a housekeeping gene to be interrogated on up 48 samples. They were used primarily to investigate how IL-17A influences osteogenesis (Chapter 4) and adipogenesis (Chapter 4) over the course of a differentiation experiment.

2.5.3 – RNA extraction

Before any genomic work was performed, the bench areas were wiped with RNAse AWAY^{TM} (ThermoFisher) to minimise potential RNA contamination from the environment. RNA extraction was performed using Norgen Total RNA Purification Kit. The purification of RNA in this kit is based on spin column chromatography without the use of phenol or chloroform.

After differentiation, the cells in a monolayer had the differentiation media aspirated and were washed with PBS. 350µL of Buffer RL was then added directly to the culture plate. This was allowed to incubate for 5 minutes at room temperature with constant gentle agitation to lyse the cells. This lysate was transferred into labelled Eppendorfs and then had 200µL of 100% ethanol

added and vortexed to mix well. These lysates could then be frozen at -80ºC until all lysates were ready for further extraction.

This lysate is then added to the column which was inserted into a collection tube and subsequently bound by centrifuging at *3500xg* for 1 minute. The flowthrough in the collection tube was then discarded. After this stage, any leftover genomic DNA contamination is removed via on-column DNAse treatment. Norgen's RNase-Free DNase I Kit was used for this. Each column had 100µL of Enzyme Incubation Buffer A and 15µL of DNAse I added. Columns were then centrifuged at 14000*xg* for 1 minute, at the end of this the flowthrough was discarded.

The columns then had 3 washes to thoroughly remove any nonbound containments, 400µL of Wash Solution A was added to each column and centrifuged at 14000*xg* for 1 minute and the flowthrough was discarded. After the final wash, the columns were centrifuged for a further 2 minutes at 14000*xg* to dry the resin thoroughly.

The dried columns were then transferred into fresh elution tubes. Each column had 50µL of Elution Solution A added to the column. Columns were then centrifuged for 2 minutes at 200*xg*, followed by 2 minutes at 14000*xg*. The elution tubes were then frozen at -80ºC until reverse transcription was performed.

2.5.4 – Reverse transcription for cDNA

Reverse transcription of cDNA from RNA was performed using a kit from Norgen in a programmed thermocycler. The reverse transcription master mix (Fluidigm) contained a mix of deoxyribonucleotide triphosphate, oligo-dTs, random primers, RNAse inhibitors and reverse transcriptase. Due to subsequent pre-amplification steps in using the Fluidigm system, RNA extracted from the previous step was analysed using a NanoDrop-1000 to record RNA concentration and purity based on 260/280 and 260/230 ratios for each sample. For reverse transcription a target range of 50-60ng of RNA was used per reaction; therefore the 5µl reaction contained 1µl of reverse transcription master mix and a 4µl mixture of RNA and nuclease-free water. For example, if a sample had an RNA concentration of 25ng/µl, then for

reverse transcription its reaction would contain 1µl reverse transcription master mix, 2µl of RNA and 2µl of nuclease-free water.

The reverse transcription master mix, RNA and nuclease-free water mix were added to individual wells, the plates were then sealed, vortexed and centrifuged before being placed into the thermocycler. The reverse transcription reaction was conducted using the following parameters: 5 minutes at 25°C, 30 minutes at 42°C, 5 minutes at 85°C and then were held at 4°C. The generated cDNA was stored at -20°C until future use.

2.5.5 – Pre-amplification

For pre-amplification (PA) a mixture of all the selected 48 TaqMan probes (listed in the relevant chapter) was diluted in tris-ethylenediaminetetraacetic acid (TE) buffer to a final concentration of 0.2x. This mix then had 1.25µl added per well of a 96-well PCR plate, which was supplemented with 1.5µl nuclease-free water, 1µl PA master mix (Fluidigm) and 1.25µl of cDNA generated earlier. This gave a total reaction volume of 5µl/well. Samples were then vortexed to mix and centrifuged before being put into the thermocycler to undergo PA. All samples underwent 14 PA cycles using the following settings: 2 minutes at 95°C, denaturing at 15 seconds at 95°C, annealing at 60°C for 4 minutes (the last two steps acting as the 14 cycles) before being held at 4°C. After PA, all samples were diluted 1:5 by the addition of 20µl of TE/well. Samples were then stored at -20°C until qPCR.

2.5.6 – qPCR

The Fluidigm 48.48 IFC chip is single-use and requires priming before it can be loaded with samples and run. In order to prime the chip 150µl of control line fluid (Fluidigm) is carefully added into the two accumulator regions (Figure 2.2). The chip is then loaded into a Fluidigm MX Loader which then runs a 12-minute priming script.

After completion of this script the chip was loaded with assays and samples (Figure 2.2). For the assays, each Taqman 3µl was added to 3µl of assay loading reagent (Fluidigm), from this 6µl mixture 5µl was added carefully to the appropriate well on the chip taking care to avoid any air bubbles which

could block the fluid lines. For the samples 3µl of Taqman universal master mix and 0.3µl of GE sample loading reagent was added to 2.7µl of the PA diluted cDNA from the previous step to give a 6µl mix from which 5µl was added to the appropriate well on the chip. After all the samples and assays were loaded onto the chip, the chip was placed back into the Fluidigm MX Loader to run a 1-hour load & mix script before being transferred into the BioMark^{TM} HD System.

The qPCR run was managed by the Data Collection software associated with the BioMark^{TM} HD System. The pre-determined script ran a GE 48x48 Standard v1 protocol, which contained 40 PCR cycles for around 1.5 hours.
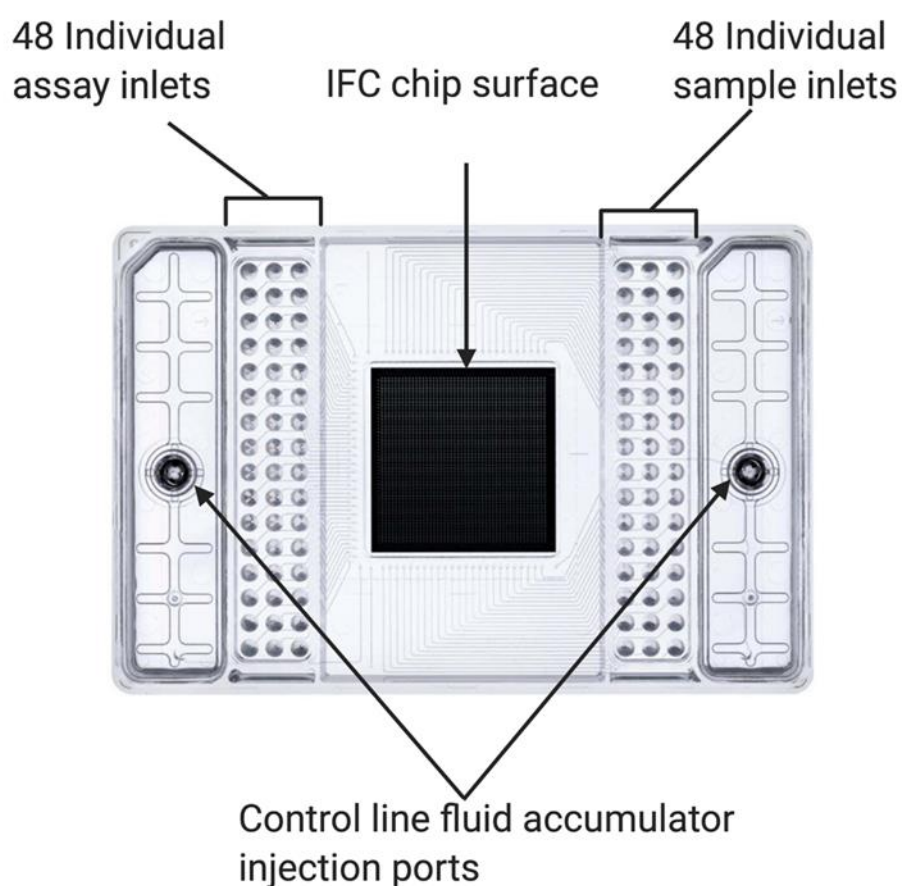
Figure 2.2: Image of a Fluidigm 48.48 IFC gene expression chip

2.5.7 – Data analysis

Following completion of the run, the data was analysed using Fluidigm Real-Time PCR Analysis software. This allowed for the generation of the cycle threshold (CT) value for each gene, and the exclusion of any genes that did not meet the expression threshold. All genes were normalised to the expression of a housekeeping gene was *hypoxanthine-guanine phosphoribosyltransferase 1 (HPRT1)*, which produced the ΔCT values. Normalisation occurred via the use of this equation

$$\Delta CT = CT \text{ target gene} - CT \text{ housekeeping gene}$$

This data was then exported into Microsoft Excel for further analysis. In order to determine relative expression ΔCT values were put into the equation: $2^{-\Delta CT}$. Hierarchal clustering was worked out by exporting relative expression values into Cluster 3.0 software. Relative expression values for genes with less than 80% expression across all samples were excluded first. The remaining data was then Log transformed with both the genes and arrays being centred on their means. Finally, the arrays were analysed using Spearman Rank Correlation, which produced a final .cdt file that was exported into Java TreeView V1.1.6r4, which produced the heatmaps of hierarchal clustering.

The genes that showed a high degree of clustering, were further analysed to investigate for any significant differences in expression, using the ΔΔCT methodology (365). This was performed by normalising gene expression changes to a control sample which in this work was an undifferentiated MSC: $\Delta\Delta CT = \Delta CT_{Sample} - \Delta CT_{Undifferentiated\ MSC}$. Once the ΔΔCT value was obtained, relative expression was worked out using $2^{-\Delta\Delta CT}$. These values could then be further analysed for any significant differences.

2.6 – Histology

Some patient samples that showed several spinous process segments with connecting intra-spinous ligament were selected to be used for histology to gain a clearer view of the micro-environment at the spinal enthesis (Figure 2.1).

2.6.1 – Tissue preparation

2.6.1.1 – Fixation

To preserve tissue integrity and stop autolysis of the samples, which could occur over the decalcification process, samples were fixed thoroughly. Upon receipt samples were washed twice in PBS to wash out any red blood cells or other circulating immune cells, which could disrupt downstream staining. After the wash samples were immediately fixed in a 10% neutral buffered formalin solution. Samples were allowed to fix for 48 hours. After this period the samples were removed and washed three additional times with PBS to remove any residual fixative before decalcification.

2.6.1.2 – Decalcification

Due to the mineralised nature of bone being impossible to section without damaging the tissue, decalcification was performed to remove the mineral content whilst preserving the microscopic tissue structure. Slow decalcification was performed using 0.5M EDTA. This methodology is slow but causes little tissue damage compared to other faster methods utilising stronger acids (366). The decalcification of mineralised bone is achieved by chelating calcium from the bone and is seen to be pH dependent. The equation best demonstrates this:

$$Ca_{10}(PO_4)_6(OH)_2 + 8H^+ \leftrightarrow 10Ca^{2+} + 6PO_4{}^{2-} + 2H_2O$$
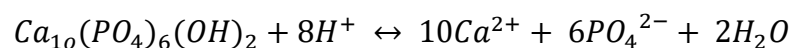
Decalcification gradually moves the calcium from the tissue into the surrounding liquid. The solution was changed every week to avoid reaction equilibrium allowing for continual progressive decalcification. To prevent tissue damage associated with over decalcification, especially in the intra-spinous ligament where maceration may occur. From the second week and every subsequent week, decalcification samples were X-rayed to look for decalcification progression. The X-ray machine used was a CS2200 (Carestream Health) with an exposure time of 0.113s at 70kV, with images captured on standard dental films read on the automated unit. Transparency of samples after X-ray was used as an indication of sufficient decalcification.

2.6.1.3 – Paraffin embedding and sectioning

Following decalcification, larger samples were cut using a scalpel into sizes that would fit into a plastic cassette (Figure 2.3). Decalcified samples were then processed for paraffin embedding, which involved a 10% neutral buffered formalin (30-minutes) through graded ethanol:

1. 70% ethanol for 1 hour
2. 90% ethanol for 1 hour
3. 95% ethanol for 1 hour
4. 100% ethanol for 1 hour
5. 100% ethanol for 2 hours
6. 100% ethanol for 2.5 hours

Then into 3 separate xylene buckets for 2x 1 hour and 1.5 hours respectively and finally into 2 buckets of molten paraffin wax for 4 and 5 hours respectively. Embedding into the paraffin blocks was performed in a Leica embedding centre using a hot paraffin dispenser and hot plate. Before the molten wax was poured into the cassettes, samples were oriented in the coronal plane (Figure 2.3). Once the wax hardens, this allows for the samples to be easily sectioned.

A Leica RM2234 microtome (Leica Microsystems) using an S+ type blade was used to section paraffin blocks. Due to wax covering the tissue sample, blocks were initially sectioned at a thickness of 10μm until the tissue was exposed. The tissue was sectioned at a thickness of 5μm, and sectioned samples were allowed to stretch and smooth out any creases by flotation in a 45ºC water bath. Samples were then lifted out onto SuperFrost Plus glass slides. Any residual water was dried from the slides by incubation overnight at 37ºC.
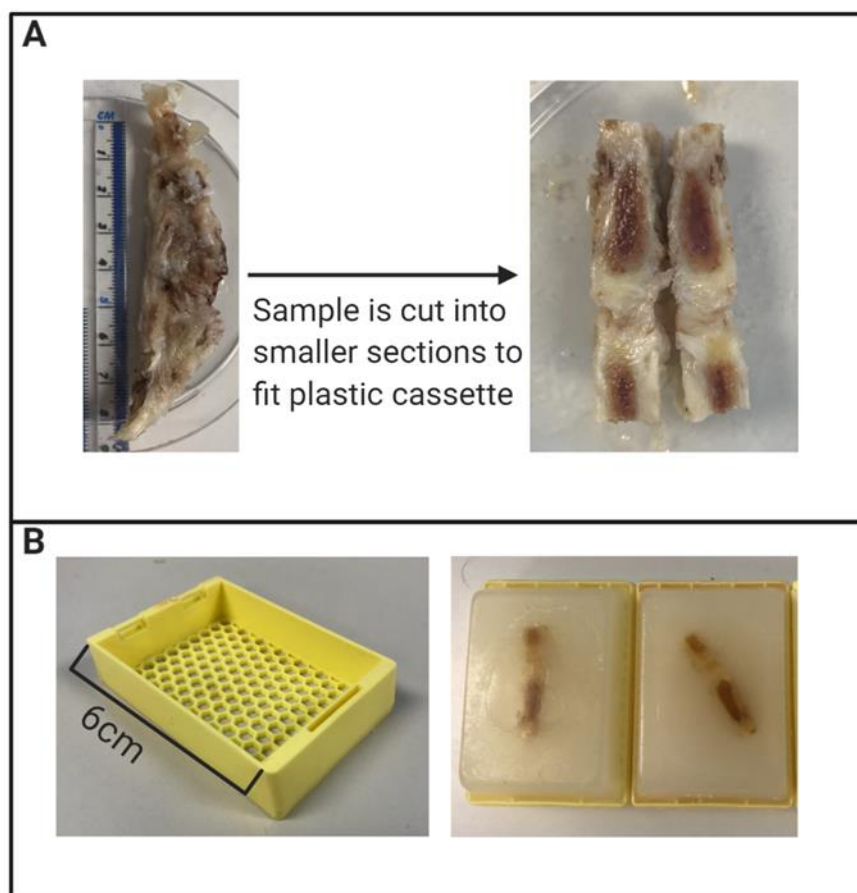
Figure 2.3: Sample preparation for histology
A) Fixed and decalcified samples were cut using a scalpel into sizes that would fit inside the plastic cassettes (B). Samples were mounted in the coronal plane to best see the tissue anatomy for staining (B).

2.6.2 – Haematoxylin and Eosin

For over a century, Haematoxylin and Eosin (H&E) have been used to identify a wide array of tissue types. The stain consists of two components: the haematoxylin stains cell nuclei a deep blue-purple colour through staining of the nucleic acids (367, 368). All extra-cellular matrix is stained non-specifically

a pink colour with Eosin, though, in areas of high proteoglycan content, this can have an element of a blue colour present (368). This makes H&E staining perfectly useful for discerning subtle variations in tissue composition such as those seen at the enthesis, where ligament transitions to fibrocartilage and subsequently into cortical bone.

Slides selected for Haematoxylin and Eosin were deparaffinised by standing the slides on a hot plate at 70ºC for 20 minutes. Residual paraffin was cleared by immersion in Xylene (3x 5 minutes). Tissue was then rehydrated by immersion in graded ethanol:

1. 100% ethanol 3x 3 minutes
2. 75% ethanol 1x 3 minutes
3. 50% ethanol 1x 3 minutes
4. Tap water 1x 2 minutes

After rehydration, slides were immersed in Harris' Haematoxylin for 2-minutes after which any no bound stain was cleared by immersion in tap water for 1-minute. The 'blueing' of the nuclei was performed by immersing the slides in Scott's tap water for 2-minutes, before washing in running tap water for 1-minute followed by immediate immersion in Eosin-Y for a further 2-minutes. After this incubation, any non-bound stain was removed by washing in tap water for 1-minute. The slides were then dehydrated using graded ethanol in an inverse protocol to the hydration of slides, and finally, slides were cleared using Xylene. The slides were then mounted using DPX medium and allowed to dry overnight at room temperature (RT) before imaging.

2.6.3 – Masson's trichrome

Masson's trichrome, as the name suggests produces three different coloured stains. Nuclei are stained black, with mature bone staining red and collagen fibres (ligaments), regenerated bone or osteoids staining blue (369). The nuclei are stained by Weigert's iron haematoxylin, which is resistant to degradation by subsequent acidic staining solutions. The acidophilic elements of the tissue, such as collagen, are stained bright red by Ponceau Fuchsin solution (370). The subsequent addition of phosphotungstic acid causes this bright red colour to be diffused out of the ligamentous tissue but leaves the

mature bone stained red (371). The ligamentous tissue is then stained with methylene blue to create the counterstain and the trichrome characteristic of Masson's trichrome staining. Masson's trichrome was used to provide an insight into any micro-damage or bone remodelling present at the site of the spinal enthesis.

Selected slides for Masson's trichrome staining were dewaxed and rehydrated in the same way as described in 2.6.2. After slides were rehydrated, they were immersed in Wiegert's iron haematoxylin for 10-minutes. They were then placed in 1% acid-alcohol for 15-seconds before being immersed in running tap water for 1-minute. This was followed by immersion in Ponceau fuchsin for 5-minutes, with a subsequent 1-minute wash in running tap water. Slides were subsequently placed into phosphotungstic acid for 15-minutes, before a final wash in running tap water for 1-minute. Finally, slides were stained using methyl blue for 1-minute before being dehydrated and mounted as described in 2.6.2.

2.6.4 – Imaging

Slides were scanned on a Leica Aperio AT2 at an original magnification of x20 and images were captured using its software Aperio Imagescope (Leica). Areas of interest around the entheseal insertion site at the spinous process were imaged at an appropriate magnification to look for potential channels of communication between the spinous process and the intra-spinous ligament.

2.7 – Statistical analysis

All data were analysed for statistical significance using IBM SPSS Statistics 26 software package. Data were assessed for normality using a Shapiro-Wilks Test. Any data that was found to be normally distributed underwent subsequent parametric testing, whilst those that were found to be not normally distributed ($p < 0.05$) were further analysed using non-parametric equivalent tests. The tests used for each experiment are specified in the respective chapters. For all data, *p-value* of <0.05 was considered significant (*$p < 0.05$, **$p < 0.01$, ***$p < 0.001$ and ****$p < 0.0001$).

Chapter 3 – Characterisation of MSCs at the human spinal enthesis

3.1 – Introduction

Mesenchymal stem/stromal cells (MSCs) were initially characterised in the bone marrow of guinea pigs in 1970 (347). These cells were initially defined as a high proliferative population of plastic adherent cells, that formed colonies on plastic dishes (347). Since this initial classification MSCs have been identified in almost every post-natal tissue in the human body (348, 349). They are capable of differentiating under the appropriate conditions into bone, fat and cartilage lineages (359). Interestingly they are also known to be capable of some immunomodulation (372), this combined with their tri-lineage potential gives them an important role in both normal tissue repair and in disease (20).

For a population of cells to be definable as MSCs they must meet the minimum criteria as set forth by the International Society for Cellular Therapy (ISCT). Cells must be plastic adherent when under normal culture conditions, and tri-lineage differentiation capable (being adipogenesis, chondrogenesis and osteogenesis). Finally, they must also display the appropriate surface markers. Positive (≥95%) expression for cluster of differentiation (CD) markers 73, 90 and 105. At the same time as being negative (≤2%) in expression for markers associated with haemopoietic cell lineages these being; CD14 (myeloid lineage marker), CD19 (B cell marker), CD34 (haematopoietic stem cell marker), CD45 (pan-leukocyte marker) and Human Leukocyte Antigen – DR isotype (HLA-DR, seen on antigen-presenting cells) (359).

However, since these initial criteria were established, it has been recognised that CD34 - depending on tissue origin and other factors - may not be a good negative marker for MSCs. Some adipose tissue-derived MSCs *in* vivo display a low expression of CD34 (373-375), this negative expression requirement for CD34 is likely due to *in vitro* expansion conditions altering surface marker expressions. Similarly, HLA-DR expression on MSCs is upregulated by stimulation with interferon-γ (IFN-γ) (376, 377).

3.1.1 – Identification of CD271+ MSCs

The expression of CD73, CD90 and CD105 are stable on MSCs in both *in vivo* and *in vitro* conditions; they are not specific markers for MSCs and are displayed on other cell types. For example, positive expression for CD73, CD90 and CD105 is seen on dermal fibroblasts isolated from the foreskin (378), and populations of endothelial progenitor cells display CD73 and CD105 (379). With populations of CD90, in particular, seen in the bone marrow and ligamentous tissue (380) which are not MSCs, the need for more specific markers to truly isolate MSC populations can be seen.

One candidate molecule to be explored is CD271 or low-affinity nerve growth factor receptor (LNGFR), which is part of the tumour necrosis factor superfamily (381). The PEB consists primarily of bone marrow and CD271+ MSCs are seen to be specific to bone marrow; expression is also seen on bone lining cells (382-385). Importantly - unlike CD73, CD90 and CD105 - CD271 is not displayed on fibroblasts (386). The CD271+CD45$^{lo/-}$ MSC phenotype also meets all of the criteria defined by the ISCT, being positive for CD73, CD90, CD105, plastic adherent and tri-lineage differentiation capable (382, 387, 388).

3.1.2 – Functional differences in MSC populations

Differentiation of MSCs is broadly a two-step process, lineage commitment or the differentiation into lineage progenitor cells and then their subsequent maturation into mature differentiated cells. These differentiation pathways are regulated by several key pathways, some of which act across numerous differentiation routes. These pathways are covered in more detail in later chapters.

Osteogenesis and adipogenesis are the two most relevant differentiation pathways when relating to AS, with adipogenesis associated with the early formation of fatty tissues at the enthesis preceding new bone formation at these sites (21, 58, 389). The master regulators of osteogenesis and adipogenesis are runt-related transcription factor 2 (RUNX2) (390) and peroxisome proliferator-activated receptor γ (PPARγ) (391). Respectively

these two transcription factors also suppress each other's actions when undergoing differentiation (392, 393).

MSCs are known to display a preference for differentiating down specific lineages based on their tissue origin (394-396). Adipose tissue-derived MSCs have a significantly higher adipogenic potential than MSC populations isolated from the bone marrow (397). The converse is true regarding osteogenesis with bone marrow-derived MSCs having higher osteogenic and chondrogenic potential (397, 398). The difference in the chondrogenesis is likely due to the evidence that chondrogenesis and osteogenesis follow a similar differentiation pathway (399). After the stimulus to differentiate is applied to MSCs if heading down an osteogenesis or chondrogenesis lineage single-cell RNAseq shows that they share commonly upregulated genes such as SP7 or osterix, which is not seen in adipogenic lineages (400). However, despite the evidence that tissue residency plays an important role in determining the differentiation ability of MSCs recent work shows that adipogenesis requires significantly more histone and transcriptional changes than osteogenesis, regardless of the MSC tissue origin and that as a result MSCs prefer to head down osteogenic lineages (401). This appears to go against what is seen with comparisons between MSCs populations showing different differentiation potentials.

3.1.3 – Hypotheses

This chapter of work aimed to investigate three main hypotheses:

1. Two populations of MSCs exist at the human enthesis, one in the PEB and one in the EST
2. These populations will have distinct functional differences depending on their tissue origin, with PEB MSCs being more osteogenic than matched EST MSCs
3. A population of CD271+ MSCs exists at the human spinal enthesis, at least in the PEB fragment.

3.2 – Materials and methods

3.2.1 – Enumeration of MSCs by colony forming unit fibroblast (CFU-F) assay

Following tissue digestion (section 2.2), fresh cells from PEB and EST (both n=17) had 10,000 viable cells seeded onto 10mm plastic petri dishes (in duplicate) containing 15ml of StemMACS MSC expansion media supplemented with 1% Penicillin-Streptomycin. After 48-hours dishes had all the media aspirated and were washed with PBS to remove any non-adherent cells, before having 15ml of fresh StemMACS media applied. Half media changes were performed every 3-days for the duration of the time in culture. Dishes were cultured for 14-days in a humidified incubator at 37ºC and 5% CO_2.

On the 14th day in culture, dishes had all media removed and were washed twice with PBS before being fixed for 15-minutes in a 3.7% formaldehyde solution. After fixation dishes were washed with PBS before being stained in a 1% methylene blue in borate buffer solution for 30-minutes at room temperature (RT). After staining dishes were washed with PBS until the PBS ran clear, dishes were subsequently allowed to air-dry overnight.

Dishes were scanned at 1200dpi resolution using an Epson 3590 flatbed scanner and colonies were manually counted using ImageJ software V1.8.0_112. Colonies were only counted if greater than 50 cells were present. The percentage of MSCs from each digest was calculated using the equation:

$$\%MSCs = \frac{Number\ of\ Colonies}{10,000} \times 100.$$

3.2.1.1 – Colony density and size

Variations in colony size of MSC populations are seen within bone marrow-derived MSCs indicating heterogeneity within the populations of the MSCs (385, 402, 403). To explore whether such heterogeneity exists within the MSCs from either the PEB or EST colony density and size was investigated. To work out how dense colonies of cells were after their time in culture PEB (n=7) and EST (n=7) samples that had at least 15 colonies per dish were scanned (as above in 3.2.1) and converted into an 8-bit grayscale image using

ImageJ. An 8-bit grayscale image is an image where each pixel of an image is assigned a luminance value from 0-256, which in grayscale equates to 256 representing black and 0 representing white. In terms of colony density after the image has been converted into 8-bit grayscale, areas of more stained (denser) colonies will have a richer colour and subsequently have a higher grayscale value. Converted images then have their colonies manually circled using the software and the mean of the grayscale density of all the colonies was recorded along with the standard deviation of all the colonies (402).

For the colony size, the images had their colonies circled one at a time and the area which the colony covered was recorded using ImageJ. This was repeated across a minimum of 15 colonies per dish for the seven selected samples.

3.2.2 – Flow cytometry

Culture expanded MSCs (<p3, n=3 for both PEB and EST) were assessed for the expression of the positive MSC markers: CD73, CD90 and CD105 whilst being negative for immune cell lineage markers (359). Cells were stained using the methodology explained in section 2.4, using the antibodies listed in Table 3.1. Three samples of PEB and EST had a minimum of 500,000 MSCs divided into 6 tubes after they were incubated in FACs block as described in section 2.4. Tubes were labelled for their contents:

   I.   CD45-V450, HLA-DR-FITC, CD34-PE, 7-AAD
  II.   CD19-FITC, CD14-VioGreen, CD73-PE, 7-AAD
 III.   CD90-FITC, IgG1-PE, IgG1-V450, 7-AAD
  IV.   CD105-PE, IgG1-FITC, IgG1-VioGreen, 7-AAD
   V.   Unstained control, 7-AAD
  VI.   Unstained control

Compensation was performed using compensation beads utilising the selected antibodies on each fluorophore. Data were analysed as described in section 2.4.

Surface Marker-Conjugate:	Volume Used (µl):	Clone:	Laser (nm):	Emission$_{max}$ (nm):	Company:	Isotype:
CD14-VioGreen	1	REA599	405	520	Miltenyi Biotec	Mouse IgG1
CD19-FITC	2.5	HIB19	488	520	BD Biosciences	Mouse IgG1
CD34-PE	10	563	488	578	BD Biosciences	Mouse IgG1
CD45-V450	2.5	HI30	405	448	BD Biosciences	Mouse IgG1
CD73-PE	1	AD2	488	578	Miltenyi Biotec	Mouse IgG1
CD90-FITC	2.5	F15-42-1	488	518	Bio-rad Laboratories	Mouse IgG1
CD105-PE	5	REA794	488	578	Miltenyi Biotec	Mouse IgG1
HLA-DR-FITC	10	L243	488	520	BD Biosciences	Mouse IgG1
Mouse IgG1-PE	10	MOPC-21	488	578	BD Biosciences	N/A
Mouse IgG1-FITC	5	IS5-21F5	488	520	Miltenyi Biotec	N/A
Mouse IgG1-VioGreen	5	IS5-21F5	405	520	Miltenyi Biotec	N/A
Mouse IgG1-V450	10	X40	405	448	BD Biosciences	N/A
7-AAD	5	N/A	488	647	BD Biosciences	N/A

Table 3.1: Table of antibodies used in ISCT flow cytometry

3.2.2.1 – Analysis of expression of CD271+ MSCs

The population of uncultured bone marrow-derived MSCs have previously been described as CD271+CD45$^{low/-}$ (382, 384, 388). As a result, PEB and EST digests with high viable cell counts (>1x10^6 for EST digests) were selected for flow cytometry to investigate the presence of CD271+ MSCs at the human spinal enthesis.

The enzymatic digestion process can stress the cells. There will also be a number of dead cells which will have a tendency to clump together. This clumping of dead cells can interfere with the staining and fluorescent characteristics of cells undergoing flow cytometry. To minimise any interference from such clumping after enzymatic digestion (section 2.2) 40units/ml of DNAse I was added to the digests, before being pelleted at 500xg for 10-minutes at RT. After this, cells were resuspended into FACS block as described in section 2.4.3 and were stained as described using the antibodies listed in

Table 3.2 in the following tube setups:

I.   Unstained Cells
II.   7-AAD only
III. Isotype controls
IV.   CD73-PE, CD45-V450, CD271-PE-Vio770, 7-AAD
V.   CD90-APC, CD45-V450, CD271-PE-Vio770, 7-AAD
VI.   CD105-FITC, CD45-V450, CD271-PE-Vio770, 7-AAD

Before being investigated in the Cytoflex S cytometer (Beckham Coulter), stained cells were passed through a 70μm cell strainer to minimise any debris or clumping cells that would interfere with readings.

Surface Marker-Conjugate:	Volume Used (µl):	Clone:	Laser (nm):	Emission$_{max}$ (nm):	Company:	Isotype:
CD45-V450	15	HI30	405	448	BD Biosciences	Mouse IgG1
CD73-PE	7.5	AD2	488	578	Miltenyi Biotec	Mouse IgG1
CD90-APC	7.5	5E10	633	660	BD Biosciences	Mouse IgG1
CD105-FITC	7.5	43A4E1	488	520	Miltenyi Biotec	Mouse IgG1
CD271-PE-Vio770	30	ME20.4-1.H4	488	775	Miltenyi Biotec	Mouse IgG1
Mouse IgG1-V450	10	X40	405	448	BD Biosciences	N/A
Mouse IgG1-PE	10	MOPC-21	488	578	BD Biosciences	N/A
Mouse IgG1-APC	10	IS5-21F5	633	660	Miltenyi Biotec	N/A
Mouse IgG1-FITC	10	IS5-21F5	488	520	Miltenyi Biotec	N/A
Mouse IgG1-PE-Vio770	10	IS5-21F5	488	775	Miltenyi Biotec	N/A
7-AAD	10	N/A	488	647	BD Biosciences	N/A

Table 3.2: Antibodies used for CD271 flow cytometry phenotyping

3.2.3 – Adipogenesis

The adipogenic potential of cells from both the PEB and EST (both n=11) was assessed using Oil Red O staining after adipogenesis in differentiation media. Culture expanded cells <P3 were seeded at a density of 50,000 cells/well (in duplicate) in 24-well plastic culture plates and were cultured in an adipogenic differentiation media. This adipogenic media has been used extensively by prior studies (384, 404, 405) and contained: DMEM, 10% FCS, 10% horse serum, 0.5mM isobutylmethylxanthine, 60µM indomethacin and 0.5mM hydrocortisone. Control wells were seeded at the same density and into the same 24-well plastic culture plates but were cultured using DMEM with 10% FCS only. Plates were incubated at 37°C and 5% CO_2 for 3 weeks with half media changes every 3 days.

On the 21st day after initiation of adipogenesis cells were stained using an Oil Red O solution. A stock solution of 0.5% Oil Red O in isopropanol was first prepared. This solution was then incubated in a water bath at 37°C for at least 30 minutes. After incubation the solution was further diluted with 3 parts Oil Red O solution to 2 parts deionised water. This was then filtered through a 0.8µm filter then a 0.22µm filter.

Prior to staining with the diluted Oil Red O solution wells had all their media aspirated and were gently washed twice with PBS. Wells were then fixed with 10% formalin for ten minutes at room temperature. At the end of incubation, the formalin was removed, and the wells had two more washes with PBS. The filtered Oil Red O solution was then added and allowed to stain any lipid vesicles for 30 minutes, at the end of the staining cells were washed with PBS to remove and excess Oil Red O. Stained wells were stored in 1ml of PBS to prevent drying out and rupture of stained vesicles. An Olympus CKX41 light microscope with an Olympus C-7070 camera attachment was used to take images at 3 locations of each well. ImageJ software was used to analyse Oil Red O stained area, hence quantifying adipogenesis (406).

3.2.4 – Chondrogenesis

The chondrogenic potential of MSC was assessed by culturing 250,000 cells (in triplicate) for both PEB (n=4) and EST (n=4) in a chondrogenic media for 3 weeks at 37°C and 5% CO_2 with half media changes three times per week.

MSCs were pelleted in Eppendorf tubes by centrifuging at 650xg for 5 minutes. After this they were cultured in chondrogenic media. The chondrogenic media (CM) consisted of high glucose DMEM, antibiotics, 40 µg/ml L-proline, 1.5 mg/ml bovine serum albumin, 4.7 µg/ml linoleic acid, 1× insulin–transferrin–selenium (ITS), 50 µg/ml L-ascorbic acid-2-phosphate, 100nM dexamethasone and 10 ng/ml TGF-β3. Control MSCs were pelleted into Eppendorf tubes at the same density and were cultured for the same duration except only in DMEM with 10% FCS.

Glycosaminoglycan (GAG) content of the pellets was assessed on the 21st day of differentiation. The CM was carefully aspirated taking care not to disturb the pellet, which was then washed twice gently with PBS. The pellet was then dissolved by the addition of 100µl of 1mg/ml papain and overnight incubation in a water bath at 65°C. The following day the contents were mixed well and frozen at -20°C until GAG content could be assessed.

The GAG content of differentiated MSCs was assessed using the Blyscan™ Glycosaminoglycan Assay (Bicolor Limited) (388). This assay was conducted following the manufacturer's instructions. Briefly, the papain digest solution was thawed and had 1ml of the dye reagent added and was incubated for 30 minutes with vortexing every 5 minutes to ensure thorough mixing. The dye (1,9-dimethylmethylene blue) binds to sulphated glycosaminoglycans (sGAG). After incubation any unbound dye was removed by centrifuging at 12,000 rotations per minute (rpm) for 10 minutes, this pelleted the bound sGAG-dye complex. Any non-bound dye was aspirated from the Eppendorfs leaving the pellet intact. After this 500µl of dissociation reagent was added, and the tubes were vortexed and incubated for ~10 minutes or until all the dye has dissociated. Tubes were then centrifuged at 12,000 rpm for a further 10 minutes to remove any foam. A 96-well plate then had 200µl of the dissociate

dye transferred into each well, which was then placed in a Cytation 5 Imaging Plate Reader (Biotek) with absorbance measured at 656nm.

3.2.5 – Osteogenesis

The osteogenic potential of MSCs was assessed using two qualitative methods (alizarin red and alkaline phosphatase) or a quantitative calcium deposition assay. In triplicate MSCs from both the PEB and EST (both n=11) were cultured in an osteogenic media (OM) containing low glucose DMEM supplemented with 10% FCS, 100nM dexamethasone, 10mM β-glycerophosphate, 0.05mM ascorbic acid and antibiotics (382, 384, 388). Control wells had MSCs seeded at the same density into the same plastic culture plates and were supplemented with DMEM with 10% FCS for their duration in culture. Cells had half media changes twice per week and were cultured at 37°C and 5% CO_2 for the duration of their time in culture.

Wells which were used for alizarin red or alkaline phosphatase staining had 10,000 cells/well seeded into 12-well plastic culture plates. Alizarin red (3.2.5.1) wells were cultured for 3 weeks, whilst alkaline phosphatase (3.2.5.2) were cultured for 2 weeks (405). Calcium deposition assays (3.2.5.3) had 3,000 cells seeded per well in a 48-well plastic culture plate and were cultured for 2 weeks (227).

3.2.5.1 – Alizarin red staining

Prior to staining a 70% ethanol solution was placed in a -20ºC freezer and was allowed to cool overnight. Plates had their media aspirated and the wells were gently washed twice with PBS. After the final PBS wash, wells were fixed for 1 hour using the cold 70% ethanol. After fixation, wells were rinsed once with distilled water, before being stained for 10 minutes using the alizarin red solution at RT. After staining wells were washed three times with PBS to remove any leftover alizarin red solution, plates were allowed to dry overnight before being scanned at 1200dpi resolution using an Epson 3590 flatbed scanner.

3.2.5.2 – Alkaline phosphatase staining

Alkaline phosphatase was performed using Fast blue RR Salt and Naphthol AS-MS phosphate alkaline solution. After differentiation wells had their media gently aspirated and were washed gently twice with PBS. After the final PBS wash wells were fixed using a fixative solution consisting of 3 parts acetone to 2 parts citrate working solution for 30 seconds. After fixation wells were washed twice with deionised water, importantly wells were not allowed to dry during this step. After the final wash the prepared Fast blue dye mixture was added to the wells and allowed to stain for 30 minutes at room temperature in the dark. At the end of the staining, the Fast-blue dye mixture was aspirated, and the wells were washed twice with deionised water. Plates were allowed to dry overnight and stained wells were scanned at 1200dpi resolution using Epson 3590 flatbed scanner.

3.2.5.3 – Calcium deposition assay

The calcium deposited by differentiated MSCs was assessed as a measurement of mineralisation. On the 14th day of differentiation, the osteogenic media was carefully aspirated, and the wells were washed twice with PBS gently, taking care not to disturb the cell monolayer and any deposited calcium. After the final PBS wash, wells were exposed to 100µl of 600mM hydrochloric acid for 4 hours at 4°C with constant gentle agitation. Flat bottom 96-well plates were loaded with 5µl of sample/well (in duplicate), a Sentinel Calcium Kit (Sentinel Diagnostics) was then used to determine calcium content as per manufacturer's instructions. In brief, the kit contains 0.3mmol/l of cresolpthalein complexone, which when in the presence of calcium ions at pH>10 reacts to form a red coloured complex. The intensity of this complex is proportional to the amount of calcium ions in the sample and can be quantified by measuring the absorbance at 600nm in a Cytation 5 Imaging Plate Reader (Biotek).

3.2.6 – Statistical analysis

As described in section 2.7 data were tested for normality using Shapiro-Wilk's Test. All data comparing the differentiation potentials between PEB and EST were analysed using paired tests, either Paired T-Tests for parametric data or

Wilcoxon signed-rank test for non-parametric data. Except for colony area analysis, as individual colonies cannot be directly paired between PEB and EST, data were analysed using a Mann-Whitney U Test.

A linear regression model was used to test if increasing age was associated with the decreased adipogenic potential of MSCs, with a slope being shown to be significantly different from 0, supporting the Mann-Whitney U Test used to compare the two age groups which had differentiation data.

3.3 – Results

3.3.1 – Matched EST has a higher proportion of colony forming cells than PEB

Cells from both PEB and EST digests were shown to be plastic adherent under standard culture conditions. Plastic adherent cells from both PEB and EST digests also formed colonies after 14 days in culture (Figure 3.1).
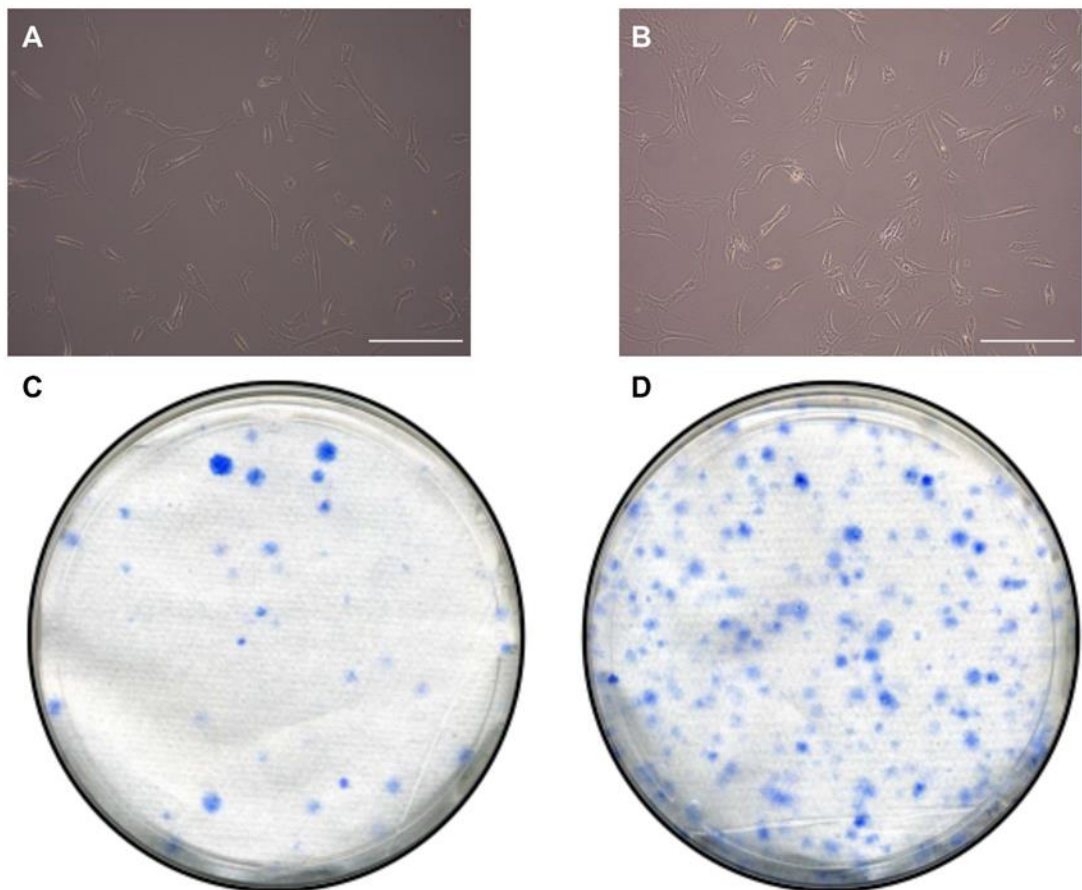
Figure 3.1: Plastic adherent cells form colonies from both PEB and EST digests

Representative images of MSCs 12 days after digestion adhering to plastic culture flasks from both the PEB (A) and EST (B). Representative stained colonies from patient-matched PEB (C) and EST (D) MSCs show greater heterogeneity in colony size in PEB MSCs than EST MSCs. Scale bar = 250μm.

EST digests formed significantly more (7.2-fold) colonies than matched PEB digests ($p<0.001$, Figure 3.2). The significantly higher colony count in EST digests meant, that as a proportion of all viable cells after sample digestion colony forming cells constitute 0.65% (range: 0.02-3.16%), compared to 0.09% (range 0.01-1.53%). Sample age did not correlate with the number of colonies formed per 10,000 viable cells from either PEB or EST.
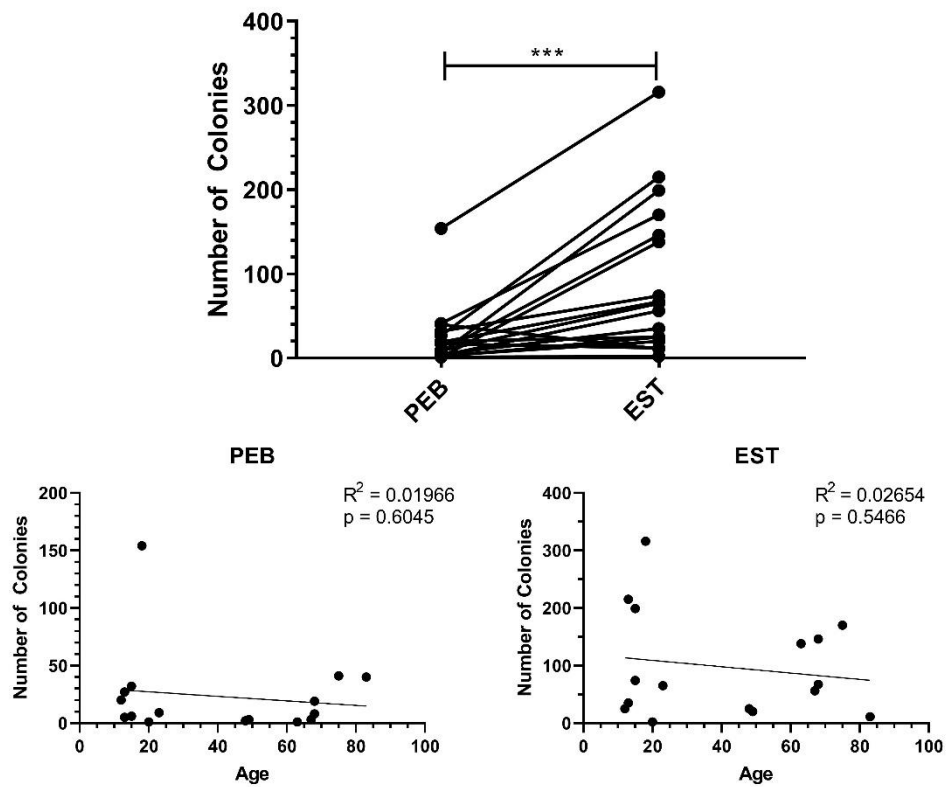
Figure 3.2: EST digests have significantly more colony forming cells than matched PEB

*EST have significantly more colony forming cells than matched PEB. The large range of colonies per 10,000 was not seen to be related to donor sample age. Wilcoxon matched-pairs signed-rank test was used to analyse colonies/10,000 viable cells. *** = p<0.001.*

3.3.1.1 – PEB show significantly larger colonies than matched EST colonies

Over the course of MSC enumeration experiments colonies from PEB displayed a greater heterogeneity in the size of their colonies compared to matched EST. The colonies from PEB were seen to be larger in general, though there was also a larger range of colony sizes. Comparatively, EST colonies were seen to be more numerous, but smaller and more uniform in size across each dish (Figure 3.1).

Indeed, PEB colonies were shown to be nearly 2-fold larger than matched EST colonies (Figure 3.3, p<0.0001). Though not only were they larger, but there was a greater degree of variance in colony sizes in PEB dishes compared to EST dishes. Additionally, PEB colonies have a median area of $11.12\pm89.29mm^2$ compared to EST colonies mean area of $5.41\pm37.49mm^2$, which equates to a 1.98-fold increase for the standard deviation of PEB colony area compared to EST colonies. However, the density of the colonies was not seen to be significantly different between PEB and EST colonies (Figure 3.3).
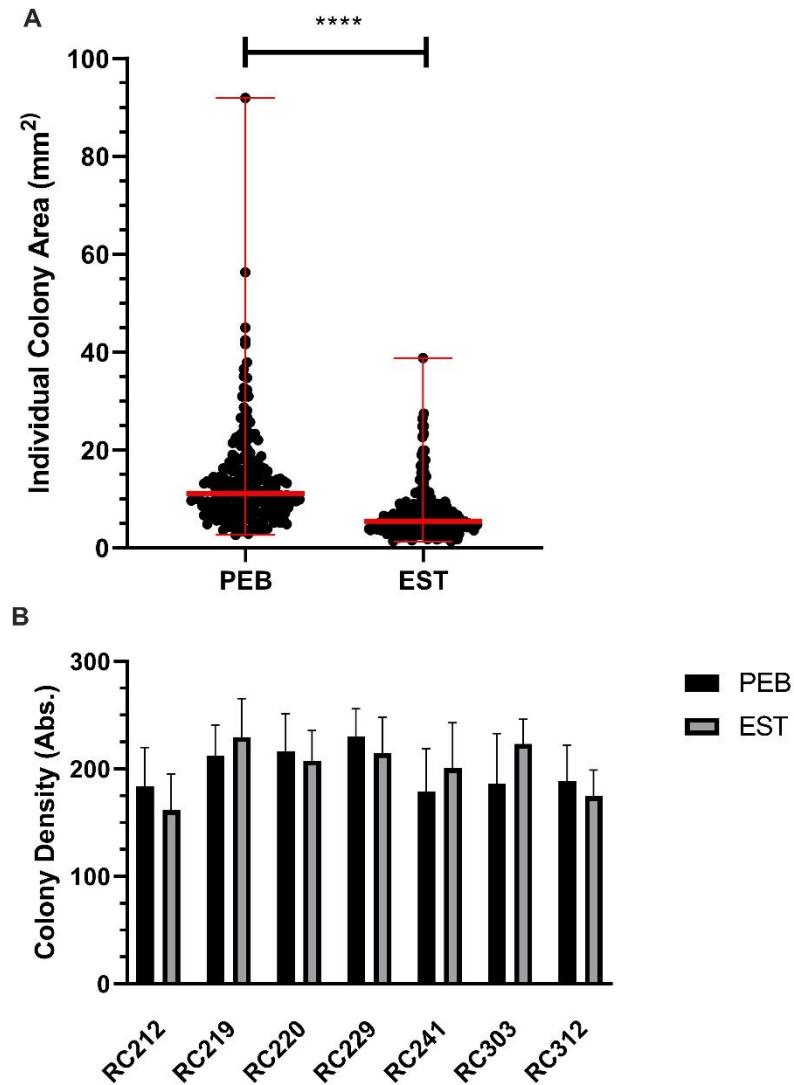
Figure 3.3: PEB MSCs form significantly larger colonies than matched EST

A) Individual colonies of MSCs from the PEB are significantly larger than those from EST sources. There was also a greater degree of variation in colony size for PEB MSCs than those from the EST. B) Colony density between PEB and EST MSCs was not seen to be significantly different with both sources producing colonies of similar density. Mann-Whitney U test was used to compare colony area. **** = p<0.0001. Red lines represent median ± range.

3.3.2 – Culture expanded cells from both PEB and EST display surface markers consistent with MSCs

In accordance with the ISCT minimum criteria for the definition of MSCs, cells had to display the correct surface markers (being positive for CD73, CD90 and CD105 whilst also being negative for haematopoietic lineage markers (359)). After gating out of doublets and dead cells (Figure 3.4), culture-expanded cells (p3) from both the PEB (n=3) and EST (n=3) were seen to display greater than 90% expression for CD73, CD90 and CD105 (EST Figure 3.5, PEB Figure 3.6). Culture expanded EST MSCs showed mean±standard deviation (SD) expression of 98.62%±0.11 for CD73, 93.60%±5.370 for CD90 and 98.45%±0.10 for CD105. PEB MSCs displayed 98.80%±1.76 for CD74, 97.06%±1.76 for CD90 and 98.53%±0.41 for CD105.

Cells from both EST and PEB cultures were negative for expression of CD14, CD19, CD34, CD45 and HLA-DR. However, whilst EST MSCs showed mean±SD expression of: 1.45%±1.03 for CD14, 1.09%±0.95 for CD19, 0.3%±0.3 for CD45 and 1.7%±0.85 for HLA-DR, one sample did show some CD34 expression (Figure 3.5).

Culture expanded MSCs from the PEB had a mean expression of: 0.52%±0.55 for CD14, 0.77%±0.57 for CD19, 0.63%±1.09 for CD34, 0.25%±0.44 for CD45 and 1.00%±1.56 for HLA-DR (Figure 3.6).
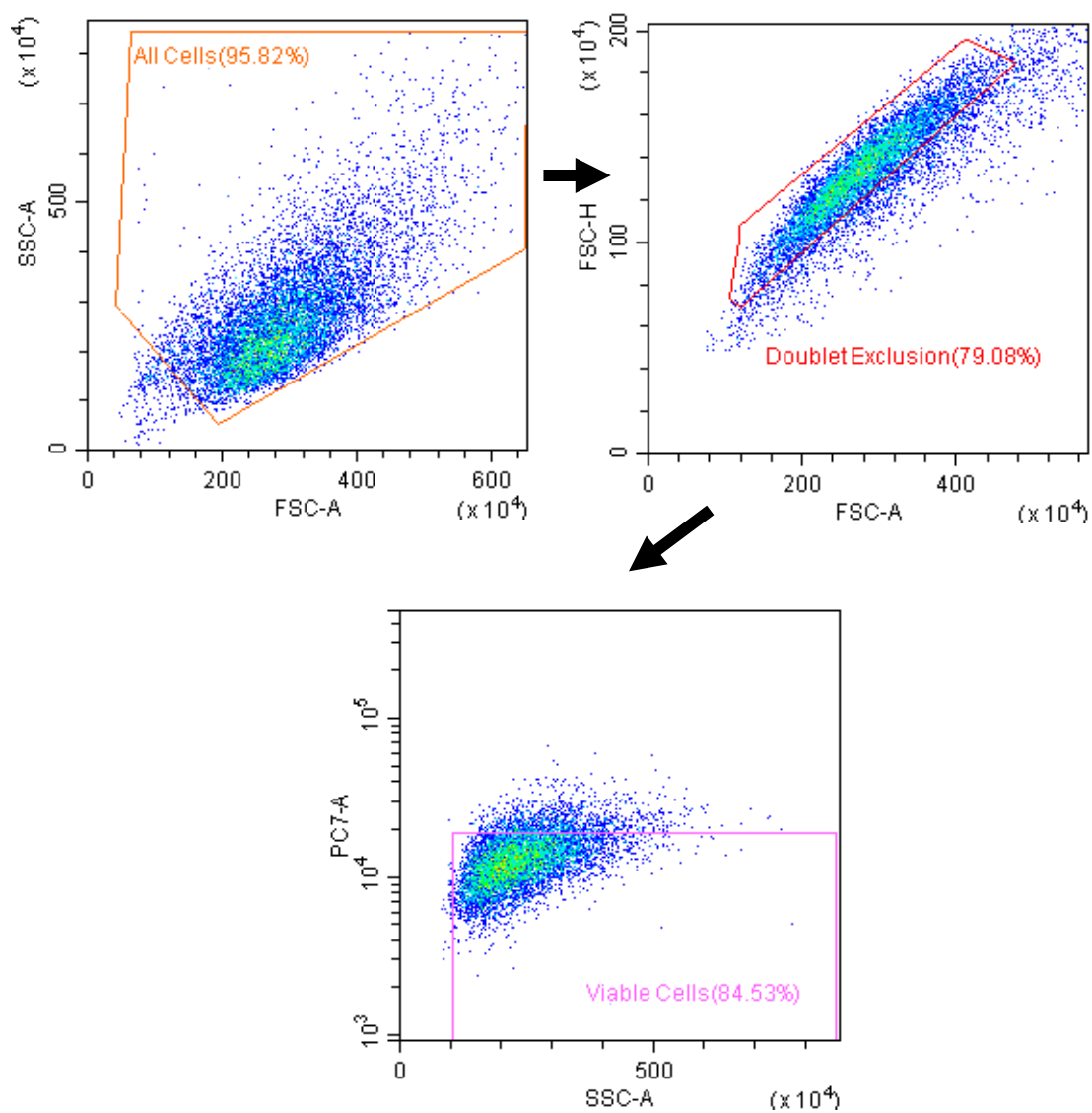
Figure 3.4: Gating strategy for culture expanded MSCs

Intact cellular bodies were gated for, after which doublets were discriminated against based off their forward height/area profiles. Viable cells were gated for based on their exclusion of uptake of 7-AAD.
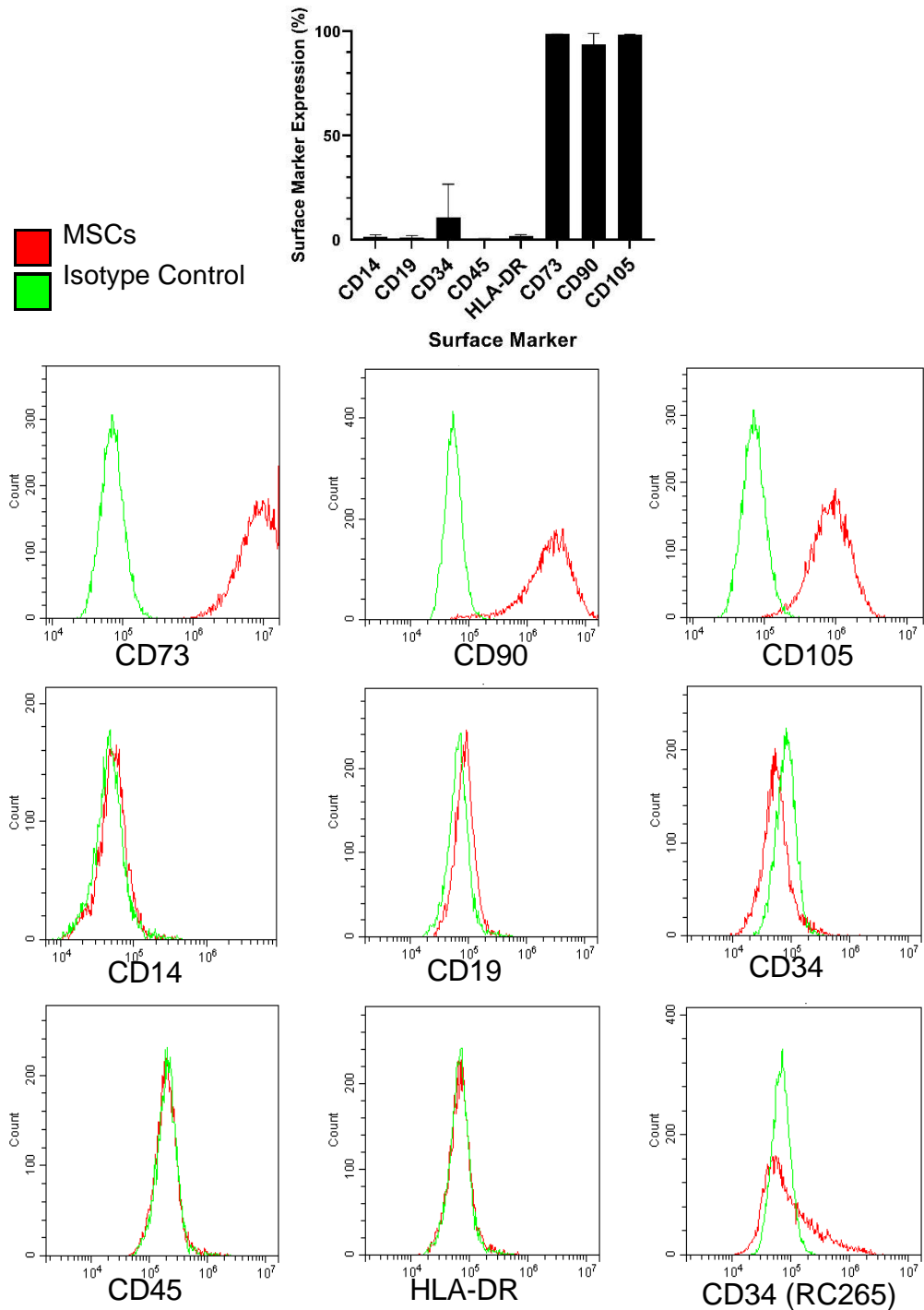
Figure 3.5: Expression of ISCT surface markers on EST MSCs

Culture expanded EST MSCs (n=3) show greater than 90% expression for CD73, CD90 and CD105, and also being negative for CD14, CD19, CD34, CD45 and HLA-DR. One sample showed some CD34 expression, though the majority of its cells were still negative as seen by the peak on CD34 (RC265) flow histogram. Error bars = mean ± SD.
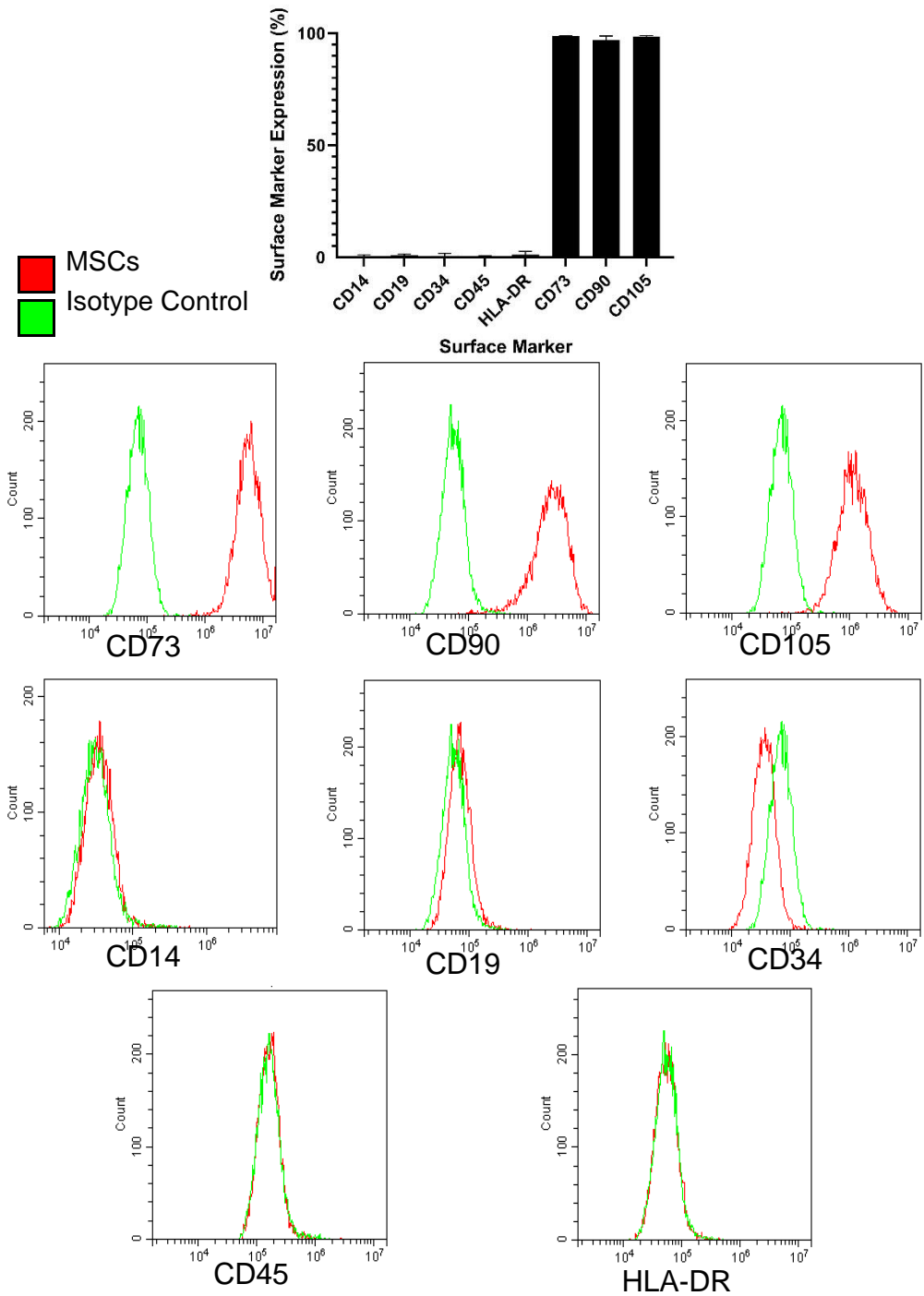
Figure 3.6: Expression of ISCT markers on PEB MSCS

Culture expanded PEB MSCs (n=3) all showed greater than 90% expression for CD73, CD90 and CD105, and also being negative for expression of CD14, CD19, CD34, CD45 and HLA-DR. Error bars = mean ± SD.

3.3.3 – CD271+ MSCs exist in the PEB but not the EST

Uncultured bone marrows MSCs have previously been defined as having population of CD271+ MSCs (382, 388, 405), after digestion $CD45^{low}CD271^{+}$ MSCs were identified in the PEB (n=6, Figure 3.7). When gating off $CD45^{low}CD271^{+}$ MSCs had greater than 95+/-12.63% median expression for CD73, 55.54+/-55.15% CD90 and 37.62+/-36.55 CD105% (Figure 3.7).

However, the EST (n=2) fraction of entheseal digests did not have any measurable populations of $CD45^{low}CD271+$ MSCs (Figure 3.8). The low viable cell count meant that only a low number of cells fell within the determined gates for $CD45^{low}CD271+$, and those that did were so few in number it could not be confidently stated that there is a clear population. When gating off CD45- cells, there were clear populations of CD73+CD90+CD105+ MSCs.
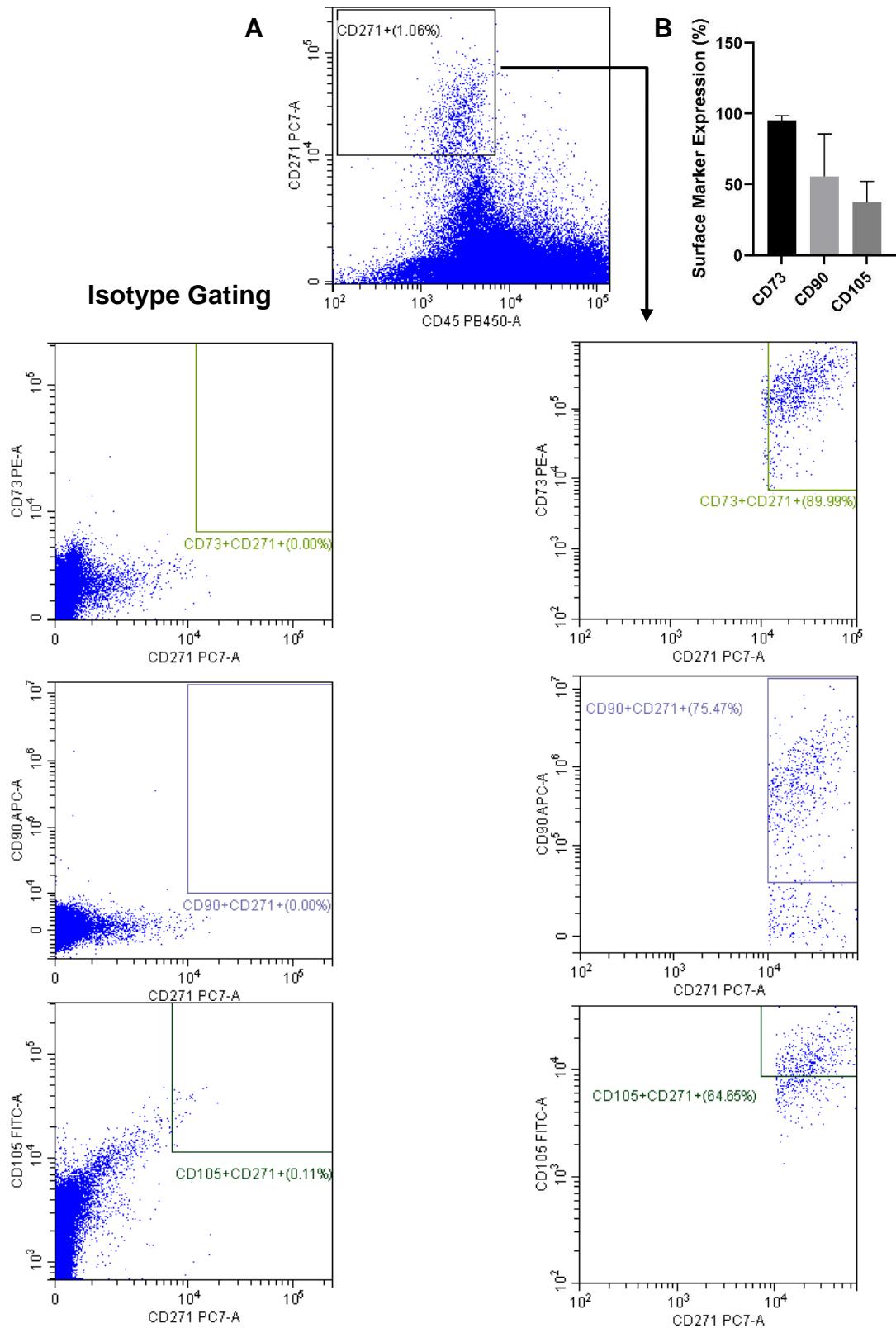
Figure 3.7: Representative population of CD271+ MSCs at the PEB

Representative flow cytometry plots of MSCs at the PEB. (A) CD271+ MSCs represented ~0.9% of total viable cells. CD271+ MSCs display CD73, CD90 and CD105 surface marker expression (B). Gating for CD271+CD45^{low} MSCs was carried out on isotype controls.
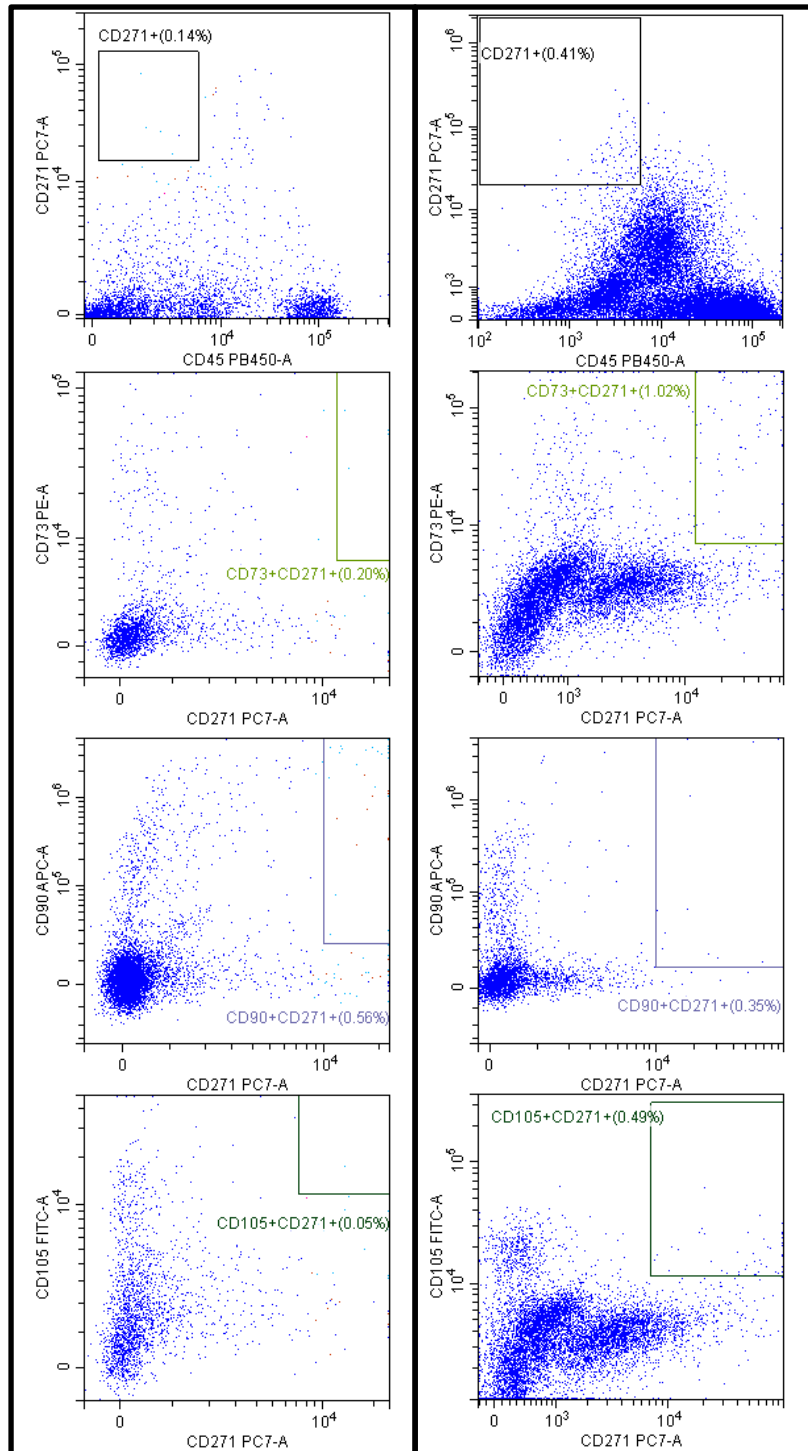
Figure 3.8: CD271+ MSCs are not abundant at the EST

There are no clear populations of CD271+ MSCs in the EST, with insufficient cells falling within the determined gate. However, gating off CD45- cells showed CD73+CD90+CD105+ MSCs are in the EST from both samples.

3.3.4 – MSCs from both PEB and EST are tri-lineage capable

3.3.4.1 – Adipogenesis

Culture expanded cells from both the PEB and the EST were capable of undergoing adipogenic differentiation when stimulated by adipogenic media compared to a control media (Figure 3.9). There were however significant differences in their differentiation potentials, with EST cells having a significantly higher (p<0.001) adipogenic potential than matched PEB cells. This was demonstrated by a 4.9-fold increase in Oil Red O stained lipid vesicles in EST cultures compared to matched PEB.

In particular for EST MSCs their adipogenic potential showed a wide range in the area stained by Oil Red O. A linear regression analysis of sample ages against Oil Red O stained area demonstrated for EST cells a significantly non-zero slope (p<0.0001) decreasing with age. There were no significant differences relating to the gender of the sample.

This pattern appeared to be consistent for PEB cells undergoing adipogenesis. The exceptionally poor adipogenic potential of PEB cells, in general, meant that any potential differences were not seen to be significant despite similar trending.
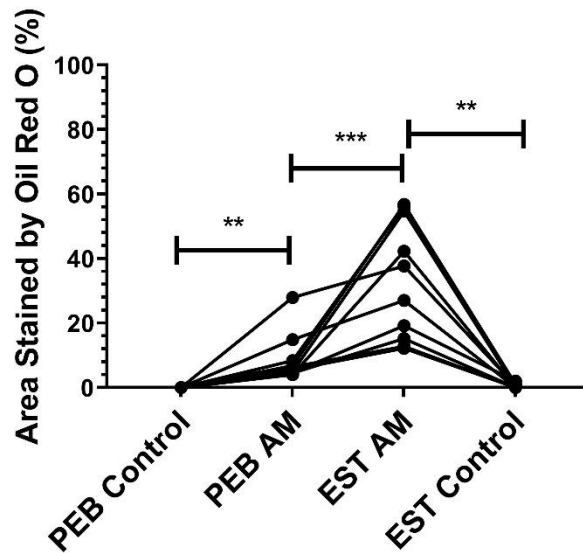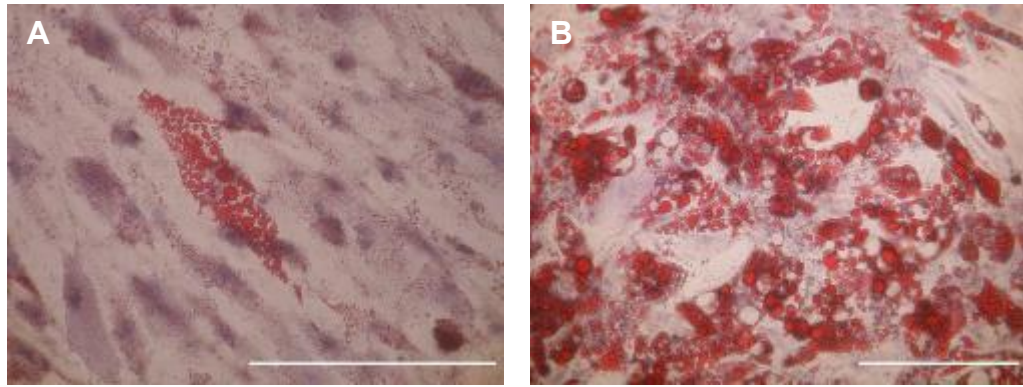
Figure 3.9: Oil Red O stained differentiated MSCs from both PEB and EST

Representative images of Oil Red O stained adipocytes differentiated from both PEB (A) and EST (B) MSCs. EST MSCs produce a significantly greater area covered by Oil Red O stained adipocytes than matched PEB MSCs (C). Scale bar = 100μm. **=p<0.01, ***=p<0.001
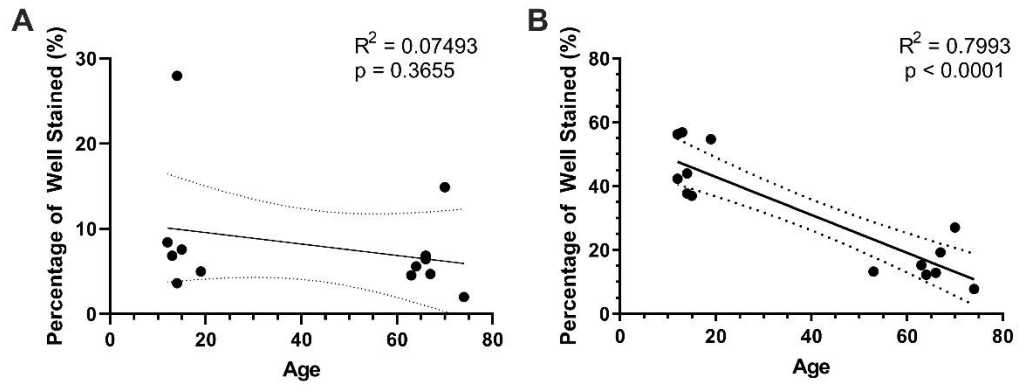
Figure 3.10: Age related changes in adipogenesis of PEB and EST MSCs

A) PEB MSCs show little age affected influence on their adipogenic potential, though there is a small trend it is not seen to be significant. At the same time as EST MSCs (B) show significant loss of adipogenic potential with increased age, with a Linear regression with a significantly non-zero slope (p<0.0001) supported by an R^2 value of 0.7993.

3.3.4.2 – Chondrogenesis

Both MSCs from the PEB and EST can differentiate into chondrocytes. PEB and EST MSCs after a three-week chondrogenesis assay have significantly increased sGAG levels compared to control pellet, but there is no significant difference between their chondrogenic ability, with sGAG level remaining at similar levels between matched samples (Figure 3.11).
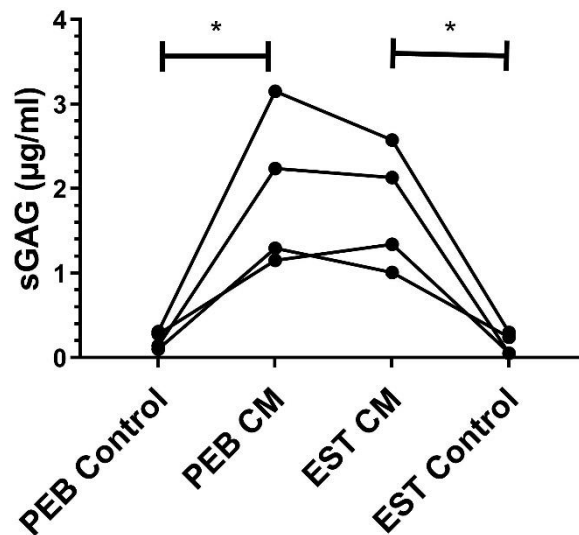
Figure 3.11: sGAG levels after chondrogenesis in both PEB and EST
*Both PEB and EST MSCs are capable of chondrogenesis with a significant increase in sGAG levels compared to controls, but there is no significant difference between the two. * = p<0.05.*

3.3.4.3 – Osteogenesis

The osteogenic potential between PEB and EST MSCs was significantly different. This was seen in both the qualitative alizarin red staining at 3 weeks post differentiation induction and the quantitative calcium assays at 2 weeks post-induction. Alkaline phosphatase and alizarin red staining showed that MSCs from both the PEB and EST underwent osteogenic differentiation, though there was seen to be a large variance in alizarin red staining for PEB MSCs after osteogenic differentiation. Comparatively EST MSCs showed visually similar levels of alizarin red staining across the samples (Figure 3.12).

PEB MSCs produce significantly more calcium than matched EST MSCs (2.75-fold increase, $p<0.01$, Figure 3.12, Figure 3.13). The alizarin red staining in particularly (combined with the calcium deposition assays) showed that PEB MSCs had a large variation in their osteogenic potential (PEB range: 18.39-171.7µg/ml, Figure 3.12). EST MSCs have particularly poor osteogenic potential (median: 20.48µg/ml), the range in osteogenic potential was smaller compared to PEB MSCs (EST range: 12.08-37.5µg/ml). MSCs from both the PEB and EST did not have measurable calcium deposition when cultured in a control media after 2-weeks. Subsequent investigation into whether the large variance in osteogenesis for PEB MSCs was related to the patient age for that sample, showed that patient age was not responsible for the differences in osteogenic potential in PEB MSCs (Figure 3.14).
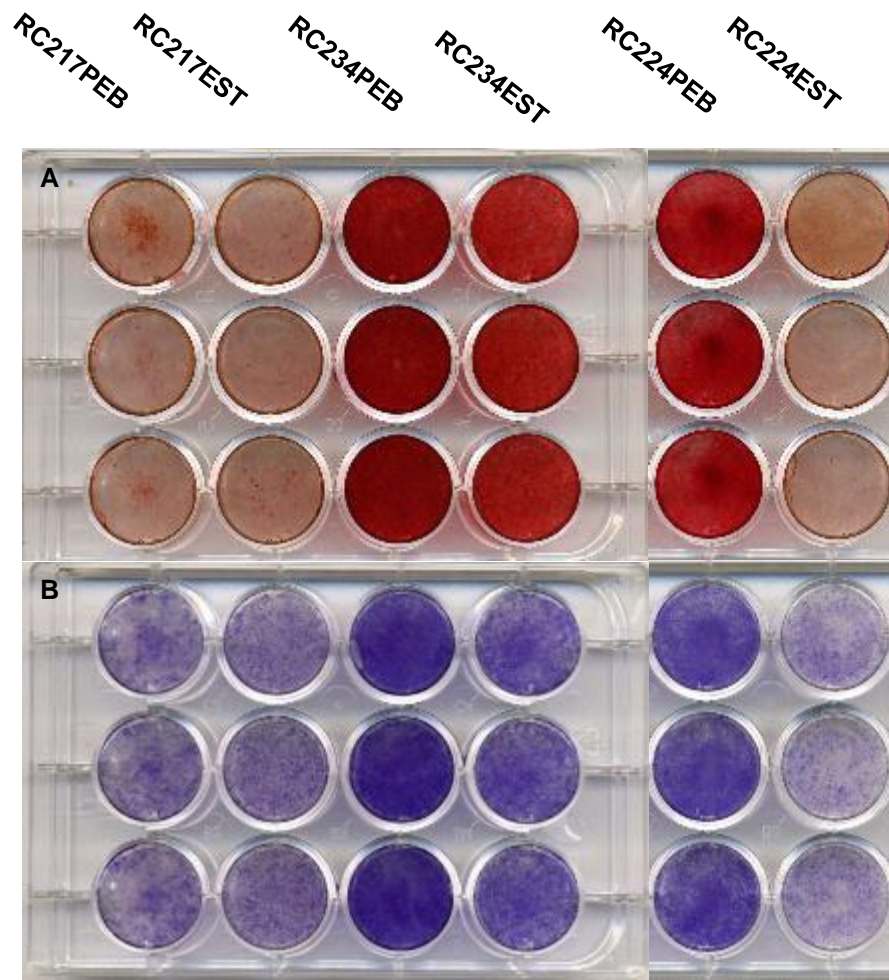
Figure 3.12: Alizarin red and alkaline phosphatase staining of PEB and EST MSCs

Representative images showing the variation in the osteogenic potential between different patient samples in particular for PEB samples. A) Alizarin red staining of PEB shows that whilst there is a greater osteogenic potential for PEB MSCs, there is a great deal of variation between samples. RC217B has a lower potential compared to RC234B. B) Alkaline phosphatase staining of the same patient samples shows a similar pattern with low alkaline phosphatase staining correlating with low alizarin red stains seen in (A).
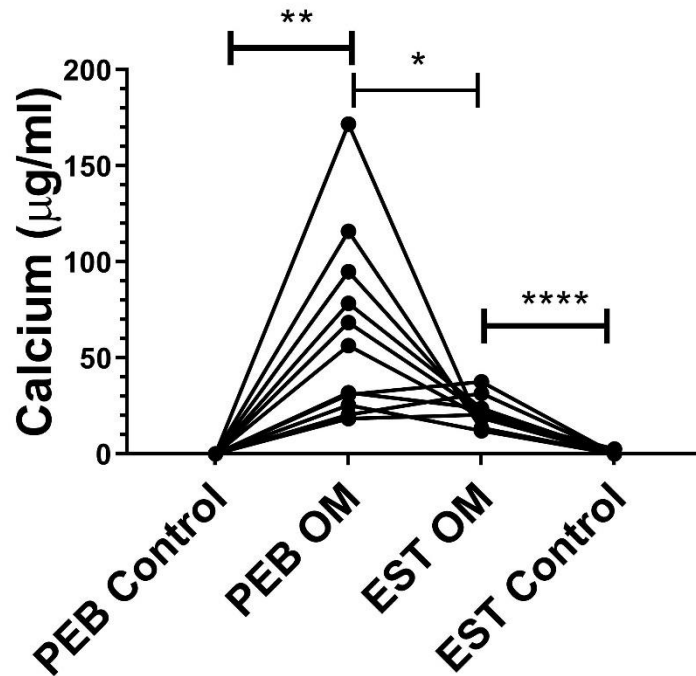
Figure 3.13: Calcium deposition in both PEB and EST MSCs

*Both PEB and EST MSCs are capable of osteogenic differentiation, with PEB MSCs producing significantly more calcium than matched EST MSCs. *=p<0.05, **=p<0.01, ****=p<0.0001.*
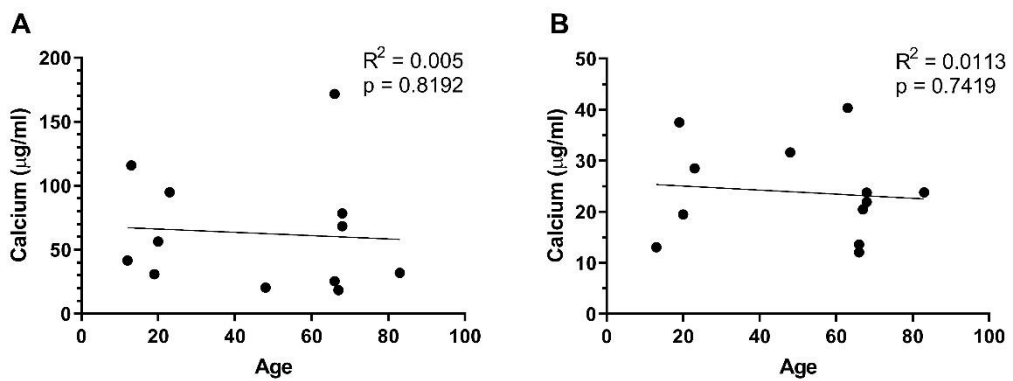
Figure 3.14: Age influences on osteogenesis for PEB and EST MSCs

Osteogenic potential for both PEB (A) and EST (B) MSCs was not seen to significantly influence the osteogenic potential of cells.

3.4 – Discussion

Traditionally ligaments have been thought either incapable of naturally repairing or having exceptionally slow repair due to their naturally low fibroblastic cells in the ligamentous body being mainly composed of extracellular matrix (>96% being collagen, proteoglycans, elastin) (407-409). However, with the new bone formation or syndesmophytes seen in AS observed at the ligamentous insertion into the bone (58), populations of MSCs must be [at the] present insertion sites.

This chapter identified two distinct populations of MSCs at the human spinal enthesis, which are seen to have significantly different differentiation potentials. This would fit with the notion that MSC populations display significant preferential differentiation potentials based on their tissue origin (397, 410).

As a proportion of viable cells after digestion EST MSCs had a significantly higher (7.2-fold) percentage of colony forming cells when compared to matched PEB MSCs. This is likely due to the tissue of origin of these digests, ligaments are largely seen to be acellular (407) and avascular meaning that there is a lower total number of cells which was also seen with our digests. Compared to bone marrow, which is what the PEB consists of, has a higher proportion of immune cells, as can be seen by the higher percentage of CD45+ cells in fresh digests. The percentage of colony-forming cells is similar to other studies conducted after enzymatic digestion which saw ~0.2-1.89% being colony-forming cells (405, 411, 412) The larger average colony size for PEB MSCs compared to EST is likely a reflection of this. Comparisons between periosteum derived MSCs, another type of connective soft tissue, and bone marrow-derived MSCs, show bone marrow-derived MSCs have significantly larger colony area and lower total colony counts compared to matched periosteum (385).

The classical phenotype of AS is the neo-osteogenesis seen at the spinal enthesis, it has long been seen that fatty depositions at the enthesis are visible using MRI and precede new bone formation at these sites (21). Both populations of MSCs identified at the human spinal enthesis are capable of

adipogenesis, but EST MSCs produce significantly more adipocytes than matched PEB MSCs. This would fit with the anatomy as entheseal attachment sites often have a fat pad to act as a cushioning mechanism to help disperse the high mechanical strain applied to this region (51, 413). This is also supported by the low levels of CD34 staining seen in one of the samples used to assess for ISCT surface markers. CD34 is seen on MSC populations derived from adipose tissues, and these populations have higher adipogenic potential than when compared to CD34- MSC populations (373, 397, 414).

The large variation within EST MSCs adipogenesis was seen to be significantly correlated with the patient's age. The older the patient at the time of the sample digestion the worse the adipogenic potential of their MSCs. This seems to be slightly counterintuitive, as with increasing age the higher the fat content observed within the bone marrow space (415).

As mentioned above whilst the fatty corners are seen to precede new bone formation in AS, the endpoint is still neo-osteogenesis and as both PEB and EST MSCs are capable of osteogenesis provides the basic mechanism for bone formation. PEB MSCs showed significantly higher calcium deposition than matched EST MSCs. At the same time populations of CD271+ MSCs were identified in PEB digests, whilst no significant populations were observable in the EST digests. CD271+ MSCs have significantly higher osteogenic potential than CD271- MSCs (374), which could be a partial explanation as to the significant differences between the osteogenic potential of the two MSC sources. However, it would be rash to suggest that this is the sole reason for the increased osteogenic potential of PEB MSCs when tissue origin is known to play a significant role in differentiation potential. As both iliac crest and vertebral body MSCs display CD271+ cells, yet the vertebral body has a significantly higher osteogenic potential (384). The large variation seen within the osteogenic potential of PEB MSCs could not be identified by this work, especially given the much smaller variation seen within EST MSCs osteogenic potential. The smaller variation within the EST MSC population is likely due to the tissue specificity, as the ligamentous tissue is devoid of bone the MSCs do not need large osteogenic potentials. It is important to acknowledge that the differences in differentiation potential between MSCs

from both the PEB and EST could be attributed to cells being slightly more differentiated into progenitors as opposed to traditional stem cells. Adipogenesis requires more histone modification than osteogenesis in MSCs and as a result, cells isolated from more fatty tissues are more adipogenic, likely due to being more adipo-progenitors than MSCs (401, 416).Interestingly when osteoblasts that were dedifferentiated back into MSCs, they displayed an epigenetic memory favouring a redifferentiation back down an osteogenic lineage (417). This could also help explain the strong preferences of MSCs from both the EST and PEB to differentiate down lineages that fit with the anatomical location they were isolated from.

In conclusion, the establishment that there are two functionally distinct populations of MSCs at the human spinal enthesis capable of tri-lineage differentiation provides the groundwork for how pathological changes seen in AS are implemented. In particular the evidence that MSCs from the EST are capable of osteogenic differentiation and rapid high levels of adipogenesis provides a rationale for the fatty corners at the enthesis seen in early AS.

Chapter 4 – Pro-Inflammatory cytokine influences on adipogenesis and osteogenesis

4.1 – Introduction

Ankylosing spondylitis is a typical spondylarthritis characterised by inflammation driven damage and subsequent over repair in the axial skeleton, namely at the entheseal attachment sites (1, 51). An array of cytokines some involved in the IL-17/IL-23 axis and those which are not are involved in the inflammatory changes seen in AS (20). TNF and IL-17A are both seen to be critically involved with the pharmacological antagonism of TNF, eventually reducing new bone formation (30, 418), whilst long-term results are awaited for IL-17A inhibition.

4.1.1 – Osteogenesis

Pro-inflammatory cytokines are known to play a role in normal tissue repair and in particular in fracture repairs; TNF and IL-17A are shown to be heavily involved in bone repair with knockouts of either showing impaired bone healing after fracture (20, 60, 128).

Despite the evidence of IL-17A involvement in bone repair, the exact role of IL-17A in new bone formation in AS is largely still to be elucidated with experimental findings sometimes producing contradictory findings. Resident MSC populations display enhanced osteogenic differentiation when stimulated with IL-17A (59, 419, 420), with the resulting differentiated osteoblasts becoming activated via JAK2/STAT3 signalling associated with osteogenesis (67). These *in vitro* findings are supported by *in vivo* mouse models, where IL-17A knockout mice are seen to have impaired bone regeneration after a tibial drill-hole fracture (60), and in humans, IL-17A levels are seen to be elevated in the days following the fracture and are associated with callus formation (178). Mycobacterium tuberculosis induced AS utilising HLA-B27 rat models saw significant suppression of new bone formation (420).

However, some reports show IL-17A significantly reduces the osteogenic potential of cells, though these cells usually come from sources where high osteogenesis is an unfavourable outcome, such as pre-osteoblast calvarial

cells (179, 181). Also, elevated systemic levels of IL-17A are associated with bone loss (421), such as that seen in psoriatic arthritis, where inhibition is associated with preventing bone erosion (422, 423). This highlights the need for further research into the role of IL-17A on osteogenesis in AS at disease-relevant sites, given the discrepancies amongst the literature.

TNF has a well-established role in driving osteoclastogenesis in inflammatory arthritides (424-426). However, in AS TNF inhibition has been associated with reduced pathological new bone formation at the enthesis (30). The reasons for these two opposing mechanisms has been suggested to be down to concentrations of TNF (427, 428), with higher concentrations showing impaired osteogenesis and increased osteoclastogenesis (134, 139, 140, 429) whilst lower concentrations stimulate osteogenesis (139, 420, 430, 431). TNF is known to synergise with IL-17A to cause even, more significant increases in osteogenesis than either cytokine individually in MSCs (420, 432, 433).

4.1.2 – Adipogenesis

In AS formation of fatty tissues around the enthesis after the initial bone loss is seen to precede the characteristic new bone formation and subsequent syndesmophytes (21, 434). However, despite this very little work has been conducted into investigating how these fatty changes occur and how the inflammation seen in AS affects this new adipogenesis.

The effects of inflammatory cytokines have been investigated when looking at different diseases, in particular diabetes and obesity. IL-17A knockout mice show enhanced diet-induced obesity (435) and an expansion of bone marrow adipose tissue with increasing adipogenesis seen by an increase in leptin levels (436). In the mouse-derived 3T3-L1 pre-adipocytes cell line IL-17A stimulation prevented adipocyte differentiation (435, 437). The suppression of maturation of adipocytes from either MSCs or 3T3-L1 cell lines by IL-17A occurs via suppression of the master adipogenic regulator transcripts *PPARGγ* and *CEBPβ* (438). Human bone marrow MSCs adipogenesis is also suppressed by IL-17A stimulation (439).

TNF is also known to suppress adipogenesis both from the 3T3-L1 cell line (440, 441) and from human MSC populations where M1 macrophages secreting TNF reduced the adipogenesis of these MSCs (442). This loss of adipogenic function could be partially rescued by TNF inhibition (442).

In differentiated adipocytes, stimulation using IL-17A causes an increase in the secretion of IL-6 and also increase adipolysis of these adipocytes, further breaking down fatty tissues (437, 439). At the same time as co-stimulation with TNF causes a synergistic upregulation of these cytokines and other chemoattractants of CD4+ T cells, namely CCL20 (443).

4.1.3 – Hypotheses

Given the known reciprocal relationship between MSC mediated osteogenesis and adipogenesis (400, 401) and the evidence that IL-17A and TNF participate in both osteogenesis and adipogenesis, it is important to investigate how adipogenesis from these disease-relevant cells is affected by IL-17A and TNF, whilst also investigating how osteogenesis may be influenced.

This chapter of work aimed to investigate four main hypotheses:

1. IL-17A and/or TNF significantly increases the osteogenic potential of MSCs from either the PEB or EST
2. IL-17A and/or TNF significantly suppresses the adipogenic potential of MSCs from either the PEB or EST
3. Adipogenically suppressed MSCs show significant downregulation in gene transcripts associated with adipocyte maturation
4. Cytokine stimulation of MSCs undergoing adipogenesis induces significant changes in genetic transcripts relating to MSC stromal function and immune cell immunomodulation

4.2 – Materials and Methods

4.2.1 – Receptor expression on PEB and EST MSCs

Culture expanded MSCs (<p3, n=3 for both PEB and EST) were assessed for expression of the cytokine receptors IL-17RA (CD217) and TNFRI (CD120a). Cells were stained using the methodology explained in section 2.4.3, using the antibodies listed in Table 4.1. Three samples of PEB and EST had a minimum of 500,000 MSCs divided into 6 tubes after they were incubated in FACs block as described above section 2.4.3.   Tubes were labelled for their contents:

    I.   TNFRI-APC, 7-AAD

    II.   IL-17RA-Alexa Fluor® 647, 7-AAD

    III.   IgG1-Alexa Fluor® 647, 7-AAD

    IV.   IgG2a-APC, 7-AAD

    V.   Unstained control, 7-AAD

    VI.   Unstained control

Compensation was performed using Compensation beads using the selected antibodies on each fluorophore. Data were analysed as described in section 2.4.3.

Surface Marker-Conjugate:	Volume Used (µl):	Clone:	Laser (nm):	Emission$_{max}$ (nm):	Company:	Isotype:
IL-17RA (CD217)-Alexa Fluor® 647	2.5	BG/hIL17AR	633	660	Biolegend	Mouse IgG1
TNFRI (CD120α)-APC	2.5	W15099A	633	660	Biolegend	Mouse IgG2a
Mouse IgG1-Alexa Fluor® 647	2.5	X40	633	660	Biolegend	N/A
Mouse IgG2a-APC	2.5	MOPC-173	633	660	Biolegend	N/A
7-AAD	5	N/A	488	647	BD Biosciences	N/A

Table 4.1: Table of antibodies used for cytokine receptor testing

4.2.2 – Pro-Inflammatory cytokine influences on osteogenesis

The influences of the SpA associate cytokines IL-17A and TNF on osteogenesis was conducted at concentrations used in similar works. IL-17A was used at 50ng/ml and TNF was used at 1ng/ml (83, 420, 433).

MSCs from both the PEB and EST were seeded at 3,000 cells per well into 48-well plastic culture plates. Osteogenic media was applied to the wells as described in section 3.2.5, except that cells were supplemented with either 5% or 10% FCS. Due to the variations in osteogenic potential of MSCs two different concentrations of FCS were selected to ensure that any changes induced by the pro-inflammatory cytokines were observable and not masked by either poor osteogenic potential for EST MSCs or maxed out the osteogenic potential of PEB MSCS. Cultures for 5% and 10% FCS were either supplemented from day 0 with;

    I.   no cytokine control
    II.   IL-17A
    III. TNF
    IV. IL-17A & TNF.

Cultures were differentiated for 2-weeks with half media and cytokine changes every 3 days. On day 14, osteogenesis was assessed by calcium deposition quantification using the same method described in section 3.2.5.3.

4.2.2.1 – IL-17A influences on osteogenic differentiation

IL-17A was the only cytokine to consistently increase osteogenesis from both PEB and EST MSCs, it was selected to investigate transcriptional changes in osteogenic differentiation. The transcriptional changes associated with IL-17A stimulation during osteogenesis were investigated using a 48*48 gene chip. RNA extractions, reverse transcription, pre-amplification, and chip running were all performed as described in section 2.5. All samples were assessed for a 260/280 purity of between 1.8-2.0, with mRNA ranging from 18.2 to 50.0ng/μl for EST MSCs and 18.3 to 50.4ng/μl for PEB MSCs.

PEB and EST (both n=4) MSCs were osteogenically differentiated with either no stimulation or IL-17A (50ng/ml) for 2-weeks in osteogenic media (section

3.2.5) with either 5% or 10% FCS. RNA was extracted at Day 0 (undifferentiated MSCs), Day 7 and Day 14. TaqMan probes for 47 targeted osteogenic, adipogenic and stromal supportive genes and one housekeeping gene were used to investigate IL-17A influences on osteogenesis (Table 4.2).

Gene:	Gene Name:	Gene ID:	Group:
ACAN	Aggrecan	Hs00153936_m1	Chondrogenesis
ALPL	Alkaline Phosphatase	Hs01029144_m1	Osteogenesis
BMP1	Bone Morphogenetic Protein 1	Hs00241807_m1	Osteogenesis
BMP2	Bone Morphogenetic Protein 2	Hs00154192_m1	Osteogenesis
BMP6	Bone Morphogenetic Protein 6	Hs01099594_m1	Osteogenesis
BMP7	Bone Morphogenetic Protein 7	Hs00233476_m1	Osteogenesis
CEBPA	CCAAT/enhancer binding protein alpha	Hs00269972_s1	Adipogenesis
CEBPB	CCAAT/enhancer binding protein beta	Hs00942496_s1	Adipogenesis
COL1A1	Collagen type I alpha 1	Hs00164004_m1	Osteogenesis
COL1A2	Collagen type I alpha 2 chain	Hs01028956_m1	Osteogenesis
COMP	Cartilage Oligomeric Matrix Protein	Hs00164359_m1	Chondrogenesis
CTNNB1	Catenin beta 1	Hs00355045_m1	Osteogenesis
CXCL12	C-X-C motif chemokine ligand 12	Hs00171022_m1	Stromal
CXCL2	C-X-C motif chemokine ligand 2	Hs00601975_m1	Stromal
DKK1	Dickkopf WNT signaling pathway inhibitor 1	Hs00183740_m1	Osteogenesis
DKK2	Dickkopf WNT signaling pathway inhibitor 2	Hs00205294_m1	Osteogenesis
DLK1	Delta like non-canonical Notch ligand 1	Hs00171584_m1	Adipogenesis
FABP4	Fatty acid binding protein 4	Hs00609791_m1	Adipogenesis
FRZB	Frizzled-related protein	Hs00173503_m1	Osteogenesis
GDF2 (BMP9)	Growth differentiation factor 2	Hs00211913_m1	Osteogenesis
GSK3B	Glycogen synthase kinase 3 beta	Hs00275656_m1	Adipogenesis
HPRT	Hypoxanthine phosphoribosyltransferase 1	Hs99999909_m1	Housekeeping
JAK1	Janus kinase 1	Hs01026983_m1	Signalling
JAK2	Janus kinase 2	Hs01078136_m1	Signalling
JAK3	Janus kinase 3	Hs00169663_m1	Signalling
LEPR	Leptin receptor	Hs00174492_m1	Adipogenesis
OMD	Osteomodulin	Hs01060466_m1	Osteogenesis
PDGFRL	Platelet derived growth factor receptor like	Hs00185122_m1	Adipogenesis
PDPN (E11)	Podoplanin	Hs00366766_m1	Osteogenesis
PPARG	Peroxisome proliferator activated receptor gamma	Hs01115513_m1	Adipogenesis

RUNX2	Runt related transcription factor 2	Hs01047973_m1	Osteogenesis
SOST	Sclerostin	Hs00228830_m1	Osteogenesis
SOX9	SRY-box 9	Hs00165814_m1	Chondrogenesis
SP7	Sp7 transcription factor	Hs01866874_s1	Osteogenesis
STAT1	Signal transducer and activator of transcription 1	Hs01013996_m1	Signalling
STAT2	Signal transducer and activator of transcription 2	Hs01013123_m1	Signalling
STAT3	Signal transducer and activator of transcription 3	Hs00374280_m1	Signalling
STAT4	Signal transducer and activator of transcription 4	Hs01028017_m1	Signalling
STAT5A	Signal transducer and activator of transcription 5A	Hs00234181_m1	Signalling
STAT5B	Signal transducer and activator of transcription 5B	Hs00273500_m1	Signalling
STAT6	Signal transducer and activator of transcription 6	Hs00598625_m1	Signalling
TGFBR2	Transforming growth factor beta receptor 2	Hs00234253_m1	Osteogenesis
TGFBR3	Transforming growth factor beta receptor 3	Hs01114246_g1	Osteogenesis
TNFRSF11B	TNF receptor superfamily member 11b	Hs00900358_m1	Osteogenesis
WNT10B	WNT family member 10B	Hs00928823_m1	Osteogenesis
WNT3	WNT family member 3	Hs00902255_m1	Osteogenesis
WNT6	WNT family member 6	Hs00362452_m1	Osteogenesis
WNT7B	WNT family member 7B	Hs00536497_m1	Osteogenesis

Table 4.2: TaqMan probes used to investigate osteogenesis

4.2.3 – Pro-Inflammatory cytokine influences on adipogenesis

4.2.3.1 – IL-17A titrations

Due to the limited work conducted on IL-17A's influence on MSC adipogenesis a concentration titration was performed to identify the appropriate concentration going forward. One was not performed for TNF due to the low concentration (1ng/ml) already used.

Five concentrations of IL-17A were selected to be investigated:

I. 10ng/ml
II. 25ng/ml
III. 50ng/ml
IV. 100ng/ml
V. 200ng/ml.

MSCs from both the EST and PEB (n=3 for both) were differentiated in adipogenic media (section 3.2.3) for 3 weeks supplemented with either no IL-17A or one of the concentrations described. Oil Red O staining was used at the end of differentiation to determine cytokine influences.

4.2.3.2 – IL-17A and TNF influences on adipogenesis

MSCs from the PEB and the EST (n=5) were seeded at 50,000 cells per well in 24-well plastic culture plates and supplemented with adipogenic media as described in section 3.2.3. Wells were either supplemented with:

I. no cytokine control
II. IL-17A (50ng/ml)
III. TNF (1ng/ml)
IV. IL-17A (50ng/ml) & TNF (1ng/ml)

Plates were cultured for three weeks with half media changes every 3 days; on the 21st after initiation wells were fixed and stained for adipocytes using Oil Red O as described in section 3.2.3**.**

4.2.3.3 – Gene expression changes in adipogenesis with IL-17A stimulation

Gene expression changes over the course of adipogenesis and the influence of IL-17A on them was investigated using a time course differentiation experiment. RNA extractions, reverse transcription, pre-amplification and chip running were all performed as described in section 2.5. TaqMan probes for 47 genes of interest relating to adipogenesis and stromal function were targeted (Table 4.3). All samples were assessed for a 260/280 purity of between 1.8-2.0, with a mRNA quantity ranging from 20.1 to 73.9ng/μl for EST MSCs and 19.5 to 61.5ng/μl for PEB MSCs.

MSCs from the PEB and EST (n=4) were seeded at a density of 50,000 cells per well in a 24-well plastic culture plate, and either unstimulated or stimulated with IL-17A (50ng/ml). Wells had half media changes every 3 days. RNA extractions were performed on Day 0 (undifferentiated MSCs), Day 3, Day 5, Day 7, Day 15 and Day 21 into differentiation. At each time point from Day 3, wells were also stained using Oil Red O to look for lipid vesicle formation.

Gene:	Gene Name:	Assay ID:	Group:
ABCA1	ATP binding cassette subfamily A member 1	Hs01059137_m1	Adipogenesis
ABCG1	ATP binding cassette subfamily G member 1	Hs00245154_m1	Adipogenesis
ADIPOQ	Adiponectin	Hs00605917_m1	Adipogenesis
AGPAT2	1-acylglycerol-3-phosphate O-acyltransferase 2	Hs00944961_m1	Adipogenesis
CCL20	C-C motif chemokine ligand 20	Hs01011368_m1	Immunomodulatory
CCL8	C-C motif chemokine ligand 8	Hs04187715_m1	Immunomodulatory
CEBPA	CCAAT/enhancer binding protein alpha	Hs00269972_s1	Adipogenesis
CEBPB	CCAAT/enhancer binding protein beta	Hs00942496_s1	Adipogenesis
CIDEA	Cell death inducing DFFA like effector A	Hs00154455_m1	Adipogenesis

Gene	Description	Assay ID	Category
CIDEC	Cell death inducing DFFA like effector C	Hs00535724_gH	Adipogenesis
CXCL12	C-X-C motif chemokine ligand 12	Hs00171022_m1	Stromal
CXCL2	C-X-C motif chemokine ligand 2	Hs00601975_m1	Stromal
FABP4	Fatty acid binding protein 4	Hs00609791_m1	Adipogenesis
GSK3B	Glycogen synthase kinase 3 beta	Hs00275656_m1	Adipogenesis
HPRT	Hypoxanthine phosphoribosyltransferase 1	Hs99999909_m1	Housekeeping
IL17RA	Interleukin 17 receptor A	Hs01056316_m1	Cytokine receptor
IL17RB	Interleukin 17 receptor B	Hs00218889_m1	Cytokine receptor
IL17RC	Interleukin 17 receptor C	Hs00994305_m1	Cytokine receptor
IL17RD	Interleukin 17 receptor D	Hs00296982_m1	Cytokine receptor
IL17RE	Interleukin 17 receptor E	Hs00979824_m1	Cytokine receptor
IL6	Interleukin 6	Hs00174131_m1	Immunomodulatory
JAK1	Janus kinase 1	Hs01026983_m1	Signalling
JAK2	Janus kinase 2	Hs01078136_m1	Signalling
JAK3	Janus kinase 3	Hs00169663_m1	Signalling
LEP	Leptin	Hs00174877_m1	Adipogenesis
LEPR	Leptin receptor	Hs00174492_m1	Adipogenesis
LPL	Lipoprotein lipase	Hs00173425_m1	Adipogenesis
LRP1	LDL receptor related protein 1	Hs00233856_m1	Adipogenesis
MAPK1	Mitogen-activated protein kinase 1	Hs01046839_m1	Adipogenesis
MAPK3	Mitogen-activated protein kinase 3	Hs00385075_m1	Adipogenesis
PLIN1	Perilipin 1	Hs00160173_m1	Adipogenesis
PLIN5	Perilipin 5	Hs00965990_m1	Adipogenesis
PPARG	Peroxisome proliferator activated receptor gamma	Hs01115513_m1	Adipogenesis
PREF1	Pre-adipocyte factor 1	Hs00171584_m1	Adipogenesis
SCARB1	Scavenger receptor class B receptor 1	Hs00969821_m1	Adipogenesis
SLC25A4	Solute carrier family 25 member 4	Hs00154037_m1	Adipogenesis

SLC2A4	Solute carrier family 2 member 4	Hs00168966_m1	Adipogenesis
STAT1	Signal transducer and activator of transcription 1	Hs01013996_m1	Signalling
STAT2	Signal transducer and activator of transcription 2	Hs01013123_m1	Signalling
STAT3	Signal transducer and activator of transcription 3	Hs00374280_m1	Signalling
STAT4	Signal transducer and activator of transcription 4	Hs01028017_m1	Signalling
STAT5A	Signal transducer and activator of transcription 5A	Hs00234181_m1	Signalling
STAT5B	Signal transducer and activator of transcription 5B	Hs00273500_m1	Signalling
STAT6	Signal transducer and activator of transcription 6	Hs00598625_m1	Signalling
TNF	Tumour necrosis factor	Hs99999043_m1	Immunomodulatory
TNFRSF1A	TNF Receptor Superfamily Member 1A	Hs01042313_m1	Cytokine receptor
TNFRSF1B	TNF Receptor Superfamily Member 1B	Hs00153550_m1	Cytokine receptor
UCP3	Uncoupling protein 3	Hs01106052_m1	Adipogenesis

Table 4.3: TaqMan probes used for IL-17A influence on adipogenesis

4.3 – Results

4.3.1 – MSCs from PEB and EST express IL-17RA and TNFRI

To demonstrate the presence of receptors for IL-17A and TNF and demonstrate that they would respond to the cytokine signalling. Culture expanded MSCs from both the PEB and EST displayed IL-17RA and TNFRI (Figure 4.1).
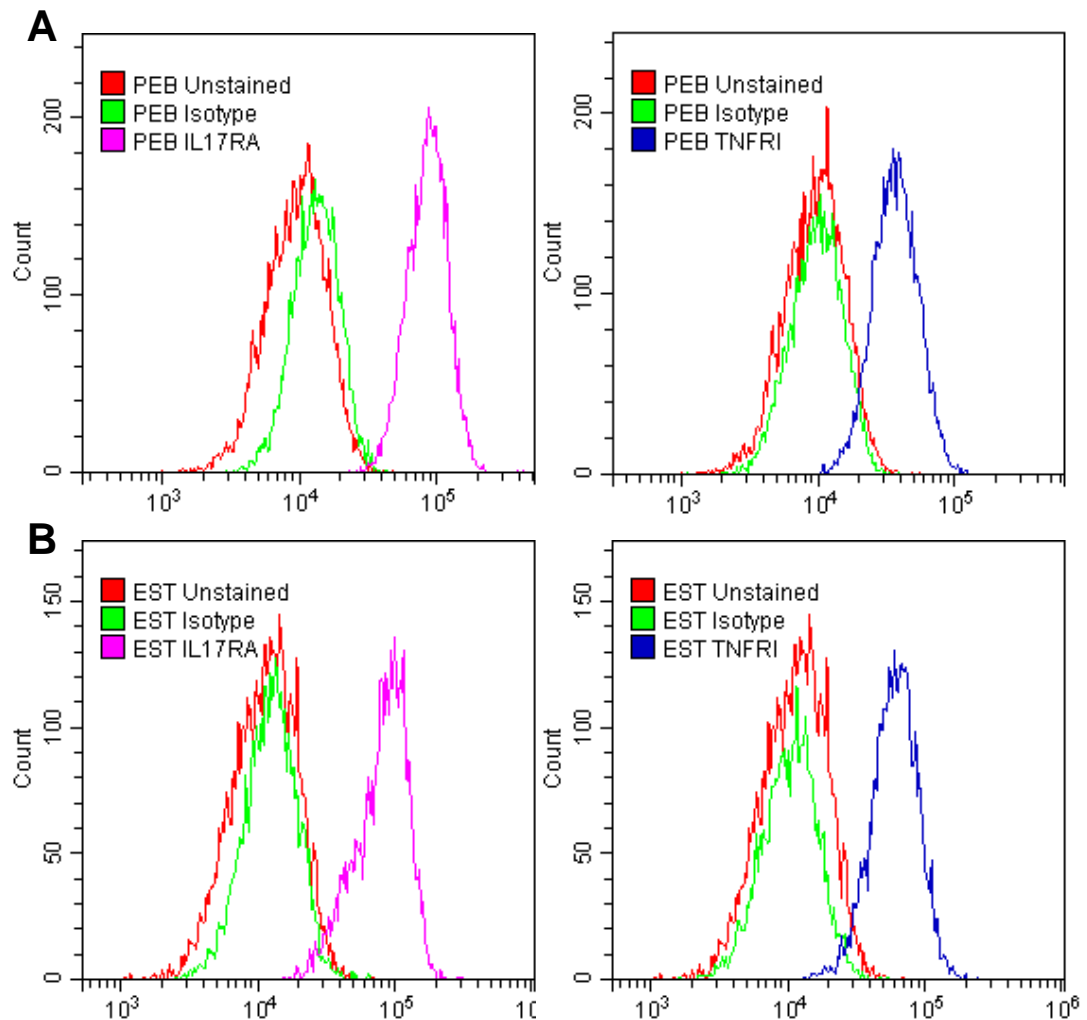
Figure 4.1: IL-17RA and TNFRI expression on PEB and EST MSCs

MSCs from both the PEB (A) and EST (B) showed positive expression for both IL-17RA and TNFRI, with greater than 95% expression for both PEB and EST for IL-17RA and greater than 85% for PEB and 95% for EST for TNFRI.

4.3.2 – IL-17A moderately increases osteogenesis

Due to the high osteogenic potential in PEB MSCs, two concentrations of FCS were used for this section, either a 5% or 10% FCS concentration in osteogenic medium.

PEB MSCs cultured in a 5% FCS osteogenic media stimulation with IL-17A caused a 2-fold increase in calcium deposition ($p<0.01$) compared to an unstimulated control culture. Compared to in a 10% FCS osteogenic media, this was a 1.3-fold increase ($p<0.05$, Figure 4.2) in calcium deposition for PEB MSCs after osteogenesis. Interestingly, TNF stimulation in either a 5% or 10% FCS did not cause any significant increases in calcium deposition in PEB MSCs, though there was a small increase of 1.3-fold for 5% FCS. Co-stimulation with both IL-17A and TNF in a 5% FCS osteogenic media caused a significant 1.65-fold increase ($p<0.05$) in calcium accumulation, though this was not seen in 10% FCS osteogenic media, there was a 1.34-fold increase, but this was not significant.

EST MSCs have a generally poor osteogenic potential, which was further evidenced by the large variability and some sample producing almost no calcium after osteogenesis in a 5% FCS osteogenic media. However, when cultured in a 10% FCS osteogenic media stimulation with IL-17A caused a modest 1.34-fold increase ($p<0.01$, Figure 4.2) in calcium deposition, which was also seen when co-stimulating with IL-17A and TNF where a 1.32-fold increase ($p<0.05$) in calcium deposition was seen. TNF stimulation alone did not cause a significant change in calcium deposition for EST MSCs in a 10% FCS osteogenic media.
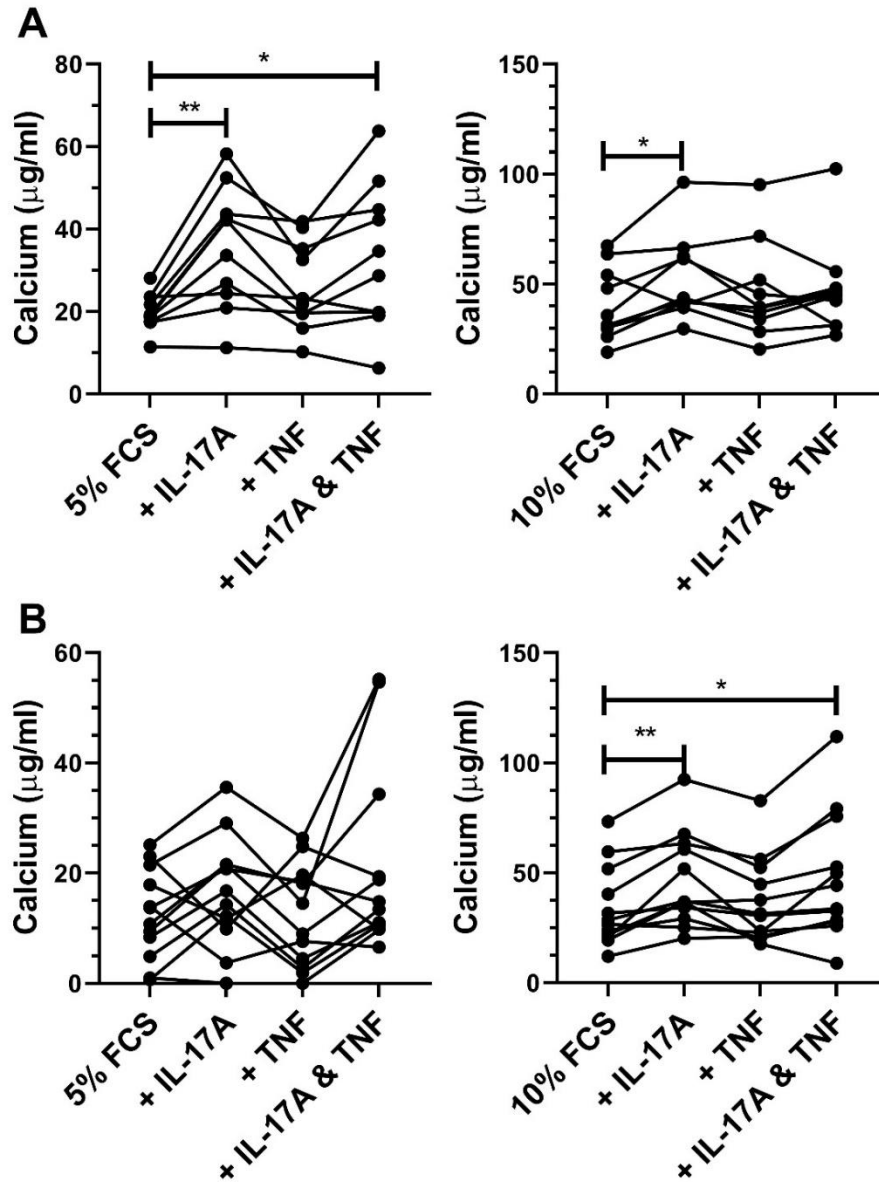
Figure 4.2: IL-17A moderately increases osteogenesis in both PEB and EST MSCs

After analysis using repeated measures one-way ANOVA with Tukey Post-Hoc testing PEB MSCs (A) showed moderate significant increases in calcium accumulation when stimulated with IL-17A in either a 5% or 10% FCS osteogenic media, whilst in a 5% FCS osteogenic media co-stimulation with IL-17A and TNF induced a significant increase. Freidman's test with Dunn's multiple comparisons of EST MSCs (B) showed a significant increase in calcium deposition in a 10% FCS osteogenic media when stimulated with either IL-17A or a combination of IL-17A and TNF. * = p<0.05, ** = p<0.01

4.3.3 – IL-17A suppresses two key osteogenic transcripts in both PEB and EST MSCs

4.3.3.1 – PEB MSCs

The moderate increases seen in PEB MSCs osteogenic potential by IL-17A were seen over the course of their two-week differentiation. Though no significant changes were seen when looking at calcium deposition for either a 5% or 10% FCS osteogenic media at either day 7 or day 14 after initiation Figure 4.3. The patterns of increase were similar to those seen in Figure 4.2.
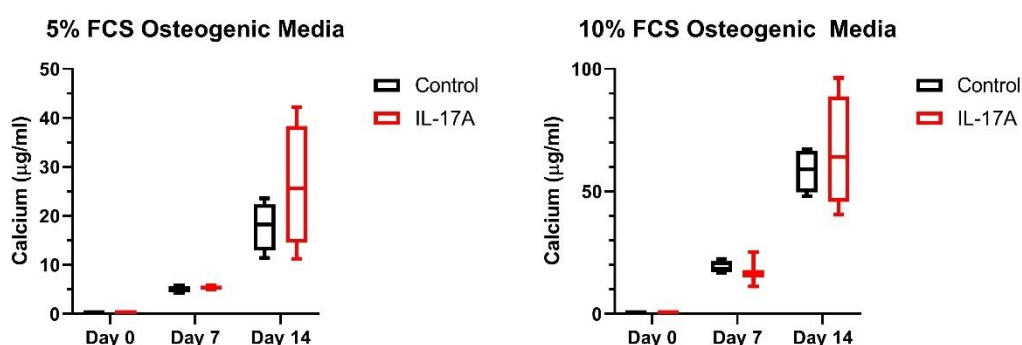
Figure 4.3: Increasing calcium accumulation over 2 weeks of osteogenesis for PEB MSCs

On day 7, after initiation, there were no obvious differences for calcium deposition by PEB MSCs (n=4) for either 5% or 10% FCS osteogenic media. This was the same on day 14, IL-17A was trending to deposit more calcium than matched unstimulated wells.

The hierarchal clustering of PEB in either a 5% (Figure 4.4) or 10% (Figure 4.5) FCS osteogenic media showed clear clustering between undifferentiated MSCs, MSCs at Day 7 of differentiation and finally MSCs at Day 14 of differentiation. The clustering did not show clearly defined clusters for cells stimulated with IL-17A, with relative expression looking at similar levels to unstimulated cells of the same patient and at the same time point.
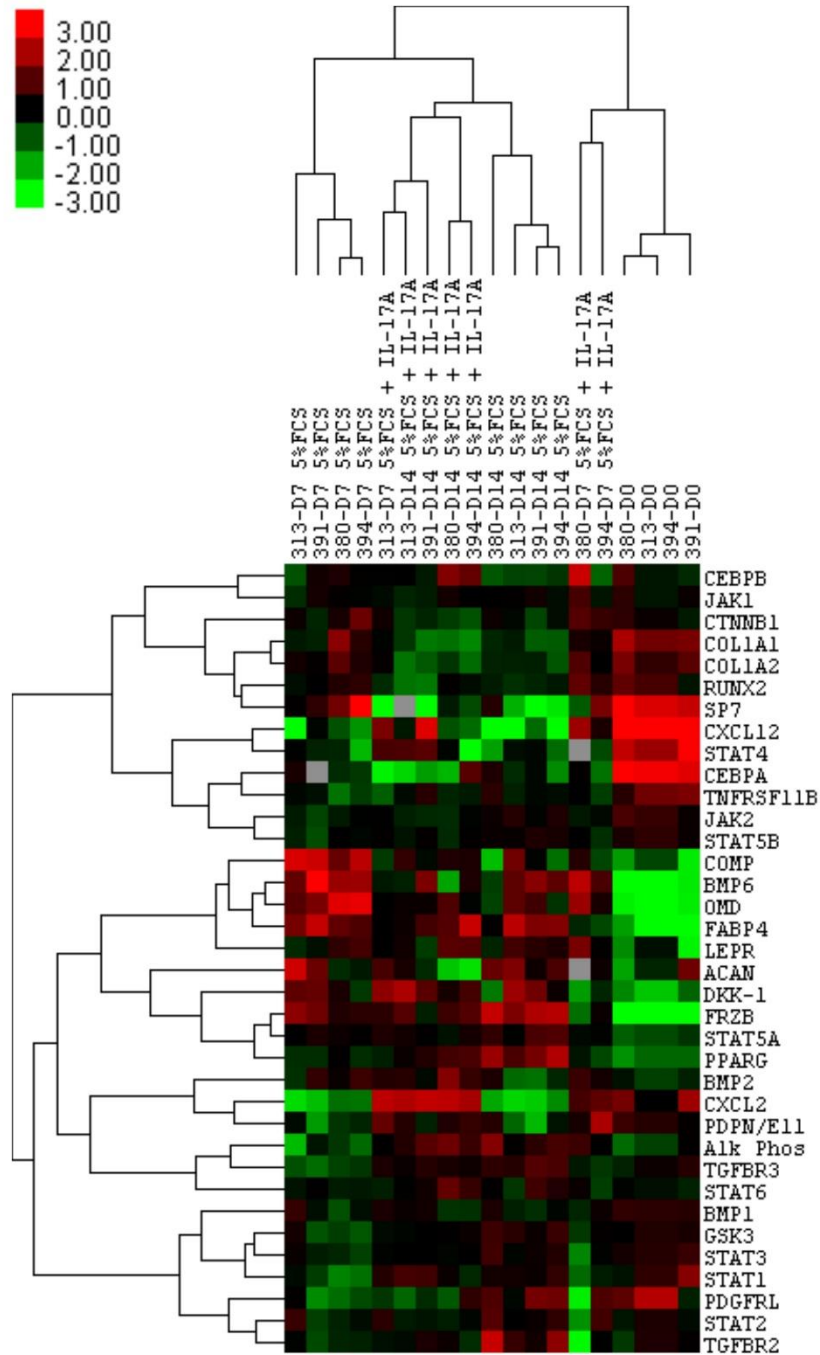
Figure 4.4: Hierarchal clustering of PEB MSCs in a 5% FCS osteogenic media +/- IL-17A

PEB MSCs (n = 4) undergoing 14 day osteogenesis ± IL-17A. Hierarchical clustering demonstrates the distinct clustering of unstimulated MSCs undergoing osteogenesis away from MSCs stimulated by IL-17A. Colour denotes the relative expression compared to Hypoxanthine Phosphoribosyltransferase 1 (HPRT1), with green representing low, black representing equal, red representing higher, and grey representing below detection. Numbers denote the sample ID, and D indicates the days in culture.
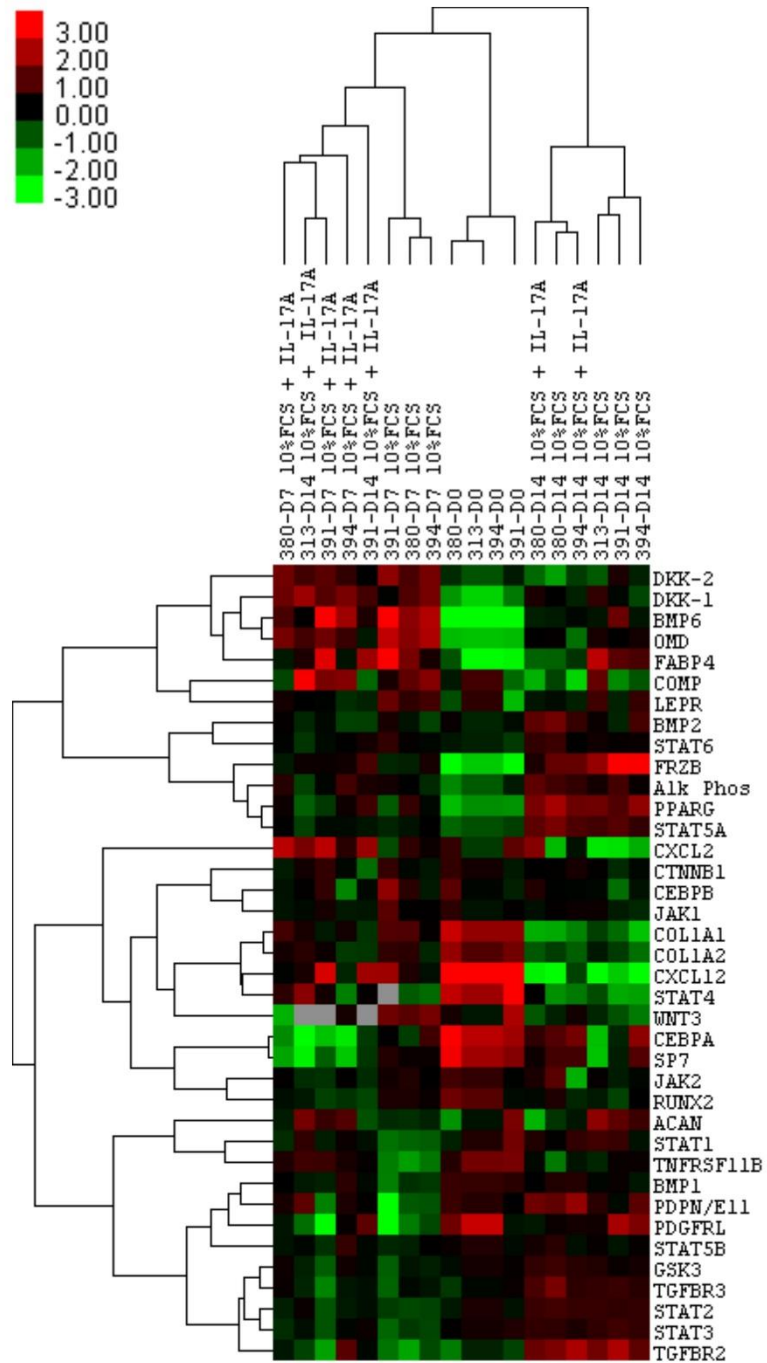
Figure 4.5: Hierarchal clustering of PEB MSCs undergoing osteogenesis in a 10% FCS osteogenic media

PEB MSCs (n = 4) undergoing 14 day osteogenesis ± IL-17A. Hierarchical clustering demonstrates the distinct clustering of unstimulated MSCs undergoing osteogenesis away from MSCs stimulated by IL-17A. Colour denotes the relative expression compared to Hypoxanthine Phosphoribosyltransferase 1 (HPRT1), with green representing low, black representing equal, red representing higher, and grey representing below detection. Numbers denote the sample ID, and D indicates the days in culture.

Genes that showed a high degree of clustering for both 5% and 10% FCS osteogenic media were selected for further paired T-test statistical testing to look for any significant differences in expression induced by IL-17A stimulation.

For both 5% and 10% FCS osteogenic media stimulation with IL-17A showed minor significant changes in osteogenic transcripts. Two regulators of osteogenesis *OMD* and *BMP2* had comparable levels of expression between both control wells and IL-17A stimulated wells. Though at Day 7 *BMP2* for both 5% (Figure 4.6A) and 10% FCS (Figure 4.6B) had higher expression but did reach statistical difference when stimulated by IL-17A compared to the control wells. Interestingly, looking at the expression for transcripts associated with mineralisation *ALPL* and *E11 (PDPN)* at Day 7, expression was higher for the IL-17A stimulated well compared to the control well and did not see much more increase in expression by Day 14 whilst the control well at Day 14 matched the levels of expression. A 5% FCS osteogenic media at Day 7 *ALPL* expression was significantly elevated by IL-17A stimulation compared to the control well ($p<0.05$, Figure 4.6A).

Interestingly, *RUNX2* and *SP7* appeared to be suppressed by IL-17A stimulation, which was a significant suppression in a 10% FCS osteogenic media (Figure 4.6B). On Day 7 *SP7* was significantly downregulated by IL-17A stimulation ($p<0.05$), and *RUNX2* was significantly suppressed at Day 14 ($p<0.05$) but IL-17A stimulation compared to control wells.
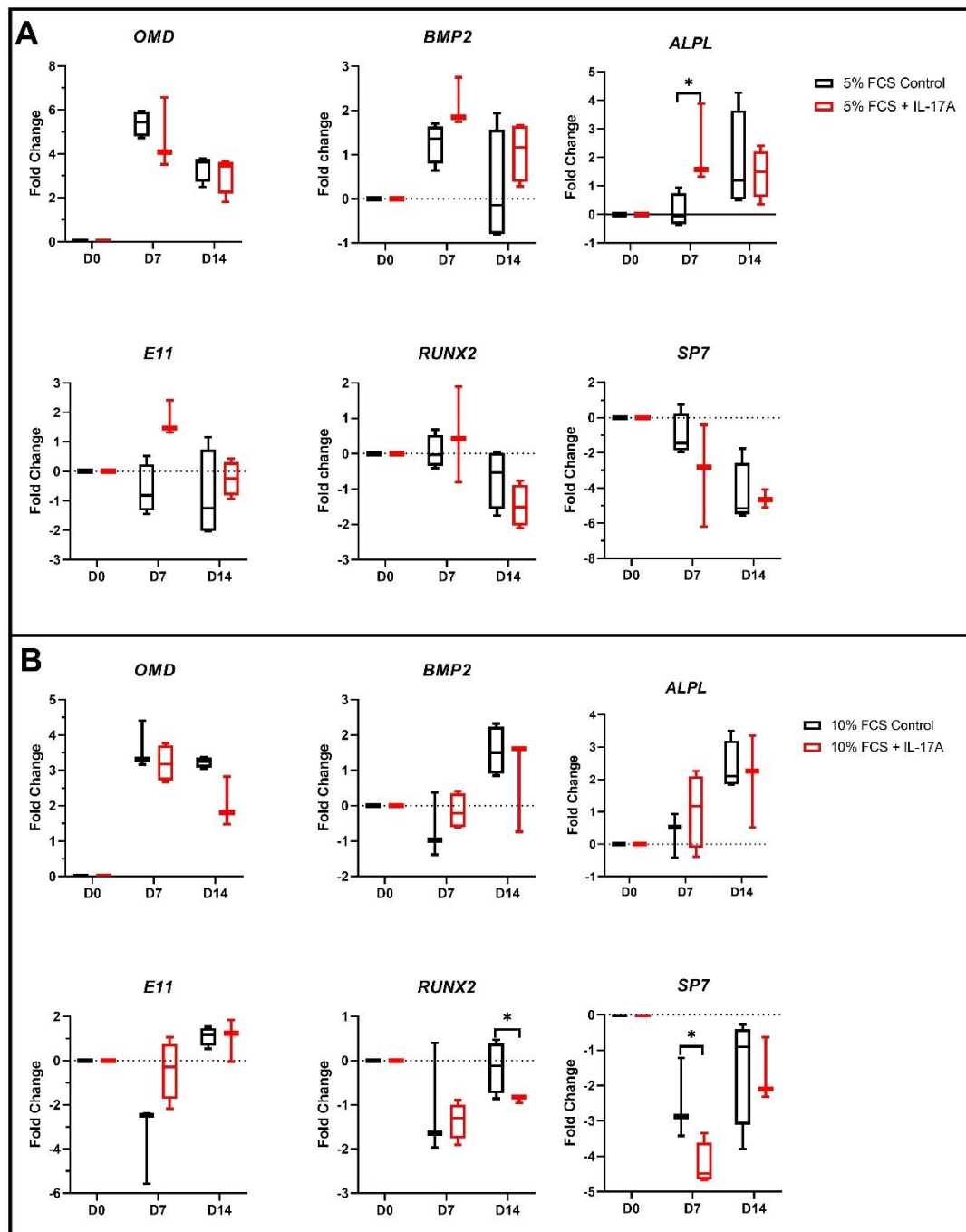
Figure 4.6: Osteogenic transcript changes in PEB MSCs with IL-17A stimulation

*PEB MSCs (n=4 for both) undergoing a 14 day osteogenic differentiation in either a 5% (A) or 10% (B) FCS osteogenic media +/- IL-17A. Using Paired T-tests transcripts relating to mineralisation (ALPL) showed significant early increases at Day 7 in 5% FCS, whilst RUNX2 and SP7 were suppressed by IL-17A. * = p<0.05*

4.3.3.2 – EST MSCs

In a 5% FCS osteogenic differentiation media, EST MSCs showed early elevation of calcium deposition at Day 7 when stimulated with IL-17A, which became significantly elevated ($p<0.05$) at Day 14 (Figure 4.7). However, in a 10% FCS osteogenic media, there were no significant changes in calcium deposition when EST MSCs were stimulated with IL-17A at either time point.
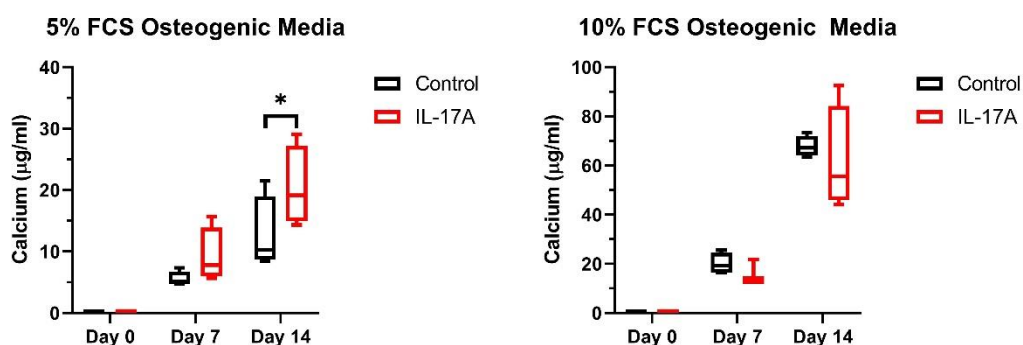
Figure 4.7: Increases in calcium deposition by EST MSCs after a 2 weeks osteogenesis +/- IL-17A

*Addition of IL-17A caused a significant increase in calcium deposition in a 5% FCS osteogenic media at Day 14 (n=4). There wasn't a significant increase in calcium deposition for EST MSCs for a 10% FCS osteogenic media when stimulated by IL-17A (n=4). Analysed using paired T-tests. * = p<0.05*

There was clear clustering of EST MSCs for both 5% FCS (Figure 4.8) and 10% FCS (Figure 4.9). Importantly undifferentiated MSCs were seen in their own distinct cluster for both 5% and 10% FCS osteogenic media. For EST MSCs in a 5% FCS osteogenic media, all the conditions clustered together with unstimulated control wells showing clustering together at both time points were also seen for the IL-17A stimulated wells (Figure 4.8). Compared to EST MSCs in a 10% osteogenic media, clustering was seen primarily related to time with Day 7 for both control and IL-17A wells clustering together and the same for Day 14 (Figure 4.9).
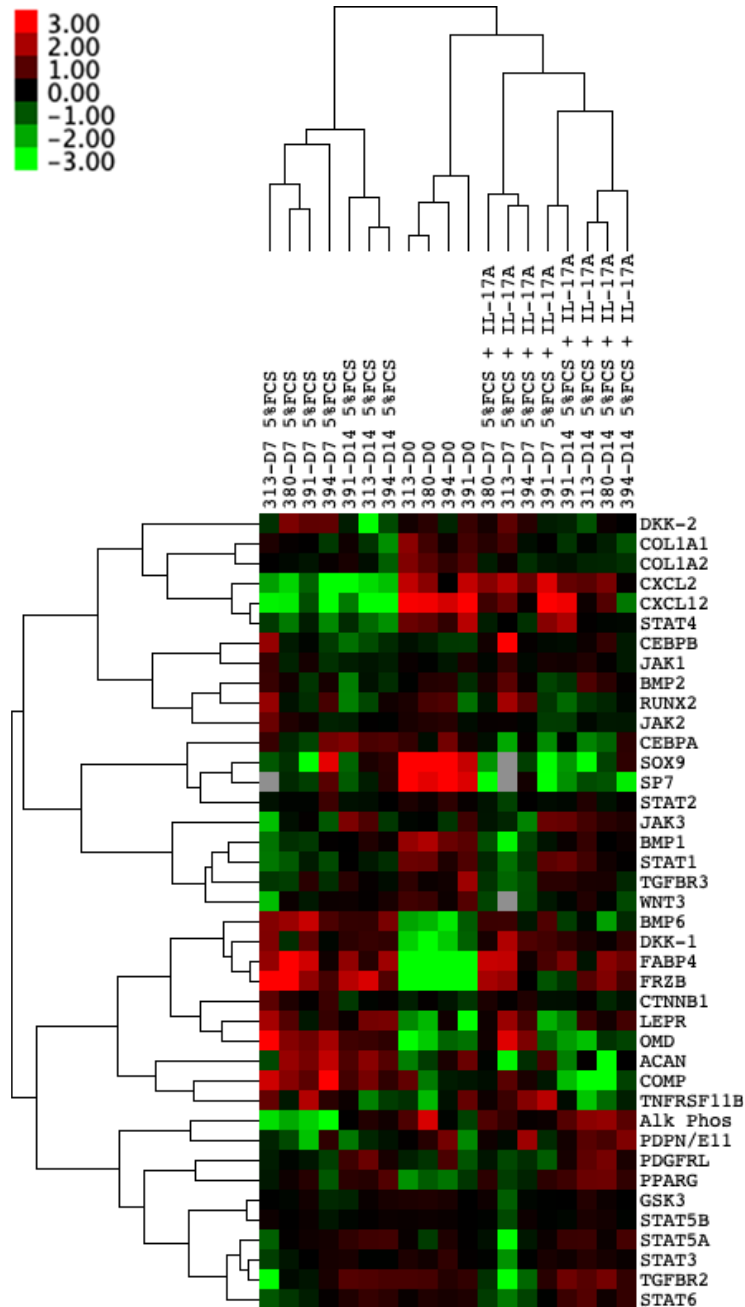
Figure 4.8: Hierarchal clustering of EST MSCs undergoing 14 day differentiation in 5% FCS osteogenic media +/- IL-17A

EST MSCs (n = 4) undergoing 14 day osteogenesis ± IL-17A. Hierarchical clustering demonstrates the distinct clustering of unstimulated MSCs undergoing osteogenesis away from MSCs stimulated by IL-17A. Colour denotes the relative expression compared to Hypoxanthine Phosphoribosyltransferase 1 (HPRT1), with green representing low, black representing equal, red representing higher, and grey representing below detection. Numbers denote the sample ID, and D indicates the days in culture.
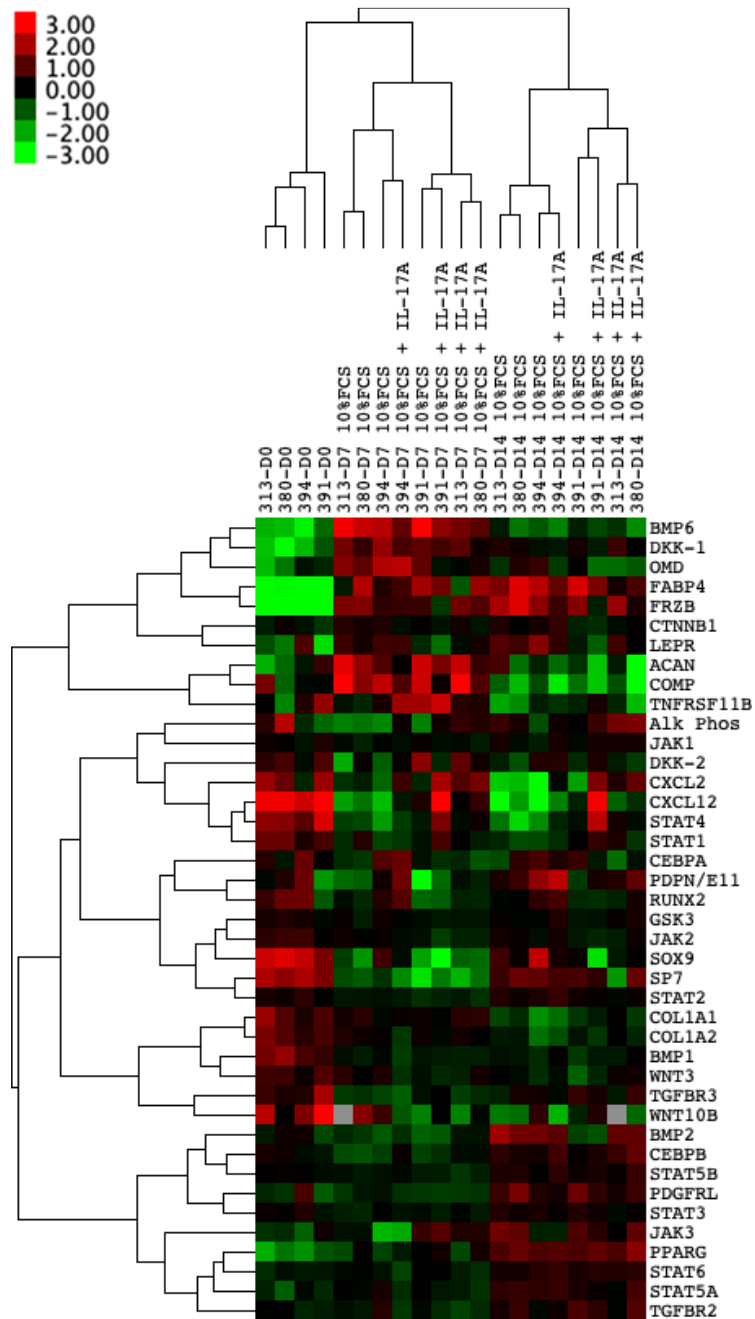
Figure 4.9: Hierarchal clustering of EST MSCs undergoing 14 day differentiation in 10% FCS osteogenic media +/- IL-17A

EST MSCs (n = 4) undergoing 14 day osteogenesis ± IL-17A. Hierarchical clustering demonstrates the distinct clustering of unstimulated MSCs undergoing osteogenesis away from MSCs stimulated by IL-17A. Colour denotes the relative expression compared to Hypoxanthine Phosphoribosyltransferase 1 (HPRT1), with green representing low, black representing equal, red representing higher, and grey representing below detection. Numbers denote the sample ID, and D indicates the days in culture.

After investigating clustering for both the 5% and 10% FCS osteogenic media, genes displaying high clustering and noticeable visual differences were selected for subsequent paired T-tests to look for differences between control and IL-17A stimulation.

As with PEB MSCs, EST MSCs in both 5% (Figure 4.10A) and 10% (Figure 4.10B) FCS osteogenic media stimulated with IL-17A showed significant increases with transcripts associated with mineralisation and osteoblast proliferation. *ALPL* in both the 5% and 10% FCS osteogenic media was significantly upregulated by IL-17A stimulation compared to the control. For the 5% FCS osteogenic media, whilst at Day 7 there was a higher increase in *ALPL* expression associated with IL-17A this only became significant at Day 14 ($p<0.05$). The inverse is true in the 10% FCS osteogenic media where IL-17A induced a significant increase in *ALPL* expression at Day 7 ($p<0.01$), which became non-significant by Day 14 with the control wells matching expression levels. Interestingly, expression of *E11* matched this pattern with significant increases in expression induced by IL-17A on Day 14 for 5% FCS osteogenic media ($p<0.05$) and a significant increase compared to control wells on Day 7 ($p<0.05$) for 10% FCS osteogenic media. *BMP2* as an inducer of osteogenesis from MSCs (66) was seen to be significantly elevated by IL-17A stimulation at Day 7 ($p<0.05$) compared to control well in 10% FCS osteogenic media, though at Day 14 this had inverted with IL-17A showing significantly lower *BMP2* expression compared to control wells ($p<0.001$). No significant differences for *BMP2* were observed in 5% FCS osteogenic media.

IL-17A induced suppression of other osteogenic transcripts, *OMD, RUNX2* and *SP7*. In a 5% FCS osteogenic media, the addition of IL-17A saw trended suppression of all the aforementioned transcripts, and for *OMD* at Day 14 this was a significant suppression ($p<0.01$). With *SP7* showing significant suppression by IL-17A at Day 7 ($p<0.05$). These patterns of suppression were also observed in a 10% FCS osteogenic media, with *OMD* being significantly suppressed at Day 7 ($p<0.05$), *RUNX2* at Day 14 being significantly suppressed ($p<0.05$), along with *SP7* at the same time point ($p<0.05$).
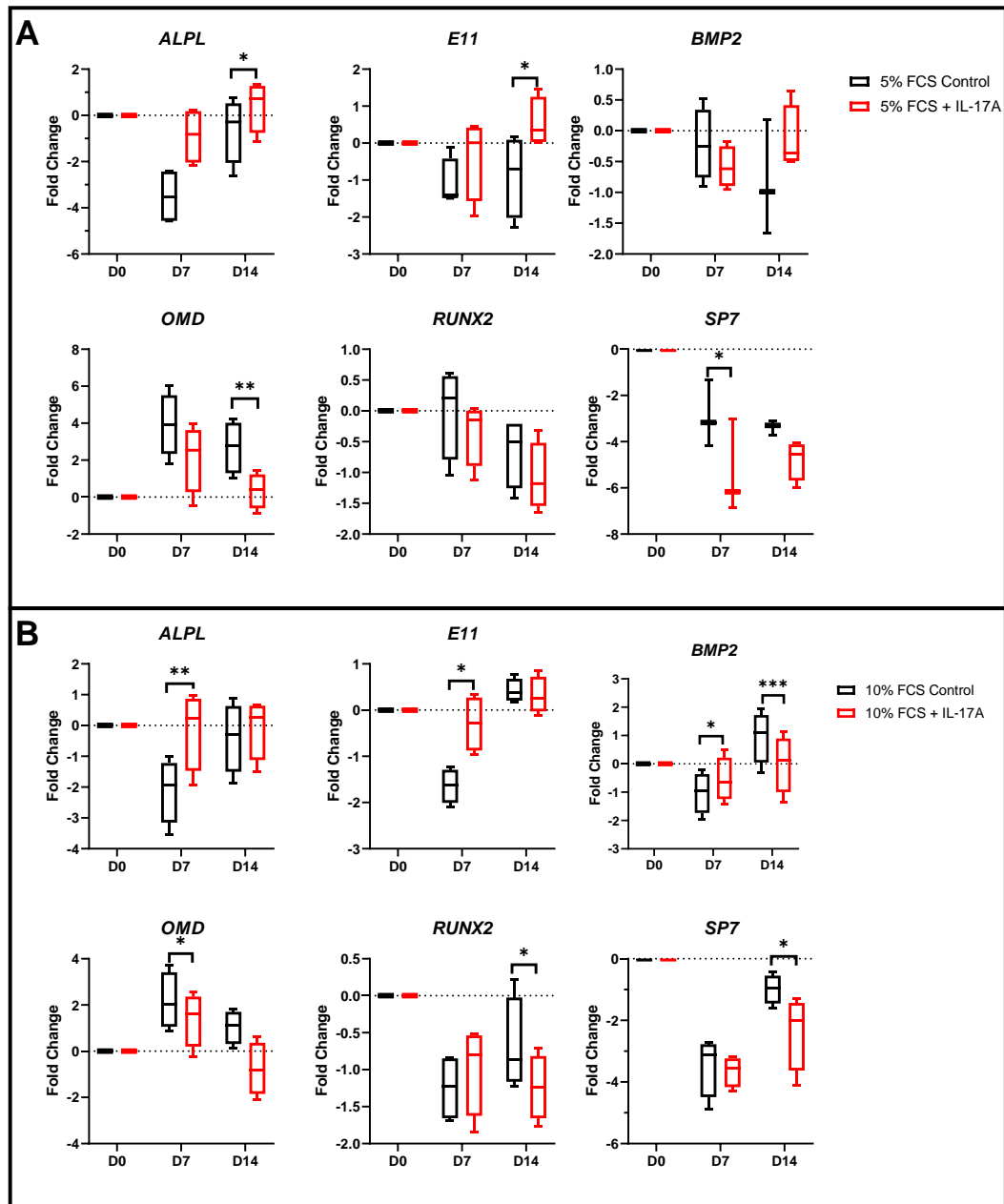
Figure 4.10: IL-17A significantly influences osteogenic transcripts in EST MSCs

EST MSCs (n=4 for both) undergoing osteogenesis have significant increases in osteogenic transcript relating mineralisation and early osteogenesis for both 5% (A) and 10% (B) FCS osteogenic media with IL-17A stimulation. Other transcription factors RUNX2 and SP7 are both suppressed by IL-17A. $8 =p<0.05$, $** = p<0.01$, $*** = p<0.001$.

4.3.4 – IL-17A and TNF suppress adipogenesis from PEB and EST MSCs

Adipogenesis for MSCs from both the PEB and the EST had significant decreases in Oil Red O staining (p<0.05 both) from the lowest concentration of IL-17A used at 10ng/ml (Figure 4.11). The amount of adipogenic suppression was greater at larger concentrations of IL-17A with an eventual levelling off at around 50ng/ml; as a result of this, to keep it consistent with osteogenic assays for all subsequent adipogenesis assays, IL-17A was used at 50ng/ml.
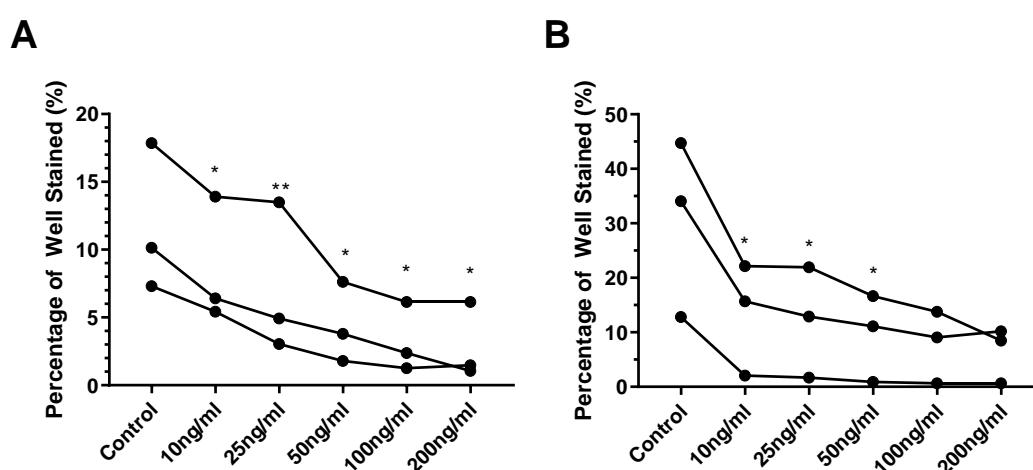
Figure 4.11: IL-17A at all tested concentrations suppress adipogenesis from both PEB and EST MSCs

*The addition of IL-17A at 10ng/ml caused a significant decrease in adipogenesis from both PEB (A) and EST (B) MSCs, with increasing concentrations also showing significant inhibition of adipogenesis. Increasing concentrations of IL-17A decreased adipogenesis compared to lower concentrations for PEB MSCS, whilst EST MSCs appeared to show maximal inhibition at lower levels. * = p<0.05, ** = p<0.01.*

The addition of either IL-17A ($p<0.05$ for both PEB and EST), TNF ($p<0.05$ for PEB, $p<0.01$ for EST) or a combination ($p<0.05$ for both) significantly suppressed the adipogenic potential of both MSCs from both the PEB and the EST (Figure 4.12). IL-17A is the strongest single driver in suppressing adipogenesis from both PEB and EST MSCs, with a 3.75-fold decrease and a 1.95-fold decrease in Oil Red O staining, respectively. This is in contrast to TNF where in PEB MSCs, there was a 2.06-fold decrease and for EST MSCs a 1.22-fold decrease. Of interest was when IL-17A and TNF co-stimulation levels of adipogenic inhibition for both PEB and EST MSCs are comparable levels to IL-17A alone. For PEB MSCs co-stimulation induced a 7.85-fold decrease and in EST MSCs a 1.87-fold decrease in Oil Red O staining. Though this was not seen to be significantly lower when compared to TNF alone. Stimulation of IL-17A caused a change in lipid vesicle morphology, and they are seen to be smaller in size and more numerous or immature compared to the larger mature vesicles seen in control wells.
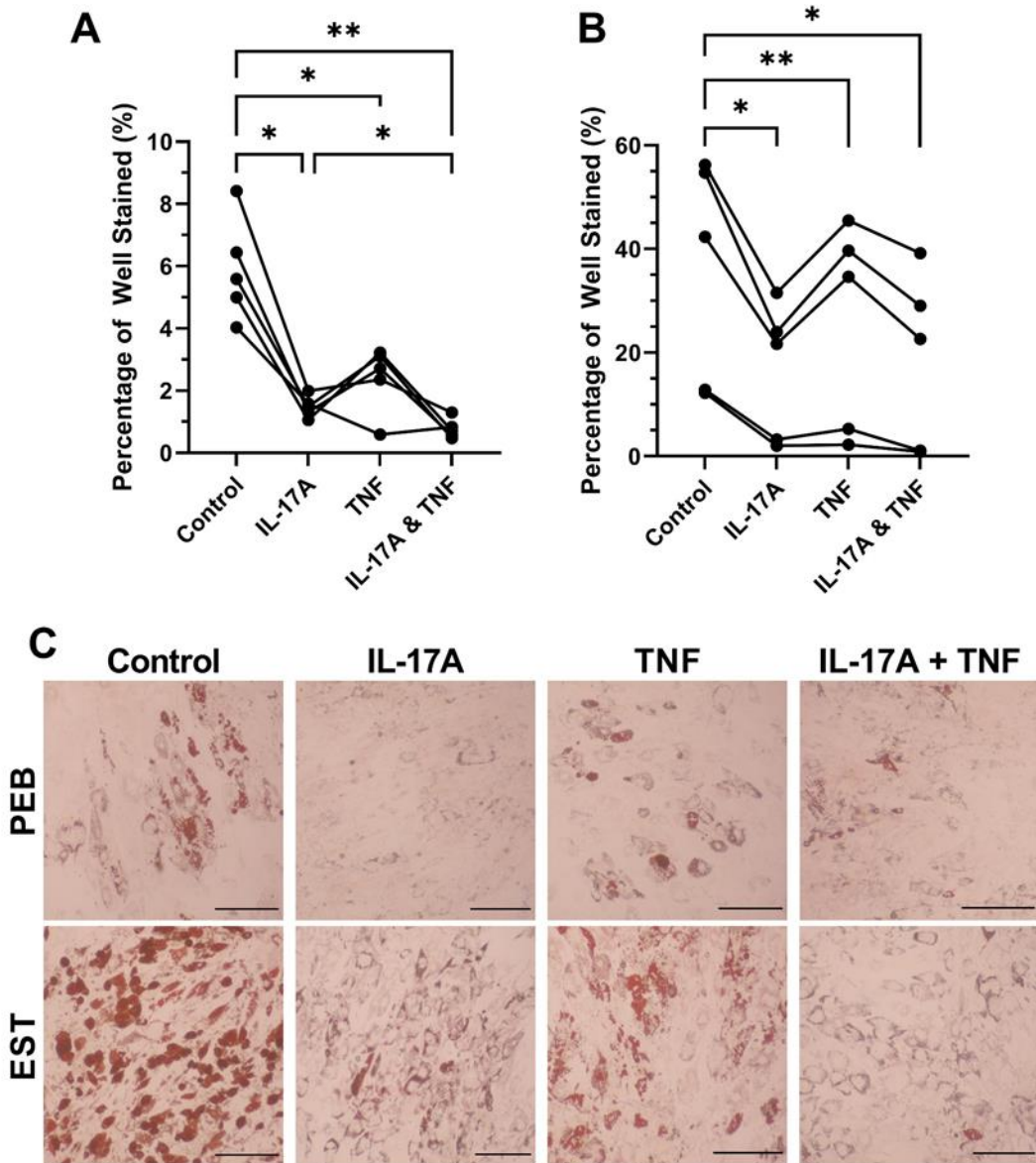
Figure 4.12: IL-17A and TNF inhibit adipogenesis from both PEB and EST MSCs

The addition of IL-17A, TNF or a combination of them both caused significant reductions in adipogenesis for MSCs from both the PEB (A) and the EST (B). Representative images of MSCs after adipogenesis when stimulated by either IL-17A, TNF or a combination of them both (C). * = p<0.05, ** = p<0.01. Scale bar = 100μm.

4.3.5 – IL-17A stimulation suppresses gene expression associated with adipogenesis.

The visual changes in lipid vesicle formation seen during IL-17A were investigated using a time course adipogenic differentiation with RNA extractions at 5 separate time points as well as Oil Red O staining.

The addition of IL-17A caused a significant increase in the number of vesicles stained for Oil Red O in both PEB (Figure 4.13) and EST (Figure 4.14) MSCs (both $p<0.05$) at Day 3 after initiation. However, by Day 5 this difference in staining had closed to near-identical levels and the same was seen at Day 7. On Day 15 there was a significant reduction in Oil Red O staining for both EST ($p<0.01$) and PEB ($p<0.05$) when stimulated with IL-17A compared to control well. This was also seen on Day 21 with IL-17A inducing significant suppression of adipogenesis for both PEB and EST MSCs.
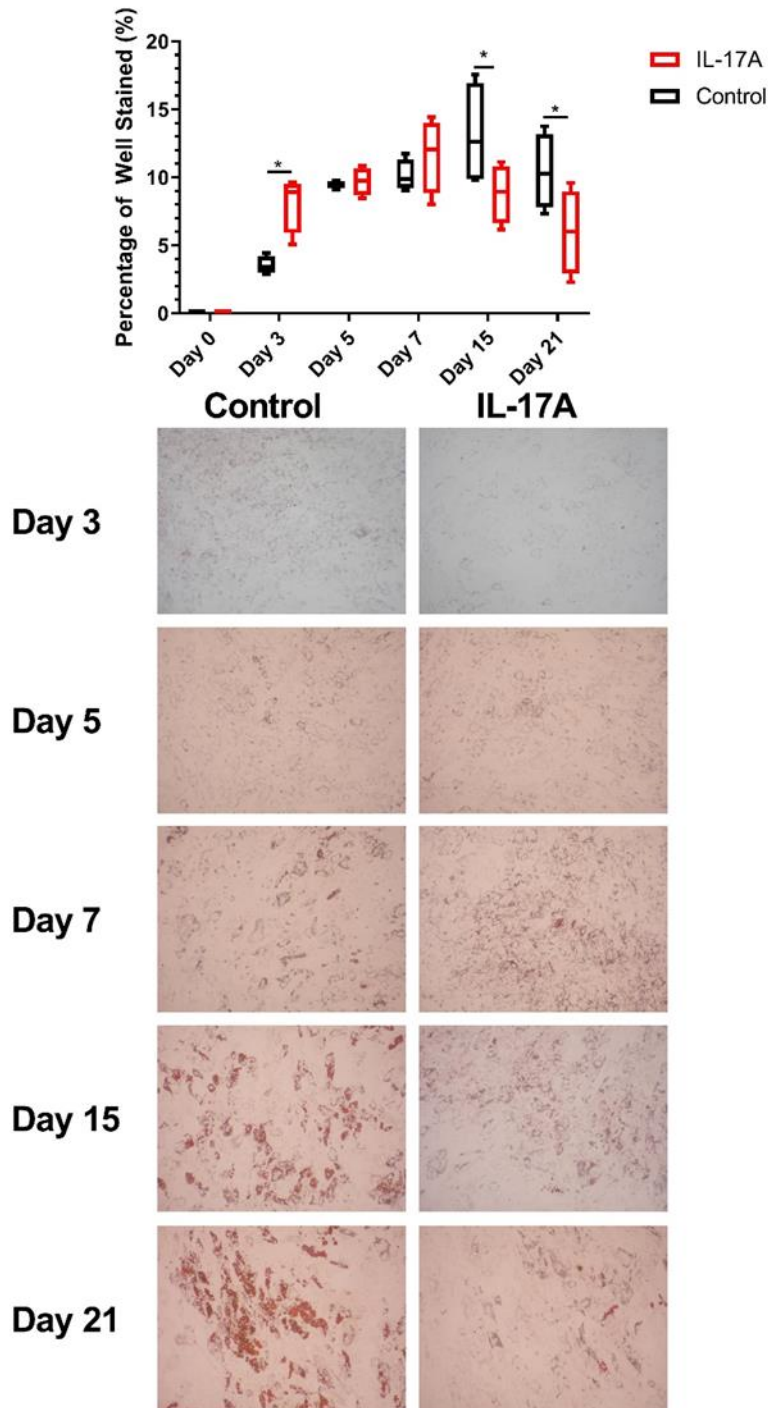
Figure 4.13: IL-17A associated suppression of adipogenesis over 21 day differentiation in PEB MSCs

*IL-17A shows a significant increase in Oil Red O stained area on Day 3 after initiation of adipogenesis compared to the control well. The suppressive effects of IL-17A are only seen from Day 15 onwards where there is a significant decrease in Oil Red O stained area compared to the control well. N=4, * = p<0.05.*
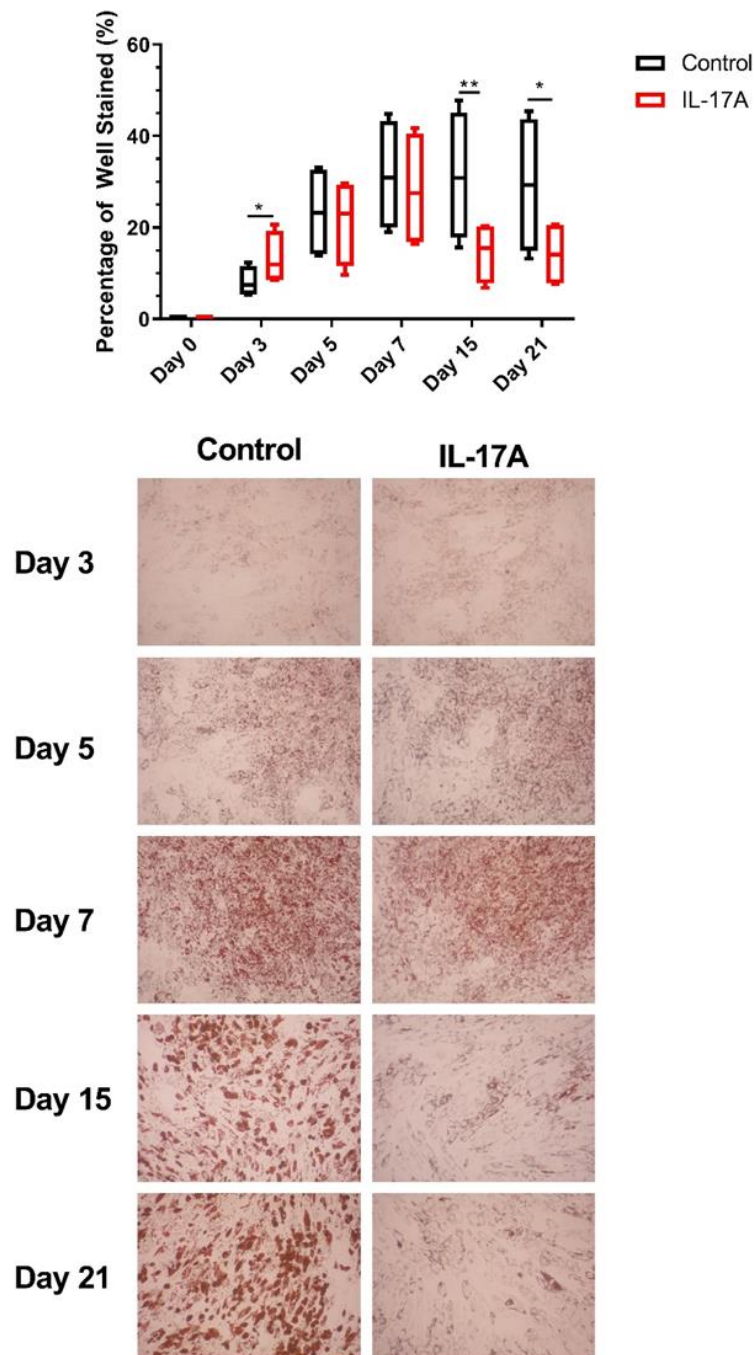
Figure 4.14: IL-17A associated suppression of adipogenesis over 21 day differentiation in EST MSCs

IL-17A shows a significant increase in Oil Red O stained area on Day 3 after initiation of adipogenesis compared to the control well. The suppressive effects of IL-17A are only seen from Day 15 onwards where there is a significant decrease in Oil Red O stained area compared to the control well. As the control wells adipocytes appear to mature from Day 15, those which are stimulated by IL-17A appear to be held in an immature vesicle phase with limited vesicle fusion. N=4, * = p<0.05, ** = p<0.01.

The hierarchal clustering of EST MSCs over a time course of adipogenesis with or without IL-17A stimulation showed cleared clustering of an array of genes associated with not only adipogenesis but also some immunomodulatory transcripts (Figure 4.15). The clustering was split into three main clusters of undifferentiated MSCs, control well and wells, which were stimulated with IL-17A all showing different expressions of transcripts.
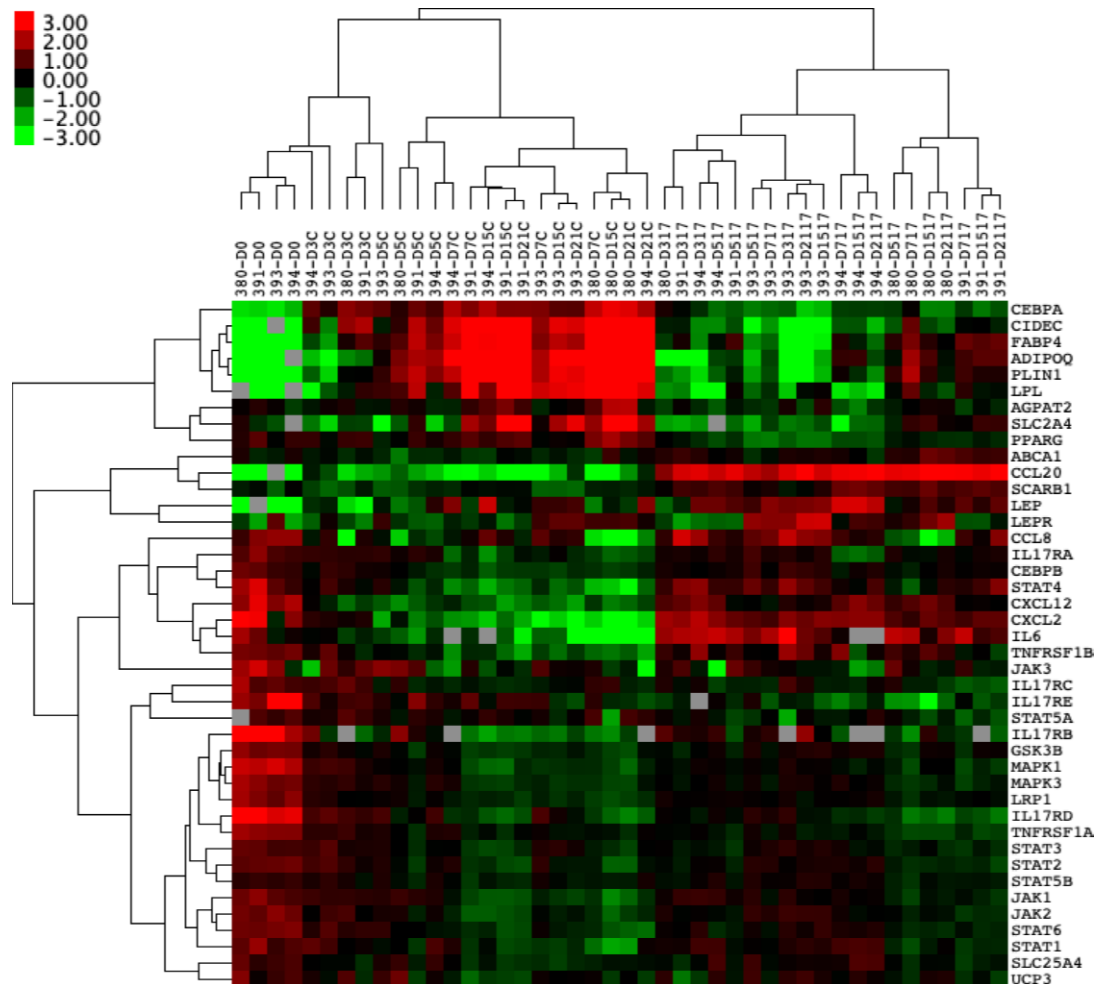
Figure 4.15: Hierarchal clustering of EST MSCs undergoing 21 day adipogenesis +/- IL-17A

EST MSCs (n = 4) undergoing 21-day adipogenesis ± IL-17A. Hierarchical clustering demonstrates the distinct clustering of unstimulated MSCs undergoing osteogenesis away from MSCs stimulated by IL-17A. Colour denotes the relative expression compared to Hypoxanthine Phosphoribosyltransferase 1 (HPRT1), with green representing low, black representing equal, red representing higher, and grey representing below detection. Numbers denote the sample ID, and D indicates the days in culture.

In EST MSCs despite the early elevation at Day 3 of Oil Red O staining in IL-17A stimulation compared to control wells (Figure 4.14), this was not reflected in genetic transcription regulation. The master regulator of adipogenesis *PPARγ* (391, 444) was significantly downregulated by IL-17A compared to a control well at Day 3 ($p<0.05$), with larger levels of suppression seen at Day 15 ($p<0.01$) and Day 21 ($p<0.001$, Figure 4.15). With significant suppression by IL-17A of PPARγ co-regulator *CEBPα* seen from as early as Day 3 ($p<0.01$) that remained significantly suppressed at every other time point, this suggests at an alternate explanation for the increase Oil Red O staining seen at Day 3 after IL-17A stimulation.

The observed lipid vesicle morphology changes when EST MSCs were stimulated with IL-17A (Figure 4.12, Figure 4.13) and their more immature appearance is supported by the suppression of genes associated with mature vesicles and proteins associated with vesicle fusion. Two transcripts that showed high degrees of clustering and are associated with mature adipocytes were *FABP4* and *ADIPOQ*, both showed significant downregulation in IL-17A stimulated cultures from Day 7 onwards ($p<0.01$ for both). At this time point in the Oil Red O staining the forming of mature adipocytes start with greater numbers being present in the two subsequent time points in the control well. With only a few number seen in IL-17A stimulated well, in fact reducing in the two subsequent time points.

Supporting the low number of mature adipocytes seen in IL-17A stimulated wells significant downregulation was compared to control wells of vesicle fusion proteins needed for adipocyte maturation. *PLIN1* and *CIDEC,* both vesicle fusion proteins, were significantly downregulated from Day 3 ($p<0.05$ for both) and remained so for the remainder of the time in culture.

Two other genes of interest that show high clustering were *CXCL12* and *CCL20.* Whereas *CXCL12* expression decreased in control well over the course of adipogenesis, when stimulated with IL-17A expression of *CXCL12* remained significantly elevated from Day 3 compared to the control wells ($p<0.05$) and at all remaining time points. At the same time, *CCL20* was significantly upregulated by stimulation of IL-17A compared to the control wells from Day 3 ($p<0.01$, Figure 4.15) and at all subsequent time points.
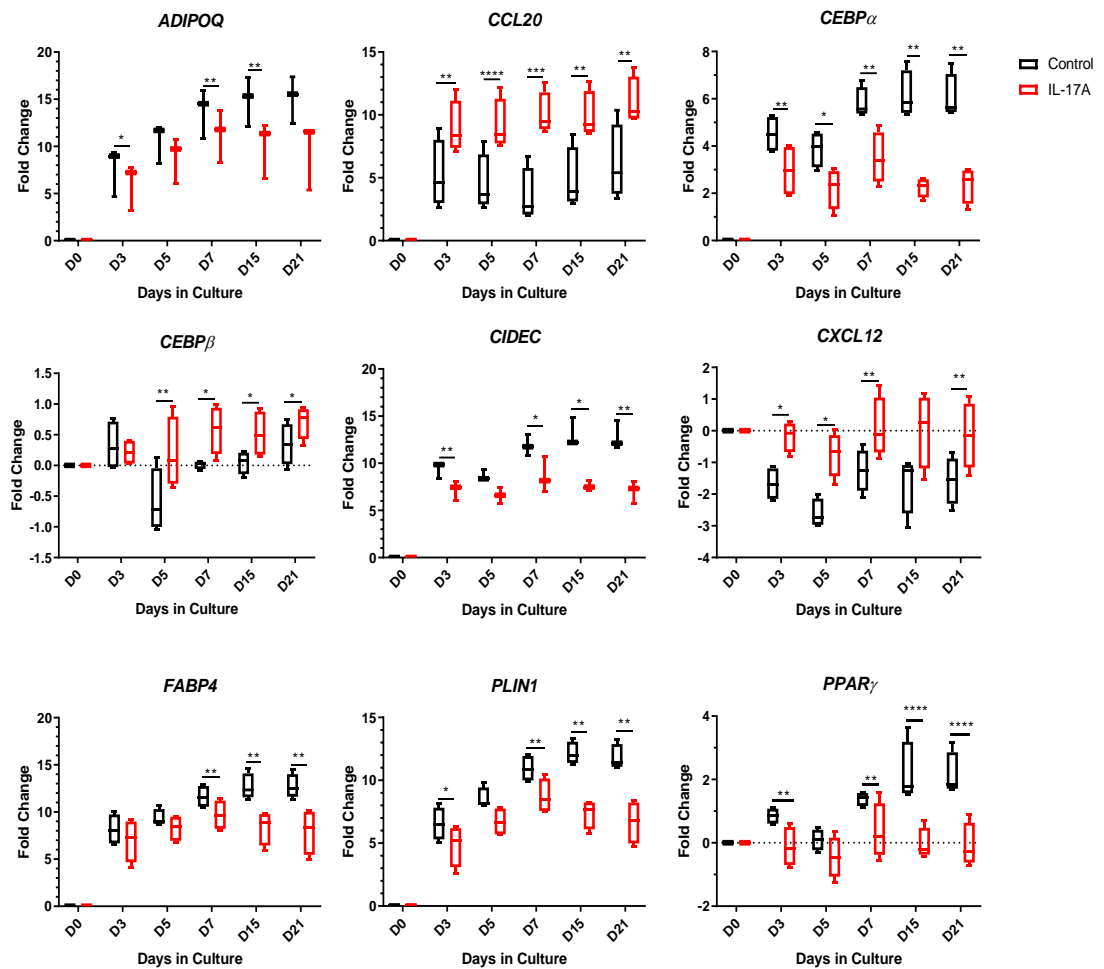
Figure 4.16: Changes in adipogenic and immunomodulatory transcripts induced by IL-17A during adipogenesis

EST MSCs (n = 4) undergoing 21 day adipogenesis ± IL-17A. Transcripts relating to adipogenesis and vesicle fusion (paired t-tests) show significant downregulation by the stimulation of IL-17A. Transcripts relating to MSC stromal support (CXCL12) and inflammatory cell migration (CCL20) show significant upregulation by the stimulation of IL-17A compared to a control adipogenic media. * = p<0.05, ** = p<0.01, *** = p<0.001, and **** = p<0.0001

When looking at the clustering of PEB MSCs, due to the poor adipogenic potential of these cells, often it was hard to detect gene expression changes as they were very subtle in some cases. Though the clustering was not as clear as EST MSCs, clusters were still evident, and similar gene clustering was seen between undifferentiated MSCs, control wells and well that were stimulated with IL-17A (Figure 4.17).
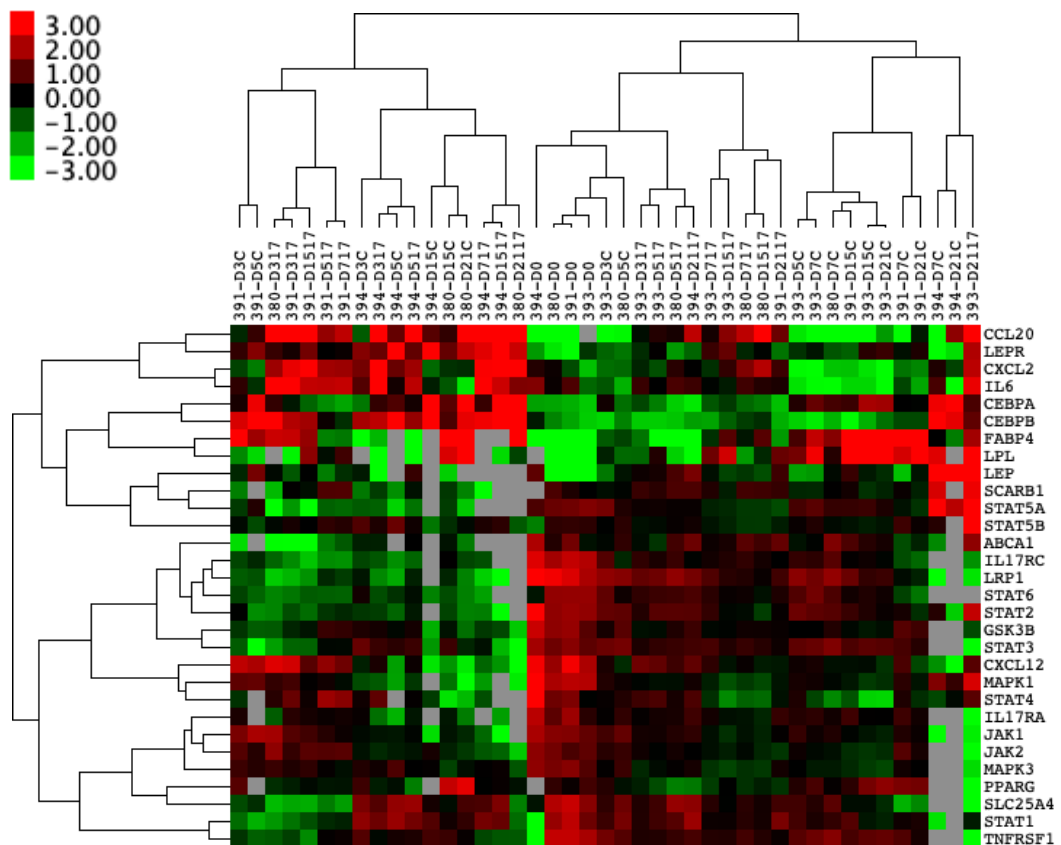
Figure 4.17: Hierarchal clustering of PEB MSCs undergoing 21 days adipogenesis +/- IL-17A

PEB MSCs (n = 4) undergoing 21 day adipogenesis ± IL-17A. Hierarchical clustering demonstrates the distinct clustering of unstimulated MSCs undergoing osteogenesis away from MSCs stimulated by IL-17A. Colour denotes the relative expression compared to Hypoxanthine Phosphoribosyltransferase 1 (HPRT1), with green representing low, black representing equal, red representing higher, and grey representing below detection. Numbers denote the sample ID, and D indicates the days in culture.

Despite the poor adipogenic potential of PEB MSCs, the transcripts relating to immunomodulation and vesicle fusion all showed the same suppression patterns by IL-17A as EST MSCs. *PPARγ* was only seen to be significantly suppressed ($p<0.05$, Figure 4.18) at Day 15 of adipogenesis by IL-17A. Adipogenic transcripts for mature adipocytes (*FABP4)* was seen to be significantly downregulated from as early as Day 5 ($p<0.01$) in PEB MSCs by IL-17A, which was supported by the suppression of the vesicle fusion proteins CIDEC and PLIN1 which were seen to be suppressed from Day 5 ($p<0.05$) for *PLIN1* and Day 7 ($p<0.01$) for *CIDEC* with continued suppression for the remainder of the time in culture. The poor adipogenic potential of PEB MSCs was also supported by the similar expression of the stromal support marker *CXCL12* when comparing between control and stimulated wells, as it was upregulated by IL-17A in EST MSCs.
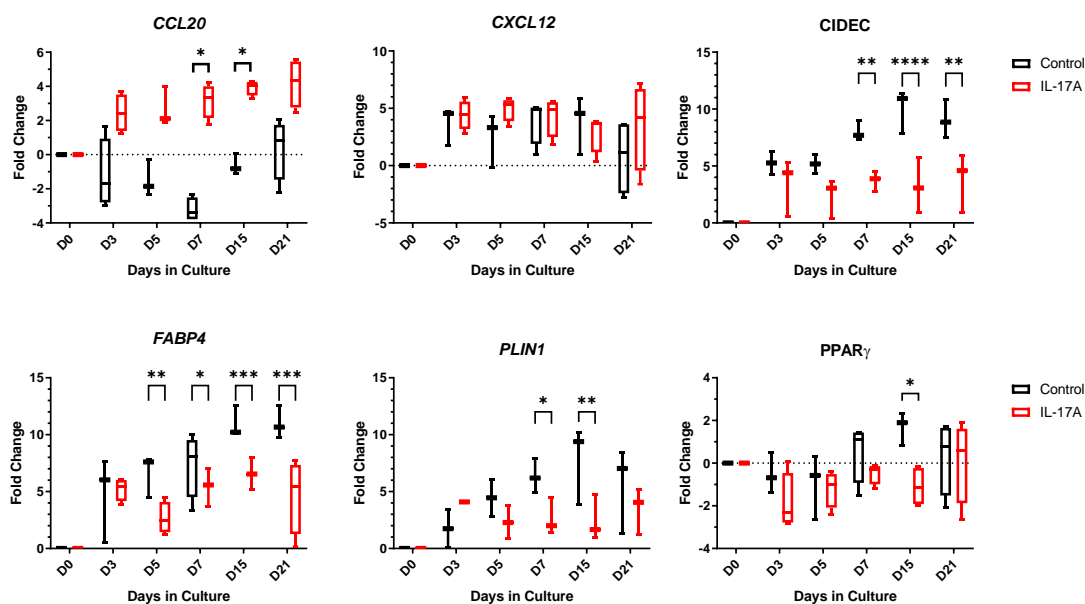
Figure 4.18: Adipogenic and immunomodulatory transcripts influenced by IL-17A in PEB MSCs undergoing adipogenesis

*PEB MSCs (n=4) undergoing adipogenesis showed significant suppression of transcripts associated with adipogenesis and immunomodulation. Though the stromal support marker CXCL12 was not significantly changed. * = p<0.05, ** = p<0.01, *** = p<0.001, **** = p<0.0001.*

4.4 – Discussion

The human spinal enthesis is an area that by its very nature is subjected to continual loading and an array of biomechanical stresses (51, 445). As a result of this continual loading, the normal axial enthesis shows microdamage which needs to be repaired via immune system interventions (51, 445). During this tissue repair process, the immune system involves an array of cytokines, though these same cytokines which normally help tissue repair can also facilitate AS pathogenesis with IL-17A and TNF being particularly prevalent in normal tissue repair (20).

Briefly for osteogenic assays, it is important to acknowledge the limitations associated with *in vitro* differentiation assays, with their reliance on corticosteroids for differentiation induction, and the difficulty in extrapolating the results to the *in vivo* scenario. Dexamethasone is essential in the initial stages of *in vitro* osteogenic differentiation and is likely to play an inhibitory role in any inflammatory cytokine signalling.

While some studies have reported that TNF increases MSCs' osteogenic potential (433), we found that TNF only increased spinal MSC osteogenesis in PEB-derived MSCs in 5% FCS osteogenic media. Further work would be needed to fully determine why this is the case across these populations of MSCs, though these cells may require an additional stimulus to respond to TNF in an osteogenic manner. Dual stimulation with IL-17A and TNF significantly increased the osteogenic potential of both PEB and EST MSCs, matching the previously reported synergistic effects on the osteogenic potential of MSCs from bone marrow and synovium (420, 433).

When stimulated with IL-17A both PEB and EST MSCs showed moderate but significant increases in osteogenic potential; this broadly fits with other studies investigating the effects of IL-17A on osteogenesis. Multipotential cells isolated from the facet capsule showed increased osteogenesis when stimulated with IL-17A (67), in fact in murine fracture models IL-17A knockout mice show an impaired fracture response associated with decreased osteoblastic differentiation (60). This impaired fracture repair by IL-17A knockouts could be rescued by supplementation of IL-17A, demonstrating

increase MSC differentiation down an osteoblastic lineage (60). Other work looking at bone marrow-derived MSCs also shows an increase in osteogenesis induced by IL-17A stimulation (419, 432, 433).

Changes in osteogenic transcripts associated with IL-17A stimulation suggested that IL-17A drives a rapid differentiation of MSCs from EST MSCs into osteoblasts. *BMP2* is a known potent inducer of osteoblastogenesis (446). Indeed sera from SpA patients show significantly higher levels of BMP2 compared to osteoarthritis, which is associated with bone loss (447). The levels of BMP2 also correlated with increased IL-17A levels in the sera (447), which fits with what this chapter found where IL-17A stimulation of MSCs also induced increased *BMP2* expression. There is a reported synergistic effect between BMP2 and IL-17A where co-stimulation enhanced ectopic bone formation in *in vivo* bone implants of rabbits (419). The stimulation of osteogenesis by IL-17A was also seen with increased expression of *ALPL* and *E11* which are osteoblastic lineage marker (383, 448, 449).

However, IL-17A caused significant decreases in three transcripts associated with osteogenesis and are seen to be downstream of BMP2's signalling pathway. Silencing of *OMD* in human dental pulp stem cells caused significant downregulation of *ALPL* and mineralisation and was reported to synergise with BMP2 to enhance more mineralised bone in rat mandible defects (450). The decreases in *RUNX2* and *SP7* given the elevation of *BMP2* caused by IL-17A is surprising given that both *RUNX2* and *SP7* are not only heavily involved in osteogenesis but are known to be induced by BMP2 stimulation (451, 452). This could be due to the early increases in differentiation as decreasing numbers of cells are capable of differentiation, as RUNX2 expression is seen to decrease in expression over time in culture (67). It is possible that any effect IL-17A may have had on increasing Run2 expression in line with the elevated *BMP2* expression may have occurred at earlier time points and was subsequently missed by the time points selected in this study. The same is likely true of the lack of changes seen in the previously reported JAK2/STAT3 induced osteogenesis activated by IL-17A (67), where this study extracted RNA at set time points up to 3 days after the last stimulation given the rapid

phosphorylation of these pathways gene expression was most likely missed (453).

A potential alternate pathway *to RUNX2* involves tissue-nonspecific alkaline phosphatase which in AS MSCs is seen to be overactive in driving mineralisation (454) and when bone marrow-derived MSCs were stimulated with TNF or IL-1β they showed a decrease in *RUNX2* expression associated with an increase in mineralisation in collagen-rich environments driven by tissue-nonspecific alkaline phosphatase (455). With mineralisation only requiring the presence of collagen and tissue-nonspecific alkaline phosphatase (456), this could explain the decreased *RUNX2* transcripts with increased osteogenesis given the fact that *in vivo,* the enthesis is a collagen-rich environment and this is where new bone is preferentially formed. Though further work is needed to fully elucidate any mechanisms.

The SpA-associated cytokines IL-17A and TNF caused significant reductions in the adipogenic potential of both EST MSCs and PEB MSCs, with a greater impact of IL-17A adipocyte vesicle maturation suppression. *CIDEC* and *PLIN1*, which are both transcripts that enable the fusion of lipid vesicles to progress into more mature adipocytes (457), were seen to be significantly downregulated in EST and PEB MSCs stimulated with IL-17A. This was supported by the significant downregulation of *PPARγ*, meaning that subsequent transcripts associated with mature adipocytes (*CEBPα*, *FABP4*, and *ADIPOQ*) (444) were further downregulated.

Notably, *CXCL12* remains at levels similar to those of undifferentiated MSCs in cultures stimulated IL-17A, which suggests that IL-17A inhibits the differentiation of EST MSCs into adipocytes, whilst maintaining their ability to attract immune-lineage cells. Interestingly, *CXCL12* expression levels in PEB MSCs were comparable between control wells which in EST MSCs saw a significant decrease compared to IL-17A stimulated wells. This would support the poorer adipogenic potential seen in PEB MSCs where more of the cells are maintaining in their undifferentiated state or acting as a more supportive role than EST MSCs.

Though literature for IL-17A's role in the formation of the fatty tissues is sparse, our findings are similar to those seen in investigations on obesity and

the potential role of IL-17A in developing insulin resistance (435, 439). IL-17A induced the downregulation of proteins associated with protection against lipolysis (*PLIN1* (458)). The *in vitro* findings show the IL-17A suppression of adipogenesis and augmentation of osteogenesis. In AS after inflammation there is an increase in adipogenesis and the formation of shiny corners, these disappear over the following months after which the new bone is typically seen (21, 434). This is also in keeping with the known MSC biology, where full commitment to osteogenesis or adipogenesis represents two different fates (401).

Chapter 5 – Translation towards human disease

5.1 – Introduction

5.1.1 – Spinal enthesis

The enthesis organ concept has long been recognised as the keystone of the progression and indeed initiation of AS and other SpA diseases (52, 413). The enthesis is the area in which the ligament transitions into fibrocartilage which anchors to the bone. In the case of the present thesis the spinous process was studied. Like other entheses, the human spinal enthesis is an area subjected to continual loading throughout life (51, 445). The normal continual loading at both the peripheral and axial entheseal tissues is associated with microcracks in health, thus affording an opportunity for direct cellular communication between bone and soft tissue (51, 445). Throughout the various entheseal attachments of the body there is an abundance of adipocytes, which are likely to play a role in shock absorption at the anchorage sites (52, 459).

Due to the microcracks that develop in healthy physiological "wear and tear" responses, these regions may facilitate both MSCs capable of differentiating down the stromal lineages required for repair, but also populations of immune cells which secrete the cytokines associated with fracture repair (20). Immune cells such as ILC3's (86), γδ T cells (88) CD4+ and CD8+ T cells are all resident to the spinal enthesis (89); other cells such as neutrophils, NK cells and more T cells - as well as other local MSCs - may need to be recruited to the site of the damage to aid in tissue repair (460). A parallel to the microcracks seen in healthy spinal entheseal bone is that of long bone fracture repair, wherein the hours and early days after injury there is a rapid increase in pro-inflammatory cytokines (178, 460). In particular, there is an increase in TNF, which is known to encourage the chemotaxis of MSCs towards the site of injury via upregulation in expression of ICAM-1 and VCAM-1 (131-133).

Beyond TNF, the GWAS studies incriminating the IL-23/17 axis, mouse models of enthesitis dependent on IL-23 and the amelioration of psoriatic arthritis under IL-23/17 pathway blockade turned attention to this pathway (60,

227). A recently emergent pathway is IL-36 (5, 461), there is already evidence of elevated serum levels of IL-36 in psoriasis patients (223, 462). Though its exact potential role is yet to be elucidated it is known to promote lymphocyte infiltration in arthritis and psoriasis (461).

5.1.2 – IL-17A's role and AS serum

It is important to acknowledge that whilst a lot of *in vitro* work on MSCs is conducted using cytokine stimulation in either a single or co-stimulatory fashion with other molecules, *in vivo* this is not the case. Single cytokine stimulation still proves valuable especially when targeting the key drivers of disease. In the case of AS, these are TNF and IL-17A where *in vitro* both cytokines drive osteogenesis in MSC populations (67, 430-432, 463). Inhibition of TNF *in vivo* is shown to diminish neo-osteogenesis in AS (77, 464), with IL-17A blockers still awaiting long term follow-ups but showing early efficacy in reducing new bone (80, 81). The use of AS serum *in vitro* is an important bridge between *in vitro* and the *in vivo* settings due to the plethora of other growth factors and cytokines present in AS serum. Some of which will have synergistic influences together and influence differentiation outcomes, especially in pathways as sensitive as adipogenesis (31, 465, 466).

The Bath ankylosing spondylitis disease activity index (BASDAI) is a graded scoring system ranging from 1 (no/minimal disease activity) up to 10 (highly active disease). Importantly higher BASDAI scores are seen to be associated with increased levels of C-reactive protein (CRP) in patient serum (467, 468). High levels of CRP correlate with increased disease activity and elevated associated new bone formation (468). The use of NSAIDs, anti-TNF and anti-IL-17A helps to slow new bone formation in AS but is also associated with a reduction in CRP levels in patient serums providing evidence for a link between the CRP levels and levels of IL-17A in AS serum (79, 265, 469).

More recently, studies have started stimulating cells either using AS patient serum or serum from stimulated T cell serums. The use of AS serum which has a significantly elevated level of IL-17A induced elevated osteogenesis from bone-derived cells of the facet capsule, this increased osteogenesis was also attenuated by IL-17A inhibition (67). However, IL-17A shares a receptor

complex with IL-17F, which is also shown to be secreted by cells resident to the enthesis in response to injury (59, 83). The current clinically licenced monoclonal antibodies against IL-17 are IL-17A specific, and it is reported that IL-17A inhibition decrease osteogenesis. Dual neutralisation of IL-17A and IL-17F in vitro leads to a greater knockdown of osteogenesis (83). This is relevant as bimekizumab, a dual IL-17A/F blocker, will soon enter the marketplace for psoriasis and spondyloarthropathy. The use of *in vitro* models of AS is still important and point towards the key players *in vivo*, though more models should look towards multi-cytokine stimulations or serum uses given the reported synergism not only between IL-17A/F but also of IL-17 and TNF (83, 420, 443).

The formation of fatty tissues at the enthesis is shown to precede syndesmophyte formation, however, to date the removal of this fat tissue has yet to be resolved, as in late-stage AS the tissue becomes heavily mineralised with little fat or soft tissue remaining (21, 58). Adiposity is associated with low-grade inflammation via increased secretion of TNF, IL-1, IL-6 and IL-8, these are implicated in increased IL-17A secretion from activated T cells (160, 161, 470). Obesity or excessive white adipose tissue has been implicated with psoriasis as a result of this excessive inflammation resulting in IL-17A production (471, 472). IL-17A's is shown to delay the differentiation of MSCs into adipocytes and also impair glucose uptake by increasing lipolysis and the breakdown of adipocytes (435, 439). This would suggest at a role of the fatty tissues at the enthesis, maintaining a low-grade inflammatory state which eventually results in adipolysis and the neo-osteogenesis at the enthesis.

5.1.3 – Hypotheses

This chapter of work aimed to investigate four main hypotheses:

1. The human spinal enthesis contains fat cells in the EST and the PEB has discontinuations in the cortical bone, allowing for potential communication.
2. MSCs from both the EST and PEB express ICAM-1 and VCAM-1 which is upregulated by TNF stimulation.
3. MSCs from both the EST and PEB are capable of secreting T cell chemoattractants when stimulated by IL-17A and TNF.
4. Inhibition of IL-17A in AS serum rescues the adipogenic potential of EST MSCs, which have adipocytes broken down by IL-17A stimulation.

5.2 – Materials and methods

5.2.1 – Histology of the spinal enthesis

To investigate for any discontinuation in the cortical bone of the spinous process, after fixation and mounting in paraffin blocks samples had a minimum of 10 serial sections sectioned. These 10 sections were then stained for either H&E or Masson's Trichrome as described in section 2.6. After staining sections were observed under a microscope to look for discontinuations. A discontinuation was only defined if it was present in the same spot of sequential sections, or was seen to be either reducing or gaining in size across sequential sections. This was done to rule out any discontinuations due to artefacts or a cutting errors during the preparation of the slides.

5.2.2 – Stimulation for ICAM-1 and VCAM-1

Expression of MSC adhesion molecules ICAM-1 and VCAM-1 was investigated using flow cytometry. 50,000 MSCs/well were seeded into 24-well plastic culture plates and allowed to expand until there was >95% confluence. MSCs from both the PEB and EST (n=3 for both) were stimulated for 48-hours using either:

I.   IL-17A (50ng/ml) (83, 420, 432)
II.   TNF (1ng/ml) (83, 420, 432)
III.   IL-17A (50ng/ml) and TNF (1ng/ml) (83, 420, 432)
IV.   IL-36γ (100ng/ml) (223, 473)
V.   Unstimulated control

After 48-hours wells had the media aspirated, and MSCs were disassociated from the plastic culture plates using the trypsin. As soon as MSCs were observed to be detaching from the plastic wells, the trypsin was aspirated into FACS tubes and diluted in 5x the trypsin's volume of PBS to reduce its action. Tubes were then centrifuged at 400g for 5-minutes in preparation for staining using the methodology explained in section 2.4.3, using the antibodies listed in Table 5.1. Compensation was performed using compensation beads using the selected antibodies on each fluorophore. Data was analysed as described in section 2.4.3.

Surface Marker-Conjugate:	Volume Used (µl):	Clone:	Laser (nm):	Emission$_{max}$ (nm):	Company:	Isotype:
ICAM-1 (CD54)-PE	2.5	HA58	488	578	BD Biosciences	Mouse IgG1
VCAM-1 (CD106)-FITC	2.5	51-10C9	488	520	BD Biosciences	Mouse IgG1
Mouse IgG1-PE	5	MOPC-21	488	578	BD Biosciences	N/A
Mouse IgG1-FITC	5	IS5-21F5	488	520	Miltenyi Biotec	N/A
7-AAD	5	N/A	488	647	BD Biosciences	N/A

Table 5.1: Table of antibodies used for ICAM-1 and VCAM-1 staining

5.2.3 – Stimulation for CCL20 and IL-8 protein expression

Protein expression for both CCL20 and IL-8 by PEB and EST was assessed using sandwich ELISAs on the stimulated supernatant. Briefly, a specific monoclonal antibody is coated onto a 96-well plastic plate overnight. Standards and samples are then added to the wells, where the secreted proteins bind to the immobilized capture antibody. Next, a biotinylated monoclonal anti-human detection antibody is added, creating the antibody-antigen antibody 'sandwich'. Avidin-horseradish peroxidase and TMB are added which combines to create a blue colour with an intensity proportionate to the amount of bound protein. A stop solution consisting of H_2SO_4 is added which stops the reaction, changing from a blue to a yellow colour which can be read at 450nm on a microplate reader.

5.2.3.1 – CCL20

Culture expanded MSCs from both PEB and EST (n=6) were plated and allowed to expand to confluence in a 96-well plate, and they were subsequently stimulated with either IL-17A (100 ng/mL), TNF (10 ng/mL), or IL-17A and TNF for 48-hours. These concentrations were selected due to other studies investigating the immunomodulation of MSCs using either IL-17A or TNF (474, 475). CCL20 levels in the supernatant were measured by ELISA (Biolegend), as per the manufacturer's instruction.

5.2.3.2 – IL-8

To investigate the concentrations of the IL-17A monoclonal antibody Ixekizumab (TALTZ) to use, MSCs from both the PEB and EST were stimulated using IL-17A looking for IL-8 protein secretion. 10,000 cells were seeded per well into 96-well flat-bottom plastic culture plates and allowed to reach >95% confluence before stimulation.

5.2.3.2.1 – IL-17A titration

To confirm IL-8 secretion from MSCs, n=2 from both the PEB and EST were stimulated using four different concentrations of IL-17A for 48-hours:

   I.   0ng/ml
   II.   1ng/ml
   III.   25ng/ml
   IV.   50ng/ml
   V.   100ng/ml

After 48-hours supernatant was collected and IL-8 concentration was measured by ELISA (Invitrogen)

5.2.3.2.2 – Ixekizumab (TALTZ) titration

Using the established IL-17A concentration from section 5.2.3.2.1, n=4 MSCs from both the PEB and EST had 10,000 cells/well plated into 96-well flat bottom plastic culture plates, and once >95% confluences cells were stimulated for 48-hours using IL-17A (50ng/ml) +/- Ixekizumab at varying concentrations:

   I.   Unstimulated
   II.   IL-17A + 0µg/ml Ixekizumab
   III.   IL-17A + 0.5µg/ml Ixekizumab
   IV.   IL-17A + 10µg/ml Ixekizumab
   V.   IL-17A + 20µg/ml Ixekizumab
   VI.   IL-17A + 80µg/ml Ixekizumab

After 48-hours supernatant was collected and IL-8 concentration was measured by ELISA.

5.2.4 – AS Serum influences on adipogenesis

Serum from 10 AS patients (Table 5.2, Yorkshire Research Ethics Committee REC 02/55) was pooled together to investigate its influence on the adipogenic potential of EST MSCs and whether IL-17A inhibition by ixekizumab had any effect. The pooled serum was tested using ELISA as per the manufacturer's instructions (Invitrogen) for the presence of IL-17A and TNF.

MSCs from the EST (n=3) were seeded at 50,000 cells per well in 24-well plastic culture plates and supplemented with adipogenic media as described in section 3.2.3, except some wells did not receive FCS but instead the AS serum. Wells were either supplemented with:

I. Adipogenic media + 10% FCS
II. Adipogenic media + 10% FCS + Ixekizumab (20μg/ml)
III. Adipogenic media + 10% AS Serum
IV. Adipogenic media + 10% AS Serum + Ixekizumab (20μg/ml)
V. Adipogenic media + 20% AS Serum
VI. Adipogenic media + 20% AS Serum+ Ixekizumab (20μg/ml)

Plates were cultured for two weeks with half media changes every 3 days, on the 14th day after initiation wells were fixed and stained for adipocytes using Oil Red O as described in section 3.2.3.

Sex:	Age:	BASDAI:	CRP:
M	33	5.6	10
M	39	10	25
F	34	9.7	33
M	29	7.63	32
M	31	8.53	15
F	35	5.15	21
M	28	3	46
M	51	6.5	48
M	35	7.66	32
M	37	7.1	55

Table 5.2: AS patients' serum

5.2.5 – IL-17A effects on adipolysis

To investigate IL-17A effects on adipolysis EST MSCs had 50,000 cells seed per well in a 24-well plastic culture plate and supplemented with adipogenic media +/- IL-17A (50ng/ml), with half media changes every 3 days. Wells were either unstimulated, constantly supplemented with IL-17A or were unstimulated until Day 7 (n=3) or Day 14 (n=3) at which point they were supplemented with IL-17A for the reminder of their time in culture. On the 21st day after initiation, the supernatant was extracted and frozen at -20°C until glycerol content could be measured using an adipolysis kit (Sigma-Aldrich).

5.3 – Results

5.3.1 – Discontinuations exist in the cortical bone of the spinous process

Staining of sections of the spinous process and its entheseal attachment from the interspinous ligament using both H&E and Masson's trichrome staining showed an array of anatomical features that may be relevant for entheseal soft tissue and adjacent bone stromal and immune cell communication.

The cortical bone of the spinous process was not uniform, in fact, on the stained slides there are several areas of bone discontinuations presenting as potential channels of communication between the EST and the PEB. These were evident in both the H&E stained slides (Figure 5.1) as well as those stained with Masson's trichrome (Figure 5.2). The bone of the spinous process was seen to have areas of mature or mineralised bone (red areas) and areas which are regenerated and not fully mineralised stained blue (369), with these regenerated areas seen more prevalently around the entheses attachment areas. The EST also showed large areas of fatty deposit, which fits with the known fatty pads seen at entheseal attachment sites around the body (51).

The same staining was also applied to an AS spinous process sample, the same staining patterns were observed in the section. With discontinuations in the cortical bone at the enthesis observed, and very prevalent fatty tissue deposits seen in the EST (Figure 5.3, Figure 5.4). In addition, there was also evidence of neo-osteogenesis protruding into the EST, suggesting at the formation of the syndesmophytes characteristic of later stage AS. The presence of mineralised bone was largely absent from this sample; this was surprising given the sample came from a 78 year old female (Figure 5.4).
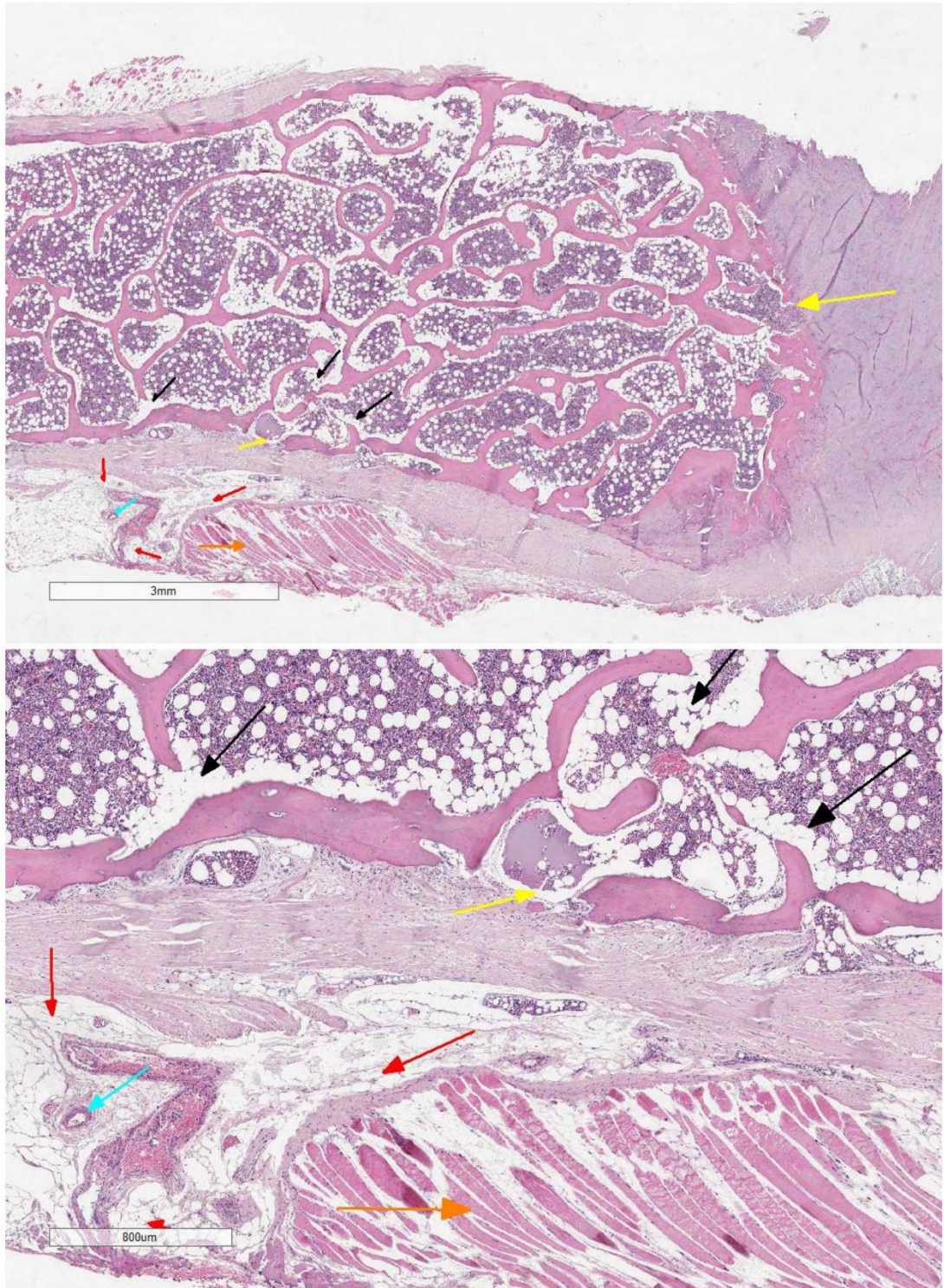
Figure 5.1: Haematoxylin and Eosin stained section of spinous process

Haematoxylin and Eosin stained section of spinous process and interspinous ligament show the discontinuations in the cortical bone (yellow arrow), as well fat cells in the EST component (red arrows). Fatty bone marrow (black arrows), muscles (orange arrows) and blood vessels (cyan arrows) are also observable.
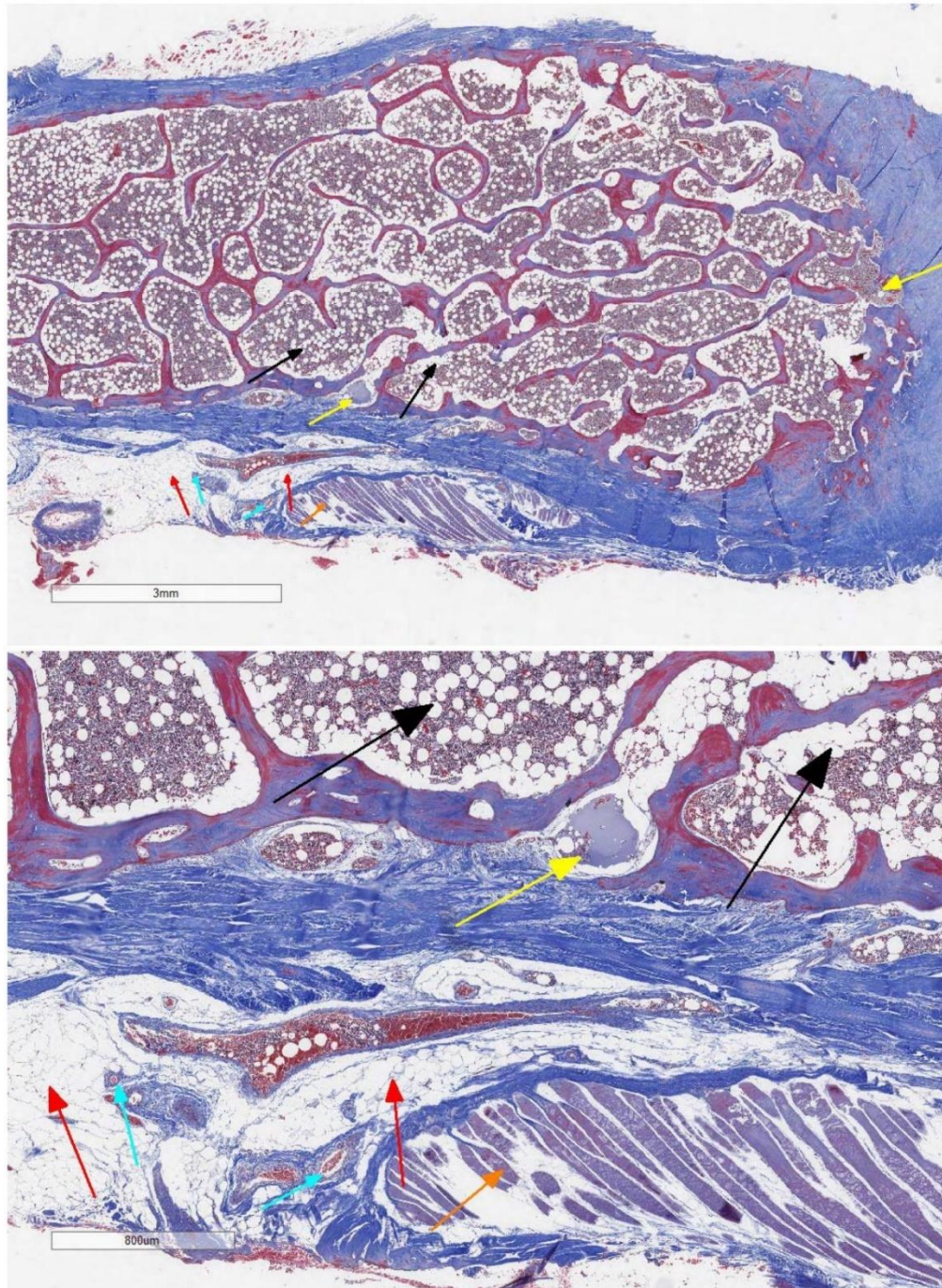
Figure 5.2: Masson's trichrome stained section of spinous process

Masson's trichrome stained section of spinous process and interspinous ligament show the discontinuations in the cortical bone (yellow arrow), as well fat cells in the EST component (red arrows). Fatty bone marrow (black arrows), muscles (orange arrows) and blood vessels (cyan arrows) are also observable. Mineralised bone is stained red by Masson's trichrome, whilst immature or regenerated bone is stained teal opposing the darker blue of ligamentous tissue.
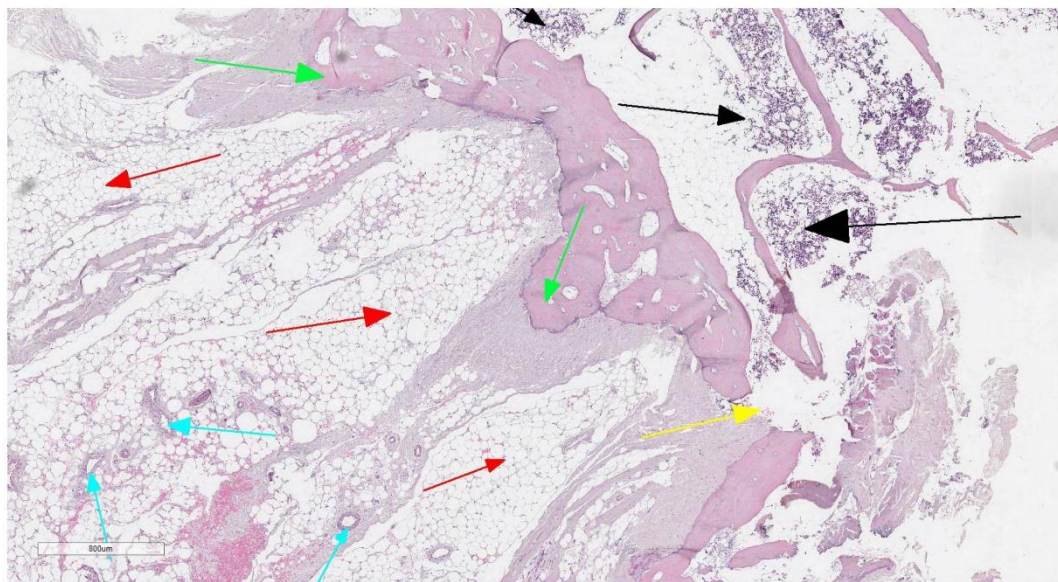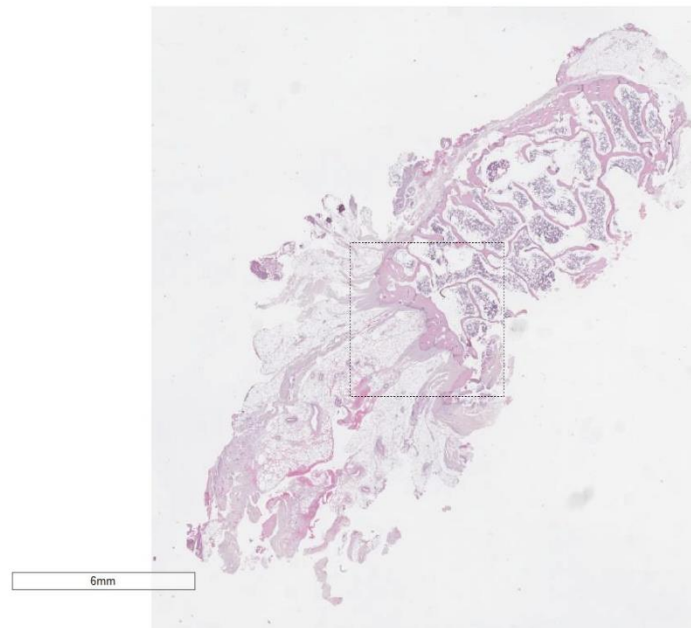
Figure 5.3: Haematoxylin and Eosin stained section of AS spinous process

Haematoxylin and Eosin stained section of spinous process and interspinous ligament show the discontinuations in the cortical bone (yellow arrow), as well fat cells in the EST component (red arrows) opposing the fat seen in the bone marrow (black arrows). Areas of neo-osteogenesis associated with AS are highlighted by the green arrows. Blood vessels are also evident throughout the EST (cyan arrows).
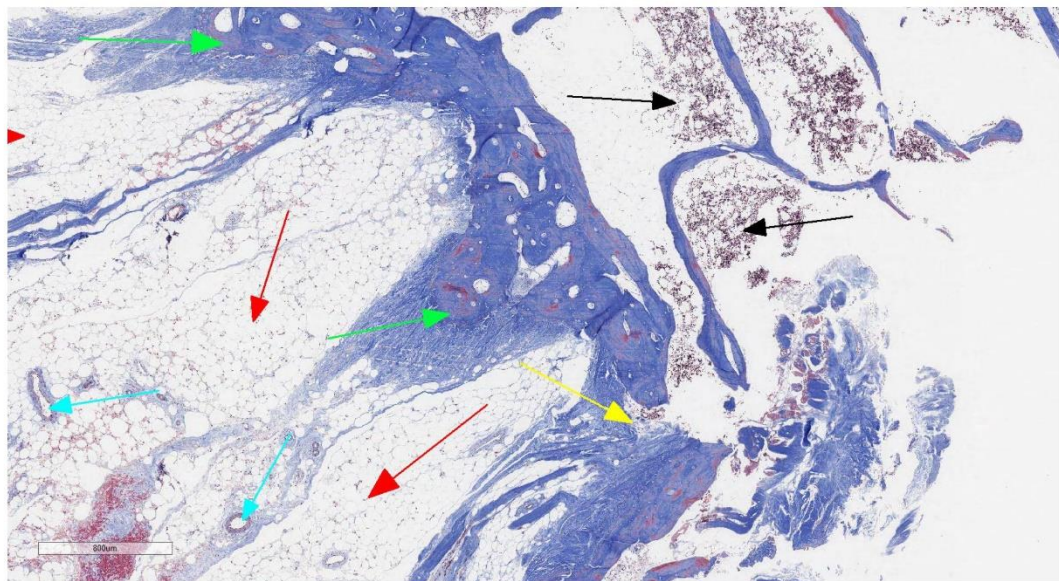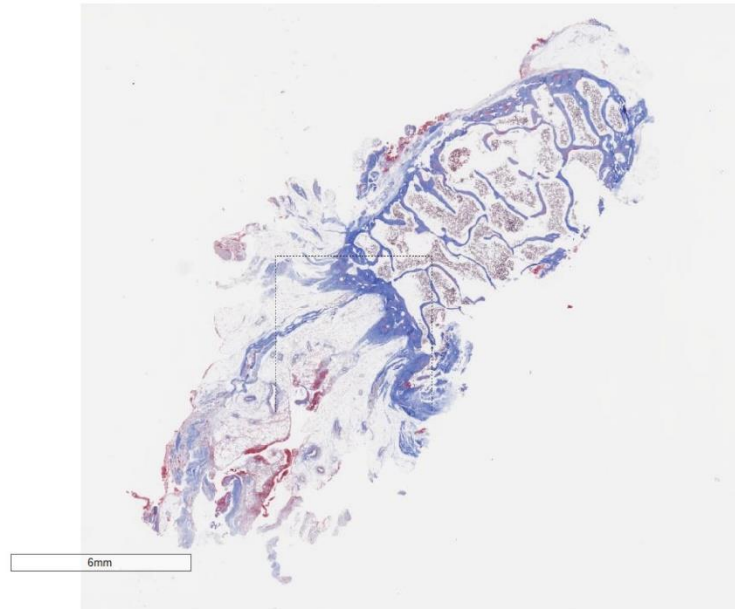
Figure 5.4: Masson's trichrome stained section of AS spinous process
Masson's trichrome stained section of spinous process and interspinous ligament show the discontinuations in the cortical bone (yellow arrow), as well fat cells in the EST component (red arrows) and the bone marrow (black arrows). Areas of neo-osteogenesis associated with AS are highlighted by the green arrows. Mineralised bone is stained red by Masson's trichrome, whilst immature or regenerated bone is stained teal opposing the darker blue of ligamentous tissue. Blood vessels are also evident throughout the EST (cyan arrows).

5.3.2 – ICAM-1 and VCAM-1 expression is upregulated by TNF in EST and PEB MSCs

ICAM-1 and VCAM-1 are both adhesion markers associated with the motility of MSCs, and increased expression is associated with increased MSCs motility (115, 131). TNF stimulation significantly increased the expression of ICAM-1 in both PEB (Figure 5.5) and EST (Figure 5.6, $p<0.05$) MSCs, and this was also seen when co-stimulating with IL-17A where there was also significant increases in ICAM-1 expression ($p<0.01$ PEB MSCs, $p<0.05$ EST MSCs), though there was no clear synergistic effects involving co-stimulation and increased ICAM-1 expression. IL-17A increased ICAM-1 expression on its own in both PEB and EST, though this was only a significant increase in PEB MSCS ($p<0.01$). This was also seen with IL-36γ stimulation where there was a significant increase in ICAM-1 expression for both PEB ($p<0.05$) and EST ($p<0.05$) MSCs.

VCAM-1 expression was at much lower levels than that of ICAM-1 on both PEB and EST when comparing median fluorescent intensities. With the presence of TNF in the stimulation being the driving force for significant upregulation of VCAM-1 expression in both PEB (Figure 5.7, $p<0.05$) and EST (Figure 5.8, $p<0.05$) MSCs. IL-17A alone showed no significant effects on VCAM-1 expression, co-stimulation with TNF resulted in a significant increase of VCAM-1 expression for both the PEB ($p<0.05$) and EST ($p<0.05$). Stimulation with IL-36γ in PEB did cause a modest significant increase in VCAM-1 expression in PEB ($p<0.01$) MSCs, but it did not significantly influence expression on EST MSCs.
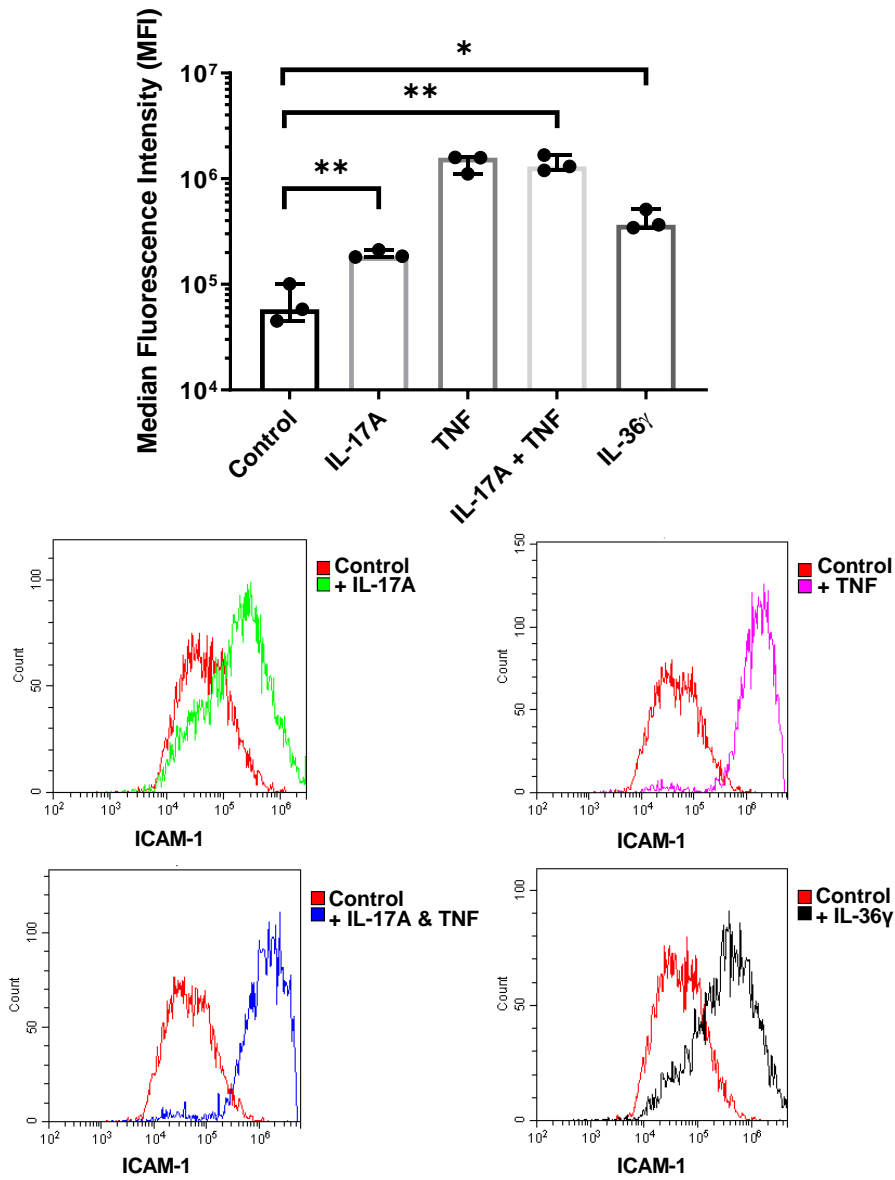
Figure 5.5: Changes in expression of ICAM-1 on PEB MSCs when stimulated by IL-17, TNF or IL-36γ

ICAM-1 was significantly upregulated by stimulation of any tested cytokine, with TNF being the most potent. There were no synergistic effects observed between TNF and IL-17A co-stimulation. Differences in MFI were investigated using Paired T-tests. * = p<0.05, ** = p<0.01.
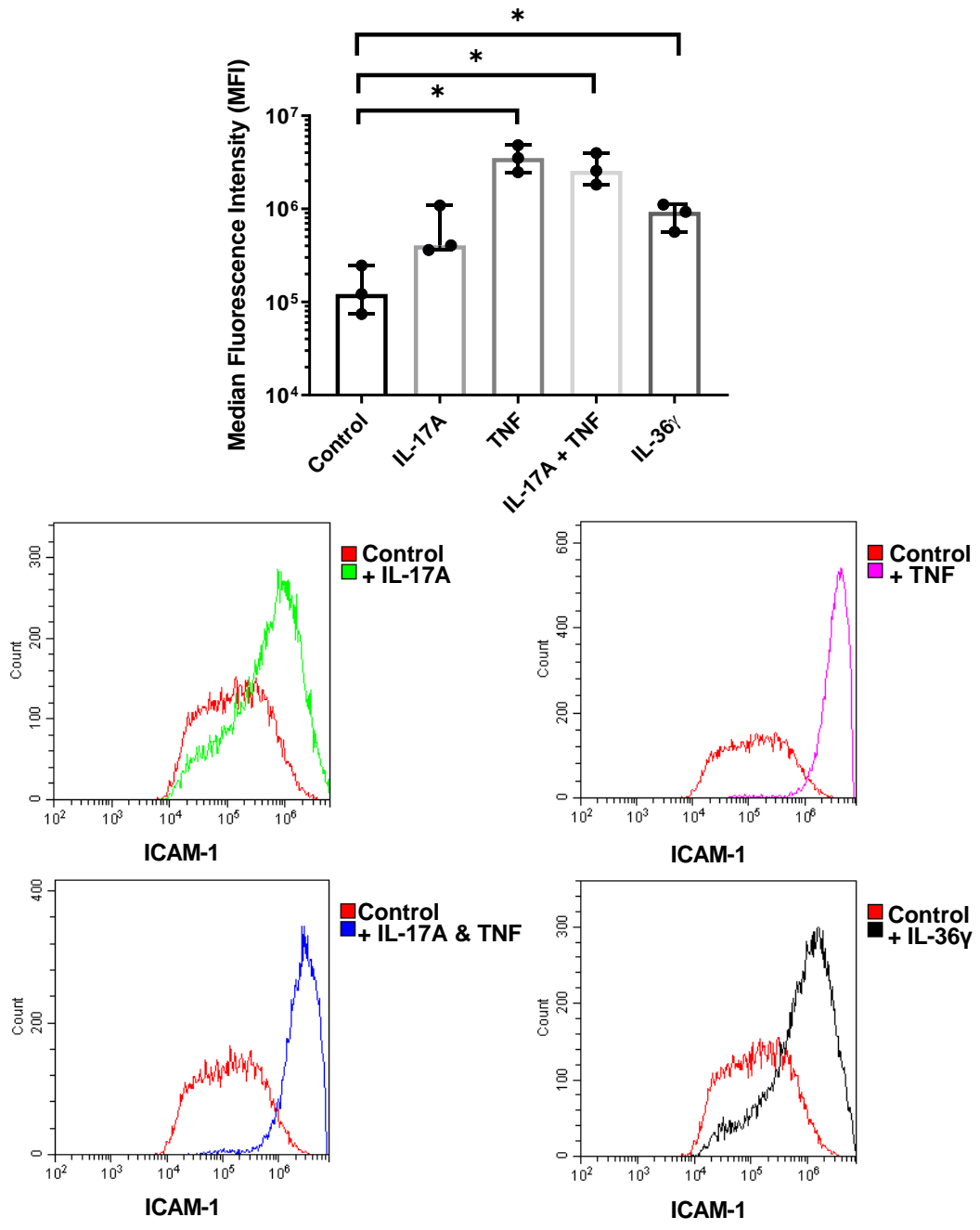
Figure 5.6: Changes in expression of ICAM-1 on EST MSCs when stimulated by IL-17, TNF or IL-36γ

*ICAM-1 was significantly upregulated by stimulation of any tested cytokine, with TNF being the most potent. There were no synergistic effects observed between TNF and IL-17A co-stimulation. Differences in MFI were investigated using Paired T-tests. * = p<0.05.*
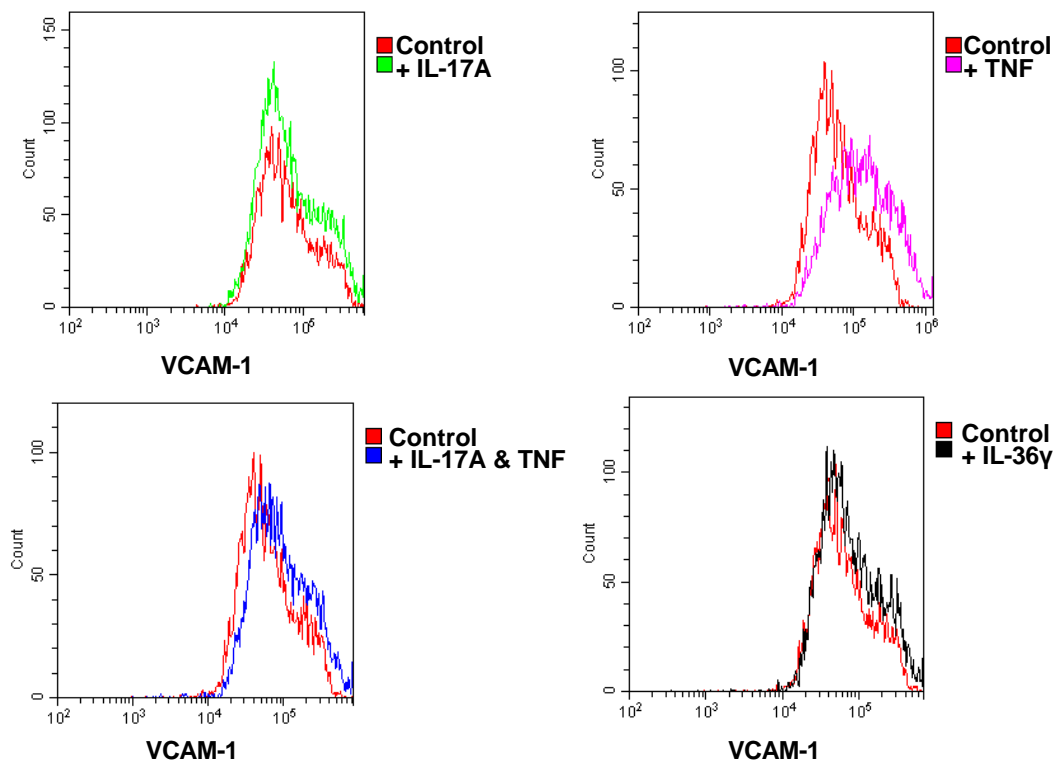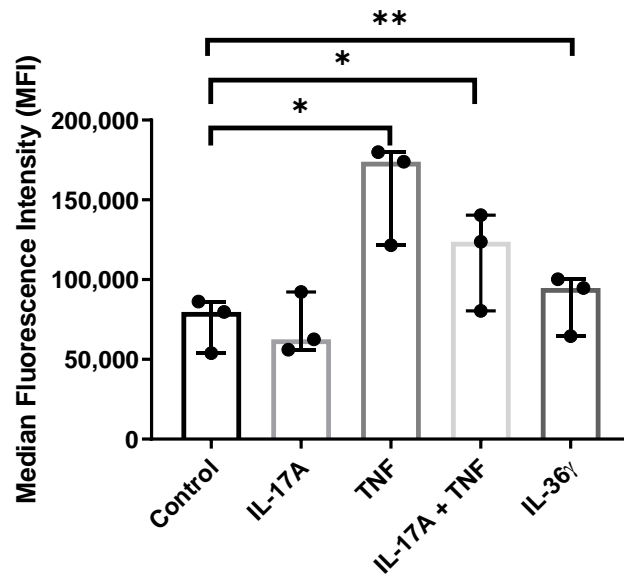
Figure 5.7: Changes in expression of VCAM-1 on PEB MSCs when stimulated by IL-17, TNF or IL-36γ

*VCAM-1 was significantly upregulated by using either TNF or IL-36γ. There were no synergistic effects observed between TNF and IL-17A co-stimulation. Differences in MFI were investigated using Paired T-tests. * = p<0.05, ** = p<0.01.*
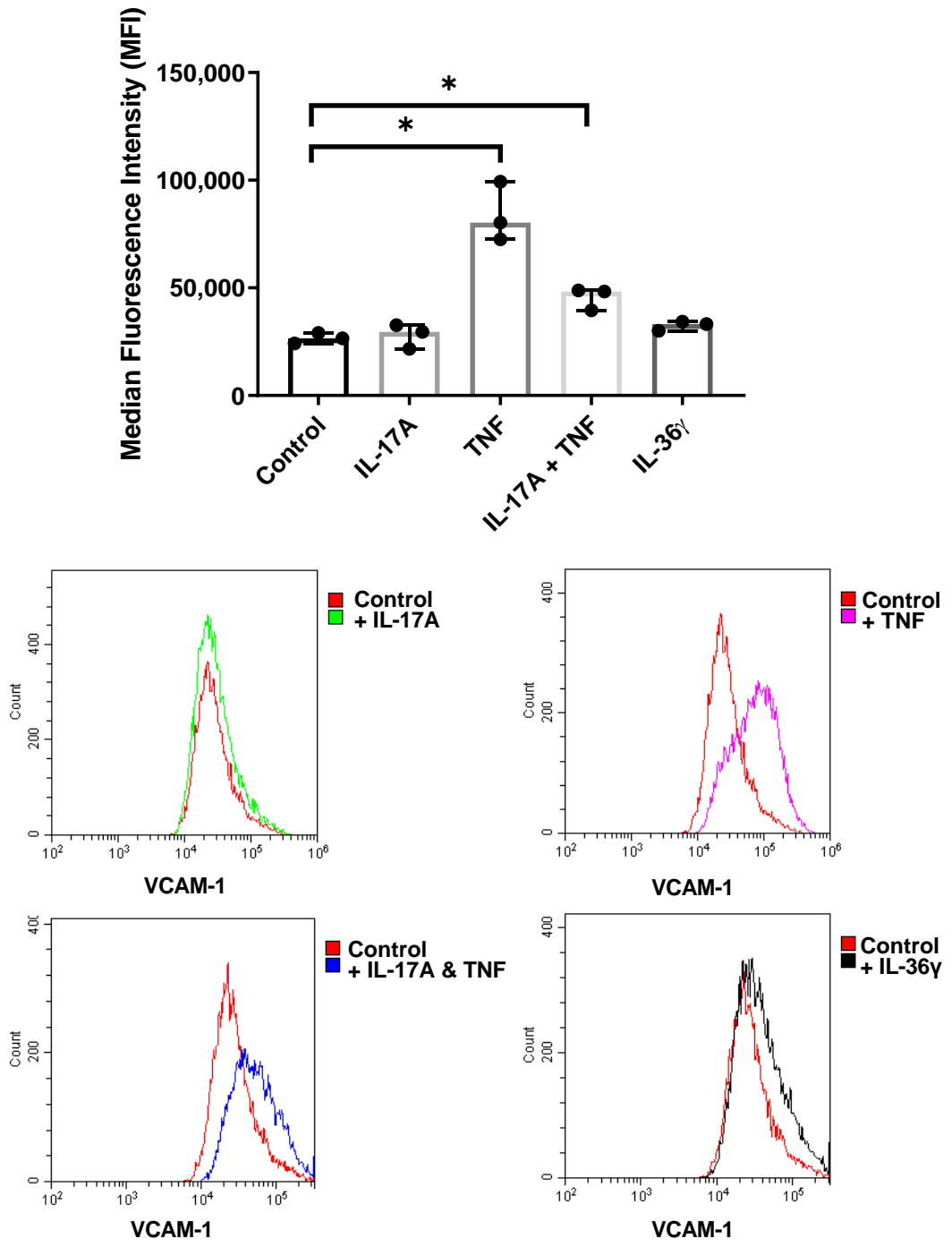
Figure 5.8: Changes in expression of VCAM-1 on EST MSCs when stimulated by IL-17, TNF or IL-36γ

*VCAM-1 was significantly upregulated by using either TNF or IL-17A and TNF. There were no synergistic effects observed between TNF and IL-17A co-stimulation. Differences in MFI were investigated using Paired T-tests. * = p<0.05.*

5.3.3 – PEB and EST MSCs secrete CCL20 and IL-8 when stimulated with pivotal AS related cytokines

Stimulations alone of either IL-17A or IL-17F did not induce secretion of CCL20 from either PEB or EST MSCs, and when IL-17A and IL-17F were co-stimulated together there was no significant CCL20 expression. TNF on its own did induce a small amount of CCL20 protein from both PEB and EST MSCs, in fact this was seen to be a significant increase for EST MSCs ($p<0.05$).

However, when stimulating with both IL-17A or IL-17F and TNF there was a synergistic effect resulting in significant increases in CCL20 protein expression in both PEB ($p<0.001$ for IL-17A/TNF, $p<0.01$ for IL-17F/TNF) and EST ($p<0.0001$ for IL-17A/TNF, $p<0.001$ for IL-17F/TNF). IL-17A is a more potent co-stimulatory partner with TNF than IL-17F, with IL-17A resulting in a median 1.36-fold increase for PEB MSCs and a 1.17-fold increase for EST MSCs. EST MSCs secreted significantly more CCL20 than PEB MSCs when stimulated by IL-17A/TNF ($p<0.01$), though this was not significantly increased when stimulated with IL-17F/TNF where there was an increase in CCL20 protein from EST MSCs compared to PEB MSCs (Figure 5.9).
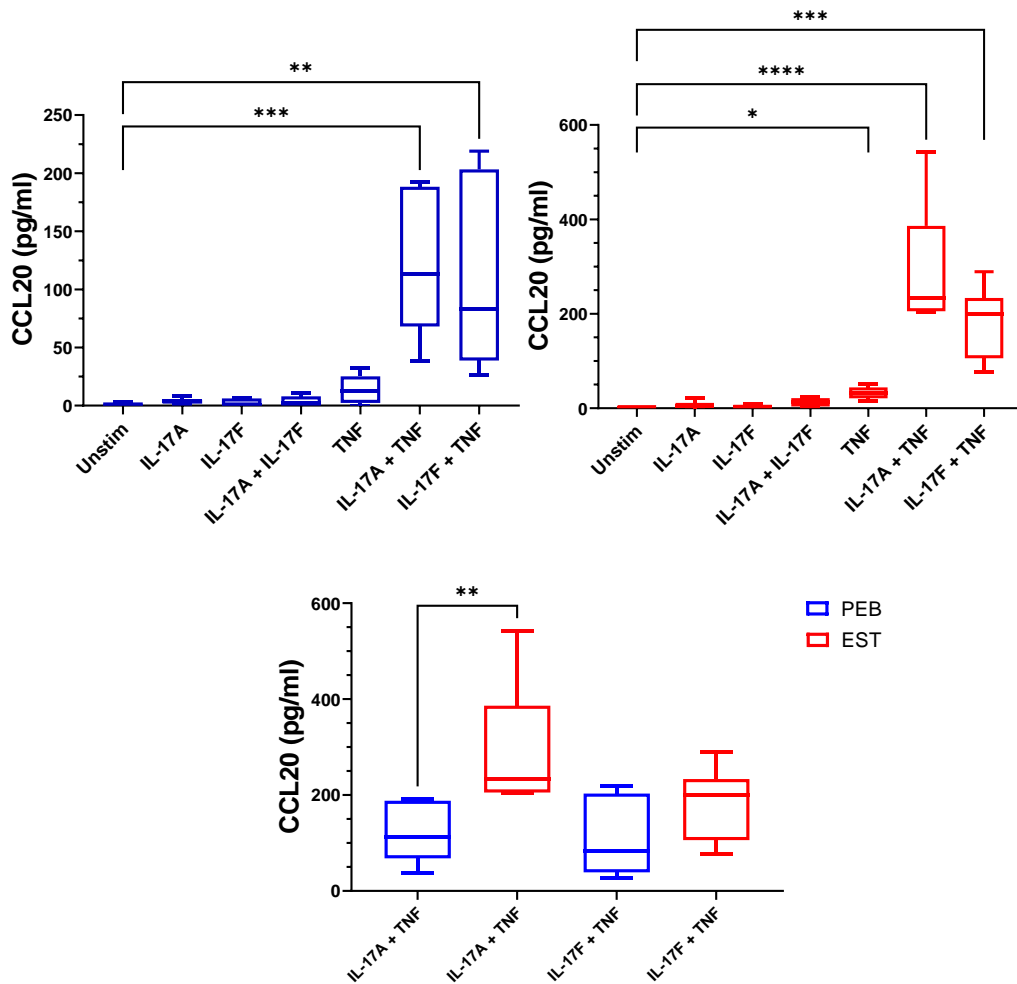
Figure 5.9: CCL20 expression from both PEB and EST MSCs induced by IL-17 and TNF

IL-17 and TNF synergise to induce CCL20 protein secretion from both PEB and EST MSCs, where individual stimulation does not induce significant expression of CCL20. Except for TNF from EST MSCs where there is a small but significant increase in CCL20 expression. EST MSCs secrete significantly more CCL20 protein than PEB MSCs when stimulated by IL-17A and TNF. CCL20 expression was analysed by Friedman's test with Dunn's post-hoc comparing to unstimulated MSCs. Mann-Whitney U test was used to compare CCL20 expression between PEB and EST MSCs. * = p<0.05, ** = p<0.01, *** = p<0.001, **** = p<0.0001.

Both PEB (n=2) and EST (n=2) MSCs secreted IL-8 in increasing quantities with increasing stimulation by IL-17A (Figure 5.10A), with IL-17A stimulation at 100ng/ml inducing a significant increase in IL-8 secretion ($p<0.01$). IL-8 secretion was completely suppressed to comparable levels with unstimulated MSCs for both PEB (n=4, Figure 5.10B) and EST (n=4, Figure 5.10C) MSCs when pre-incubated before stimulation with any tested concentration of the IL-17A monoclonal antibody Ixekizumab. As with CCL20 EST MSCs secreted more IL-8 than PEB MSCs when stimulated with IL-17A.
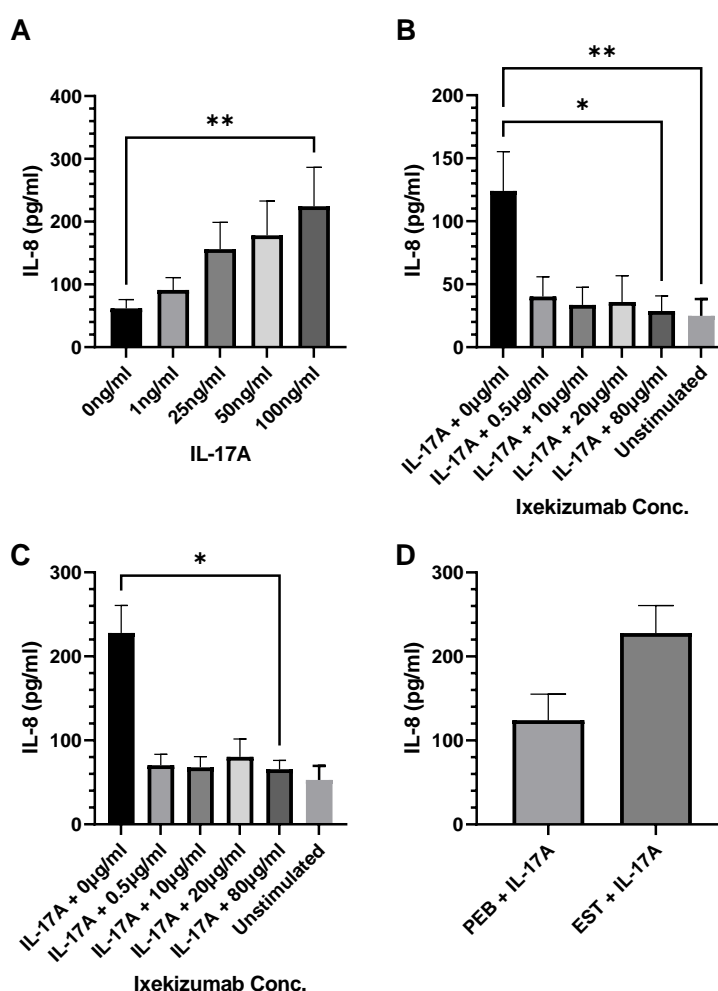
Figure 5.10: IL-8 expression is induced by IL-17A and suppressed by IL-17A inhibition with ixekizumab

(A) IL-8 secretion increased with increasing IL-17A concentration for both PEB and EST MSCs. Ixekizumab suppressed IL-8 secretion by inhibiting IL-17A signalling for both PEB (B) and EST (C) MSCs. (D) EST secrete more IL-8 than PEB MSCs. (A, B, C) analysed using Friedman's test with Dunn's post-hoc. (D) analysed using Paired T-test. * = p<0.05, ** = p<0.01.

5.3.4 – AS serum significantly suppressed adipogenesis

AS serum used at either 10% or 20% caused significant (10% = $p<0.0001$, 20% = $p<0.01$) reduction in adipogenesis when compared to a control adipogenic media with 10% FCS. The addition of Ixekizumab did not rescue the adipogenic potential for either the 10% or 20% AS serum (Figure 5.11). However, after ELISA measurement there were no detectable levels of IL-17A or TNF in the pooled AS serum.

The addition of AS serum maintained the morphology of EST MSCs in the adipogenic media. It was noted that EST MSCs in an adipogenic media supplemented with 10% FCS showed a different cell morphology with lower total observable cellularity, and much more rounded adipocyte shaped cells. Conversely, with the addition of AS serum either 10% or 20%, cells showed a much more fibroblastic or spindle shape morphology. There were visibly more cells in the same area compared to either undifferentiated MSCs cultured for the same duration in DMEM + 10% FCS or the adipogenic media with 10% FCS (Figure 5.12). This points towards the AS serum not only suppressing adipogenesis but also inducing a rapid proliferation of cells, both at 10% and 20% serum.
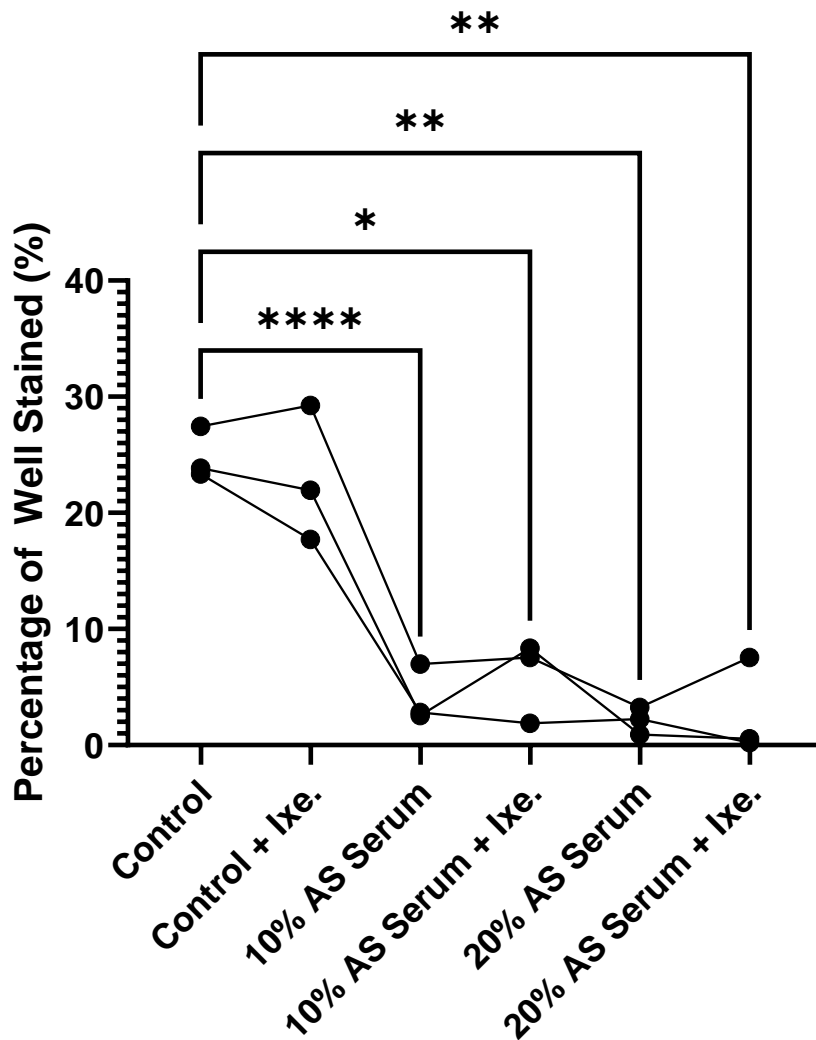
Figure 5.11: AS serum significantly reduces adipogenesis from EST MSCs

The use of TALTZ (Ixekixumab) did not significantly influence the adipogenic potential of EST MSCs. Whilst AS serum used at either 10% or 20% significantly reduced the amount of area covered by Oil Red O stained adipocytes, which was not increased by the addition of a monoclonal IL-17A inhibitor. Analysed using RM ANOVA with Tukey's post-hoc test. * = p<0.05, ** = p<0.01, **** = p<0.0001.
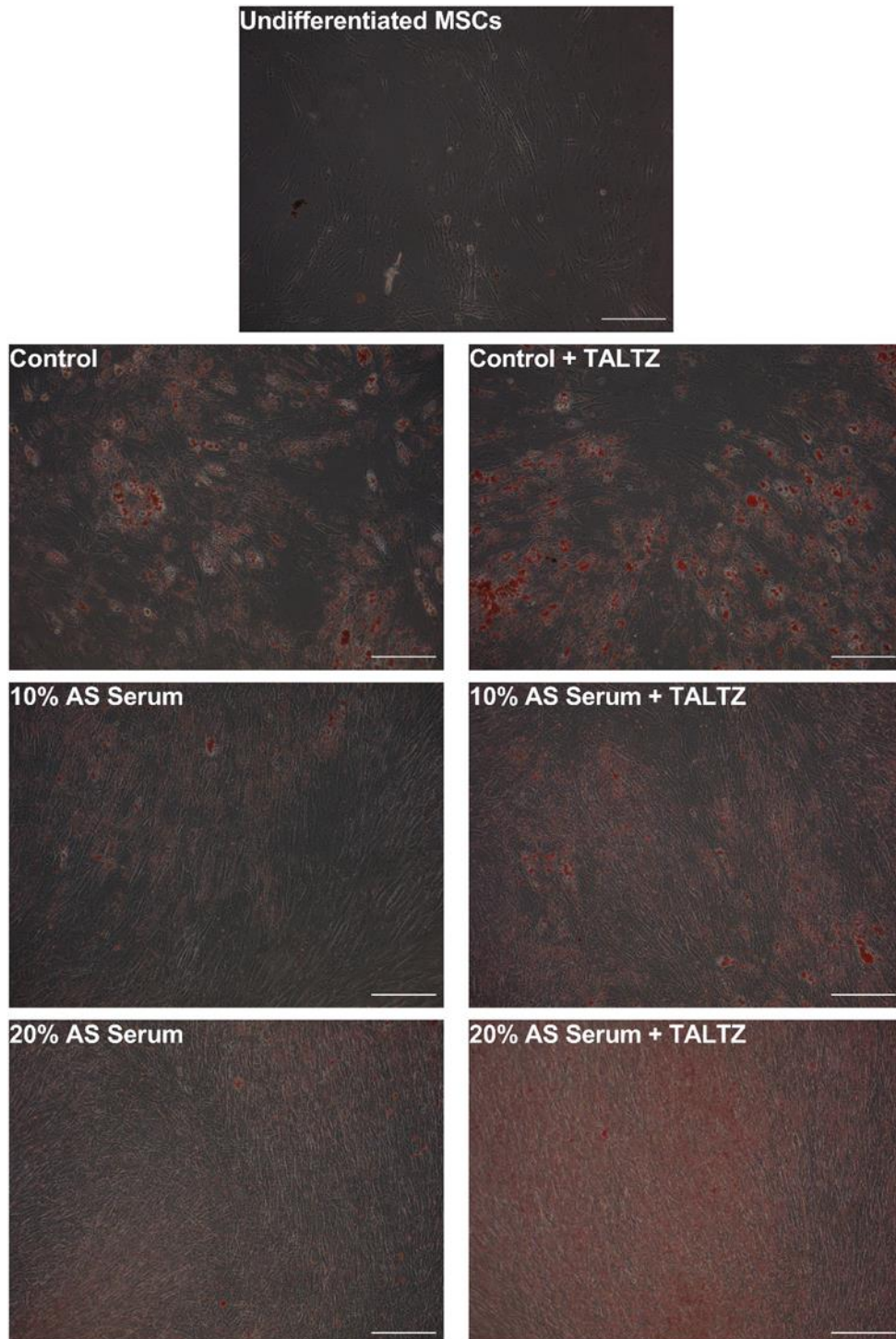
Figure 5.12: Images of differences in cell morphology between FCS and AS Serum in adipogenic media

Comparative images from the same region of the well of EST MSCs under differing adipogenic conditions. The presence of AS serum either 10% or 20% visually increased the number of cells, and cells maintained a more spindle shape like undifferentiated MSCs. Whilst adipogenically differentiated MSCs showed a rounder more adipocytic cell morphology. Scale bar = 250μm.

5.3.5 – Continual IL-17A stimulation increases glycerol content associated with increased adipolysis

IL-17A was shown to significantly decrease transcripts associated with adipogenesis, and transcripts that protect against adipolysis (section 4.3.5). Preliminary work was investigated to see if IL-17A induces the breakdown of adipocytes. EST MSCs from as early as Day 7 reached their maximum area stained with Oil Red O (section 4.3.5). Two separate time course stimulations were run, with either addition of IL-17A from either Day 7 (n=3) or Day 14 (n=3) into their 21 day differentiation did not significantly increase glycerol content in the supernatant. When a continual stimulus of IL-17A was applied throughout the 21 day differentiation there was a significant increase in glycerol content in the supernatant (n=6, $p<0.05$, Figure 5.13).
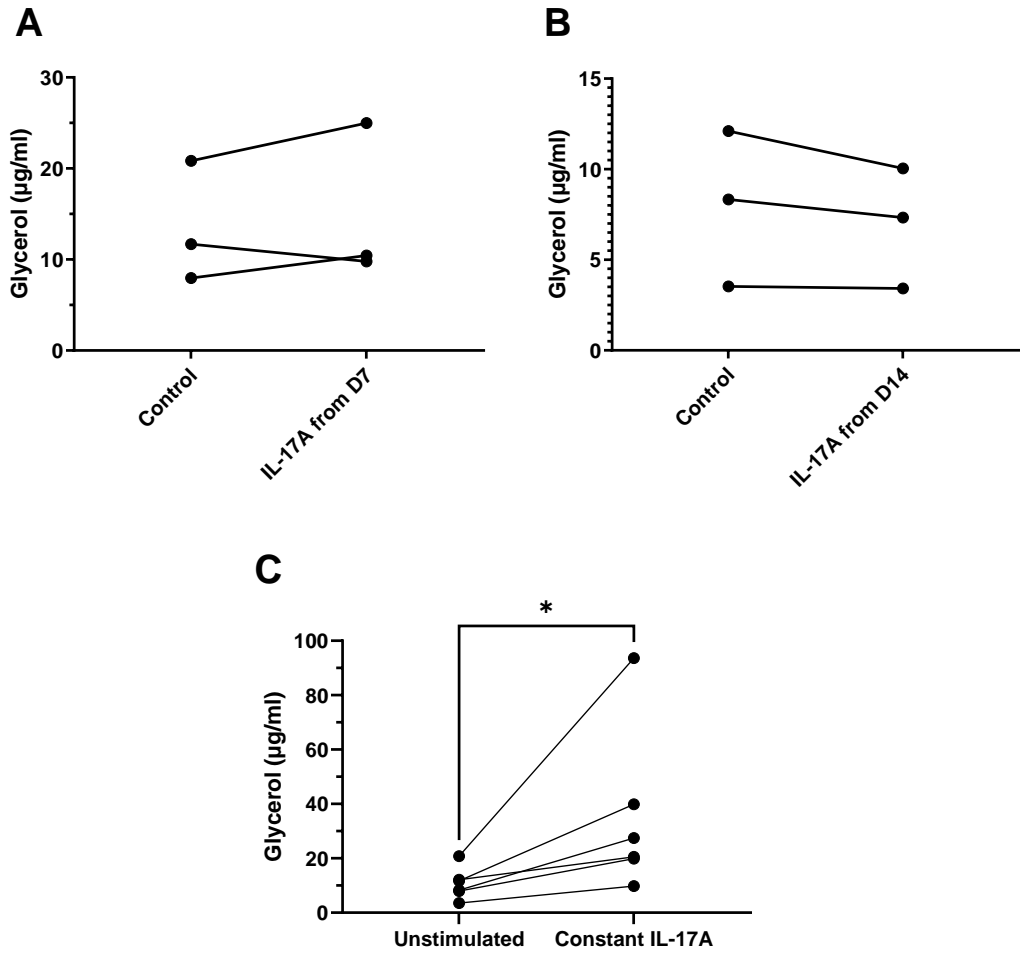
Figure 5.13: Constant IL-17A increases adipolysis of EST MSCs

The addition of IL-17A to EST MSCs after Day 7 (A) or Day 14 (B) did not affect the glycerol content in the supernatant and hence did not increase adipolysis. Constant stimulation with IL-17A during adipogenesis significantly increased glycerol content and hence adipolysis. (A, B) analysed using RM ANOVA with Dunn's post-hoc. (C) analysed using paired T-test. * = p<0.05

5.4 – Discussion

The spinal entheseal attachment site is an area of high mechanical stresses and strains which result in microdamage either to the ligament or the cortical bone of the spinous process (445). This is seen by the prevalent areas of remodelled or regenerated bone in the spinous process, particularly around the entheseal attachment sites whilst the internal trabecular bone showed more mineralised bone with few areas of remodelling. The AS spinous process showed large areas of new bone formation into the ligament characteristic of the syndesmophytes observed in late-stage AS (58, 476).

The EST fraction in both the AS and healthy sample had large areas of fat cells, this was particularly evident in the AS sample. There were also large areas of fat in the bone marrow of the PEB. There was also evidence of discontinuations in the cortical bone of the spinous process, allowing for the potential communication and indeed movement of MSCs or other cell types between the PEB and the EST in response to tissue damage (351, 477).

The resulting microdamage from normal entheseal strains and stresses needs repair of the damaged bone. The PEB at the spinous process is known to contain a large array of immune cells such as ILC3s (86), γδ T cells (88) and both CD4+ and CD8+ T cells (89) which are all capable of IL-17A and TNF production. These two cytokines are the most targeted in AS and have revolutionised disease management. It turns out that they also have important roles in bone formation as a by-product of bone repair following damage (20, 77, 81, 178). Both IL-17A and TNF are reported to increase osteogenesis from MSC populations (67, 182, 419, 432), and this was shown in the case of IL-17A in section 4.3.2. In addition to this role in differentiation, TNF is reported to increase the expression of cellular adhesion markers ICAM-1 and VCAM-1 (114-116). In the case of bone repair the increase in TNF levels is thought to encourage migration of MSCs to the fracture site associated with upregulation of ICAM-1 and VCAM-1 (131-133). This was also seen in this chapter, where the addition of TNF was the most potent driver in the up-regulation of the expression of either ICAM-1 or VCAM-1. Supported by the lack of synergy with IL-17A in increasing expression, TNF is likely the main driver behind the upregulation of ICAM-1 and VCAM-1 and hence is a ready candidate capable

of enhancing the potential migratory ability of MSCs to the sites of damage at the enthesis. The migration of MSCs to the site of tissue damage also plays an additional role aside from differentiation into the osteoblasts or adipocytes to repair the damage.

Beyond direct osteogenic capabilities, MSCs are known to play a role in modulating the immune system via secretion of immune cell chemoattractants such as CCL20 and resultant immune chemotaxis could further fine tune cytokine responses at sites of injury (355). CCL20 is a known T cell chemoattractant via its interaction with C-C Motif Chemokine Receptor 6 (CCR6) (356), importantly populations of CCR6+ T cells exist at the human enthesis (357). Significant CCL20 secretion was only observed when co-stimulation of either IL-17A and TNF or IL-17F and TNF was applied to PEB and EST MSCs. There were low levels of expression in EST MSCs when stimulated by TNF alone, which is likely attributable to the significantly higher ability of EST MSCs to secrete CCL20 than PEB MSCs.

The secretion of IL-8 by both PEB and EST MSCs was also demonstrated, and this provides a direct avenue for innate immune cell recruitment to sites of damage and in particular of neutrophils. This is shown by increasing concentrations of IL-17A resulted in increasing IL-8, which could be suppressed by the addition of ixekizumab. CCL20 and IL-8 are both secreted at significantly higher levels by EST MSCs than PEB MSCs further highlighting the functional differences between these two MSC populations. Notably, in the EST several blood vessels were observed in the AS H&E stained section. This would provide easy access to the tissue in response to tissue damage and the associated inflammation-driven over repair seen in AS.

A problem with many *in vitro* work is the use of only single or co-stimulatory factors when investigating the differentiation ability of MSCs, considering that *in vivo* the sera in which the MSCs are located contains an array of additional cytokines and growth factors all of which may influence the differentiation ability of MCSs (31, 478). The use of AS serum is usually associated with elevated levels of IL-17A (31), however, the pooled serum used in this chapter did not have any detectable IL-17A or TNF via ELISA. This is either due to it being below the detection sensitivity of the ELISA, or the fact that as the serum

had been frozen at -20°C for an extended period protein degradation may have occurred on the cytokines of interest. The AS serum did however still significantly impair the adipogenic potential of EST MSCs, though the exact mechanism could not be determined, as IL-17A inhibition did not rescue this impairment. Interestingly it appeared to cause a rapid proliferation of MSCs and with the cells maintain a more undifferentiated morphology, similar to what was seen in section 4.3.5, where IL-17A maintained expression of stromal support transcripts in MSCs undergoing adipogenesis. Though this would need to be confirmed using markers of MSCs proliferation such as KI-67 (479).

Preliminary experiments built on the previous sections work where IL-17A suppressed the adipogenic potential of MSCs from both PEB and EST MSCs. The addition of IL-17A to adipogenically differentiated human bone marrow MSCs for 7 days induced significant decreases in Oil Red O stain and also a significant increase in glycerol content in the supernatant (439). This study did not see the same glycerol increase when adipogenically differentiated EST MSCs were stimulated after 14 or 7 days with IL-17A. However, this could be due to the significantly higher adipogenic potential of EST MSCs compared to PEB MSCs. Though there was a significant increase in glycerol content when EST MSCs undergoing adipogenesis were continually stimulated with IL-17A. This fits with what was seen in section 4.3.5 were from Day 15 Oil Red O stained area decreased from a peak in at Day 7, suggesting that adipolysis is occurring induced by IL-17A. This could help explain the resolution of the fat deposition seen to precede the osteogenesis in AS (21).

In conclusion, the evidence that the cortical bone of the PEB is not uniform and does contain discontinuations suggests the potential for MSC movement between the two tissues. When combined with the evidence that drivers of AS IL-17A and TNF upregulate the expression of MSC adhesion and migratory markers ICAM-1, this supports the idea that EST MSCs can migrate to the damaged bone, attract more immune cells, both innate and adaptive lineages respectively via IL-8 and CCL-20, exacerbating inflammation and still differentiate into the osteogenesis characteristic of AS at the enthesis.

Chapter 6 – General discussion

6.1 – Key findings

This work established two distinct populations of MSCs at the human spinal enthesis and investigated their responses to AS relevant cytokine stimulation including TNF and IL-17A - the latter of which is derived from innate and adaptive lymphocytes.

Mesenchymal stem cells were identified both in the PEB or the spinous process and at the EST or the interspinous ligament. These two populations of MSCs are functionally distinct, with CD45⁻CD271⁺ MSCs identified at the PEB but not at the EST. This could help explain the significant differences seen between matched PEB and EST. It was previously established that MSCs display a tissue specificity regarding their differentiation potential, with MSCs isolated from adipose tissues showing significantly increase adipogenesis than MSCs isolated from bone sources (397). This fits with what was seen in this study, where EST MSCs displayed a significantly higher adipogenic potential than their matched PEB MSCs, and adipocyte accumulation was noted in normal EST tissue. However, there were also large areas of fat cells located in the bone marrow of the PEB suggesting that PEB MSCs may already be further differentiated down an osteogenic lineage than their EST MSCs counterparts, whilst still maintaining a low degree of plasticity between the two early phases of differentiation (401).

The interspinous ligament as an entheseal attachment site when stained for H&E or Masson's trichrome highlighted large areas of adipocytes in close proximity to the enthesis insertion with entheseal adipogenic accumulation previously being reported at other enthesis sites (51). Combined with one sample showing low levels of CD34, a marker for adipose-derived MSCs would help explain the high adipogenic potential compared to PEB MSCs (374). Per-entheseal bone MSCs had a significantly higher osteogenic potential than matched EST MSCs, supporting the notion that tissue origin of MSCs plays an important role in differentiation potential. Neo-osteogenesis in AS is seen at entheseal soft tissue sites and this thesis showed EST MSCs resident at these sites that are prone to soft tissue osteogenesis with relatively

increased osteogenesis potential following cytokine stimulation that offers new insight into the putative mechanism for AS neo-osteogenesis.

Ankylosing spondylitis may be driven by excessive tissue repair in response to the development of normal microcracks which occur in the human spine naturally over time (51, 52, 445). The tissue repair is thought to be driven primarily by an aberrant immune response; in particular the IL-17/IL-23 axis alongside TNF have been heavily implicated in AS pathogenesis (1, 17, 20, 61, 480). It is reported that IL-17A and TNF drive osteogenesis both independently from one another as well as acting to synergistically enhance osteogenesis is reported (59, 60, 420, 431, 432). Importantly the enthesis is the site of preferred new bone formation in AS and the ossification of the enthesis and the attached ligament is a major cause of the discomfort and pain affiliated with the AS (20, 35, 52). Therefore, the presence of MSCs both at PEB and EST which respond in a moderate but significant increase in osteogenesis when stimulated by the AS relevant cytokine IL-17A demonstrates that these are the cells responsible for the pathogenic changes seen in the latter stages of AS.

However, there were no significant increases when both EST and PEB MSCs were stimulated by TNF, with no reported synergistic enhancement of osteogenesis when stimulating with both TNF and IL-17A. This goes against what has been previously identified, but as discussed in section 4.4 the literature considering the influence of both TNF and IL-17A on osteogenesis is mixed and depends on a range of factors (20). IL-17A asserts its influences on osteogenesis from both PEB and EST MSCs by inducing an early increase in differentiated cells. This was demonstrated on Day 7 after initiation transcripts associated with osteoblast (*ALPL, E11)* and *BMP2,* which is a regulator of osteogenesis via acting on *RUNX2* and *SP7* (448, 450, 452, 481), were significantly upregulated by IL-17A stimulation. However, by day 14 these elevations in transcripts were not significant, though counter-intuitively both *RUNX2* and *SP7* were significantly downregulated by IL-17A stimulation. Given that the syndesmophytes form at the entheseal attachment, the increased osteogenesis induced by IL-17A in EST MSCs fit with what is seen in disease. This is important as the majority of work looking at MSCs in relation

to AS has been using MSCs taken from bone marrow-derived sources which given the mentioned differences in tissue specificity may have had a differing response to the same cytokines.

The main novelty of this work lies in the observed findings that may be relevant to the early phases of AS, in particular the formation of the fat at the vertebral bodies seen to precede the osteogenesis at the enthesis annulus soft tissue (21). Most of the work involving IL-17A and adipogenesis is mainly related to studies involving obesity and diabetes (435, 437, 472). Both IL-17A and TNF significantly impaired the adipogenic potential of both PEB and EST MSCs, IL-17A caused a more potent reduction in adipogenesis and visibly changed the morphology of the lipid vesicles. How this IL-17A impact on adipogenesis *in vivo* might impact on new bone formation requires further evaluation. Three major transcript functions were either significantly suppressed or upregulated by IL-17A stimulation. Stimulation changed the morphology of the lipid vesicles by holding them in a more immature state, with lots of small vesicles not fusing to create the classical mature adipocyte. This was supported by the downregulation of *PLIN1* and *CIDEC* both are key transcripts needed to support vesicle fusion to develop into mature adipocytes (457), and as a secondary function *PLIN1* is associated with protection against adipolysis or breaking down of the adipocytes (482). The transcripts associated with mature adipocytes (*FABP4, ADIPOQ*) were also significantly suppressed by IL-17A.

The importance at the loss of protection conferred by PLIN1 would help rationalise the loss of the fat seen in the vertebral corners as AS progresses and new bone is deposited. However, it must be acknowledged that *in vivo* in AS that new bone formation follows the post-inflammatory phase of the disease and there is virtually no knowledge of *in vivo* levels of IL-17A in this setting. Preliminary published work supports this idea where constant IL-17A stimulation of EST MSCs undergoing adipogenesis had significantly increased levels of glycerol, which is a product of lipid break down (439). Combining this with the elevated expression of *CXCL12*, an MSC stromal support marker, when stimulated by IL-17A during adipogenesis suggests that MSCs stimulated by IL-17A are prevented from going down an adipogenic lineage and with the increased osteogenesis pushed down a more osteogenic

lineage by IL-17A stimulation. There is an established reciprocity between the early phases of osteogenesis and adipogenesis in MSCs (401). This suggests that IL-17A may be holding MSCs in a more immature pre-adipocyte phase with the known increased osteogenesis induced by IL-17A this could help explain the phenotypic changes from fatty tissues towards neo-osteogenesis at the enthesis (67, 357).

It is now firmly established that the normal spinal enthesis has an immune system including innate and adaptive lymphocytes that can be induced to secrete MSC relevant cytokines including IL-17 and IL-22. Accordingly, the impact of cytokines on MSC stromal supportive function for lymphocytes was investigated. At the same time stimulation with IL-17A during adipogenesis saw an increase in the transcript for *CCL20* which is a CCR6+CD4+ T cell chemoattractant (356, 357). In undifferentiated MSCs both from the PEB and EST when stimulated with both IL-17A and TNF there is a significant increase in CCL20 secretion.

Intraosseous MSCs and fat cells occurring within the vertebral bodies in AS would naturally be incriminated in spinal corner adipogenesis due to their PEB location. These MSCs adipogenesis was impaired by IL-17A or TNF.   This may be relevant to AS as the fat changes at entheses are a post-inflammatory phase phenomenon. Entheseal soft tissue MSCs were also capable of adipogenic differentiation and showed the same negative outcome with cytokine stimulation. Given the cortical bone of the spinous process had discontinuations between the EST and PEB, this allows for the possibility of MSC migration between the two tissues. This migration is evidenced by previous work showing that MSCs migrate towards TNF elevated in fracture sites via up-regulation of ICAM-1 and VCAM-1 (131, 483). Though chemotaxis was not assessed, when stimulated with TNF both PEB and EST MSCs showed significant upregulation in the expression of both ICAM-1 and VCAM-1, which would enable the migration of EST to the site of damage at the PEB and hence rapidly form the fat cells seen in early AS. Whilst also facilitating the migration of MSCs to the enthesis to differentiate down an osteogenic lineage and begin to produce the characteristic phenotype of AS being the new bone formation into the enthesis.

6.2 – Study limitations

This study does have its limitations, namely as all MSCs used for differentiation experiments in this study came from healthy patients with no known underlying inflammatory condition. Ideally, MSCs would come from patients with AS, however, it is unusual for patients with AS to have corrective spinal surgeries and those which do usually have it late-stage and hence the majority of the soft tissue is mineralised and of limited use. When comparing between AS and healthy control MSCs they both follow the same responses to IL-17A, though AS MSCs appear to have a higher innate osteogenic response (67).

It is important to acknowledge the limitations associated with *in vitro* differentiation assays, with their reliance on corticosteroids for differentiation induction, and the difficulty in extrapolating the results to the *in vivo* scenario. Dexamethasone important in the initial stages of *in vitro* osteogenic differentiation is likely to play an inhibitory role in any inflammatory cytokine signalling. At the same time, most work is usually only stimulated using either solitary or co-stimulation of cytokines, which has its benefits but *in vivo,* as mentioned in section 5.1.2, the serum in these tissues is full of extra cytokines and growth factors all at significantly lower concentrations than those used *in vitro* (31, 146, 148).

Some of the aforementioned limitations were addressed by the preliminary use of AS serum in an adipogenic experiment, however, there were no detectable levels of either IL-17A or TNF in the serum so what induced the significant downregulation in adipogenesis of EST MSCs could not be determined. Either these cytokines were below detection or had degraded due to prolonged storage at -20°C, up to 15 years. Cytokine serum levels in AS are in the pg/ml range and can often fall below the detection of some assays (31, 146, 148). The use of AS serum in osteogenesis induces an increase in osteogenesis, which can be reversed by the inhibition of IL-17A (67).

The increase in ICAM-1 expression when MSCs were stimulated by TNF, and the supporting evidence of discontinuations seen in the cortical bone revealed by histology provides the groundwork for further proof that MSCs can migrate

between the two tissues in response to damage. However, this could not be demonstrated by this study. This could be subsequently investigated using transwell migration assays using conditioned media from activated T cells isolated from the enthesis. Where conditioned media with known disease-relevant cytokines would stimulate the MSCs and induce migration to the increased concentration of these cytokines which *in vivo* would be associated with tissue damage (89, 460, 480).

6.3 – Clinical relevance and future directions

The role of IL-17A in osteogenesis is well established now and with the growing evidence that inhibition of IL-17A in AS reduces new osteogenesis, this study only adds more backing to that concept (80-82). Ixekizumab is a monoclonal antibody specific for IL-17A and in this work it blocked IL-8 release from MSCs following IL-17A stimulation. This may provide an unappreciated mechanism for disruption of the IL-23/17 axis pathway towards the recruitment of neutrophils to inflammatory lesions.

IL-17F also signals through the same receptor complex as IL-17A and induces osteogenesis at a milder level (194, 195). More recently IL-17F has been seen to signal through an IL-17RC homodimer, raising the possibility for IL-17RA independent induced osteogenesis (183). Recent work showed that bimekizumab, a dual inhibitor of IL-17A and IL-17F showed significant reductions in IL-17A and IL-17F driven osteogenesis from human periosteal cells (83). Future work regarding osteogenesis and EST or PEB MSCs should involve either the use of AS serum or an expanded potential of cytokines notably the IL-36 family.

The effects of IL-17A and TNF in driving osteogenesis in MSCs is well studied. However, the early phases of AS remain largely enigmatic, in particular the formation and resolution of the fat seen at the vertebral bodies in AS. This study provided a mechanism through which this could be addressed, via the migration of EST MSCs to the site of damage via upregulation of ICAM-1 and the subsequent rapid adipogenic differentiation and IL-17A's subsequent influence in resolving this fat formation. Being able to identify the formation of this new fatty tissue and understanding how it can transition towards new bone

formation in AS is important and provides potential opportunities to intervene early and prevent or reduce new bone formation.

Future work to address this and provide a better understanding of the functional differences between these two distinct populations of MSCs would be of great benefit. This would be accomplished with the use of single-cell RNAseq on purified populations from both the PEB and EST. Also given the currently poorly understood IL-17A signalling pathway would best be understood using similar techniques on populations of MSCs both unstimulated and those after being differentiated and stimulated by IL-17A.

That being said, it is remarkable that the normal spinal enthesis has resident MSC populations and a complex innate and adaptive immune system in health (484).   The work in this thesis has been used to advocate a novel model for AS and SpA pathogenesis whereby these cells and cytokines fine tune tissue repair. Genetic polymorphisms in AS, gut barrier dysfunction and dysbiosis and other factors likely skew this response towards excessive tissue repair responses typical of AS. Hence, it could be argued that the normal physiology and *in vitro* models using cytokines critical to human AS is a valid approach to investigating disease (20, 357).

6.4 – Concluding remarks

The driving forces behind the neo-osteogenesis in the later stages of AS and how the IL-23/IL-17 axis amongst others contributes to this is starting to emerge. In advanced AS, new bone formation at the enthesis leading to bamboo spines is irreversible. Therefore, it is of much better value to understand the early phases of AS and how these normal tissue repair responses can lead to fat at the corners of the enthesis and the subsequent new bone.

This project identified two populations of MSCs at the human spinal enthesis which are functionally distinct in their differentiation potentials, with the ability to mimic the anatomical changes seen in AS. Importantly, this study gave a potential mechanism for interactions with the local immune system and the changes seen in early AS which should be carried forward with further work to better improve the understanding of AS.

Appendix A – Patient samples

Sample ID:	Sex:	Age:
RC121	M	69
RC143	M	43
RC144	M	65
RC147	F	36
RC151	F	66
RC152	F	24
RC154	M	78
RC160	F	56
RC166	M	70
RC167	F	14
RC175	F	44
RC176	M	78
RC183	M	69
RC184	M	47
RC185	F	18
RC194 (AS)	F	78
RC195	F	17
RC197	F	55
RC198	M	32
RC200	F	35
RC202	F	34
RC210	M	71
RC211	F	80
RC212	F	18
RC217	F	66
RC219	M	68
RC220	F	75
RC221	M	48
RC222	F	12
RC223	F	19
RC224	F	13
RC229	F	12
RC232	F	68
RC233	F	12
RC234	F	20
RC241	M	15
RC242	M	23
RC243	M	45
RC244	F	43
RC250	F	68
RC265	M	67
RC300	F	14
RC302	M	14

RC303	M	83
RC311	M	49
RC312	M	13
RC313	M	63
RC317	M	66
RC359	F	64
RC380	F	15
RC390	F	50
RC391	F	14
RC393	F	53
RC394	M	74
RC433	F	64
RC434	F	54
RC435	F	27
RC501	M	42
RC509	M	18
RC570	F	24
RC571	F	17

Appendix B – Reagents

Product:	Manufacturer:
Absolute Ethanol	Sigma
Acetone	Sigma
Alizarin Red	Sigma
β-Mercaptoethanol	Sigma
Bovine Serum Albumin	Sigma
Citrate Concentrated Solution	Sigma
Collagenase I Type A, AOF	Worthington
Dimethyl Sulphoxide (DMSO)	Sigma
DNase I	Norgen Biotek
DPX Mounting Media	Sigma
Dulbecco's Modified Eagle Medium (DMEM) Low Glucose	Gibco
Dulbecco's Modified Eagle Medium (DMEM) High Glucose	Gibco
Eosin Y	Sigma
Ethylenedinitrilotetraacetic Acid (EDTA)	Fisher Scientific
Fast Blue RR Salt Tablets	Sigma
Foetal Bovine Serum	Biosera
Formalin (10% Neutral Buffered)	Sigma
Haematoxylin (Harris')	Fisher Scientific
Haematoxylin (Weigert's)	Sigma
Horse Serum	Gibco
Hydrochloric Acid	Sigma

Isopropanol	Sigma
Methanol	Sigma
Methylene Blue	Sigma
Naphtol AX-MX Phosphate	Sigma
Nuclease Free Water	Ambion
Oil Red O	Sigma
Phosphate Buffered Saline (PBS) Tablets	Sigma
Penicillin/Streptomycin	Gibco
StemMACS MSC Expansion Media	Miltenyi Biotec
Toluidine Blue	Sigma
Trypan Blue Solution	Sigma
Xylene	Fisher Scientific

Appendix C – Standard solutions

Activated papain enzyme digestion solution (GAG assay)

For 100 mM sodium phosphate buffer/5 mM EDTA/10 mM L-cysteine (0.125 mg/ml papain): Just before use, add 63 mg of L-cysteine hydrochloride hydrate in 40 ml papain buffer and sterile filter using syringe and 20 µm filter. Transfer 1 ml of papain solution to a microcentrifuge tube using a syringe and 20-gauge needle then add 125 µg/ml papain enzyme.

Alizarin red staining solution (Osteogenesis)

Prepared by dissolving 342 mg Alizarin Red (Sigma) in 25 ml of dH2O and pH adjusted to 4.1

Borate buffer (CFU-F assay)

10mM borate buffer: 1.91g disodium tetraborate dehydrate (Sigma) dissolved in 500 ml dH2O and pH adjusted to 8.8 with 1M boric acid (made up by dissolving 6.183g boric acid (Sigma) in 100 ml dH2O = 1M)

Cell freezing media

90% FCS (Biosera) + 10% DMSO (Sigma).

Citrate fixative (ALP assay)

6 ml acetone (Sigma) and 4 ml of 1:50 dilution of citrate concentrate solution (Sigma)

EDTA decalcification solution

0.5 M EDTA solution (pH 7.4): 186.1 g EDTA disodium dehydrate (Fisher Scientific) dissolved in 800 ml dH2O. The disodium salt of EDTA will not go into solution until the pH of the solution is adjusted to ~8.0 by the addition of NaOH. The pH was therefore first adjusted to 8.0 with approximately 20 g of

Sodium Hydroxide pellets (NaOH) (Fisher Scientific) and following complete dissolution adjusted to 7.4 with neat HCl (Sigma).

Fast Blue solution (ALP assay)

One Fast blue salt tablet (Sigma) dissolved in 48 ml of dH2O with the addition of 2 ml of 0.25% Naphthol AX-MX phosphate solution (Sigma)

FACS Buffer

500 ml PBS + 1% w/v bovine serum albumin (5 g) (Sigma) + 200 µl EDTA 0.5M (Fisher Scientific)

Fc blocking buffer

1 ml aliquots containing 10% mouse serum (Sigma), 1% human IgG (Sigma) in FACS Buffer

HCL solution (Calcium assay)

0.5N HCl; 26.5 ml of 37% HCl (Fisher Scientific) in 473.5 ml dH2O.

Methylene blue solution (CFU-F assay)

1% w/v methylene blue solution: 1 g methylene blue (Sigma) dissolved in 100 ml of 10mM borate buffer (pH 8.0).

Naphthol AS-MX Phosphate Substrate

20 mg of Naphthol AX-MX phosphate (Sigma) dissolved in 1 ml Ethylene Glycol

Monoethyl Ether (Sigma)

Oil red (Adipogenesis)

Prepared at 0.5% by dissolving 50 mg Oil red (Sigma) in 10 ml of isopropanol (Sigma), incubated for 30 minutes at 37° C and then diluted 3:2 w/v with dH2O, filtered twice using a 45 μm filter (Millex) for the first filtration followed by a 22 μm filter (Millex) to remove any undissolved material.

Papain buffer extract (GAG assay)

For 100 ml of 100 mM sodium phosphate buffer/5 mM EDTA (pH 6.5): To 90 ml of dH2O add 0.653 g sodium phosphate dibasic (Na2HPO4, MW 142.0), 0.648 g of sodium dihydrogen phosphate (NaH2PO4, MW 120.0) and 1 ml of 500 mM EDTA (Sigma). Adjust pH to 6.5 using HCl and make up the volume to 100 ml using dH2O then filter sterile.

Phosphate buffer saline

1 PBS tablet (Sigma) dissolved in 200 ml dH2O

Tris-buffered saline

16 g Sodium chloride (NaCl), 0.4 g Potassium chloride (KCl) and 6 g Tris base (all from Sigma) dissolved in 800 ml dH2O adjust pH to 7.4 with HCl and make up the volume to 1L with dH2O

Appendix D – Plasticware, consumables and equipment

Item:	Manufacturer:
12-Well Culture Plate	Corning
24-Well Culture Plate	Corning
48-Well Culture Plate	Corning
96-Well Culture Plate	Corning
6-Well Culture Plate	Corning
10mm Culture Dish	Corning
5ml Bijous	StarLab
Cell Strainer	Corning
2ml Cryovials	Sarstedt
Falcon Tubes	Corning
FACS Tubes	Corning
Filters	Millex
Histology Cassettes	Scientific Laboratory Supplies
Microtome Blades (CellEdge R+)	Cell Path
Pipette Tips	Gilson
Safe-Lock Tubes	Eppendorf
Scalpel (Blade Sizes 10 and 22)	Swann-Morton
Stripette	Corning
SuperFrost Plus Microscope Slides	Thermo Fisher
T25, T75 and T150 Culture Flasks	Corning
96-Well PCR Plate	Thermo Fisher
PCR Tubes and Caps	Star Lab

Equipment:	Manufacturer:
Bone Rongeur (Stille-Luer)	Sklar
Cell Culture Cabinet (Class II)	Nuaire
Centrifuge	Eppendorf
Digital Camera (Microscope)	Olympus
-20°C Freezer	Liebherr
-80°C Freezer	Panasonic
Freezing Container	CoolCell
2-4°C Fridge	Lec Medical
Fume Hood	
Haemocytometer	Hawksley
Hot Plate – SH3 (Histology)	Stuart Scientific
37°C Incubator	Sanyo
Microcentrifuge	StarLab
Inverted Light Microscope	Olympus
Nanodrop Spectrophotometer	Thermo Fisher
Plate Reader	Biotek
Vortex	StarLab
Water Bath	Grant
Weighing Scale	Mettler Toledo
X-Ray Machine (CS2200)	Carestream Health

Appendix E – Ethics

UNIVERSITY OF LEEDS

The Leeds Teaching Hospitals **NHS**
NHS Trust

Title of Study: Understanding Osteogenesis in Health, Development and Disease

Childs assent form ages 6-9: On agreement to participate one copy of this form should be kept by the participant, one copy placed in patient's notes and one copy retained by the research team.

Patient Name: .... Patient NHS ID: ....
Patient D.O.B. Year:..................... Month:..................... Sex...........

Please circle all you agree (or if unable, to be completed by parent / guardian on their behalf)		
1. Have you read all (or had read to you) the information about this study?	Yes	No
2. Have you asked all the questions you want to about the study and had chance to talk about it with your mum or dad or guardian?	Yes	No
3. Have you had your questions answered in a way you understand?	Yes	No
4. Do you understand what this study is about?	Yes	No
5. Do you understand that if you do take part in this study you will not be given any special treatment or reward?	Yes	No
6. Do you understand that anything written down about you will not be shown to anyone else, and that nobody else will be told anything about you?	Yes	No
7. Is it ok for us to write down things that the doctors and nurses say about how you are?	Yes	No
8. Do you understand that it is ok to decide that you don't want to take part in this study even after you have already said you will and that nobody will be cross?	Yes	No
9. If we don't use everything straight away is it ok for us to keep what's left over for future research?	Yes	No
10. Are you happy to take part?	Yes	No

If any answers are 'no' or you don't want to take part, don't sign your name!
If you do want to take part, you can write your name below

Child's agreement
I agree to take part in this study.

Name:.. Date: ....

Investigator/Sub-investigator
I have explained the study to the above named participant and he/she has indicated his/her willingness to participate
Name (BLOCK CAPITALS): ....

Signed: .... Date: ....

<u>Understanding Osteogenesis in Health, Development and Disease</u>

PATIENT CONSENT FORM: On agreement to participate one copy of this form should be kept by the participant, one copy placed in patient's notes and one copy retained by the research team.

Patient name..   Patient NHS ID.......................................

Patient DOB: Year.............................. Month................................   Sex............

Please circle as appropriate

1. I have read the patient information sheet for the above study.   Yes/No

2. I have had the opportunity to ask questions about the study and to discuss it with family and friends if I so wish to.   Yes/No

3. I understand the purpose of the study, and how I will be involved.   Yes/No

4. I understand, and accept, that if I take part in the study I may not gain direct personal benefit from it.   Yes/No

5. I understand that all information collected in the study will be held in confidence and that, if it is presented or published, all my personal details will be removed.   Yes/No

6. I confirm that I will be taking part in this study of my own free will, and I understand that I am free to withdraw from the study at any time without giving a reason and without affecting my future care or legal rights.   Yes/No

7. I understand that relevant sections of my medical notes, may be looked at by individuals from the NHS Trust and regulatory authorities and that specific information relevant to the research may be passed to individuals at the University of Leeds. I give permission for these individuals to have access to my records.   Yes/No

8. I give permission for any tissue samples I donate to be sent to third parties including industrial partners as part of this study.   Yes/No

9. I give permission for any tissue samples I donate to be retained for future studies, subject to proper ethical approval.   Yes/No

10. I have spoken to Dr..

11. I agree to take part in this research study.

<u>PATIENT:</u>
Signed: .... Date ....

Name (BLOCK CAPITALS)..

<u>Investigator/Sub-investigator</u>

I have explained the study to the above named participant and he/she has indicated his/her willingness to participate

Signed.. Date..................

Understanding osteogenesis in health, development and disease. Version 2.0, 22/11/2016
IRAS Project ID: 197636

Understanding Osteogenesis in Health, Development and Disease

PARENT/GUARDIAN CONSENT FORM: On agreement to participate one copy of this form should be kept by the participant, one copy placed in patient's notes and one copy retained by the research team.

Patient name..   Patient NHS ID..

Patient DOB: Year............................. Month.............................   Patient sex: ....

Please circle as appropriate

1. I have read the patient information sheet for the above study.   Yes/No

2. I have had the opportunity to ask questions about the study and to discuss it with my child/ward, family and friends if I so wish to.   Yes/No

3. I understand the purpose of the study, and how my child/ward will be involved. I am satisfied that my child/ward also understands to the best of their ability.   Yes/No

4. I understand, and accept, that if my child/ward takes part in the study he/she or I may not gain direct personal benefit from it.   Yes/No

5. I understand that all information collected in the study will be held in confidence and that, if it is presented or published, all personal details will be removed.   Yes/No

6. I confirm that my child/ward will be taking part in this study of his/her own free will, and I understand that I am free to withdraw my child/ward from the study at any time without giving a reason and without affecting his/her future care or my legal rights.   Yes/No

7. I understand that relevant sections of my child's/ward's medical notes, may be looked at by individuals from the NHS Trust, regulatory authorities and that specific information relevant to the research may be passed to individuals at the University of Leeds. I give permission for this to happen   Yes/No

8. I give permission for any tissue samples donated to be sent to third parties including industrial partners as part of this study.   Yes/No

9. I give permission for any tissue samples donated to be retained for future studies, subject to proper ethical approval.   Yes/No

10. I have spoken to Dr...

11. I agree to allow my child/ward take part in this research study.

Parent / guardian

Signed: .... Date ....

Name (BLOCK CAPITALS)...

Investigator/Sub-investigator

I have explained the study to the above named parent or guardian of the participating minor who has indicated their willingness to allow his/her child to take part.

Signed... Date................................

Understanding osteogenesis in health, development and disease. Version 2.0, 22/11/2016,
IRAS Project ID: 197636

UNIVERSITY OF LEEDS

Understanding Osteogenesis in Health, Development and Disease

PATIENT CONSENT FORM: On agreement to participate one copy of this form should be kept by the participant, one copy placed in patient's notes and one copy retained by the research team.

Patient name... Patient NHS ID..

Patient DOB: Year.............................. Month.............................. Sex...........

Please circle as appropriate

1. I have read the patient information sheet for the above study. Yes/No

2. I have had the opportunity to ask questions about the study and to discuss it with family and friends if I so wish to. Yes/No

3. I understand the purpose of the study, and how I will be involved. Yes/No

4. I understand, and accept, that if I take part in the study I may not gain direct personal benefit from it. Yes/No

5. I understand that all information collected in the study will be held in confidence and that, if it is presented or published, all my personal details will be removed. Yes/No

6. I confirm that I will be taking part in this study of my own free will, and I understand that I am free to withdraw from the study at any time without giving a reason and without affecting my future care or legal rights. Yes/No

7. I understand that relevant sections of my medical notes, may be looked at by individuals from the NHS Trust and regulatory authorities and that specific information relevant to the research may be passed to individuals at the University of Leeds. I give permission for these individuals to have access to my records. Yes/No

8. I give permission for any tissue samples I donate to be sent to third parties including industrial partners as part of this study. Yes/No

9. I give permission for any tissue samples I donate to be retained for future studies, subject to proper ethical approval. Yes/No

10. I have spoken to Dr...

11. I agree to take part in this research study.

PATIENT:
Signed: .... Date ....

Name (BLOCK CAPITALS)..

Investigator/Sub-investigator

I have explained the study to the above named participant and he/she has indicated his/her willingness to participate

Signed... Date...................

Understanding osteogenesis in health, development and disease. Version 2.0, 22/11/2016
IRAS Project ID: 197636

Bibliography

1. Watad, A., Bridgewood, C., Russell, T., Marzo-Ortega, H., Cuthbert, R. and McGonagle, D. The Early Phases of Ankylosing Spondylitis: Emerging Insights From Clinical and Basic Science. *Front Immunol.* 2018, **9**(2668), p.2668.
2. Moll, J.M., Haslock, I., Macrae, I.F. and Wright, V. Associations between ankylosing spondylitis, psoriatic arthritis, Reiter's disease, the intestinal arthropathies, and Behcet's syndrome. *Medicine (Baltimore).* 1974, **53**(5), pp.343-364.
3. Generali, E., Bose, T., Selmi, C., Voncken, J.W. and Damoiseaux, J. Nature versus nurture in the spectrum of rheumatic diseases: Classification of spondyloarthritis as autoimmune or autoinflammatory. *Autoimmun Rev.* 2018, **17**(9), pp.935-941.
4. Deodhar, A., Miossec, P. and Baraliakos, X. Is undifferentiated spondyloarthritis a discrete entity? A debate. *Autoimmun Rev.* 2018, **17**(1), pp.29-32.
5. Bridgewood, C., Watad, A., Cuthbert, R.J. and McGonagle, D. Spondyloarthritis: new insights into clinical aspects, translational immunology and therapeutics. *Curr Opin Rheumatol.* 2018, **30**(5), pp.526-532.
6. Ostrowska, M., Maslinski, W., Prochorec-Sobieszek, M., Nieciecki, M. and Sudol-Szopinska, I. Cartilage and bone damage in rheumatoid arthritis. *Reumatologia.* 2018, **56**(2), pp.111-120.
7. Stolwijk, C., van Onna, M., Boonen, A. and van Tubergen, A. Global Prevalence of Spondyloarthritis: A Systematic Review and Meta-Regression Analysis. *Arthritis Care Res (Hoboken).* 2016, **68**(9), pp.1320-1331.
8. Brown, M.A., Li, Z. and Cao, K.L. Biomarker development for axial spondyloarthritis. *Nat Rev Rheumatol.* 2020, **16**(8), pp.448-463.
9. Griffiths, C.E.M., Armstrong, A.W., Gudjonsson, J.E. and Barker, J. Psoriasis. *Lancet.* 2021, **397**(10281), pp.1301-1315.
10. Van Praet, L., Jacques, P., Van den Bosch, F. and Elewaut, D. The transition of acute to chronic bowel inflammation in spondyloarthritis. *Nat Rev Rheumatol.* 2012, **8**(5), pp.288-295.
11. Baumgart, D.C. and Sandborn, W.J. Crohn's disease. *Lancet.* 2012, **380**(9853), pp.1590-1605.

12. Palm, O., Moum, B., Ongre, A. and Gran, J.T. Prevalence of ankylosing spondylitis and other spondyloarthropathies among patients with inflammatory bowel disease: a population study (the IBSEN study). *J Rheumatol.* 2002, **29**(3), pp.511-515.

13. Brewerton, D.A., Hart, F.D., Nicholls, A., Caffrey, M., James, D.C. and Sturrock, R.D. Ankylosing spondylitis and HL-A 27. *Lancet.* 1973, **1**(7809), pp.904-907.

14. Chatzikyriakidou, A., Voulgari, P.V. and Drosos, A.A. What is the role of HLA-B27 in spondyloarthropathies? *Autoimmun Rev.* 2011, **10**(8), pp.464-468.

15. Bowness, P. HLA-B27. *Annu Rev Immunol.* 2015, **33**, pp.29-48.

16. Dashti, N., Mahmoudi, M., Aslani, S. and Jamshidi, A. HLA-B*27 subtypes and their implications in the pathogenesis of ankylosing spondylitis. *Gene.* 2018, **670**, pp.15-21.

17. Tsui, F.W., Tsui, H.W., Akram, A., Haroon, N. and Inman, R.D. The genetic basis of ankylosing spondylitis: new insights into disease pathogenesis. *Appl Clin Genet.* 2014, **7**, pp.105-115.

18. Li, Z. and Brown, M.A. Progress of genome-wide association studies of ankylosing spondylitis. *Clin Transl Immunology.* 2017, **6**(12), p.e163.

19. International Genetics of Ankylosing Spondylitis, C., Cortes, A., Hadler, J., Pointon, J.P., Robinson, P.C., Karaderi, T., Leo, P., Cremin, K., Pryce, K., Harris, J., Lee, S., Joo, K.B., Shim, S.C., Weisman, M., Ward, M., Zhou, X., Garchon, H.J., Chiocchia, G., Nossent, J., Lie, B.A., Forre, O., Tuomilehto, J., Laiho, K., Jiang, L., Liu, Y., Wu, X., Bradbury, L.A., Elewaut, D., Burgos-Vargas, R., Stebbings, S., Appleton, L., Farrah, C., Lau, J., Kenna, T.J., Haroon, N., Ferreira, M.A., Yang, J., Mulero, J., Fernandez-Sueiro, J.L., Gonzalez-Gay, M.A., Lopez-Larrea, C., Deloukas, P., Donnelly, P., Australo-Anglo-American Spondyloarthritis, C., Groupe Francaise d'Etude Genetique des, S., Nord-Trondelag Health, S., Spondyloarthritis Research Consortium of, C., Wellcome Trust Case Control, C., Bowness, P., Gafney, K., Gaston, H., Gladman, D.D., Rahman, P., Maksymowych, W.P., Xu, H., Crusius, J.B., van der Horst-Bruinsma, I.E., Chou, C.T., Valle-Onate, R., Romero-Sanchez, C., Hansen, I.M., Pimentel-Santos, F.M., Inman, R.D., Videm, V., Martin, J., Breban, M., Reveille, J.D., Evans, D.M., Kim, T.H., Wordsworth, B.P. and Brown,

M.A. Identification of multiple risk variants for ankylosing spondylitis through high-density genotyping of immune-related loci. *Nat Genet.* 2013, **45**(7), pp.730-738.

20. Russell, T., Bridgewood, C., Rowe, H., Altaie, A., Jones, E. and McGonagle, D. Cytokine "fine tuning" of enthesis tissue homeostasis as a pointer to spondyloarthritis pathogenesis with a focus on relevant TNF and IL-17 targeted therapies. *Semin Immunopathol.* 2021, **43**(2), pp.193-206.

21. Baraliakos, X., Boehm, H., Bahrami, R., Samir, A., Schett, G., Luber, M., Ramming, A. and Braun, J. What constitutes the fat signal detected by MRI in the spine of patients with ankylosing spondylitis? A prospective study based on biopsies obtained during planned spinal osteotomy to correct hyperkyphosis or spinal stenosis. *Ann Rheum Dis.* 2019, **78**(9), pp.1220-1225.

22. Braun, J. and Sieper, J. Ankylosing spondylitis. *The Lancet.* 2007, **369**(9570), pp.1379-1390.

23. Wanders, A., Landewé, R., Dougados, M., Mielants, H., van der Linden, S. and van der Heijde, D. Association between radiographic damage of the spine and spinal mobility for individual patients with ankylosing spondylitis: can assessment of spinal mobility be a proxy for radiographic evaluation? *Annals of the Rheumatic Diseases.* 2005, **64**(7), p.988.

24. Zhu, W., He, X., Cheng, K., Zhang, L., Chen, D., Wang, X., Qiu, G., Cao, X. and Weng, X. Ankylosing spondylitis: etiology, pathogenesis, and treatments. *Bone Res.* 2019, **7**, p.22.

25. Cooper, C., Carbone, L., Michet, C.J., Atkinson, E.J., O'Fallon, W.M. and Melton, L.J., 3rd. Fracture risk in patients with ankylosing spondylitis: a population based study. *J Rheumatol.* 1994, **21**(10), pp.1877-1882.

26. Vosse, D., Landewé, R., van der Heijde, D., van der Linden, S., van Staa, T.P. and Geusens, P. Ankylosing spondylitis and the risk of fracture: results from a large primary care-based nested case-control study. *Ann Rheum Dis.* 2009, **68**(12), pp.1839-1842.

27. Marzo-Ortega, H., McGonagle, D., Jarrett, S., Haugeberg, G., Hensor, E., O'Connor, P., Tan, A.L., Conaghan, P.G., Greenstein, A. and Emery, P. Infliximab in combination with methotrexate in active ankylosing spondylitis: a clinical and imaging study. *Annals of the Rheumatic Diseases.* 2005, **64**(11), pp.1568-1575.

28. Bochkova, A.G., Levshakova, A.V., Bunchuk, N.V. and Braun, J. Spinal inflammation lesions as detected by magnetic resonance imaging in patients with early ankylosing spondylitis are more often observed in posterior structures of the spine. *Rheumatology (Oxford).* 2010, **49**(4), pp.749-755.

29. Poddubnyy, D., Hermann, K.G., Callhoff, J., Listing, J. and Sieper, J. Ustekinumab for the treatment of patients with active ankylosing spondylitis: results of a 28-week, prospective, open-label, proof-of-concept study (TOPAS). *Ann Rheum Dis.* 2014, **73**(5), pp.817-823.

30. Callhoff, J., Sieper, J., Weiss, A., Zink, A. and Listing, J. Efficacy of TNFalpha blockers in patients with ankylosing spondylitis and non-radiographic axial spondyloarthritis: a meta-analysis. *Ann Rheum Dis.* 2015, **74**(6), pp.1241-1248.

31. Korkosz, M., Czepiel, M., Gula, Z., Stec, M., Weglarczyk, K., Rutkowska-Zapala, M., Gruca, A., Lenart, M., Baran, J., Gasowski, J., Blyszczuk, P. and Siedlar, M. Sera of patients with axial spondyloarthritis (axSpA) enhance osteoclastogenic potential of monocytes isolated from healthy individuals. *BMC Musculoskelet Disord.* 2018, **19**(1), p.434.

32. Garrett, S., Jenkinson, T., Kennedy, L.G., Whitelock, H., Gaisford, P. and Calin, A. A new approach to defining disease status in ankylosing spondylitis: the Bath Ankylosing Spondylitis Disease Activity Index. *J Rheumatol.* 1994, **21**(12), pp.2286-2291.

33. Braun, J., Pham, T., Sieper, J., Davis, J., van der Linden, S., Dougados, M. and van der Heijde, D. International ASAS consensus statement for the use of anti-tumour necrosis factor agents in patients with ankylosing spondylitis. *Ann Rheum Dis.* 2003, **62**(9), pp.817-824.

34. van der Heijde, D., Sieper, J., Maksymowych, W.P., Dougados, M., Burgos-Vargas, R., Landewé, R., Rudwaleit, M. and Braun, J. 2010 Update of the international ASAS recommendations for the use of anti-TNF agents in patients with axial spondyloarthritis. *Ann Rheum Dis.* 2011, **70**(6), pp.905-908.

35. Cohen, J.D., Cunin, P., Farrenq, V., Oniankitan, O., Carton, L., Chevalier, X. and Claudepierre, P. Estimation of the Bath Ankylosing Spondylitis Disease Activity Index cutoff for perceived symptom relief in patients with spondyloarthropathies. *J Rheumatol.* 2006, **33**(1), pp.79-81.

36. Mustafa, K.N., Hammoudeh, M. and Khan, M.A. HLA-B27 Prevalence in Arab Populations and Among Patients with Ankylosing Spondylitis. *J Rheumatol.* 2012, **39**(8), pp.1675-1677.

37. Akassou, A., Yacoubi, H., Jamil, A., Dakka, N., Amzazi, S., Sadki, K., Niamane, R., Elhassani, S. and Bakri, Y. Prevalence of HLA-B27 in Moroccan healthy subjects and patients with ankylosing spondylitis and mapping construction of several factors influencing AS diagnosis by using multiple correspondence analysis. *Rheumatol Int.* 2015, **35**(11), pp.1889-1894.

38. Abdelrahman, M.H., Mahdy, S., Khanjar, I.A., Siam, A.M., Malallah, H.A., Al-Emadi, S.A., Sarakbi, H.A. and Hammoudeh, M. Prevalence of HLA-B27 in Patients with Ankylosing Spondylitis in Qatar. *Int J Rheumatol.* 2012, **2012**, p.860213.

39. van Lunteren, M., Sepriano, A., Landewe, R., Sieper, J., Rudwaleit, M., van der Heijde, D. and van Gaalen, F. Do ethnicity, degree of family relationship, and the spondyloarthritis subtype in affected relatives influence the association between a positive family history for spondyloarthritis and HLA-B27 carriership? Results from the worldwide ASAS cohort. *Arthritis Res Ther.* 2018, **20**(1), p.166.

40. Cho, S.M., Jung, S.H. and Chung, Y.J. A Variant in RUNX3 Is Associated with the Risk of Ankylosing Spondylitis in Koreans. *Genomics Inform.* 2017, **15**(2), pp.65-68.

41. Australo-Anglo-American Spondyloarthritis, C., Reveille, J.D., Sims, A.M., Danoy, P., Evans, D.M., Leo, P., Pointon, J.J., Jin, R., Zhou, X., Bradbury, L.A., Appleton, L.H., Davis, J.C., Diekman, L., Doan, T., Dowling, A., Duan, R., Duncan, E.L., Farrar, C., Hadler, J., Harvey, D., Karaderi, T., Mogg, R., Pomeroy, E., Pryce, K., Taylor, J., Savage, L., Deloukas, P., Kumanduri, V., Peltonen, L., Ring, S.M., Whittaker, P., Glazov, E., Thomas, G.P., Maksymowych, W.P., Inman, R.D., Ward, M.M., Stone, M.A., Weisman, M.H., Wordsworth, B.P. and Brown, M.A. Genome-wide association study of ankylosing spondylitis identifies non-MHC susceptibility loci. *Nat Genet.* 2010, **42**(2), pp.123-127.

42. Timms, A.E., Crane, A.M., Sims, A.M., Cordell, H.J., Bradbury, L.A., Abbott, A., Coyne, M.R., Beynon, O., Herzberg, I., Duff, G.W., Calin, A., Cardon, L.R.,

Wordsworth, B.P. and Brown, M.A. The interleukin 1 gene cluster contains a major susceptibility locus for ankylosing spondylitis. *Am J Hum Genet.* 2004, **75**(4), pp.587-595.

43. Li, L., Shi, B., Zheng, W., Xing, W., Zhao, Y., Li, F., Xin, D., Jin, T., Zhu, Y. and Yang, X. Association of IL-1A and IL-1B polymorphisms with ankylosing spondylitis among the Chinese Han population: a case-control study. *Oncotarget.* 2017, **8**(17), pp.28278-28284.

44. Evans, D.M., Spencer, C.C., Pointon, J.J., Su, Z., Harvey, D., Kochan, G., Oppermann, U., Dilthey, A., Pirinen, M., Stone, M.A., Appleton, L., Moutsianas, L., Leslie, S., Wordsworth, T., Kenna, T.J., Karaderi, T., Thomas, G.P., Ward, M.M., Weisman, M.H., Farrar, C., Bradbury, L.A., Danoy, P., Inman, R.D., Maksymowych, W., Gladman, D., Rahman, P., Spondyloarthritis Research Consortium of, C., Morgan, A., Marzo-Ortega, H., Bowness, P., Gaffney, K., Gaston, J.S., Smith, M., Bruges-Armas, J., Couto, A.R., Sorrentino, R., Paladini, F., Ferreira, M.A., Xu, H., Liu, Y., Jiang, L., Lopez-Larrea, C., Diaz-Pena, R., Lopez-Vazquez, A., Zayats, T., Band, G., Bellenguez, C., Blackburn, H., Blackwell, J.M., Bramon, E., Bumpstead, S.J., Casas, J.P., Corvin, A., Craddock, N., Deloukas, P., Dronov, S., Duncanson, A., Edkins, S., Freeman, C., Gillman, M., Gray, E., Gwilliam, R., Hammond, N., Hunt, S.E., Jankowski, J., Jayakumar, A., Langford, C., Liddle, J., Markus, H.S., Mathew, C.G., McCann, O.T., McCarthy, M.I., Palmer, C.N., Peltonen, L., Plomin, R., Potter, S.C., Rautanen, A., Ravindrarajah, R., Ricketts, M., Samani, N., Sawcer, S.J., Strange, A., Trembath, R.C., Viswanathan, A.C., Waller, M., Weston, P., Whittaker, P., Widaa, S., Wood, N.W., McVean, G., Reveille, J.D., Wordsworth, B.P., Brown, M.A., Donnelly, P., Australo-Anglo-American Spondyloarthritis, C. and Wellcome Trust Case Control, C. Interaction between ERAP1 and HLA-B27 in ankylosing spondylitis implicates peptide handling in the mechanism for HLA-B27 in disease susceptibility. *Nat Genet.* 2011, **43**(8), pp.761-767.

45. Vecellio, M., Roberts, A.R., Cohen, C.J., Cortes, A., Knight, J.C., Bowness, P. and Wordsworth, B.P. The genetic association of RUNX3 with ankylosing spondylitis can be explained by allele-specific effects on IRF4 recruitment that alter gene expression. *Ann Rheum Dis.* 2016, **75**(8), pp.1534-1540.

46. Vecellio, M., Cortes, A., Roberts, A.R., Ellis, J., Cohen, C.J., Knight, J.C., Brown, M.A., Bowness, P. and Wordsworth, B.P. Evidence for a second ankylosing spondylitis-associated RUNX3 regulatory polymorphism. *RMD Open.* 2018, **4**(1), p.e000628.

47. Apel, M., Uebe, S., Bowes, J., Giardina, E., Korendowych, E., Juneblad, K., Pasutto, F., Ekici, A.B., McManus, R., Ho, P., Bruce, I.N., Ryan, A.W., Behrens, F., Bohm, B., Traupe, H., Lohmann, J., Gieger, C., Wichmann, H.E., Padyukov, L., Fitzgerald, O., Alenius, G.M., McHugh, N.J., Novelli, G., Burkhardt, H., Barton, A., Reis, A. and Huffmeier, U. Variants in RUNX3 contribute to susceptibility to psoriatic arthritis, exhibiting further common ground with ankylosing spondylitis. *Arthritis Rheum.* 2013, **65**(5), pp.1224-1231.

48. Boyle, L.H., Goodall, J.C., Opat, S.S. and Gaston, J.S. The recognition of HLA-B27 by human CD4(+) T lymphocytes. *J Immunol.* 2001, **167**(5), pp.2619-2624.

49. DeLay, M.L., Turner, M.J., Klenk, E.I., Smith, J.A., Sowders, D.P. and Colbert, R.A. HLA-B27 misfolding and the unfolded protein response augment interleukin-23 production and are associated with Th17 activation in transgenic rats. *Arthritis Rheum.* 2009, **60**(9), pp.2633-2643.

50. Ambarus, C.A., Yeremenko, N. and Baeten, D.L. Altered cytokine expression by macrophages from HLA-B27-positive spondyloarthritis patients without evidence of endoplasmic reticulum stress. *Rheumatol Adv Pract.* 2018, **2**(1), p.rky014.

51. Benjamin, M. and McGonagle, D. The enthesis organ concept and its relevance to the spondyloarthropathies. *Adv Exp Med Biol.* 2009, **649**, pp.57-70.

52. Benjamin, M. and McGonagle, D. The anatomical basis for disease localisation in seronegative spondyloarthropathy at entheses and related sites. *J Anat.* 2001, **199**(Pt 5), pp.503-526.

53. Reilly, G.C. and Currey, J.D. The development of microcracking and failure in bone depends on the loading mode to which it is adapted. *J Exp Biol.* 1999, **202**(Pt 5), pp.543-552.

54. Dimitriou, R., Tsiridis, E. and Giannoudis, P.V. Current concepts of molecular aspects of bone healing. *Injury.* 2005, **36**(12), pp.1392-1404.

55. Sato, K., Suematsu, A., Okamoto, K., Yamaguchi, A., Morishita, Y., Kadono, Y., Tanaka, S., Kodama, T., Akira, S., Iwakura, Y., Cua, D.J. and Takayanagi, H. Th17 functions as an osteoclastogenic helper T cell subset that links T cell activation and bone destruction. *J Exp Med.* 2006, **203**(12), pp.2673-2682.

56. Adamopoulos, I.E., Tessmer, M., Chao, C.C., Adda, S., Gorman, D., Petro, M., Chou, C.C., Pierce, R.H., Yao, W., Lane, N.E., Laface, D. and Bowman, E.P. IL-23 is critical for induction of arthritis, osteoclast formation, and maintenance of bone mass. *J Immunol.* 2011, **187**(2), pp.951-959.

57. Adamopoulos, I.E. Inflammation in bone physiology and pathology. *Curr Opin Rheumatol.* 2018, **30**(1), pp.59-64.

58. Baraliakos, X., Listing, J., Rudwaleit, M., Haibel, H., Brandt, J., Sieper, J. and Braun, J. Progression of radiographic damage in patients with ankylosing spondylitis: defining the central role of syndesmophytes. *Ann Rheum Dis.* 2007, **66**(7), pp.910-915.

59. Croes, M., Oner, F.C., van Neerven, D., Sabir, E., Kruyt, M.C., Blokhuis, T.J., Dhert, W.J.A. and Alblas, J. Proinflammatory T cells and IL-17 stimulate osteoblast differentiation. *Bone.* 2016, **84**, pp.262-270.

60. Ono, T., Okamoto, K., Nakashima, T., Nitta, T., Hori, S., Iwakura, Y. and Takayanagi, H. IL-17-producing gammadelta T cells enhance bone regeneration. *Nat Commun.* 2016, **7**, p.10928.

61. McGonagle, D.G., McInnes, I.B., Kirkham, B.W., Sherlock, J. and Moots, R. The role of IL-17A in axial spondyloarthritis and psoriatic arthritis: recent advances and controversies. *Ann Rheum Dis.* 2019, **78**(9), pp.1167-1178.

62. Appel, H., Kuhne, M., Spiekermann, S., Köhler, D., Zacher, J., Stein, H., Sieper, J. and Loddenkemper, C. Immunohistochemical analysis of hip arthritis in ankylosing spondylitis: evaluation of the bone-cartilage interface and subchondral bone marrow. *Arthritis Rheum.* 2006, **54**(6), pp.1805-1813.

63. Rudwaleit, M., van der Heijde, D., Landewé, R., Listing, J., Akkoc, N., Brandt, J., Braun, J., Chou, C.T., Collantes-Estevez, E., Dougados, M., Huang, F., Gu, J., Khan, M.A., Kirazli, Y., Maksymowych, W.P., Mielants, H., Sørensen, I.J., Ozgocmen, S., Roussou, E., Valle-Oñate, R., Weber, U., Wei, J. and Sieper, J. The development of Assessment of SpondyloArthritis international Society classification

criteria for axial spondyloarthritis (part II): validation and final selection. *Ann Rheum Dis.* 2009, **68**(6), pp.777-783.

64. Sawicki, L.M., Lütje, S., Baraliakos, X., Braun, J., Kirchner, J., Boos, J., Heusch, P., Ruhlmann, V., Herrmann, K., Umutlu, L., Quick, H.H., Antoch, G. and Buchbender, C. Dual-phase hybrid (18) F-Fluoride Positron emission tomography/MRI in ankylosing spondylitis: Investigating the link between MRI bone changes, regional hyperaemia and increased osteoblastic activity. *J Med Imaging Radiat Oncol.* 2018, **62**(3), pp.313-319.

65. Wang, C.M., Tsai, S.C., Lin, J.C., Wu, Y.J., Wu, J. and Chen, J.Y. Association of Genetic Variants of RANK, RANKL, and OPG with Ankylosing Spondylitis Clinical Features in Taiwanese. *Mediators Inflamm.* 2019, **2019**, p.8029863.

66. Zheng, G., Xie, Z., Wang, P., Li, J., Li, M., Cen, S., Tang, S., Liu, W., Ye, G., Li, Y., Wang, S., Wu, X., Su, H., Wu, Y. and Shen, H. Enhanced osteogenic differentiation of mesenchymal stem cells in ankylosing spondylitis: a study based on a three-dimensional biomimetic environment. *Cell Death Dis.* 2019, **10**(5), p.350.

67. Jo, S., Wang, S.E., Lee, Y.L., Kang, S., Lee, B., Han, J., Sung, I.H., Park, Y.S., Bae, S.C. and Kim, T.H. IL-17A induces osteoblast differentiation by activating JAK2/STAT3 in ankylosing spondylitis. *Arthritis Res Ther.* 2018, **20**(1), p.115.

68. Bleil, J., Maier, R., Hempfing, A., Sieper, J., Appel, H. and Syrbe, U. Granulation Tissue Eroding the Subchondral Bone Also Promotes New Bone Formation in Ankylosing Spondylitis. *Arthritis Rheumatol.* 2016, **68**(10), pp.2456-2465.

69. Lories, R.J., Luyten, F.P. and de Vlam, K. Progress in spondylarthritis. Mechanisms of new bone formation in spondyloarthritis. *Arthritis Res Ther.* 2009, **11**(2), p.221.

70. Baeten, D., Ostergaard, M., Wei, J.C., Sieper, J., Jarvinen, P., Tam, L.S., Salvarani, C., Kim, T.H., Solinger, A., Datsenko, Y., Pamulapati, C., Visvanathan, S., Hall, D.B., Aslanyan, S., Scholl, P. and Padula, S.J. Risankizumab, an IL-23 inhibitor, for ankylosing spondylitis: results of a randomised, double-blind, placebo-controlled, proof-of-concept, dose-finding phase 2 study. *Ann Rheum Dis.* 2018, **77**(9), pp.1295-1302.

71. Deodhar, A., Gensler, L.S., Sieper, J., Clark, M., Calderon, C., Wang, Y., Zhou, Y., Leu, J.H., Campbell, K., Sweet, K., Harrison, D.D., Hsia, E.C. and van der Heijde, D. Three Multicenter, Randomized, Double-Blind, Placebo-Controlled Studies Evaluating the Efficacy and Safety of Ustekinumab in Axial Spondyloarthritis. *Arthritis Rheumatol.* 2019, **71**(2), pp.258-270.

72. Gordon, K.B., Strober, B., Lebwohl, M., Augustin, M., Blauvelt, A., Poulin, Y., Papp, K.A., Sofen, H., Puig, L., Foley, P., Ohtsuki, M., Flack, M., Geng, Z., Gu, Y., Valdes, J.M., Thompson, E.H.Z. and Bachelez, H. Efficacy and safety of risankizumab in moderate-to-severe plaque psoriasis (UltIMMa-1 and UltIMMa-2): results from two double-blind, randomised, placebo-controlled and ustekinumab-controlled phase 3 trials. *Lancet.* 2018, **392**(10148), pp.650-661.

73. van Tok, M.N., Satumtira, N., Dorris, M., Pots, D., Slobodin, G., van de Sande, M.G., Taurog, J.D., Baeten, D.L. and van Duivenvoorde, L.M. Innate Immune Activation Can Trigger Experimental Spondyloarthritis in HLA-B27/Huβ2m Transgenic Rats. *Front Immunol.* 2017, **8**, p.920.

74. van Tok, M.N., Na, S., Lao, C.R., Alvi, M., Pots, D., van de Sande, M.G.H., Taurog, J.D., Sedgwick, J.D., Baeten, D.L. and van Duivenvoorde, L.M. The Initiation, but Not the Persistence, of Experimental Spondyloarthritis Is Dependent on Interleukin-23 Signaling. *Front Immunol.* 2018, **9**, p.1550.

75. Breban, M., Glatigny, S., Cherqaoui, B., Beaufrère, M., Lauraine, M., Rincheval-Arnold, A., Gaumer, S., Guénal, I. and Araujo, L.M. Lessons on SpA pathogenesis from animal models. *Seminars in Immunopathology.* 2021.

76. Schulz, M., Dotzlaw, H. and Neeck, G. Ankylosing spondylitis and rheumatoid arthritis: serum levels of TNF-alpha and Its soluble receptors during the course of therapy with etanercept and infliximab. *Biomed Res Int.* 2014, **2014**, p.675108.

77. Baraliakos, X., Haibel, H., Listing, J., Sieper, J. and Braun, J. Continuous long-term anti-TNF therapy does not lead to an increase in the rate of new bone formation over 8 years in patients with ankylosing spondylitis. *Ann Rheum Dis.* 2014, **73**(4), pp.710-715.

78. Lubrano, E., Massimo Perrotta, F., Manara, M., D'Angelo, S., Addimanda, O., Ramonda, R., Punzi, L., Olivieri, I.,

Salvarani, C. and Marchesoni, A. Predictors of Loss of Remission and Disease Flares in Patients with Axial Spondyloarthritis Receiving Antitumor Necrosis Factor Treatment: A Retrospective Study. *J Rheumatol.* 2016, **43**(8), pp.1541-1546.

79. Wei, J.C., Kim, T.H., Kishimoto, M., Ogusu, N., Jeong, H. and Kobayashi, S. Efficacy and safety of brodalumab, an anti-IL17RA monoclonal antibody, in patients with axial spondyloarthritis: 16-week results from a randomised, placebo-controlled, phase 3 trial. *Ann Rheum Dis.* 2021.

80. Mease, P., Walsh, J.A., Baraliakos, X., Inman, R., de Vlam, K., Wei, J.C., Hunter, T., Gallo, G., Sandoval, D., Zhao, F., Dong, Y., Bolce, R. and Marzo-Ortega, H. Translating Improvements with Ixekizumab in Clinical Trial Outcomes into Clinical Practice: ASAS40, Pain, Fatigue, and Sleep in Ankylosing Spondylitis. *Rheumatol Ther.* 2019, **6**(3), pp.435-450.

81. Marzo-Ortega, H., Mease, P.J., Rahman, P., Navarro-Compan, V., Strand, V., Dougados, M., Combe, B., Wei, J.C., Baraliakos, X., Hunter, T., Sandoval, D., Li, X., Zhu, B., Bessette, L. and Deodhar, A. Impact of Ixekizumab on Work Productivity in Patients with Ankylosing Spondylitis: Results from the COAST-V and COAST-W Trials at 52 Weeks. *Rheumatol Ther.* 2020, **7**(4), pp.759-774.

82. Deodhar, A., van der Heijde, D., Gensler, L.S., Kim, T.H., Maksymowych, W.P., Ostergaard, M., Poddubnyy, D., Marzo-Ortega, H., Bessette, L., Tomita, T., Leung, A., Hojnik, M., Gallo, G., Li, X., Adams, D., Carlier, H., Sieper, J. and Group, C.-X.S. Ixekizumab for patients with non-radiographic axial spondyloarthritis (COAST-X): a randomised, placebo-controlled trial. *Lancet.* 2020, **395**(10217), pp.53-64.

83. Shah, M., Maroof, A., Gikas, P., Mittal, G., Keen, R., Baeten, D., Shaw, S. and Roberts, S.J. Dual neutralisation of IL-17F and IL-17A with bimekizumab blocks inflammation-driven osteogenic differentiation of human periosteal cells. *RMD Open.* 2020, **6**(2).

84. Balazcs, E., Sieper, J., Bickham, K., Mehta, A., Frontera, N., Stryszak, P., Popmihajlov, Z. and Peloso, P.M. A randomized, clinical trial to assess the relative efficacy and tolerability of two doses of etoricoxib versus naproxen in patients with ankylosing spondylitis. *BMC Musculoskelet Disord.* 2016, **17**(1), p.426.

85. Wang, R., Dasgupta, A. and Ward, M.M. Comparative efficacy of non-steroidal anti-inflammatory drugs in ankylosing spondylitis: a Bayesian network meta-analysis of clinical trials. *Ann Rheum Dis.* 2016, **75**(6), pp.1152-1160.

86. Cuthbert, R.J., Fragkakis, E.M., Dunsmuir, R., Li, Z., Coles, M., Marzo-Ortega, H., Giannoudis, P.V., Jones, E., El-Sherbiny, Y.M. and McGonagle, D. Brief Report: Group 3 Innate Lymphoid Cells in Human Enthesis. *Arthritis Rheumatol.* 2017, **69**(9), pp.1816-1822.

87. Gaur, P., Misra, R. and Aggarwal, A. Natural killer cell and gamma delta T cell alterations in enthesitis related arthritis category of juvenile idiopathic arthritis. *Clin Immunol.* 2015, **161**(2), pp.163-169.

88. Cuthbert, R.J., Watad, A., Fragkakis, E.M., Dunsmuir, R., Loughenbury, P., Khan, A., Millner, P.A., Davison, A., Marzo-Ortega, H., Newton, D., Bridgewood, C. and McGonagle, D.G. Evidence that tissue resident human enthesis gammadeltaT-cells can produce IL-17A independently of IL-23R transcript expression. *Ann Rheum Dis.* 2019, **78**(11), pp.1559-1565.

89. Watad, A., Rowe, H., Russell, T., Zhou, Q., Anderson, L.K., Khan, A., Dunsmuir, R., Loughenbury, P., Borse, V., Rao, A., Millner, P.A., Bragazzi, N.L., Amital, H., Cuhtbert, R., Wittmann, M., Sharif, K., Kenna, T., Brown, M.A., Newton, D., Bridgewood, C. and McGonagle, D.G. Normal human enthesis harbours conventional CD4+ and CD8+ T cells with regulatory features and inducible IL-17A and TNF expression. *Ann Rheum Dis.* 2020, **79**(8), pp.1044-1054.

90. Bridgewood, C., Watad, A., Russell, T., Palmer, T.M., Marzo-Ortega, H., Khan, A., Millner, P.A., Dunsmuir, R., Rao, A., Loughenbury, P., Wittmann, M., Cuthbert, R.J. and McGonagle, D.G. Identification of myeloid cells in the human enthesis as the main source of local IL-23 production. *Ann Rheum Dis.* 2019, **78**(7), pp.929-933.

91. Sherlock, J.P., Joyce-Shaikh, B., Turner, S.P., Chao, C.C., Sathe, M., Grein, J., Gorman, D.M., Bowman, E.P., McClanahan, T.K., Yearley, J.H., Eberl, G., Buckley, C.D., Kastelein, R.A., Pierce, R.H., Laface, D.M. and Cua, D.J. IL-23 induces spondyloarthropathy by acting on ROR-gammat+ CD3+CD4-CD8- entheseal resident T cells. *Nat Med.* 2012, **18**(7), pp.1069-1076.

92. Cambre, I., Gaublomme, D., Burssens, A., Jacques, P., Schryvers, N., De Muynck, A., Meuris, L., Lambrecht, S.,

Carter, S., de Bleser, P., Saeys, Y., Van Hoorebeke, L., Kollias, G., Mack, M., Simoens, P., Lories, R., Callewaert, N., Schett, G. and Elewaut, D. Mechanical strain determines the site-specific localization of inflammation and tissue damage in arthritis. *Nat Commun.* 2018, **9**(1), p.4613.

93. Gracey, E., Burssens, A., Cambre, I., Schett, G., Lories, R., McInnes, I.B., Asahara, H. and Elewaut, D. Tendon and ligament mechanical loading in the pathogenesis of inflammatory arthritis. *Nat Rev Rheumatol.* 2020, **16**(4), pp.193-207.

94. Hannu, T. Reactive arthritis. *Best Pract Res Clin Rheumatol.* 2011, **25**(3), pp.347-357.

95. Laasila, K. and Leirisalo-Repo, M. Recurrent reactive arthritis associated with urinary tract infection by Escherichia coli. *J Rheumatol.* 1999, **26**(10), pp.2277-2279.

96. Schiellerup, P., Krogfelt, K.A. and Locht, H. A comparison of self-reported joint symptoms following infection with different enteric pathogens: effect of HLA-B27. *J Rheumatol.* 2008, **35**(3), pp.480-487.

97. Townes, J.M., Deodhar, A.A., Laine, E.S., Smith, K., Krug, H.E., Barkhuizen, A., Thompson, M.E., Cieslak, P.R. and Sobel, J. Reactive arthritis following culture-confirmed infections with bacterial enteric pathogens in Minnesota and Oregon: a population-based study. *Annals of the Rheumatic Diseases.* 2008, **67**(12), pp.1689-1696.

98. Das, S. and Khader, S. Yin and yang of interleukin-17 in host immunity to infection. *F1000Research.* 2017, **6**, pp.741-741.

99. Alnahas, S., Hagner, S., Raifer, H., Kilic, A., Gasteiger, G., Mutters, R., Hellhund, A., Prinz, I., Pinkenburg, O., Visekruna, A., Garn, H. and Steinhoff, U. IL-17 and TNF-α Are Key Mediators of Moraxella catarrhalis Triggered Exacerbation of Allergic Airway Inflammation. *Frontiers in Immunology.* 2017, **8**, pp.1562-1562.

100. Ehlers, S. Role of tumour necrosis factor (TNF) in host defence against tuberculosis: implications for immunotherapies targeting TNF. *Annals of the Rheumatic Diseases.* 2003, **62 Suppl 2**(Suppl 2), pp.ii37-ii42.

101. Shen, H., Goodall, J.C. and Gaston, J.S. Frequency and phenotype of T helper 17 cells in peripheral blood and synovial fluid of patients with reactive arthritis. *J Rheumatol.* 2010, **37**(10), pp.2096-2099.

102. Chowdhury, A.C., Chaurasia, S., Mishra, S.K., Aggarwal, A. and Misra, R. IL-17 and IFN-γ producing NK and γδ-T cells are preferentially expanded in synovial fluid of patients with reactive arthritis and undifferentiated spondyloarthritis. *Clin Immunol.* 2017, **183**, pp.207-212.

103. Singh, R., Aggarwal, A. and Misra, R. Th1/Th17 cytokine profiles in patients with reactive arthritis/undifferentiated spondyloarthropathy. *J Rheumatol.* 2007, **34**(11), pp.2285-2290.

104. Singh, A.K., Misra, R. and Aggarwal, A. Th-17 associated cytokines in patients with reactive arthritis/undifferentiated spondyloarthropathy. *Clin Rheumatol.* 2011, **30**(6), pp.771-776.

105. Mielants, H., Veys, E.M., Cuvelier, C. and de Vos, M. Ileocolonoscopic Findings in Seronegative Spondylarthropathies. *Rheumatology.* 1988, **XXVII**(suppl_2), pp.95-105.

106. Mäki-Ikola, O., Nissilä, M., Lehtinen, K., Leirisalo-Repo, M., Toivanen, P. and Granfors, K. Antibodies to Klebsiella pneumoniae, Escherichia coli and Proteus mirabilis in the sera of patients with axial and peripheral form of ankylosing spondylitis. *Br J Rheumatol.* 1995, **34**(5), pp.413-417.

107. Holbrook, J., Lara-Reyna, S., Jarosz-Griffiths, H. and McDermott, M. Tumour necrosis factor signalling in health and disease. *F1000Res.* 2019, **8**.

108. Grine, L., Dejager, L., Libert, C. and Vandenbroucke, R.E. An inflammatory triangle in psoriasis: TNF, type I IFNs and IL-17. *Cytokine Growth Factor Rev.* 2015, **26**(1), pp.25-33.

109. Takahashi, H., Tsuji, H., Ishida-Yamamoto, A. and Iizuka, H. Plasma trough levels of adalimumab and infliximab in terms of clinical efficacy during the treatment of psoriasis. *J Dermatol.* 2013, **40**(1), pp.39-42.

110. Bose, F., Petti, L., Diani, M., Moscheni, C., Molteni, S., Altomare, A., Rossi, R.L., Talarico, D., Fontana, R., Russo, V., Altomare, G. and Reali, E. Inhibition of CCR7/CCL19 axis in lesional skin is a critical event for clinical remission induced by TNF blockade in patients with psoriasis. *Am J Pathol.* 2013, **183**(2), pp.413-421.

111. Bandzar, S., Gupta, S. and Platt, M.O. Crohn's disease: a review of treatment options and current research. *Cell Immunol.* 2013, **286**(1-2), pp.45-52.

112. Nanda, K.S., Cheifetz, A.S. and Moss, A.C. Impact of antibodies to infliximab on clinical outcomes and serum

infliximab levels in patients with inflammatory bowel disease (IBD): a meta-analysis. *Am J Gastroenterol.* 2013, **108**(1), pp.40-47; quiz 48.

113. Mast, B.A. and Schultz, G.S. Interactions of cytokines, growth factors, and proteases in acute and chronic wounds. *Wound Repair Regen.* 1996, **4**(4), pp.411-420.

114. Lukacs, N.W., Chensue, S.W., Strieter, R.M., Warmington, K. and Kunkel, S.L. Inflammatory granuloma formation is mediated by TNF-alpha-inducible intercellular adhesion molecule-1. *J Immunol.* 1994, **152**(12), pp.5883-5889.

115. Chang, C.C., Chu, C.F., Wang, C.N., Wu, H.T., Bi, K.W., Pang, J.H. and Huang, S.T. The anti-atherosclerotic effect of tanshinone IIA is associated with the inhibition of TNF-alpha-induced VCAM-1, ICAM-1 and CX3CL1 expression. *Phytomedicine.* 2014, **21**(3), pp.207-216.

116. Li, Z., Hodgkinson, T., Gothard, E.J., Boroumand, S., Lamb, R., Cummins, I., Narang, P., Sawtell, A., Coles, J., Leonov, G., Reboldi, A., Buckley, C.D., Cupedo, T., Siebel, C., Bayat, A., Coles, M.C. and Ambler, C.A. Epidermal Notch1 recruits RORgamma(+) group 3 innate lymphoid cells to orchestrate normal skin repair. *Nat Commun.* 2016, **7**, p.11394.

117. Sander, A.L., Henrich, D., Muth, C.M., Marzi, I., Barker, J.H. and Frank, J.M. In vivo effect of hyperbaric oxygen on wound angiogenesis and epithelialization. *Wound Repair Regen.* 2009, **17**(2), pp.179-184.

118. Kanno, E., Kawakami, K., Ritsu, M., Ishii, K., Tanno, H., Toriyabe, S., Imai, Y., Maruyama, R. and Tachi, M. Wound healing in skin promoted by inoculation with Pseudomonas aeruginosa PAO1: The critical role of tumor necrosis factor-alpha secreted from infiltrating neutrophils. *Wound Repair Regen.* 2011, **19**(5), pp.608-621.

119. Sommer, K., Sander, A.L., Albig, M., Weber, R., Henrich, D., Frank, J., Marzi, I. and Jakob, H. Delayed wound repair in sepsis is associated with reduced local pro-inflammatory cytokine expression. *PLoS One.* 2013, **8**(9), p.e73992.

120. Ashcroft, G.S., Jeong, M.J., Ashworth, J.J., Hardman, M., Jin, W., Moutsopoulos, N., Wild, T., McCartney-Francis, N., Sim, D., McGrady, G., Song, X.Y. and Wahl, S.M. Tumor necrosis factor-alpha (TNF-alpha) is a therapeutic target for impaired cutaneous wound healing. *Wound Repair Regen.* 2012, **20**(1), pp.38-49.

121. Jin, F.Y., Nathan, C., Radzioch, D. and Ding, A. Secretory leukocyte protease inhibitor: a macrophage product induced by and antagonistic to bacterial lipopolysaccharide. *Cell.* 1997, **88**(3), pp.417-426.

122. Mori, K., Hatamochi, A., Ueki, H., Olsen, A. and Jimenez, S.A. The transcription of human alpha 1(I) procollagen gene (COL1A1) is suppressed by tumour necrosis factor-alpha through proximal short promoter elements: evidence for suppression mechanisms mediated by two nuclear-factorbinding sites. *Biochem J.* 1996, **319 (Pt 3)**, pp.811-816.

123. Beauchef, G., Bigot, N., Kypriotou, M., Renard, E., Poree, B., Widom, R., Dompmartin-Blanchere, A., Oddos, T., Maquart, F.X., Demoor, M., Boumediene, K. and Galera, P. The p65 subunit of NF-kappaB inhibits COL1A1 gene transcription in human dermal and scleroderma fibroblasts through its recruitment on promoter by protein interaction with transcriptional activators (c-Krox, Sp1, and Sp3). *J Biol Chem.* 2012, **287**(5), pp.3462-3478.

124. Hayden, M.S. and Ghosh, S. Regulation of NF-kappaB by TNF family cytokines. *Semin Immunol.* 2014, **26**(3), pp.253-266.

125. Mori, R., Kondo, T., Ohshima, T., Ishida, Y. and Mukaida, N. Accelerated wound healing in tumor necrosis factor receptor p55-deficient mice with reduced leukocyte infiltration. *FASEB J.* 2002, **16**(9), pp.963-974.

126. Gerstenfeld, L.C., Cho, T.J., Kon, T., Aizawa, T., Tsay, A., Fitch, J., Barnes, G.L., Graves, D.T. and Einhorn, T.A. Impaired fracture healing in the absence of TNF-alpha signaling: the role of TNF-alpha in endochondral cartilage resorption. *J Bone Miner Res.* 2003, **18**(9), pp.1584-1592.

127. Glass, G.E., Chan, J.K., Freidin, A., Feldmann, M., Horwood, N.J. and Nanchahal, J. TNF-alpha promotes fracture repair by augmenting the recruitment and differentiation of muscle-derived stromal cells. *Proc Natl Acad Sci U S A.* 2011, **108**(4), pp.1585-1590.

128. Chan, J.K., Glass, G.E., Ersek, A., Freidin, A., Williams, G.A., Gowers, K., Espirito Santo, A.I., Jeffery, R., Otto, W.R., Poulsom, R., Feldmann, M., Rankin, S.M., Horwood, N.J. and Nanchahal, J. Low-dose TNF augments fracture healing in normal and osteoporotic bone by up-regulating the innate immune response. *EMBO Mol Med.* 2015, **7**(5), pp.547-561.

129. Sun, T., Wang, X., Liu, Z., Liu, S. and Zhang, J. Patterns of cytokine release and evolution of remote organs from proximal femur fracture in COPD rats. *Injury.* 2011, **42**(8), pp.825-832.
130. Currie, H.N., Loos, M.S., Vrana, J.A., Dragan, K. and Boyd, J.W. Spatial cytokine distribution following traumatic injury. *Cytokine.* 2014, **66**(2), pp.112-118.
131. Fu, X., Han, B., Cai, S., Lei, Y., Sun, T. and Sheng, Z. Migration of bone marrow-derived mesenchymal stem cells induced by tumor necrosis factor-alpha and its possible role in wound healing. *Wound Repair Regen.* 2009, **17**(2), pp.185-191.
132. Xiao, Q., Wang, S.K., Tian, H., Xin, L., Zou, Z.G., Hu, Y.L., Chang, C.M., Wang, X.Y., Yin, Q.S., Zhang, X.H. and Wang, L.Y. TNF-alpha increases bone marrow mesenchymal stem cell migration to ischemic tissues. *Cell Biochem Biophys.* 2012, **62**(3), pp.409-414.
133. Lu, Z.Y., Chen, W.C., Li, Y.H., Li, L., Zhang, H., Pang, Y., Xiao, Z.F., Xiao, H.W. and Xiao, Y. TNF-alpha enhances vascular cell adhesion molecule-1 expression in human bone marrow mesenchymal stem cells via the NF-kappaB, ERK and JNK signaling pathways. *Mol Med Rep.* 2016, **14**(1), pp.643-648.
134. Martensson, K., Chrysis, D. and Savendahl, L. Interleukin-1beta and TNF-alpha act in synergy to inhibit longitudinal growth in fetal rat metatarsal bones. *J Bone Miner Res.* 2004, **19**(11), pp.1805-1812.
135. Fernandez-Vojvodich, P., Karimian, E. and Savendahl, L. The biologics anakinra and etanercept prevent cytokine-induced growth retardation in cultured fetal rat metatarsal bones. *Horm Res Paediatr.* 2011, **76**(4), pp.278-285.
136. Lehmann, W., Edgar, C.M., Wang, K., Cho, T.J., Barnes, G.L., Kakar, S., Graves, D.T., Rueger, J.M., Gerstenfeld, L.C. and Einhorn, T.A. Tumor necrosis factor alpha (TNF-alpha) coordinately regulates the expression of specific matrix metalloproteinases (MMPS) and angiogenic factors during fracture healing. *Bone.* 2005, **36**(2), pp.300-310.
137. Wang, Y., Li de, L., Zhang, X.B., Duan, Y.H., Wu, Z.H., Hao, D.S., Chen, B.S. and Qiu, G.X. Increase of TNFalpha-stimulated osteoarthritic chondrocytes apoptosis and decrease of matrix metalloproteinases 9 by NF-kappaB inhibition. *Biomed Environ Sci.* 2013, **26**(4), pp.277-283.

138. Briolay, A., Lencel, P., Bessueille, L., Caverzasio, J., Buchet, R. and Magne, D. Autocrine stimulation of osteoblast activity by Wnt5a in response to TNF-alpha in human mesenchymal stem cells. *Biochem Biophys Res Commun.* 2013, **430**(3), pp.1072-1077.

139. Li, X., Wang, J., Zhan, Z., Li, S., Zheng, Z., Wang, T., Zhang, K., Pan, H., Li, Z., Zhang, N. and Liu, H. Inflammation Intensity-Dependent Expression of Osteoinductive Wnt Proteins Is Critical for Ectopic New Bone Formation in Ankylosing Spondylitis. *Arthritis Rheumatol.* 2018, **70**(7), pp.1056-1070.

140. Kaneki, H., Guo, R., Chen, D., Yao, Z., Schwarz, E.M., Zhang, Y.E., Boyce, B.F. and Xing, L. Tumor necrosis factor promotes Runx2 degradation through up-regulation of Smurf1 and Smurf2 in osteoblasts. *J Biol Chem.* 2006, **281**(7), pp.4326-4333.

141. Ding, J., Ghali, O., Lencel, P., Broux, O., Chauveau, C., Devedjian, J.C., Hardouin, P. and Magne, D. TNF-alpha and IL-1beta inhibit RUNX2 and collagen expression but increase alkaline phosphatase activity and mineralization in human mesenchymal stem cells. *Life Sci.* 2009, **84**(15-16), pp.499-504.

142. Hah, Y.S., Kang, H.G., Cho, H.Y., Shin, S.H., Kim, U.K., Park, B.W., Lee, S.I., Rho, G.J., Kim, J.R. and Byun, J.H. JNK signaling plays an important role in the effects of TNF-alpha and IL-1beta on in vitro osteoblastic differentiation of cultured human periosteal-derived cells. *Mol Biol Rep.* 2013, **40**(8), pp.4869-4881.

143. Diarra, D., Stolina, M., Polzer, K., Zwerina, J., Ominsky, M.S., Dwyer, D., Korb, A., Smolen, J., Hoffmann, M., Scheinecker, C., van der Heide, D., Landewe, R., Lacey, D., Richards, W.G. and Schett, G. Dickkopf-1 is a master regulator of joint remodeling. *Nat Med.* 2007, **13**(2), pp.156-163.

144. Sun, W., Tian, L., Jiang, L., Zhang, S., Zhou, M., Zhu, J. and Xue, J. Sclerostin rather than Dickkopf-1 is associated with mSASSS but not with disease activity score in patients with ankylosing spondylitis. *Clin Rheumatol.* 2019, **38**(4), pp.989-995.

145. Zhang, L., Ouyang, H., Xie, Z., Liang, Z.H. and Wu, X.W. Serum DKK-1 level in the development of ankylosing spondylitis and rheumatic arthritis: a meta-analysis. *Exp Mol Med.* 2016, **48**, p.e228.

146. Liao, H.T., Lin, Y.F., Tsai, C.Y. and Chou, T.C. Bone morphogenetic proteins and Dickkopf-1 in ankylosing spondylitis. *Scand J Rheumatol.* 2018, **47**(1), pp.56-61.

147. Di, G., Kong, L., Zhao, Q. and Ding, T. MicroRNA-146a knockdown suppresses the progression of ankylosing spondylitis by targeting dickkopf 1. *Biomed Pharmacother.* 2018, **97**, pp.1243-1249.

148. Sakellariou, G.T., Iliopoulos, A., Konsta, M., Kenanidis, E., Potoupnis, M., Tsiridis, E., Gavana, E. and Sayegh, F.E. Serum levels of Dkk-1, sclerostin and VEGF in patients with ankylosing spondylitis and their association with smoking, and clinical, inflammatory and radiographic parameters. *Joint Bone Spine.* 2017, **84**(3), pp.309-315.

149. Wu, M., Chen, M., Ma, Y., Yang, J., Han, R., Yuan, Y., Hu, X., Wang, M., Zhang, X., Xu, S., Liu, R., Jiang, G., Xu, J., Shuai, Z., Zou, Y., Pan, G. and Pan, F. Dickkopf-1 in ankylosing spondylitis: Review and meta-analysis. *Clin Chim Acta.* 2018, **481**, pp.177-183.

150. Daoussis, D., Liossis, S.N., Solomou, E.E., Tsanaktsi, A., Bounia, K., Karampetsou, M., Yiannopoulos, G. and Andonopoulos, A.P. Evidence that Dkk-1 is dysfunctional in ankylosing spondylitis. *Arthritis Rheum.* 2010, **62**(1), pp.150-158.

151. Han, Q., Das, S., Hirano, M., Holland, S.J., McCurley, N., Guo, P., Rosenberg, C.S., Boehm, T. and Cooper, M.D. Characterization of Lamprey IL-17 Family Members and Their Receptors. *J Immunol.* 2015, **195**(11), pp.5440-5451.

152. Goepfert, A., Lehmann, S., Wirth, E. and Rondeau, J.M. The human IL-17A/F heterodimer: a two-faced cytokine with unique receptor recognition properties. *Sci Rep.* 2017, **7**(1), p.8906.

153. Langrish, C.L., Chen, Y., Blumenschein, W.M., Mattson, J., Basham, B., Sedgwick, J.D., McClanahan, T., Kastelein, R.A. and Cua, D.J. IL-23 drives a pathogenic T cell population that induces autoimmune inflammation. *J Exp Med.* 2005, **201**(2), pp.233-240.

154. Teunissen, M.B.M., Yeremenko, N.G., Baeten, D.L.P., Chielie, S., Spuls, P.I., de Rie, M.A., Lantz, O. and Res, P.C.M. The IL-17A-producing CD8+ T-cell population in psoriatic lesional skin comprises mucosa-associated invariant T cells and conventional T cells. *J Invest Dermatol.* 2014, **134**(12), pp.2898-2907.

155. Ciccia, F., Guggino, G., Rizzo, A., Saieva, L., Peralta, S., Giardina, A., Cannizzaro, A., Sireci, G., De Leo, G., Alessandro, R. and Triolo, G. Type 3 innate lymphoid cells producing IL-17 and IL-22 are expanded in the gut, in the peripheral blood, synovial fluid and bone marrow of patients with ankylosing spondylitis. *Ann Rheum Dis.* 2015, **74**(9), pp.1739-1747.

156. Venken, K., Jacques, P., Mortier, C., Labadia, M.E., Decruy, T., Coudenys, J., Hoyt, K., Wayne, A.L., Hughes, R., Turner, M., Van Gassen, S., Martens, L., Smith, D., Harcken, C., Wahle, J., Wang, C.T., Verheugen, E., Schryvers, N., Varkas, G., Cypers, H., Wittoek, R., Piette, Y., Gyselbrecht, L., Van Calenbergh, S., Van den Bosch, F., Saeys, Y., Nabozny, G. and Elewaut, D. RORgammat inhibition selectively targets IL-17 producing iNKT and gammadelta-T cells enriched in Spondyloarthritis patients. *Nat Commun.* 2019, **10**(1), p.9.

157. Yu, J.-S., Hamada, M., Ohtsuka, S., Yoh, K., Takahashi, S. and Miaw, S.-C. Differentiation of IL-17-Producing Invariant Natural Killer T Cells Requires Expression of the Transcription Factor c-Maf. *Frontiers in Immunology.* 2017, **8**, pp.1399-1399.

158. Toussirot, E., Laheurte, C., Gaugler, B., Gabriel, D. and Saas, P. Increased IL-22- and IL-17A-Producing Mucosal-Associated Invariant T Cells in the Peripheral Blood of Patients With Ankylosing Spondylitis. *Front Immunol.* 2018, **9**, p.1610.

159. Wright, J.F., Bennett, F., Li, B., Brooks, J., Luxenberg, D.P., Whitters, M.J., Tomkinson, K.N., Fitz, L.J., Wolfman, N.M., Collins, M., Dunussi-Joannopoulos, K., Chatterjee-Kishore, M. and Carreno, B.M. The human IL-17F/IL-17A heterodimeric cytokine signals through the IL-17RA/IL-17RC receptor complex. *J Immunol.* 2008, **181**(4), pp.2799-2805.

160. Sutton, C.E., Lalor, S.J., Sweeney, C.M., Brereton, C.F., Lavelle, E.C. and Mills, K.H. Interleukin-1 and IL-23 induce innate IL-17 production from gammadelta T cells, amplifying Th17 responses and autoimmunity. *Immunity.* 2009, **31**(2), pp.331-341.

161. Gray, E.E., Suzuki, K. and Cyster, J.G. Cutting edge: Identification of a motile IL-17-producing gammadelta T cell population in the dermis. *J Immunol.* 2011, **186**(11), pp.6091-6095.

162. Maher, B.M., Mulcahy, M.E., Murphy, A.G., Wilk, M., O'Keeffe, K.M., Geoghegan, J.A., Lavelle, E.C. and McLoughlin, R.M. Nlrp-3-driven interleukin 17 production by gammadeltaT cells controls infection outcomes during Staphylococcus aureus surgical site infection. *Infect Immun.* 2013, **81**(12), pp.4478-4489.

163. Takagi, N., Kawakami, K., Kanno, E., Tanno, H., Takeda, A., Ishii, K., Imai, Y., Iwakura, Y. and Tachi, M. IL-17A promotes neutrophilic inflammation and disturbs acute wound healing in skin. *Exp Dermatol.* 2017, **26**(2), pp.137-144.

164. Wilgus, T.A., Roy, S. and McDaniel, J.C. Neutrophils and Wound Repair: Positive Actions and Negative Reactions. *Adv Wound Care (New Rochelle).* 2013, **2**(7), pp.379-388.

165. Rodero, M.P., Hodgson, S.S., Hollier, B., Combadiere, C. and Khosrotehrani, K. Reduced Il17a expression distinguishes a Ly6c(lo)MHCII(hi) macrophage population promoting wound healing. *J Invest Dermatol.* 2013, **133**(3), pp.783-792.

166. McDaniel, J.C., Roy, S. and Wilgus, T.A. Neutrophil activity in chronic venous leg ulcers--a target for therapy? *Wound Repair Regen.* 2013, **21**(3), pp.339-351.

167. MacLeod, A.S., Hemmers, S., Garijo, O., Chabod, M., Mowen, K., Witherden, D.A. and Havran, W.L. Dendritic epidermal T cells regulate skin antimicrobial barrier function. *J Clin Invest.* 2013, **123**(10), pp.4364-4374.

168. Li, Y., Wang, Y., Zhou, L., Liu, M., Liang, G., Yan, R., Jiang, Y., Hao, J., Zhang, X., Hu, X., Huang, Y., Wang, R., Yin, Z., Wu, J., Luo, G. and He, W. Vgamma4 T Cells Inhibit the Pro-healing Functions of Dendritic Epidermal T Cells to Delay Skin Wound Closure Through IL-17A. *Front Immunol.* 2018, **9**, p.240.

169. Shelton, S.K., Bai, S.R., Jordan, J.K. and Sheehan, A.H. Ixekizumab: A Review of Its Use for the Management of Moderate to Severe Plaque Psoriasis. *Ann Pharmacother.* 2019, **53**(3), pp.276-284.

170. Lai, Y., Li, D., Li, C., Muehleisen, B., Radek, K.A., Park, H.J., Jiang, Z., Li, Z., Lei, H., Quan, Y., Zhang, T., Wu, Y., Kotol, P., Morizane, S., Hata, T.R., Iwatsuki, K., Tang, C. and Gallo, R.L. The antimicrobial protein REG3A regulates keratinocyte proliferation and differentiation after skin injury. *Immunity.* 2012, **37**(1), pp.74-84.

171. Kezic, S., Kemperman, P.M., Koster, E.S., de Jongh, C.M., Thio, H.B., Campbell, L.E., Irvine, A.D., McLean, W.H., Puppels, G.J. and Caspers, P.J. Loss-of-function mutations in the filaggrin gene lead to reduced level of natural moisturizing factor in the stratum corneum. *J Invest Dermatol.* 2008, **128**(8), pp.2117-2119.

172. Gutowska-Owsiak, D., Schaupp, A.L., Salimi, M., Selvakumar, T.A., McPherson, T., Taylor, S. and Ogg, G.S. IL-17 downregulates filaggrin and affects keratinocyte expression of genes associated with cellular adhesion. *Exp Dermatol.* 2012, **21**(2), pp.104-110.

173. Schon, M.P. and Boehncke, W.H. Psoriasis. *N Engl J Med.* 2005, **352**(18), pp.1899-1912.

174. Saunte, D.M., Mrowietz, U., Puig, L. and Zachariae, C. Candida infections in patients with psoriasis and psoriatic arthritis treated with interleukin-17 inhibitors and their practical management. *Br J Dermatol.* 2017, **177**(1), pp.47-62.

175. Hueber, W., Sands, B.E., Lewitzky, S., Vandemeulebroecke, M., Reinisch, W., Higgins, P.D., Wehkamp, J., Feagan, B.G., Yao, M.D., Karczewski, M., Karczewski, J., Pezous, N., Bek, S., Bruin, G., Mellgard, B., Berger, C., Londei, M., Bertolino, A.P., Tougas, G., Travis, S.P. and Secukinumab in Crohn's Disease Study, G. Secukinumab, a human anti-IL-17A monoclonal antibody, for moderate to severe Crohn's disease: unexpected results of a randomised, double-blind placebo-controlled trial. *Gut.* 2012, **61**(12), pp.1693-1700.

176. Lee, J.S., Tato, C.M., Joyce-Shaikh, B., Gulen, M.F., Cayatte, C., Chen, Y., Blumenschein, W.M., Judo, M., Ayanoglu, G., McClanahan, T.K., Li, X. and Cua, D.J. Interleukin-23-Independent IL-17 Production Regulates Intestinal Epithelial Permeability. *Immunity.* 2015, **43**(4), pp.727-738.

177. Song, X., Dai, D., He, X., Zhu, S., Yao, Y., Gao, H., Wang, J., Qu, F., Qiu, J., Wang, H., Li, X., Shen, N. and Qian, Y. Growth Factor FGF2 Cooperates with Interleukin-17 to Repair Intestinal Epithelial Damage. *Immunity.* 2015, **43**(3), pp.488-501.

178. Ono, T. and Takayanagi, H. Osteoimmunology in Bone Fracture Healing. *Curr Osteoporos Rep.* 2017, **15**(4), pp.367-375.

179. Kim, Y.G., Park, J.W., Lee, J.M., Suh, J.Y., Lee, J.K., Chang, B.S., Um, H.S., Kim, J.Y. and Lee, Y. IL-17 inhibits osteoblast differentiation and bone regeneration in rat. *Arch Oral Biol.* 2014, **59**(9), pp.897-905.
180. Jo, S., Lee, J.K., Han, J., Lee, B., Kang, S., Hwang, K.T., Park, Y.S. and Kim, T.H. Identification and characterization of human bone-derived cells. *Biochem Biophys Res Commun.* 2018, **495**(1), pp.1257-1263.
181. Shaw, A.T., Maeda, Y. and Gravallese, E.M. IL-17A deficiency promotes periosteal bone formation in a model of inflammatory arthritis. *Arthritis Res Ther.* 2016, **18**(1), p.104.
182. Kotake, S., Udagawa, N., Takahashi, N., Matsuzaki, K., Itoh, K., Ishiyama, S., Saito, S., Inoue, K., Kamatani, N., Gillespie, M.T., Martin, T.J. and Suda, T. IL-17 in synovial fluids from patients with rheumatoid arthritis is a potent stimulator of osteoclastogenesis. *J Clin Invest.* 1999, **103**(9), pp.1345-1352.
183. Goepfert, A., Lehmann, S., Blank, J., Kolbinger, F. and Rondeau, J.M. Structural Analysis Reveals that the Cytokine IL-17F Forms a Homodimeric Complex with Receptor IL-17RC to Drive IL-17RA-Independent Signaling. *Immunity.* 2020, **52**(3), pp.499-512.e495.
184. Akimzhanov, A.M., Yang, X.O. and Dong, C. Chromatin remodeling of interleukin-17 (IL-17)-IL-17F cytokine gene locus during inflammatory helper T cell differentiation. *J Biol Chem.* 2007, **282**(9), pp.5969-5972.
185. Iwakura, Y., Ishigame, H., Saijo, S. and Nakae, S. Functional specialization of interleukin-17 family members. *Immunity.* 2011, **34**(2), pp.149-162.
186. Kuestner, R.E., Taft, D.W., Haran, A., Brandt, C.S., Brender, T., Lum, K., Harder, B., Okada, S., Ostrander, C.D., Kreindler, J.L., Aujla, S.J., Reardon, B., Moore, M., Shea, P., Schreckhise, R., Bukowski, T.R., Presnell, S., Guerra-Lewis, P., Parrish-Novak, J., Ellsworth, J.L., Jaspers, S., Lewis, K.E., Appleby, M., Kolls, J.K., Rixon, M., West, J.W., Gao, Z. and Levin, S.D. Identification of the IL-17 receptor related molecule IL-17RC as the receptor for IL-17F. *J Immunol.* 2007, **179**(8), pp.5462-5473.
187. Ishigame, H., Kakuta, S., Nagai, T., Kadoki, M., Nambu, A., Komiyama, Y., Fujikado, N., Tanahashi, Y., Akitsu, A., Kotaki, H., Sudo, K., Nakae, S., Sasakawa, C. and Iwakura, Y. Differential roles of interleukin-17A and -17F in host

defense against mucoepithelial bacterial infection and allergic responses. *Immunity.* 2009, **30**(1), pp.108-119.

188. Rathore, J.S. and Wang, Y. Protective role of Th17 cells in pulmonary infection. *Vaccine.* 2016, **34**(13), pp.1504-1514.

189. Whibley, N., Tritto, E., Traggiai, E., Kolbinger, F., Moulin, P., Brees, D., Coleman, B.M., Mamo, A.J., Garg, A.V., Jaycox, J.R., Siebenlist, U., Kammuller, M. and Gaffen, S.L. Antibody blockade of IL-17 family cytokines in immunity to acute murine oral mucosal candidiasis. *J Leukoc Biol.* 2016, **99**(6), pp.1153-1164.

190. Boisson, B., Wang, C., Pedergnana, V., Wu, L., Cypowyj, S., Rybojad, M., Belkadi, A., Picard, C., Abel, L., Fieschi, C., Puel, A., Li, X. and Casanova, J.L. An ACT1 mutation selectively abolishes interleukin-17 responses in humans with chronic mucocutaneous candidiasis. *Immunity.* 2013, **39**(4), pp.676-686.

191. Soderstrom, C., Berstein, G., Zhang, W., Valdez, H., Fitz, L., Kuhn, M. and Fraser, S. Ultra-Sensitive Measurement of IL-17A and IL-17F in Psoriasis Patient Serum and Skin. *Aaps j.* 2017, **19**(4), pp.1218-1222.

192. van der Fits, L., Mourits, S., Voerman, J.S., Kant, M., Boon, L., Laman, J.D., Cornelissen, F., Mus, A.M., Florencia, E., Prens, E.P. and Lubberts, E. Imiquimod-induced psoriasis-like skin inflammation in mice is mediated via the IL-23/IL-17 axis. *J Immunol.* 2009, **182**(9), pp.5836-5845.

193. Fujishima, S., Watanabe, H., Kawaguchi, M., Suzuki, T., Matsukura, S., Homma, T., Howell, B.G., Hizawa, N., Mitsuya, T., Huang, S.K. and Iijima, M. Involvement of IL-17F via the induction of IL-6 in psoriasis. *Arch Dermatol Res.* 2010, **302**(7), pp.499-505.

194. Wang, Y., Kim, J., Chan, A., Whyne, C. and Nam, D. A two phase regulation of bone regeneration: IL-17F mediates osteoblastogenesis via C/EBP-beta in vitro. *Bone.* 2018, **116**, pp.47-57.

195. Nam, D., Mau, E., Wang, Y., Wright, D., Silkstone, D., Whetstone, H., Whyne, C. and Alman, B. T-lymphocytes enable osteoblast maturation via IL-17F during the early phase of fracture repair. *PLoS One.* 2012, **7**(6), p.e40044.

196. Erkol Inal, E., Gorukmez, O., Eroglu, S., Ozemri, S.S., Solak, O., Gorukmez, O. and Yakut, T. Associations between polymorphisms of IL-17F and IL-17A genes with disease activity and clinical outcome of Ankylosing Spondylitis. *Acta Reumatol Port.* 2016, **41**(3), pp.232-239.

197. Gaffen, S.L. Structure and signalling in the IL-17 receptor family. *Nat Rev Immunol.* 2009, **9**(8), pp.556-567.
198. Ramirez-Carrozzi, V., Ota, N., Sambandam, A., Wong, K., Hackney, J., Martinez-Martin, N., Ouyang, W. and Pappu, R. Cutting Edge: IL-17B Uses IL-17RA and IL-17RB to Induce Type 2 Inflammation from Human Lymphocytes. *J Immunol.* 2019, **202**(7), pp.1935-1941.
199. Li, H., Chen, J., Huang, A., Stinson, J., Heldens, S., Foster, J., Dowd, P., Gurney, A.L. and Wood, W.I. Cloning and characterization of IL-17B and IL-17C, two new members of the IL-17 cytokine family. *Proc Natl Acad Sci U S A.* 2000, **97**(2), pp.773-778.
200. Brembilla, N.C., Senra, L. and Boehncke, W.H. The IL-17 Family of Cytokines in Psoriasis: IL-17A and Beyond. *Front Immunol.* 2018, **9**, p.1682.
201. Senra, L., Stalder, R., Alvarez Martinez, D., Chizzolini, C., Boehncke, W.H. and Brembilla, N.C. Keratinocyte-Derived IL-17E Contributes to Inflammation in Psoriasis. *J Invest Dermatol.* 2016, **136**(10), pp.1970-1980.
202. Johnston, A., Fritz, Y., Dawes, S.M., Diaconu, D., Al-Attar, P.M., Guzman, A.M., Chen, C.S., Fu, W., Gudjonsson, J.E., McCormick, T.S. and Ward, N.L. Keratinocyte overexpression of IL-17C promotes psoriasiform skin inflammation. *J Immunol.* 2013, **190**(5), pp.2252-2262.
203. Angkasekwinai, P., Park, H., Wang, Y.H., Wang, Y.H., Chang, S.H., Corry, D.B., Liu, Y.J., Zhu, Z. and Dong, C. Interleukin 25 promotes the initiation of proallergic type 2 responses. *J Exp Med.* 2007, **204**(7), pp.1509-1517.
204. Natarajan, K., Mathialagan, G.D., Raghavan, S. and Shanmugam, N. The Advanced Lipoxidation end Product Precursor Malondialdehyde Induces IL-17E Expression and Skews Lymphocytes to the th17 Subset. *Cell Mol Biol Lett.* 2015, **20**(4), pp.647-662.
205. Tang, W., Smith, S.G., Beaudin, S., Dua, B., Howie, K., Gauvreau, G. and O'Byrne, P.M. IL-25 and IL-25 receptor expression on eosinophils from subjects with allergic asthma. *Int Arch Allergy Immunol.* 2014, **163**(1), pp.5-10.
206. Ramirez-Carrozzi, V., Sambandam, A., Luis, E., Lin, Z., Jeet, S., Lesch, J., Hackney, J., Kim, J., Zhou, M., Lai, J., Modrusan, Z., Sai, T., Lee, W., Xu, M., Caplazi, P., Diehl, L., de Voss, J., Balazs, M., Gonzalez, L., Jr., Singh, H., Ouyang, W. and Pappu, R. IL-17C regulates the innate

immune function of epithelial cells in an autocrine manner. *Nat Immunol.* 2011, **12**(12), pp.1159-1166.

207. Xu, M., Lu, H., Lee, Y.H., Wu, Y., Liu, K., Shi, Y., An, H., Zhang, J., Wang, X., Lai, Y. and Dong, C. An Interleukin-25-Mediated Autoregulatory Circuit in Keratinocytes Plays a Pivotal Role in Psoriatic Skin Inflammation. *Immunity.* 2018, **48**(4), pp.787-798 e784.

208. Hvid, M., Vestergaard, C., Kemp, K., Christensen, G.B., Deleuran, B. and Deleuran, M. IL-25 in atopic dermatitis: a possible link between inflammation and skin barrier dysfunction? *J Invest Dermatol.* 2011, **131**(1), pp.150-157.

209. Chang, S.H., Reynolds, J.M., Pappu, B.P., Chen, G., Martinez, G.J. and Dong, C. Interleukin-17C promotes Th17 cell responses and autoimmune disease via interleukin-17 receptor E. *Immunity.* 2011, **35**(4), pp.611-621.

210. Qian, Y., Kang, Z., Liu, C. and Li, X. IL-17 signaling in host defense and inflammatory diseases. *Cell Mol Immunol.* 2010, **7**(5), pp.328-333.

211. Vandeghinste, N., Klattig, J., Jagerschmidt, C., Lavazais, S., Marsais, F., Haas, J.D., Auberval, M., Lauffer, F., Moran, T., Ongenaert, M., Van Balen, M., Dupont, S., Lepescheux, L., Garcia, T., Hartle, S., Eyerich, K., Fallon, P.G., Brys, R. and Steidl, S. Neutralization of IL-17C Reduces Skin Inflammation in Mouse Models of Psoriasis and Atopic Dermatitis. *J Invest Dermatol.* 2018, **138**(7), pp.1555-1563.

212. Johansen, C., Vinter, H., Soegaard-Madsen, L., Olsen, L.R., Steiniche, T., Iversen, L. and Kragballe, K. Preferential inhibition of the mRNA expression of p38 mitogen-activated protein kinase regulated cytokines in psoriatic skin by anti-TNFalpha therapy. *Br J Dermatol.* 2010, **163**(6), pp.1194-1204.

213. Batalla, A., Coto, E., Gonzalez-Lara, L., Gonzalez-Fernandez, D., Gomez, J., Aranguren, T.F., Queiro, R., Santos-Juanes, J., Lopez-Larrea, C. and Coto-Segura, P. Association between single nucleotide polymorphisms IL17RA rs4819554 and IL17E rs79877597 and Psoriasis in a Spanish cohort. *J Dermatol Sci.* 2015, **80**(2), pp.111-115.

214. Johansen, C., Usher, P.A., Kjellerup, R.B., Lundsgaard, D., Iversen, L. and Kragballe, K. Characterization of the interleukin-17 isoforms and receptors in lesional psoriatic skin. *Br J Dermatol.* 2009, **160**(2), pp.319-324.

215. Kokubu, T., Haudenschild, D.R., Moseley, T.A., Rose, L. and Reddi, A.H. Immunolocalization of IL-17A, IL-17B, and their receptors in chondrocytes during fracture healing. *J Histochem Cytochem.* 2008, **56**(2), pp.89-95.

216. Yamaguchi, Y., Fujio, K., Shoda, H., Okamoto, A., Tsuno, N.H., Takahashi, K. and Yamamoto, K. IL-17B and IL-17C are associated with TNF-alpha production and contribute to the exacerbation of inflammatory arthritis. *J Immunol.* 2007, **179**(10), pp.7128-7136.

217. Liu, D., Cao, T., Wang, N., Liu, C., Ma, N., Tu, R. and Min, X. IL-25 attenuates rheumatoid arthritis through suppression of Th17 immune responses in an IL-13-dependent manner. *Sci Rep.* 2016, **6**, p.36002.

218. Gumus, P., Buduneli, E., Biyikoglu, B., Aksu, K., Sarac, F., Nile, C., Lappin, D. and Buduneli, N. Gingival crevicular fluid, serum levels of receptor activator of nuclear factor-kappaB ligand, osteoprotegerin, and interleukin-17 in patients with rheumatoid arthritis and osteoporosis and with periodontal disease. *J Periodontol.* 2013, **84**(11), pp.1627-1637.

219. Kleinschek, M.A., Owyang, A.M., Joyce-Shaikh, B., Langrish, C.L., Chen, Y., Gorman, D.M., Blumenschein, W.M., McClanahan, T., Brombacher, F., Hurst, S.D., Kastelein, R.A. and Cua, D.J. IL-25 regulates Th17 function in autoimmune inflammation. *J Exp Med.* 2007, **204**(1), pp.161-170.

220. Reynolds, J.M., Martinez, G.J., Nallaparaju, K.C., Chang, S.H., Wang, Y.H. and Dong, C. Cutting edge: regulation of intestinal inflammation and barrier function by IL-17C. *J Immunol.* 2012, **189**(9), pp.4226-4230.

221. Friedrich, M., Diegelmann, J., Schauber, J., Auernhammer, C.J. and Brand, S. Intestinal neuroendocrine cells and goblet cells are mediators of IL-17A-amplified epithelial IL-17C production in human inflammatory bowel disease. *Mucosal Immunol.* 2015, **8**(4), pp.943-958.

222. Im, E., Jung, J. and Rhee, S.H. Toll-like receptor 5 engagement induces interleukin-17C expression in intestinal epithelial cells. *J Interferon Cytokine Res.* 2012, **32**(12), pp.583-591.

223. Friedrich, M., Tillack, C., Wollenberg, A., Schauber, J. and Brand, S. IL-36gamma sustains a proinflammatory self-amplifying loop with IL-17C in anti-TNF-induced

psoriasiform skin lesions of patients with Crohn's disease. *Inflamm Bowel Dis.* 2014, **20**(11), pp.1891-1901.

224. Xie, M.H., Aggarwal, S., Ho, W.H., Foster, J., Zhang, Z., Stinson, J., Wood, W.I., Goddard, A.D. and Gurney, A.L. Interleukin (IL)-22, a novel human cytokine that signals through the interferon receptor-related proteins CRF2-4 and IL-22R. *J Biol Chem.* 2000, **275**(40), pp.31335-31339.

225. Logsdon, N.J., Jones, B.C., Josephson, K., Cook, J. and Walter, M.R. Comparison of interleukin-22 and interleukin-10 soluble receptor complexes. *J Interferon Cytokine Res.* 2002, **22**(11), pp.1099-1112.

226. Wolk, K., Kunz, S., Witte, E., Friedrich, M., Asadullah, K. and Sabat, R. IL-22 increases the innate immunity of tissues. *Immunity.* 2004, **21**(2), pp.241-254.

227. El-Zayadi, A.A., Jones, E.A., Churchman, S.M., Baboolal, T.G., Cuthbert, R.J., El-Jawhari, J.J., Badawy, A.M., Alase, A.A., El-Sherbiny, Y.M. and McGonagle, D. Interleukin-22 drives the proliferation, migration and osteogenic differentiation of mesenchymal stem cells: a novel cytokine that could contribute to new bone formation in spondyloarthropathies. *Rheumatology (Oxford).* 2017, **56**(3), pp.488-493.

228. Boniface, K., Bernard, F.X., Garcia, M., Gurney, A.L., Lecron, J.C. and Morel, F. IL-22 inhibits epidermal differentiation and induces proinflammatory gene expression and migration of human keratinocytes. *J Immunol.* 2005, **174**(6), pp.3695-3702.

229. Martin, J.C., Wolk, K., Beriou, G., Abidi, A., Witte-Handel, E., Louvet, C., Kokolakis, G., Drujont, L., Dumoutier, L., Renauld, J.C., Sabat, R. and Josien, R. Limited Presence of IL-22 Binding Protein, a Natural IL-22 Inhibitor, Strengthens Psoriatic Skin Inflammation. *J Immunol.* 2017, **198**(9), pp.3671-3678.

230. Lim, C., Hong, M. and Savan, R. Human IL-22 binding protein isoforms act as a rheostat for IL-22 signaling. *Sci Signal.* 2016, **9**(447), p.ra95.

231. Al-Sebaei, M.O., Daukss, D.M., Belkina, A.C., Kakar, S., Wigner, N.A., Cusher, D., Graves, D., Einhorn, T., Morgan, E. and Gerstenfeld, L.C. Role of Fas and Treg cells in fracture healing as characterized in the fas-deficient (lpr) mouse model of lupus. *J Bone Miner Res.* 2014, **29**(6), pp.1478-1491.

232. Duhen, T., Geiger, R., Jarrossay, D., Lanzavecchia, A. and Sallusto, F. Production of interleukin 22 but not interleukin 17 by a subset of human skin-homing memory T cells. *Nat Immunol.* 2009, **10**(8), pp.857-863.

233. Liu, Y., Yang, B., Ma, J., Wang, H., Huang, F., Zhang, J., Chen, H. and Wu, C. Interleukin-21 induces the differentiation of human Tc22 cells via phosphorylation of signal transducers and activators of transcription. *Immunology.* 2011, **132**(4), pp.540-548.

234. Ortega, C., Fernandez, A.S., Carrillo, J.M., Romero, P., Molina, I.J., Moreno, J.C. and Santamaria, M. IL-17-producing CD8+ T lymphocytes from psoriasis skin plaques are cytotoxic effector cells that secrete Th17-related cytokines. *J Leukoc Biol.* 2009, **86**(2), pp.435-443.

235. Martin, B., Hirota, K., Cua, D.J., Stockinger, B. and Veldhoen, M. Interleukin-17-producing gammadelta T cells selectively expand in response to pathogen products and environmental signals. *Immunity.* 2009, **31**(2), pp.321-330.

236. Doisne, J.M., Soulard, V., Becourt, C., Amniai, L., Henrot, P., Havenar-Daughton, C., Blanchet, C., Zitvogel, L., Ryffel, B., Cavaillon, J.M., Marie, J.C., Couillin, I. and Benlagha, K. Cutting edge: crucial role of IL-1 and IL-23 in the innate IL-17 response of peripheral lymph node NK1.1- invariant NKT cells to bacteria. *J Immunol.* 2011, **186**(2), pp.662-666.

237. Spits, H. and Cupedo, T. Innate lymphoid cells: emerging insights in development, lineage relationships, and function. *Annu Rev Immunol.* 2012, **30**, pp.647-675.

238. Chen, F., Cao, A., Yao, S., Evans-Marin, H.L., Liu, H., Wu, W., Carlsen, E.D., Dann, S.M., Soong, L., Sun, J., Zhao, Q. and Cong, Y. mTOR Mediates IL-23 Induction of Neutrophil IL-17 and IL-22 Production. *J Immunol.* 2016, **196**(10), pp.4390-4399.

239. Hue, S., Ahern, P., Buonocore, S., Kullberg, M.C., Cua, D.J., McKenzie, B.S., Powrie, F. and Maloy, K.J. Interleukin-23 drives innate and T cell-mediated intestinal inflammation. *J Exp Med.* 2006, **203**(11), pp.2473-2483.

240. Yu, R., Ding, Y., Zhu, L., Qu, Y., Zhang, C., Liu, L. and Chen, L. IL-22 mediates the oral mucosal wound healing via STAT3 in keratinocytes. *Arch Oral Biol.* 2016, **72**, pp.14-20.

241. McGee, H.M., Schmidt, B.A., Booth, C.J., Yancopoulos, G.D., Valenzuela, D.M., Murphy, A.J., Stevens, S., Flavell, R.A. and Horsley, V. IL-22 promotes fibroblast-mediated

wound repair in the skin. *J Invest Dermatol.* 2013, **133**(5), pp.1321-1329.

242. Kolumam, G., Wu, X., Lee, W.P., Hackney, J.A., Zavala-Solorio, J., Gandham, V., Danilenko, D.M., Arora, P., Wang, X. and Ouyang, W. IL-22R Ligands IL-20, IL-22, and IL-24 Promote Wound Healing in Diabetic db/db Mice. *PLoS One.* 2017, **12**(1), p.e0170639.

243. Gimblet, C., Loesche, M.A., Carvalho, L., Carvalho, E.M., Grice, E.A., Artis, D. and Scott, P. IL-22 Protects against Tissue Damage during Cutaneous Leishmaniasis. *PLoS One.* 2015, **10**(8), p.e0134698.

244. Sabat, R. and Wolk, K. Research in practice: IL-22 and IL-20: significance for epithelial homeostasis and psoriasis pathogenesis. *J Dtsch Dermatol Ges.* 2011, **9**(7), pp.518-523.

245. Meephansan, J., Ruchusatsawat, K., Sindhupak, W., Thorner, P.S. and Wongpiyabovorn, J. Effect of methotrexate on serum levels of IL-22 in patients with psoriasis. *Eur J Dermatol.* 2011, **21**(4), pp.501-504.

246. Wolk, K., Haugen, H.S., Xu, W., Witte, E., Waggie, K., Anderson, M., Vom Baur, E., Witte, K., Warszawska, K., Philipp, S., Johnson-Leger, C., Volk, H.D., Sterry, W. and Sabat, R. IL-22 and IL-20 are key mediators of the epidermal alterations in psoriasis while IL-17 and IFN-gamma are not. *J Mol Med (Berl).* 2009, **87**(5), pp.523-536.

247. Zhang, J.R., Pang, D.D., Tong, Q., Liu, X., Su, D.F. and Dai, S.M. Different Modulatory Effects of IL-17, IL-22, and IL-23 on Osteoblast Differentiation. *Mediators Inflamm.* 2017, **2017**, p.5950395.

248. Zhang, L., Li, Y.G., Li, Y.H., Qi, L., Liu, X.G., Yuan, C.Z., Hu, N.W., Ma, D.X., Li, Z.F., Yang, Q., Li, W. and Li, J.M. Increased frequencies of Th22 cells as well as Th17 cells in the peripheral blood of patients with ankylosing spondylitis and rheumatoid arthritis. *PLoS One.* 2012, **7**(4), p.e31000.

249. Martin, J.C., Beriou, G., Heslan, M., Bossard, C., Jarry, A., Abidi, A., Hulin, P., Menoret, S., Thinard, R., Anegon, I., Jacqueline, C., Lardeux, B., Halary, F., Renauld, J.C., Bourreille, A. and Josien, R. IL-22BP is produced by eosinophils in human gut and blocks IL-22 protective actions during colitis. *Mucosal Immunol.* 2016, **9**(2), pp.539-549.

250. Brand, S., Beigel, F., Olszak, T., Zitzmann, K., Eichhorst, S.T., Otte, J.M., Diepolder, H., Marquardt, A., Jagla, W.,

Popp, A., Leclair, S., Herrmann, K., Seiderer, J., Ochsenkuhn, T., Goke, B., Auernhammer, C.J. and Dambacher, J. IL-22 is increased in active Crohn's disease and promotes proinflammatory gene expression and intestinal epithelial cell migration. *Am J Physiol Gastrointest Liver Physiol.* 2006, **290**(4), pp.G827-838.

251. Sugimoto, K., Ogawa, A., Mizoguchi, E., Shimomura, Y., Andoh, A., Bhan, A.K., Blumberg, R.S., Xavier, R.J. and Mizoguchi, A. IL-22 ameliorates intestinal inflammation in a mouse model of ulcerative colitis. *J Clin Invest.* 2008, **118**(2), pp.534-544.

252. Begue, B., Verdier, J., Rieux-Laucat, F., Goulet, O., Morali, A., Canioni, D., Hugot, J.P., Daussy, C., Verkarre, V., Pigneur, B., Fischer, A., Klein, C., Cerf-Bensussan, N. and Ruemmele, F.M. Defective IL10 signaling defining a subgroup of patients with inflammatory bowel disease. *Am J Gastroenterol.* 2011, **106**(8), pp.1544-1555.

253. Song, B., Ma, Y., Liu, X., Li, W., Zhang, J., Liu, J. and Han, J. IL-22 promotes the proliferation of cancer cells in smoking colorectal cancer patients. *Tumour Biol.* 2016, **37**(1), pp.1349-1356.

254. Smith, W.L. The eicosanoids and their biochemical mechanisms of action. *Biochem J.* 1989, **259**(2), pp.315-324.

255. Sugimoto, Y., Narumiya, S. and Ichikawa, A. Distribution and function of prostanoid receptors: studies from knockout mice. *Prog Lipid Res.* 2000, **39**(4), pp.289-314.

256. Lu, L.Y., Loi, F., Nathan, K., Lin, T.H., Pajarinen, J., Gibon, E., Nabeshima, A., Cordova, L., Jamsen, E., Yao, Z. and Goodman, S.B. Pro-inflammatory M1 macrophages promote Osteogenesis by mesenchymal stem cells via the COX-2-prostaglandin E2 pathway. *J Orthop Res.* 2017, **35**(11), pp.2378-2385.

257. Takayama, K., Garcia-Cardena, G., Sukhova, G.K., Comander, J., Gimbrone, M.A., Jr. and Libby, P. Prostaglandin E2 suppresses chemokine production in human macrophages through the EP4 receptor. *J Biol Chem.* 2002, **277**(46), pp.44147-44154.

258. Graham, S., Gamie, Z., Polyzois, I., Narvani, A.A., Tzafetta, K., Tsiridis, E., Helioti, M., Mantalaris, A. and Tsiridis, E. Prostaglandin EP2 and EP4 receptor agonists in bone formation and bone healing: In vivo and in vitro evidence. *Expert Opin Investig Drugs.* 2009, **18**(6), pp.746-766.

259. Akamine, T., Jee, W.S., Ke, H.Z., Li, X.J. and Lin, B.Y. Prostaglandin E2 prevents bone loss and adds extra bone to immobilized distal femoral metaphysis in female rats. *Bone.* 1992, **13**(1), pp.11-22.

260. Schlundt, C., El Khassawna, T., Serra, A., Dienelt, A., Wendler, S., Schell, H., van Rooijen, N., Radbruch, A., Lucius, R., Hartmann, S., Duda, G.N. and Schmidt-Bleek, K. Macrophages in bone fracture healing: Their essential role in endochondral ossification. *Bone.* 2018, **106**, pp.78-89.

261. Xie, C., Liang, B., Xue, M., Lin, A.S., Loiselle, A., Schwarz, E.M., Guldberg, R.E., O'Keefe, R.J. and Zhang, X. Rescue of impaired fracture healing in COX-2-/- mice via activation of prostaglandin E2 receptor subtype 4. *Am J Pathol.* 2009, **175**(2), pp.772-785.

262. Li, M., Ke, H.Z., Qi, H., Healy, D.R., Li, Y., Crawford, D.T., Paralkar, V.M., Owen, T.A., Cameron, K.O., Lefker, B.A., Brown, T.A. and Thompson, D.D. A novel, non-prostanoid EP2 receptor-selective prostaglandin E2 agonist stimulates local bone formation and enhances fracture healing. *J Bone Miner Res.* 2003, **18**(11), pp.2033-2042.

263. Ma, X., Aoki, T. and Narumiya, S. Prostaglandin E2-EP4 signaling persistently amplifies CD40-mediated induction of IL-23 p19 expression through canonical and non-canonical NF-kappaB pathways. *Cell Mol Immunol.* 2016, **13**(2), pp.240-250.

264. Tan, A.L., Marzo-Ortega, H., O'Connor, P., Fraser, A., Emery, P. and McGonagle, D. Efficacy of anakinra in active ankylosing spondylitis: a clinical and magnetic resonance imaging study. *Ann Rheum Dis.* 2004, **63**(9), pp.1041-1045.

265. Sieper, J., Braun, J., Kay, J., Badalamenti, S., Radin, A.R., Jiao, L., Fiore, S., Momtahen, T., Yancopoulos, G.D., Stahl, N. and Inman, R.D. Sarilumab for the treatment of ankylosing spondylitis: results of a Phase II, randomised, double-blind, placebo-controlled study (ALIGN). *Ann Rheum Dis.* 2015, **74**(6), pp.1051-1057.

266. Lasiglie, D., Traggiai, E., Federici, S., Alessio, M., Buoncompagni, A., Accogli, A., Chiesa, S., Penco, F., Martini, A. and Gattorno, M. Role of IL-1 beta in the development of human T(H)17 cells: lesson from NLPR3 mutated patients. *PLoS One.* 2011, **6**(5), p.e20014.

267. Revu, S., Wu, J., Henkel, M., Rittenhouse, N., Menk, A., Delgoffe, G.M., Poholek, A.C. and McGeachy, M.J. IL-23

and IL-1beta Drive Human Th17 Cell Differentiation and Metabolic Reprogramming in Absence of CD28 Costimulation. *Cell Rep.* 2018, **22**(10), pp.2642-2653.

268. Mailer, R.K., Joly, A.L., Liu, S., Elias, S., Tegner, J. and Andersson, J. IL-1beta promotes Th17 differentiation by inducing alternative splicing of FOXP3. *Sci Rep.* 2015, **5**, p.14674.

269. Ruscitti, P., Cipriani, P., Carubbi, F., Liakouli, V., Zazzeroni, F., Di Benedetto, P., Berardicurti, O., Alesse, E. and Giacomelli, R. The role of IL-1beta in the bone loss during rheumatic diseases. *Mediators Inflamm.* 2015, **2015**, p.782382.

270. Cohen, I., Rider, P., Vornov, E., Tomas, M., Tudor, C., Wegner, M., Brondani, L., Freudenberg, M., Mittler, G., Ferrando-May, E., Dinarello, C.A., Apte, R.N. and Schneider, R. IL-1alpha is a DNA damage sensor linking genotoxic stress signaling to sterile inflammation and innate immunity. *Sci Rep.* 2015, **5**, p.14756.

271. Tang, A. and Gilchrest, B.A. Regulation of keratinocyte growth factor gene expression in human skin fibroblasts. *J Dermatol Sci.* 1996, **11**(1), pp.41-50.

272. Sauder, D.N., Orr, F.W., Matic, S., Stetsko, D., Parker, K.P., Chizzonite, R. and Kilian, P.L. Human interleukin-1 alpha is chemotactic for normal human keratinocytes. *Immunol Lett.* 1989, **22**(2), pp.123-127.

273. Barone, E.J., Yager, D.R., Pozez, A.L., Olutoye, O.O., Crossland, M.C., Diegelmann, R.F. and Cohen, I.K. Interleukin-1alpha and collagenase activity are elevated in chronic wounds. *Plast Reconstr Surg.* 1998, **102**(4), pp.1023-1027; discussion 1028-1029.

274. Beidler, S.K., Douillet, C.D., Berndt, D.F., Keagy, B.A., Rich, P.B. and Marston, W.A. Inflammatory cytokine levels in chronic venous insufficiency ulcer tissue before and after compression therapy. *J Vasc Surg.* 2009, **49**(4), pp.1013-1020.

275. Kon, T., Cho, T.J., Aizawa, T., Yamazaki, M., Nooh, N., Graves, D., Gerstenfeld, L.C. and Einhorn, T.A. Expression of osteoprotegerin, receptor activator of NF-kappaB ligand (osteoprotegerin ligand) and related proinflammatory cytokines during fracture healing. *J Bone Miner Res.* 2001, **16**(6), pp.1004-1014.

276. Lee, Y.M., Fujikado, N., Manaka, H., Yasuda, H. and Iwakura, Y. IL-1 plays an important role in the bone

metabolism under physiological conditions. *Int Immunol.* 2010, **22**(10), pp.805-816.

277. Guo, C., Yang, X.G., Wang, F. and Ma, X.Y. IL-1alpha induces apoptosis and inhibits the osteoblast differentiation of MC3T3-E1 cells through the JNK and p38 MAPK pathways. *Int J Mol Med.* 2016, **38**(1), pp.319-327.

278. Matuska, A., O'Shaughnessey, K., King, W. and Woodell-May, J. Autologous solution protects bovine cartilage explants from IL-1alpha- and TNFalpha-induced cartilage degradation. *J Orthop Res.* 2013, **31**(12), pp.1929-1935.

279. Dinarello, C.A. and van der Meer, J.W. Treating inflammation by blocking interleukin-1 in humans. *Semin Immunol.* 2013, **25**(6), pp.469-484.

280. Lugrin, J., Parapanov, R., Rosenblatt-Velin, N., Rignault-Clerc, S., Feihl, F., Waeber, B., Muller, O., Vergely, C., Zeller, M., Tardivel, A., Schneider, P., Pacher, P. and Liaudet, L. Cutting edge: IL-1alpha is a crucial danger signal triggering acute myocardial inflammation during myocardial infarction. *J Immunol.* 2015, **194**(2), pp.499-503.

281. Nishiura, R., Noda, N., Minoura, H., Toyoda, N., Imanaka-Yoshida, K., Sakakura, T. and Yoshida, T. Expression of matrix metalloproteinase-3 in mouse endometrial stromal cells during early pregnancy: regulation by interleukin-1alpha and tenascin-C. *Gynecol Endocrinol.* 2005, **21**(2), pp.111-118.

282. Sato, A., Aonuma, K., Imanaka-Yoshida, K., Yoshida, T., Isobe, M., Kawase, D., Kinoshita, N., Yazaki, Y. and Hiroe, M. Serum tenascin-C might be a novel predictor of left ventricular remodeling and prognosis after acute myocardial infarction. *J Am Coll Cardiol.* 2006, **47**(11), pp.2319-2325.

283. Lee, J.G. and Heur, M. Interleukin-1beta enhances cell migration through AP-1 and NF-kappaB pathway-dependent FGF2 expression in human corneal endothelial cells. *Biol Cell.* 2013, **105**(4), pp.175-189.

284. Rajshankar, D., Downey, G.P. and McCulloch, C.A. IL-1beta enhances cell adhesion to degraded fibronectin. *FASEB J.* 2012, **26**(11), pp.4429-4444.

285. Rider, P., Carmi, Y., Guttman, O., Braiman, A., Cohen, I., Voronov, E., White, M.R., Dinarello, C.A. and Apte, R.N. IL-1alpha and IL-1beta recruit different myeloid cells and promote different stages of sterile inflammation. *J Immunol.* 2011, **187**(9), pp.4835-4843.

286. Jiang, L., Dai, Y., Cui, F., Pan, Y., Zhang, H., Xiao, J. and Xiaobing, F.U. Expression of cytokines, growth factors and apoptosis-related signal molecules in chronic pressure ulcer wounds healing. *Spinal Cord.* 2014, **52**(2), pp.145-151.

287. Karam, R.A., Rezk, N.A., Abdel Rahman, T.M. and Al Saeed, M. Effect of negative pressure wound therapy on molecular markers in diabetic foot ulcers. *Gene.* 2018, **667**, pp.56-61.

288. Mirza, R.E., Fang, M.M., Ennis, W.J. and Koh, T.J. Blocking interleukin-1beta induces a healing-associated wound macrophage phenotype and improves healing in type 2 diabetes. *Diabetes.* 2013, **62**(7), pp.2579-2587.

289. Trebec-Reynolds, D.P., Voronov, I., Heersche, J.N. and Manolson, M.F. IL-1alpha and IL-1beta have different effects on formation and activity of large osteoclasts. *J Cell Biochem.* 2010, **109**(5), pp.975-982.

290. Lange, J., Sapozhnikova, A., Lu, C., Hu, D., Li, X., Miclau, T., 3rd and Marcucio, R.S. Action of IL-1beta during fracture healing. *J Orthop Res.* 2010, **28**(6), pp.778-784.

291. Huang, R.L., Yuan, Y., Tu, J., Zou, G.M. and Li, Q. Opposing TNF-alpha/IL-1beta- and BMP-2-activated MAPK signaling pathways converge on Runx2 to regulate BMP-2-induced osteoblastic differentiation. *Cell Death Dis.* 2014, **5**, p.e1187.

292. Hengartner, N.E., Fiedler, J., Ignatius, A. and Brenner, R.E. IL-1beta inhibits human osteoblast migration. *Mol Med.* 2013, **19**, pp.36-42.

293. Tran, T.A. Muckle-Wells syndrome: clinical perspectives. *Open Access Rheumatol.* 2017, **9**, pp.123-129.

294. Houx, L., Hachulla, E., Kone-Paut, I., Quartier, P., Touitou, I., Guennoc, X., Grateau, G., Hamidou, M., Neven, B., Berthelot, J.M., Lequerre, T., Pillet, P., Lemelle, I., Fischbach, M., Duquesne, A., Le Blay, P., Le Jeunne, C., Stirnemann, J., Bonnet, C., Gaillard, D., Alix, L., Touraine, R., Garcier, F., Bedane, C., Jurquet, A.L., Duffau, P., Smail, A., Frances, C., Grall-Lerosey, M., Cathebras, P., Tran, T.A., Morell-Dubois, S., Pagnier, A., Richez, C., Cuisset, L. and Devauchelle-Pensec, V. Musculoskeletal symptoms in patients with cryopyrin-associated periodic syndromes: a large database study. *Arthritis Rheumatol.* 2015, **67**(11), pp.3027-3036.

295. Hawkins, P.N., Lachmann, H.J., Aganna, E. and McDermott, M.F. Spectrum of clinical features in Muckle-

Wells syndrome and response to anakinra. *Arthritis Rheum.* 2004, **50**(2), pp.607-612.

296. Wang, X., Friis, T.E., Masci, P.P., Crawford, R.W., Liao, W. and Xiao, Y. Alteration of blood clot structures by interleukin-1 beta in association with bone defects healing. *Sci Rep.* 2016, **6**, p.35645.

297. Farahat, M.N., Yanni, G., Poston, R. and Panayi, G.S. Cytokine expression in synovial membranes of patients with rheumatoid arthritis and osteoarthritis. *Ann Rheum Dis.* 1993, **52**(12), pp.870-875.

298. Eklund, K.K., Leirisalo-Repo, M., Ranta, P., Maki, T., Kautiainen, H., Hannonen, P., Korpela, M., Hakala, M., Jarvinen, P. and Mottonen, T. Serum IL-1beta levels are associated with the presence of erosions in recent onset rheumatoid arthritis. *Clin Exp Rheumatol.* 2007, **25**(5), pp.684-689.

299. Guncu, G.N., Akman, A.C., Gunday, S., Yamalik, N. and Berker, E. Effect of inflammation on cytokine levels and bone remodelling markers in peri-implant sulcus fluid: a preliminary report. *Cytokine.* 2012, **59**(2), pp.313-316.

300. Karakus, E., Halici, Z., Albayrak, A., Bayir, Y., Demirci, E., Aydin, A., Ozturk-Karagoz, B., Cadirci, E., Ayan, A.K., Sahin, A. and Unal, D. Effects of Administration of Amlodipine and Lacidipine on Inflammation-Induced Bone Loss in the Ovariectomized Rat. *Inflammation.* 2016, **39**(1), pp.336-346.

301. Tosato, G. and Jones, K.D. Interleukin-1 induces interleukin-6 production in peripheral blood monocytes. *Blood.* 1990, **75**(6), pp.1305-1310.

302. Cahill, C.M. and Rogers, J.T. Interleukin (IL) 1beta induction of IL-6 is mediated by a novel phosphatidylinositol 3-kinase-dependent AKT/IkappaB kinase alpha pathway targeting activator protein-1. *J Biol Chem.* 2008, **283**(38), pp.25900-25912.

303. Scheller, J., Chalaris, A., Schmidt-Arras, D. and Rose-John, S. The pro- and anti-inflammatory properties of the cytokine interleukin-6. *Biochim Biophys Acta.* 2011, **1813**(5), pp.878-888.

304. Heink, S., Yogev, N., Garbers, C., Herwerth, M., Aly, L., Gasperi, C., Husterer, V., Croxford, A.L., Moller-Hackbarth, K., Bartsch, H.S., Sotlar, K., Krebs, S., Regen, T., Blum, H., Hemmer, B., Misgeld, T., Wunderlich, T.F., Hidalgo, J., Oukka, M., Rose-John, S., Schmidt-Supprian, M.,

Waisman, A. and Korn, T. Trans-presentation of IL-6 by dendritic cells is required for the priming of pathogenic TH17 cells. *Nat Immunol.* 2017, **18**(1), pp.74-85.

305. Wolf, J., Rose-John, S. and Garbers, C. Interleukin-6 and its receptors: a highly regulated and dynamic system. *Cytokine.* 2014, **70**(1), pp.11-20.

306. Heinrich, P.C., Behrmann, I., Muller-Newen, G., Schaper, F. and Graeve, L. Interleukin-6-type cytokine signalling through the gp130/Jak/STAT pathway. *Biochem J.* 1998, **334 (Pt 2)**, pp.297-314.

307. Mateo, R.B., Reichner, J.S. and Albina, J.E. Interleukin-6 activity in wounds. *Am J Physiol.* 1994, **266**(6 Pt 2), pp.R1840-1844.

308. Paquet, P. and Pierard, G.E. Interleukin-6 and the skin. *Int Arch Allergy Immunol.* 1996, **109**(4), pp.308-317.

309. Gallucci, R.M., Simeonova, P.P., Matheson, J.M., Kommineni, C., Guriel, J.L., Sugawara, T. and Luster, M.I. Impaired cutaneous wound healing in interleukin-6-deficient and immunosuppressed mice. *FASEB J.* 2000, **14**(15), pp.2525-2531.

310. Gallucci, R.M., Sugawara, T., Yucesoy, B., Berryann, K., Simeonova, P.P., Matheson, J.M. and Luster, M.I. Interleukin-6 treatment augments cutaneous wound healing in immunosuppressed mice. *J Interferon Cytokine Res.* 2001, **21**(8), pp.603-609.

311. Taniguchi, K., Arima, K., Masuoka, M., Ohta, S., Shiraishi, H., Ontsuka, K., Suzuki, S., Inamitsu, M., Yamamoto, K.I., Simmons, O., Toda, S., Conway, S.J., Hamasaki, Y. and Izuhara, K. Periostin controls keratinocyte proliferation and differentiation by interacting with the paracrine IL-1alpha/IL-6 loop. *J Invest Dermatol.* 2014, **134**(5), pp.1295-1304.

312. Heo, S.C., Jeon, E.S., Lee, I.H., Kim, H.S., Kim, M.B. and Kim, J.H. Tumor necrosis factor-alpha-activated human adipose tissue-derived mesenchymal stem cells accelerate cutaneous wound healing through paracrine mechanisms. *J Invest Dermatol.* 2011, **131**(7), pp.1559-1567.

313. Gallucci, R.M., Sloan, D.K., Heck, J.M., Murray, A.R. and O'Dell, S.J. Interleukin 6 indirectly induces keratinocyte migration. *J Invest Dermatol.* 2004, **122**(3), pp.764-772.

314. Grossman, R.M., Krueger, J., Yourish, D., Granelli-Piperno, A., Murphy, D.P., May, L.T., Kupper, T.S., Sehgal, P.B. and Gottlieb, A.B. Interleukin 6 is expressed in high levels in psoriatic skin and stimulates proliferation of cultured human

keratinocytes. *Proc Natl Acad Sci U S A.* 1989, **86**(16), pp.6367-6371.

315. Ball, E.M., Gibson, D.S., Bell, A.L. and Rooney, M.R. Plasma IL-6 levels correlate with clinical and ultrasound measures of arthritis in patients with systemic lupus erythematosus. *Lupus.* 2014, **23**(1), pp.46-56.

316. Kadono, T., Kikuchi, K., Ihn, H., Takehara, K. and Tamaki, K. Increased production of interleukin 6 and interleukin 8 in scleroderma fibroblasts. *J Rheumatol.* 1998, **25**(2), pp.296-301.

317. Confalone, E., D'Alessio, G. and Furia, A. IL-6 Induction by TNFalpha and IL-1beta in an Osteoblast-Like Cell Line. *Int J Biomed Sci.* 2010, **6**(2), pp.135-140.

318. Giganti, M.G., Liuni, F., Celi, M., Gasbarra, E., Zenobi, R., Tresoldi, I., Modesti, A., Bei, R. and Tarantino, U. Changes in serum levels of TNF-alpha, IL-6, OPG, RANKL and their correlation with radiographic and clinical assessment in fragility fractures and high energy fractures. *J Biol Regul Homeost Agents.* 2012, **26**(4), pp.671-680.

319. Wallace, A., Cooney, T.E., Englund, R. and Lubahn, J.D. Effects of interleukin-6 ablation on fracture healing in mice. *J Orthop Res.* 2011, **29**(9), pp.1437-1442.

320. Yoshida, Y. and Tanaka, T. Interleukin 6 and rheumatoid arthritis. *Biomed Res Int.* 2014, **2014**, p.698313.

321. Mori, T., Miyamoto, T., Yoshida, H., Asakawa, M., Kawasumi, M., Kobayashi, T., Morioka, H., Chiba, K., Toyama, Y. and Yoshimura, A. IL-1beta and TNFalpha-initiated IL-6-STAT3 pathway is critical in mediating inflammatory cytokines and RANKL expression in inflammatory arthritis. *Int Immunol.* 2011, **23**(11), pp.701-712.

322. Ohtsuji, M., Lin, Q., Nishikawa, K., Ohtsuji, N., Okazaki, H., Tsurui, H., Amano, H., Shirai, T., Nishimoto, N., Nishimura, H. and Hirose, S. IL-6 signal blockade ameliorates the enhanced osteoclastogenesis and the associated joint destruction in a novel FcgammaRIIB-deficient rheumatoid arthritis mouse model. *Mod Rheumatol.* 2015, **25**(2), pp.270-277.

323. Liang, B., Song, Z., Wu, B., Gardner, D., Shealy, D., Song, X.Y. and Wooley, P.H. Evaluation of anti-IL-6 monoclonal antibody therapy using murine type II collagen-induced arthritis. *J Inflamm (Lond).* 2009, **6**, p.10.

324. Bensaoud, N., Rostom, S., Bahiri, R. and Hajjaj-Hassouni, N. Efficacy of tocilizumab on MRI-determined bone oedema in rheumatoid arthritis. *Clin Rheumatol.* 2015, **34**(6), pp.1031-1037.

325. Addimanda, O., Possemato, N., Macchioni, P. and Salvarani, C. Efficacy and safety of tocilizumab in refractory rheumatoid arthritis: a real life cohort from a single centre. *Clin Exp Rheumatol.* 2014, **32**(4), pp.460-464.

326. Conaghan, P.G., Peterfy, C., Olech, E., Kaine, J., Ridley, D., Dicarlo, J., Friedman, J., Devenport, J. and Troum, O. The effects of tocilizumab on osteitis, synovitis and erosion progression in rheumatoid arthritis: results from the ACT-RAY MRI substudy. *Ann Rheum Dis.* 2014, **73**(5), pp.810-816.

327. Jeffery, V., Goldson, A.J., Dainty, J.R., Chieppa, M. and Sobolewski, A. IL-6 Signaling Regulates Small Intestinal Crypt Homeostasis. *J Immunol.* 2017, **199**(1), pp.304-311.

328. Kuhn, K.A., Schulz, H.M., Regner, E.H., Severs, E.L., Hendrickson, J.D., Mehta, G., Whitney, A.K., Ir, D., Ohri, N., Robertson, C.E., Frank, D.N., Campbell, E.L. and Colgan, S.P. Bacteroidales recruit IL-6-producing intraepithelial lymphocytes in the colon to promote barrier integrity. *Mucosal Immunol.* 2018, **11**(2), pp.357-368.

329. Strangfeld, A., Richter, A., Siegmund, B., Herzer, P., Rockwitz, K., Demary, W., Aringer, M., Meissner, Y., Zink, A. and Listing, J. Risk for lower intestinal perforations in patients with rheumatoid arthritis treated with tocilizumab in comparison to treatment with other biologic or conventional synthetic DMARDs. *Ann Rheum Dis.* 2017, **76**(3), pp.504-510.

330. Danese, S., Vermeire, S., Hellstern, P., Panaccione, R., Rogler, G., Fraser, G., Kohn, A., Desreumaux, P., Leong, R.W., Comer, G.M., Cataldi, F., Banerjee, A., Maguire, M.K., Li, C., Rath, N., Beebe, J. and Schreiber, S. 764 Results of Andante, a Randomized Clinical Study With an Anti-IL6 Antibody (PF-04236921) in Subjects With Crohn's Disease Who Are Anti-TNF Inadequate Responders. *Gastroenterology.* 2016, **150**(4), p.S155.

331. Dutzan, N., Abusleme, L., Bridgeman, H., Greenwell-Wild, T., Zangerle-Murray, T., Fife, M.E., Bouladoux, N., Linley, H., Brenchley, L., Wemyss, K., Calderon, G., Hong, B.Y., Break, T.J., Bowdish, D.M.E., Lionakis, M.S., Jones, S.A., Trinchieri, G., Diaz, P.I., Belkaid, Y., Konkel, J.E. and

Moutsopoulos, N.M. On-going Mechanical Damage from Mastication Drives Homeostatic Th17 Cell Responses at the Oral Barrier. *Immunity.* 2017, **46**(1), pp.133-147.

332. Bettelli, E., Carrier, Y., Gao, W., Korn, T., Strom, T.B., Oukka, M., Weiner, H.L. and Kuchroo, V.K. Reciprocal developmental pathways for the generation of pathogenic effector TH17 and regulatory T cells. *Nature.* 2006, **441**(7090), pp.235-238.

333. Ghoreschi, K., Laurence, A., Yang, X.P., Tato, C.M., McGeachy, M.J., Konkel, J.E., Ramos, H.L., Wei, L., Davidson, T.S., Bouladoux, N., Grainger, J.R., Chen, Q., Kanno, Y., Watford, W.T., Sun, H.W., Eberl, G., Shevach, E.M., Belkaid, Y., Cua, D.J., Chen, W. and O'Shea, J.J. Generation of pathogenic T(H)17 cells in the absence of TGF-beta signalling. *Nature.* 2010, **467**(7318), pp.967-971.

334. Hallmon, W.W. Occlusal trauma: effect and impact on the periodontium. *Ann Periodontol.* 1999, **4**(1), pp.102-108.

335. Luo, Z., Wang, H., Chen, J., Kang, J., Sun, Z. and Wu, Y. Overexpression and Potential Regulatory Role of IL-17F in Pathogenesis of Chronic Periodontitis. *Inflammation.* 2015, **38**(3), pp.978-986.

336. Gandhi, N.A., Pirozzi, G. and Graham, N.M.J.E.r.o.c.i. Commonality of the IL-4/IL-13 pathway in atopic diseases. *Expert Rev Clin Immunol.* 2017, **13**(5), pp.425-437.

337. Willsmore, Z.N., Woolf, R.T., Hughes, C., Menon, B., Kirkham, B., Smith, C. and Pink, A. Development of inflammatory arthritis and enthesitis in patients on dupilumab: a case series. *British Journal of Dermatology.* 2019, **181**(5), pp.1068-1070.

338. Ludwig, C.M., Haleen, H., Hsiao, J.L., Lio, P.A. and Shi, V.Y. Emerging rheumatologic reactions with Th2 blockade. *Dermatologic Therapy.* 2020, p.e14069.

339. Bowes, J., Eyre, S., Flynn, E., Ho, P., Salah, S., Warren, R.B., Marzo-Ortega, H., Coates, L., McManus, R. and Ryan, A.W. Evidence to support IL-13 as a risk locus for psoriatic arthritis but not psoriasis vulgaris. *Annals of the Rheumatic Diseases.* 2011, **70**(6), pp.1016-1019.

340. Li, Z., Burns, A.R., Miller, S.B. and Smith, C.W. CCL20, gammadelta T cells, and IL-22 in corneal epithelial healing. *FASEB J.* 2011, **25**(8), pp.2659-2668.

341. Duffin, K.C., Freeny, I.C., Schrodi, S.J., Wong, B., Feng, B.-J., Soltani-Arabshahi, R., Rakkhit, T., Goldgar, D.E. and Krueger, G.G. Association between IL13 polymorphisms

and psoriatic arthritis is modified by smoking. *Journal of Investigative Dermatology.* 2009, **129**(12), pp.2777-2783.

342. Bridgewood, C., Sharif, K., Freeston, J., Saleem, B., Russell, T., Watad, A., Khan, A., Loughenbury, P., Rao, A., Wittmann, M. and McGonagle, D. Regulation of entheseal IL-23 expression by IL-4 and IL-13 as an explanation for arthropathy development under dupilumab therapy. *Rheumatology (Oxford).* 2021, **60**(5), pp.2461-2466.

343. Lubberts, E., Joosten, L.A., van de Loo, F.A., van den Gersselaar, L.A. and van den Berg, W.B. Reduction of interleukin-17-induced inhibition of chondrocyte proteoglycan synthesis in intact murine articular cartilage by interleukin-4. *Arthritis Rheum.* 2000, **43**(6), pp.1300-1306.

344. Bessis, N., Boissier, M.C., Ferrara, P., Blankenstein, T., Fradelizi, D. and Fournier, C. Attenuation of collagen-induced arthritis in mice by treatment with vector cells engineered to secrete interleukin-13. *Eur J Immunol.* 1996, **26**(10), pp.2399-2403.

345. Silfverswärd, C.J., Larsson, S., Ohlsson, C., Frost, A. and Nilsson, O. Reduced cortical bone mass in mice with inactivation of interleukin-4 and interleukin-13. *Journal of Orthopaedic Research.* 2007, **25**(6), pp.725-731.

346. Silfverswärd, C.J., Sisask, G., Larsson, S., Ohlsson, C., Frost, A., Ljunggren, Ö. and Nilsson, O. Bone formation in interleukin-4 and interleukin-13 depleted mice. *Acta orthopaedica.* 2008, **79**(3), pp.410-420.

347. Friedenstein, A.J., Chailakhjan, R.K. and Lalykina, K.S. The development of fibroblast colonies in monolayer cultures of guinea-pig bone marrow and spleen cells. *Cell Tissue Kinet.* 1970, **3**(4), pp.393-403.

348. Mafi, R., Hindocha, S., Mafi, P., Griffin, M. and Khan, W.S. Sources of adult mesenchymal stem cells applicable for musculoskeletal applications - a systematic review of the literature. *Open Orthop J.* 2011, **5 Suppl 2**, pp.242-248.

349. Meirelles, L.d.S., Chagastelles, P.C. and Nardi, N.B. Mesenchymal stem cells reside in virtually all post-natal organs and tissues. *J Cell Sci.* 2006, **119**(11), p.2204.

350. Valenti, M.T., Dalle Carbonare, L. and Mottes, M. Osteogenic Differentiation in Healthy and Pathological Conditions. *Int J Mol Sci.* 2016, **18**(1).

351. Maerz, T., Fleischer, M., Newton, M.D., Davidson, A., Salisbury, M., Altman, P., Kurdziel, M.D., Anderson, K., Bedi, A. and Baker, K.C. Acute mobilization and migration

of bone marrow-derived stem cells following anterior cruciate ligament rupture. *Osteoarthritis Cartilage.* 2017, **25**(8), pp.1335-1344.

352. Klimczak, A. and Kozlowska, U. Mesenchymal Stromal Cells and Tissue-Specific Progenitor Cells: Their Role in Tissue Homeostasis. *Stem Cells Int.* 2016, **2016**, p.4285215.

353. Krajewska-Wlodarczyk, M., Owczarczyk-Saczonek, A., Placek, W., Osowski, A., Engelgardt, P. and Wojtkiewicz, J. Role of Stem Cells in Pathophysiology and Therapy of Spondyloarthropathies-New Therapeutic Possibilities? *Int J Mol Sci.* 2017, **19**(1).

354. Kim, M., Kim, C., Choi, Y.S., Kim, M., Park, C. and Suh, Y. Age-related alterations in mesenchymal stem cells related to shift in differentiation from osteogenic to adipogenic potential: implication to age-associated bone diseases and defects. *Mech Ageing Dev.* 2012, **133**(5), pp.215-225.

355. Kyurkchiev, D., Bochev, I., Ivanova-Todorova, E., Mourdjeva, M., Oreshkova, T., Belemezova, K. and Kyurkchiev, S. Secretion of immunoregulatory cytokines by mesenchymal stem cells. *World J Stem Cells.* 2014, **6**(5), pp.552-570.

356. Yamazaki, T., Yang, X.O., Chung, Y., Fukunaga, A., Nurieva, R., Pappu, B., Martin-Orozco, N., Kang, H.S., Ma, L., Panopoulos, A.D., Craig, S., Watowich, S.S., Jetten, A.M., Tian, Q. and Dong, C. CCR6 regulates the migration of inflammatory and regulatory T cells. *J Immunol.* 2008, **181**(12), pp.8391-8401.

357. Russell, T., Watad, A., Bridgewood, C., Rowe, H., Khan, A., Rao, A., Loughenbury, P., Millner, P., Dunsmuir, R., Cuthbert, R., Altaie, A., Jones, E. and McGonagle, D. IL-17A and TNF Modulate Normal Human Spinal Entheseal Bone and Soft Tissue Mesenchymal Stem Cell Osteogenesis, Adipogenesis, and Stromal Function. *Cells.* 2021, **10**(2), p.341.

358. Adan, A., Alizada, G., Kiraz, Y., Baran, Y. and Nalbant, A. Flow cytometry: basic principles and applications. *Crit Rev Biotechnol.* 2017, **37**(2), pp.163-176.

359. Dominici, M., Le Blanc, K., Mueller, I., Slaper-Cortenbach, I., Marini, F., Krause, D., Deans, R., Keating, A., Prockop, D. and Horwitz, E. Minimal criteria for defining multipotent mesenchymal stromal cells. The International Society for

Cellular Therapy position statement. *Cytotherapy.* 2006, **8**(4), pp.315-317.

360. Macey, M.G. *Flow Cytometry.* Human Press, 2007.
361. Wilkerson, M.J. Principles and applications of flow cytometry and cell sorting in companion animal medicine. *Vet Clin North Am Small Anim Pract.* 2012, **42**(1), pp.53-71.
362. Reggeti, F. and Bienzle, D. Flow cytometry in veterinary oncology. *Vet Pathol.* 2011, **48**(1), pp.223-235.
363. Snow, C. Flow cytometer electronics. *Cytometry A.* 2004, **57**(2), pp.63-69.
364. Ramakrishnan, R., Qin, J., Jones, R.C. and Weaver, L.S. Integrated Fluidic Circuits (IFCs) for digital PCR. *Methods Mol Biol.* 2013, **949**, pp.423-431.
365. Livak, K.J. and Schmittgen, T.D. Analysis of relative gene expression data using real-time quantitative PCR and the 2(-Delta Delta C(T)) Method. *Methods.* 2001, **25**(4), pp.402-408.
366. Savi, F.M., Brierly, G.I., Baldwin, J., Theodoropoulos, C. and Woodruff, M.A. Comparison of Different Decalcification Methods Using Rat Mandibles as a Model. *J Histochem Cytochem.* 2017, **65**(12), pp.705-722.
367. Fischer, A.H., Jacobson, K.A., Rose, J. and Zeller, R. Hematoxylin and eosin staining of tissue and cell sections. *CSH Protoc.* 2008, **2008**, p.pdb prot4986.
368. Schmitz, N., Laverty, S., Kraus, V.B. and Aigner, T. Basic methods in histopathology of joint tissues. *Osteoarthritis Cartilage.* 2010, **18 Suppl 3**, pp.S113-116.
369. Zhang, C., Yan, B., Cui, Z., Cui, S., Zhang, T., Wang, X., Liu, D., Yang, R., Jiang, N., Zhou, Y. and Liu, Y. Bone regeneration in minipigs by intrafibrillarly-mineralized collagen loaded with autologous periodontal ligament stem cells. *Sci Rep.* 2017, **7**(1), p.10519.
370. Kugler, J.H. Ponceau-fuchsin as a routine counterstain. *Stain Technol.* 1949, **24**(3), p.191.
371. Lai, M. and Lü, B. Tissue Preparation for Microscopy and Histology. In: Pawliszyn, J. ed. *Comprehensive Sampling and Sample Preparation.* Oxford: Academic Press, 2012, pp.53-93.
372. Najar, M., Fayyad-Kazan, H., Faour, W.H., Merimi, M., Sokal, E.M., Lombard, C.A. and Fahmi, H. Immunological modulation following bone marrow-derived mesenchymal stromal cells and Th17 lymphocyte co-cultures. *Inflamm Res.* 2019, **68**(3), pp.203-213.

373. Mitchell, J.B., McIntosh, K., Zvonic, S., Garrett, S., Floyd, Z.E., Kloster, A., Di Halvorsen, Y., Storms, R.W., Goh, B., Kilroy, G., Wu, X. and Gimble, J.M. Immunophenotype of human adipose-derived cells: temporal changes in stromal-associated and stem cell-associated markers. *Stem Cells.* 2006, **24**(2), pp.376-385.

374. Beckenkamp, L.R., Souza, L.E.B., Melo, F.U.F., Thome, C.H., Magalhaes, D.A.R., Palma, P.V.B. and Covas, D.T. Comparative characterization of CD271(+) and CD271(-) subpopulations of CD34(+) human adipose-derived stromal cells. *J Cell Biochem.* 2018, **119**(5), pp.3873-3884.

375. Lin, C.S., Ning, H., Lin, G. and Lue, T.F. Is CD34 truly a negative marker for mesenchymal stromal cells? *Cytotherapy.* 2012, **14**(10), pp.1159-1163.

376. Romieu-Mourez, R., François, M., Boivin, M.-N., Stagg, J. and Galipeau, J. Regulation of MHC Class II Expression and Antigen Processing in Murine and Human Mesenchymal Stromal Cells by IFN-γ, TGF-β, and Cell Density. *The Journal of Immunology.* 2007, **179**(3), pp.1549-1558.

377. Stagg, J., Pommey, S., Eliopoulos, N. and Galipeau, J. Interferon-γ-stimulated marrow stromal cells: a new type of nonhematopoietic antigen-presenting cell. *Blood.* 2006, **107**(6), pp.2570-2577.

378. Fang, F., Ni, K., Cai, Y., Ye, Z., Shang, J., Shen, S. and Xiong, C. Biological characters of human dermal fibroblasts derived from foreskin of male infertile patients. *Tissue and Cell.* 2017, **49**(1), pp.56-63.

379. Hager, G., Holnthoner, W., Wolbank, S., Husa, A.M., Godthardt, K., Redl, H. and Gabriel, C. Three specific antigens to isolate endothelial progenitor cells from human liposuction material. *Cytotherapy.* 2013, **15**(11), pp.1426-1435.

380. Lui, P.P.Y. Markers for the identification of tendon-derived stem cells in vitro and tendon stem cells in situ - update and future development. *Stem Cell Res Ther.* 2015, **6**(1), pp.106-106.

381. Thomson, T.M., Rettig, W.J., Chesa, P.G., Green, S.H., Mena, A.C. and Old, L.J. Expression of human nerve growth factor receptor on cells derived from all three germ layers. *Exp Cell Res.* 1988, **174**(2), pp.533-539.

382. Jones, E., English, A., Churchman, S.M., Kouroupis, D., Boxall, S.A., Kinsey, S., Giannoudis, P.G., Emery, P. and

McGonagle, D. Large-scale extraction and characterization of CD271+ multipotential stromal cells from trabecular bone in health and osteoarthritis: implications for bone regeneration strategies based on uncultured or minimally cultured multipotential stromal cells. *Arthritis Rheum.* 2010, **62**(7), pp.1944-1954.

383. Ilas, D.C., Baboolal, T.G., Churchman, S.M., Jones, W.G., Giannoudis, P.V., Buhring, H.J., McGonagle, D. and Jones, E. The osteogenic commitment of CD271+CD56+ bone marrow stromal cells (BMSCs) in osteoarthritic femoral head bone. *Sci Rep.* 2020, **10**(1), p.11145.

384. Fragkakis, E.M., El-Jawhari, J.J., Dunsmuir, R.A., Millner, P.A., Rao, A.S., Henshaw, K.T., Pountos, I., Jones, E. and Giannoudis, P.V. Vertebral body versus iliac crest bone marrow as a source of multipotential stromal cells: Comparison of processing techniques, tri-lineage differentiation and application on a scaffold for spine fusion. *PLoS One.* 2018, **13**(5), p.e0197969.

385. Owston, H.E., Ganguly, P., Tronci, G., Russell, S.J., Giannoudis, P.V. and Jones, E.A. Colony Formation, Migratory, and Differentiation Characteristics of Multipotential Stromal Cells (MSCs) from "Clinically Accessible" Human Periosteum Compared to Donor-Matched Bone Marrow MSCs. *Stem Cells Int.* 2019, **2019**, p.6074245.

386. Barilani, M., Banfi, F., Sironi, S., Ragni, E., Guillaumin, S., Polveraccio, F., Rosso, L., Moro, M., Astori, G., Pozzobon, M. and Lazzari, L. Low-affinity Nerve Growth Factor Receptor (CD271) Heterogeneous Expression in Adult and Fetal Mesenchymal Stromal Cells. *Sci Rep.* 2018, **8**(1), p.9321.

387. Churchman, S.M., Ponchel, F., Boxall, S.A., Cuthbert, R., Kouroupis, D., Roshdy, T., Giannoudis, P.V., Emery, P., McGonagle, D. and Jones, E.A. Transcriptional profile of native CD271+ multipotential stromal cells: evidence for multiple fates, with prominent osteogenic and Wnt pathway signaling activity. *Arthritis Rheum.* 2012, **64**(8), pp.2632-2643.

388. Cox, G., Boxall, S.A., Giannoudis, P.V., Buckley, C.T., Roshdy, T., Churchman, S.M., McGonagle, D. and Jones, E. High abundance of CD271(+) multipotential stromal cells (MSCs) in intramedullary cavities of long bones. *Bone.* 2012, **50**(2), pp.510-517.

389. Braun, J. and Baraliakos, X. Imaging of axial spondyloarthritis including ankylosing spondylitis. *Ann Rheum Dis.* 2011, **70 Suppl 1**, pp.i97-103.

390. Otto, F., Thornell, A.P., Crompton, T., Denzel, A., Gilmour, K.C., Rosewell, I.R., Stamp, G.W., Beddington, R.S., Mundlos, S., Olsen, B.R., Selby, P.B. and Owen, M.J. Cbfa1, a candidate gene for cleidocranial dysplasia syndrome, is essential for osteoblast differentiation and bone development. *Cell.* 1997, **89**(5), pp.765-771.

391. Rosen, E.D., Sarraf, P., Troy, A.E., Bradwin, G., Moore, K., Milstone, D.S., Spiegelman, B.M. and Mortensen, R.M. PPAR gamma is required for the differentiation of adipose tissue in vivo and in vitro. *Mol Cell.* 1999, **4**(4), pp.611-617.

392. Jeon, M.J., Kim, J.A., Kwon, S.H., Kim, S.W., Park, K.S., Park, S.W., Kim, S.Y. and Shin, C.S. Activation of peroxisome proliferator-activated receptor-gamma inhibits the Runx2-mediated transcription of osteocalcin in osteoblasts. *J Biol Chem.* 2003, **278**(26), pp.23270-23277.

393. Stechschulte, L.A. and Lecka-Czernik, B. Reciprocal regulation of PPARγ and RUNX2 activities in marrow mesenchymal stem cells: Fine balance between p38 MAPK and Protein Phosphatase 5. *Curr Mol Biol Rep.* 2017, **3**(2), pp.107-113.

394. Satomura, K., Krebsbach, P., Bianco, P. and Gehron Robey, P. Osteogenic imprinting upstream of marrow stromal cell differentiation. *J Cell Biochem.* 2000, **78**(3), pp.391-403.

395. Ng, T.T., Mak, K.H., Popp, C. and Ng, R.K. Murine Mesenchymal Stromal Cells Retain Biased Differentiation Plasticity Towards Their Tissue of Origin. *Cells.* 2020, **9**(3).

396. Strioga, M., Viswanathan, S., Darinskas, A., Slaby, O. and Michalek, J. Same or not the same? Comparison of adipose tissue-derived versus bone marrow-derived mesenchymal stem and stromal cells. *Stem Cells Dev.* 2012, **21**(14), pp.2724-2752.

397. Mohamed-Ahmed, S., Fristad, I., Lie, S.A., Suliman, S., Mustafa, K., Vindenes, H. and Idris, S.B. Adipose-derived and bone marrow mesenchymal stem cells: a donor-matched comparison. *Stem Cell Res Ther.* 2018, **9**(1), p.168.

398. Davies, O.G., Cooper, P.R., Shelton, R.M., Smith, A.J. and Scheven, B.A. A comparison of the in vitro mineralisation and dentinogenic potential of mesenchymal stem cells

derived from adipose tissue, bone marrow and dental pulp. *J Bone Miner Metab.* 2015, **33**(4), pp.371-382.

399. Jing, Y., Jing, J., Ye, L., Liu, X., Harris, S.E., Hinton, R.J. and Feng, J.Q. Chondrogenesis and osteogenesis are one continuous developmental and lineage defined biological process. *Sci Rep.* 2017, **7**(1), p.10020.

400. Wolock, S.L., Krishnan, I., Tenen, D.E., Matkins, V., Camacho, V., Patel, S., Agarwal, P., Bhatia, R., Tenen, D.G., Klein, A.M. and Welner, R.S. Mapping Distinct Bone Marrow Niche Populations and Their Differentiation Paths. *Cell Rep.* 2019, **28**(2), pp.302-311 e305.

401. Rauch, A., Haakonsson, A.K., Madsen, J.G.S., Larsen, M., Forss, I., Madsen, M.R., Van Hauwaert, E.L., Wiwie, C., Jespersen, N.Z., Tencerova, M., Nielsen, R., Larsen, B.D., Rottger, R., Baumbach, J., Scheele, C., Kassem, M. and Mandrup, S. Osteogenesis depends on commissioning of a network of stem cell transcription factors that act as repressors of adipogenesis. *Nat Genet.* 2019, **51**(4), pp.716-727.

402. Ganguly, P., El-Jawhari, J.J., Burska, A.N., Ponchel, F., Giannoudis, P.V. and Jones, E.A. The Analysis of In Vivo Aging in Human Bone Marrow Mesenchymal Stromal Cells Using Colony-Forming Unit-Fibroblast Assay and the CD45(low)CD271(+) Phenotype. *Stem Cells Int.* 2019, **2019**, p.5197983.

403. Gothard, D., Dawson, J.I. and Oreffo, R.O. Assessing the potential of colony morphology for dissecting the CFU-F population from human bone marrow stromal cells. *Cell Tissue Res.* 2013, **352**(2), pp.237-247.

404. Jones, E.A., English, A., Henshaw, K., Kinsey, S.E., Markham, A.F., Emery, P. and McGonagle, D. Enumeration and phenotypic characterization of synovial fluid multipotential mesenchymal progenitor cells in inflammatory and degenerative arthritis. *Arthritis Rheum.* 2004, **50**(3), pp.817-827.

405. Campbell, T.M., Churchman, S.M., Gomez, A., McGonagle, D., Conaghan, P.G., Ponchel, F. and Jones, E. Mesenchymal Stem Cell Alterations in Bone Marrow Lesions in Patients With Hip Osteoarthritis. *Arthritis Rheumatol.* 2016, **68**(7), pp.1648-1659.

406. Aldridge, A., Kouroupis, D., Churchman, S., English, A., Ingham, E. and Jones, E. Assay validation for the assessment of adipogenesis of multipotential stromal cells--

a direct comparison of four different methods. *Cytotherapy.* 2013, **15**(1), pp.89-101.

407. Frank, C.B. Ligament structure, physiology and function. *J Musculoskelet Neuronal Interact.* 2004, **4**(2), pp.199-201.

408. Rinoldi, C., Kijeńska-Gawrońska, E., Khademhosseini, A., Tamayol, A. and Swieszkowski, W. Fibrous Systems as Potential Solutions for Tendon and Ligament Repair, Healing, and Regeneration. *Adv Healthc Mater.* 2021, **10**(7), p.e2001305.

409. Ratcliffe, A., Butler, D.L., Dyment, N.A., Cagle, P.J., Jr., Proctor, C.S., Ratcliffe, S.S. and Flatow, E.L. Scaffolds for tendon and ligament repair and regeneration. *Ann Biomed Eng.* 2015, **43**(3), pp.819-831.

410. Ogata, Y., Mabuchi, Y., Shinoda, K., Horiike, Y., Mizuno, M., Otabe, K., Suto, E.G., Suzuki, N., Sekiya, I. and Akazawa, C. Anterior cruciate ligament-derived mesenchymal stromal cells have a propensity to differentiate into the ligament lineage. *Regen Ther.* 2018, **8**, pp.20-28.

411. Jones, E., English, A., Churchman, S., Kouroupis, D., Boxall, S., Kinsey, S., Giannoudis, P., Emery, P. and McGonagle, D. Large-scale extraction and characterization of CD271+ multipotential stromal cells from trabecular bone in health and osteoarthritis: Implications for bone regeneration strategies based on uncultured or minimally cultured multipotential stromal cells. *Arthritis & Rheumatism.* 2010, **62**(7), pp.1944-1954.

412. Blashki, D., Murphy, M.B., Ferrari, M., Simmons, P.J. and Tasciotti, E. Mesenchymal stem cells from cortical bone demonstrate increased clonal incidence, potency, and developmental capacity compared to their bone marrow-derived counterparts. *J Tissue Eng.* 2016, **7**, p.2041731416661196.

413. McGonagle, D., Lories, R.J., Tan, A.L. and Benjamin, M. The concept of a "synovio-entheseal complex" and its implications for understanding joint inflammation and damage in psoriatic arthritis and beyond. *Arthritis Rheum.* 2007, **56**(8), pp.2482-2491.

414. Petrenko, Y., Vackova, I., Kekulova, K., Chudickova, M., Koci, Z., Turnovcova, K., Kupcova Skalnikova, H., Vodicka, P. and Kubinova, S. A Comparative Analysis of Multipotent Mesenchymal Stromal Cells derived from Different Sources,

with a Focus on Neuroregenerative Potential. *Sci Rep.* 2020, **10**(1), p.4290.

415. Tuljapurkar, S.R., McGuire, T.R., Brusnahan, S.K., Jackson, J.D., Garvin, K.L., Kessinger, M.A., Lane, J.T., BJ, O.K. and Sharp, J.G. Changes in human bone marrow fat content associated with changes in hematopoietic stem cell numbers and cytokine levels with aging. *J Anat.* 2011, **219**(5), pp.574-581.

416. Chen, Q., Shou, P., Zheng, C., Jiang, M., Cao, G., Yang, Q., Cao, J., Xie, N., Velletri, T., Zhang, X., Xu, C., Zhang, L., Yang, H., Hou, J., Wang, Y. and Shi, Y. Fate decision of mesenchymal stem cells: adipocytes or osteoblasts? *Cell Death Differ.* 2016, **23**(7), pp.1128-1139.

417. Rui, Y., Xu, L., Chen, R., Zhang, T., Lin, S., Hou, Y., Liu, Y., Meng, F., Liu, Z., Ni, M., Tsang, K.S., Yang, F., Wang, C., Chan, H.C., Jiang, X. and Li, G. Epigenetic memory gained by priming with osteogenic induction medium improves osteogenesis and other properties of mesenchymal stem cells. *Sci Rep.* 2015, **5**, p.11056.

418. Wendling, D., Verhoeven, F. and Prati, C. Anti-IL-17 monoclonal antibodies for the treatment of ankylosing spondylitis. *Expert Opin Biol Ther.* 2019, **19**(1), pp.55-64.

419. Croes, M., Kruyt, M.C., Groen, W.M., van Dorenmalen, K.M.A., Dhert, W.J.A., Oner, F.C. and Alblas, J. Interleukin 17 enhances bone morphogenetic protein-2-induced ectopic bone formation. *Sci Rep.* 2018, **8**(1), p.7269.

420. van Tok, M.N., van Duivenvoorde, L.M., Kramer, I., Ingold, P., Pfister, S., Roth, L., Blijdorp, I.C., van de Sande, M.G.H., Taurog, J.D., Kolbinger, F. and Baeten, D.L. Interleukin-17A Inhibition Diminishes Inflammation and New Bone Formation in Experimental Spondyloarthritis. *Arthritis Rheumatol.* 2019, **71**(4), pp.612-625.

421. Uluckan, O., Jimenez, M., Karbach, S., Jeschke, A., Grana, O., Keller, J., Busse, B., Croxford, A.L., Finzel, S., Koenders, M., van den Berg, W., Schinke, T., Amling, M., Waisman, A., Schett, G. and Wagner, E.F. Chronic skin inflammation leads to bone loss by IL-17-mediated inhibition of Wnt signaling in osteoblasts. *Sci Transl Med.* 2016, **8**(330), p.330ra337.

422. Nash, P., Behrens, F., Orbai, A.M., Rathmann, S.S., Adams, D.H., Benichou, O. and Deodhar, A. Ixekizumab is efficacious when used alone or when added to conventional synthetic disease-modifying antirheumatic drugs

(cDMARDs) in patients with active psoriatic arthritis and previous inadequate response or intolerance to tumour necrosis factor inhibitors. *RMD Open.* 2018, **4**(2), p.e000692.

423. Nicola, S., Rolla, G., Monti, R. and Brussino, L. Treatment of psoriatic arthritis with secukinumab: a case series. *J Dermatolog Treat.* 2018, **29**(sup1), pp.6-8.

424. Yao, Z., Lei, W., Duan, R., Li, Y., Luo, L. and Boyce, B.F. RANKL cytokine enhances TNF-induced osteoclastogenesis independently of TNF receptor associated factor (TRAF) 6 by degrading TRAF3 in osteoclast precursors. *J Biol Chem.* 2017, **292**(24), pp.10169-10179.

425. Luo, G., Li, F., Li, X., Wang, Z.-G. and Zhang, B. TNF-α and RANKL promote osteoclastogenesis by upregulating RANK via the NF-κB pathway. *Mol Med Rep.* 2018, **17**(5), pp.6605-6611.

426. Marahleh, A., Kitaura, H., Ohori, F., Kishikawa, A., Ogawa, S., Shen, W.R., Qi, J., Noguchi, T., Nara, Y. and Mizoguchi, I. TNF-α Directly Enhances Osteocyte RANKL Expression and Promotes Osteoclast Formation. *Front Immunol.* 2019, **10**, p.2925.

427. Kotake, S. and Nanke, Y. Effect of TNFalpha on osteoblastogenesis from mesenchymal stem cells. *Biochim Biophys Acta.* 2014, **1840**(3), pp.1209-1213.

428. Karnes, J.M., Daffner, S.D. and Watkins, C.M. Multiple roles of tumor necrosis factor-alpha in fracture healing. *Bone.* 2015, **78**, pp.87-93.

429. Zuo, C., Zhao, X., Shi, Y., Wu, W., Zhang, N., Xu, J., Wang, C., Hu, G. and Zhang, X. TNF-α inhibits SATB2 expression and osteoblast differentiation through NF-κB and MAPK pathways. *Oncotarget.* 2018, **9**(4), pp.4833-4850.

430. Lavocat, F., Osta, B. and Miossec, P. Increased sensitivity of rheumatoid synoviocytes to Schnurri-3 expression in TNF-alpha and IL-17A induced osteoblastic differentiation. *Bone.* 2016, **87**, pp.89-96.

431. Daniele, S., Natali, L., Giacomelli, C., Campiglia, P., Novellino, E., Martini, C. and Trincavelli, M.L. Osteogenesis Is Improved by Low Tumor Necrosis Factor Alpha Concentration through the Modulation of Gs-Coupled Receptor Signals. *Mol Cell Biol.* 2017, **37**(8).

432. Osta, B., Roux, J.P., Lavocat, F., Pierre, M., Ndongo-Thiam, N., Boivin, G. and Miossec, P. Differential Effects of

IL-17A and TNF-alpha on Osteoblastic Differentiation of Isolated Synoviocytes and on Bone Explants from Arthritis Patients. *Front Immunol.* 2015, **6**, p.151.

433. Osta, B., Lavocat, F., Eljaafari, A. and Miossec, P. Effects of Interleukin-17A on Osteogenic Differentiation of Isolated Human Mesenchymal Stem Cells. *Front Immunol.* 2014, **5**, p.425.

434. Bennett, A.N., Rehman, A., Hensor, E.M., Marzo-Ortega, H., Emery, P. and McGonagle, D. The fatty Romanus lesion: a non-inflammatory spinal MRI lesion specific for axial spondyloarthropathy. *Ann Rheum Dis.* 2010, **69**(5), pp.891-894.

435. Zuniga, L.A., Shen, W.J., Joyce-Shaikh, B., Pyatnova, E.A., Richards, A.G., Thom, C., Andrade, S.M., Cua, D.J., Kraemer, F.B. and Butcher, E.C. IL-17 regulates adipogenesis, glucose homeostasis, and obesity. *J Immunol.* 2010, **185**(11), pp.6947-6959.

436. Scheffler, J.M., Grahnemo, L., Engdahl, C., Drevinge, C., Gustafsson, K.L., Corciulo, C., Lawenius, L., Iwakura, Y., Sjögren, K., Lagerquist, M.K., Carlsten, H., Ohlsson, C. and Islander, U. Interleukin 17A: a Janus-faced regulator of osteoporosis. *Sci Rep.* 2020, **10**(1), p.5692.

437. Lee, S.H., Jhun, J., Byun, J.-K., Kim, E.-K., Jung, K., Lee, J.E., Choi, J.Y., Park, S.-H. and Cho, M.-L. IL-17 axis accelerates the inflammatory progression of obese in mice via TBK1 and IKBKE pathway. *Immunol Lett.* 2017, **184**, pp.67-75.

438. Ahmed, M. and Gaffen, S.L. IL-17 inhibits adipogenesis in part via C/EBPα, PPARγ and Krüppel-like factors. *Cytokine.* 2013, **61**(3), pp.898-905.

439. Shin, J.H., Shin, D.W. and Noh, M. Interleukin-17A inhibits adipocyte differentiation in human mesenchymal stem cells and regulates pro-inflammatory responses in adipocytes. *Biochem Pharmacol.* 2009, **77**(12), pp.1835-1844.

440. Cawthorn, W.P., Heyd, F., Hegyi, K. and Sethi, J.K. Tumour necrosis factor-alpha inhibits adipogenesis via a beta-catenin/TCF4(TCF7L2)-dependent pathway. *Cell Death And Differentiation.* 2007, **14**(7), pp.1361-1373.

441. Pesce Viglietti, A.I., Giambartolomei, G.H., Quarleri, J. and Delpino, M.V. Brucella abortus Infection Modulates 3T3-L1 Adipocyte Inflammatory Response and Inhibits Adipogenesis. *Front Endocrinol (Lausanne).* 2020, **11**, p.585923.

442. Ma, H., Li, Y.N., Song, L., Liu, R., Li, X., Shang, Q., Wang, Y., Shao, C. and Shi, Y. Macrophages inhibit adipogenic differentiation of adipose tissue derived mesenchymal stem/stromal cells by producing pro-inflammatory cytokines. *Cell Biosci.* 2020, **10**, p.88.

443. Shinjo, T., Iwashita, M., Yamashita, A., Sano, T., Tsuruta, M., Matsunaga, H., Sanui, T., Asano, T. and Nishimura, F. IL-17A synergistically enhances TNFα-induced IL-6 and CCL20 production in 3T3-L1 adipocytes. *Biochem Biophys Res Commun.* 2016, **477**(2), pp.241-246.

444. Lowe, C.E., O'Rahilly, S. and Rochford, J.J. Adipogenesis at a glance. *J Cell Sci.* 2011, **124**(Pt 16), pp.2681-2686.

445. Hilton, R.C. and Ball, J. Vertebral rim lesions in the dorsolumbar spine. *Ann Rheum Dis.* 1984, **43**(2), pp.302-307.

446. Salazar, V.S., Gamer, L.W. and Rosen, V. BMP signalling in skeletal development, disease and repair. *Nature Reviews Endocrinology.* 2016, **12**(4), pp.203-221.

447. Briolay, A., El Jamal, A., Arnolfo, P., Le Goff, B., Blanchard, F., Magne, D. and Bougault, C. Enhanced BMP-2/BMP-4 ratio in patients with peripheral spondyloarthritis and in cytokine- and stretch-stimulated mouse chondrocytes. *Arthritis Res Ther.* 2020, **22**(1), p.234.

448. Hadjiargyrou, M., Rightmire, E.P., Ando, T. and Lombardo, F.T. The E11 osteoblastic lineage marker is differentially expressed during fracture healing. *Bone.* 2001, **29**(2), pp.149-154.

449. Ariizumi, T., Ogose, A., Kawashima, H., Hotta, T., Li, G., Xu, Y., Umezu, H., Sugai, M. and Endo, N. Expression of podoplanin in human bone and bone tumors: New marker of osteogenic and chondrogenic bone tumors. *Pathol Int.* 2010, **60**(3), pp.193-202.

450. Lin, W., Zhu, X., Gao, L., Mao, M., Gao, D. and Huang, Z. Osteomodulin positively regulates osteogenesis through interaction with BMP2. *Cell Death Dis.* 2021, **12**(2), p.147.

451. Lee, M.H., Kwon, T.G., Park, H.S., Wozney, J.M. and Ryoo, H.M. BMP-2-induced Osterix expression is mediated by Dlx5 but is independent of Runx2. *Biochem Biophys Res Commun.* 2003, **309**(3), pp.689-694.

452. Yu, S., Guo, J., Sun, Z., Lin, C., Tao, H., Zhang, Q., Cui, Y., Zuo, H., Lin, Y., Chen, S., Liu, H. and Chen, Z. BMP2-dependent gene regulatory network analysis reveals Klf4 as

a novel transcription factor of osteoblast differentiation. *Cell Death Dis.* 2021, **12**(2), p.197.

453. Ungureanu, D., Saharinen, P., Junttila, I., Hilton, D.J. and Silvennoinen, O. Regulation of Jak2 through the ubiquitin-proteasome pathway involves phosphorylation of Jak2 on Y1007 and interaction with SOCS-1. *Mol Cell Biol.* 2002, **22**(10), pp.3316-3326.

454. Liu, C.H., Raj, S., Chen, C.H., Hung, K.H., Chou, C.T., Chen, I.H., Chien, J.T., Lin, I.Y., Yang, S.Y., Angata, T., Tsai, W.C., Wei, J.C., Tzeng, I.S., Hung, S.C. and Lin, K.I. HLA-B27-mediated activation of TNAP phosphatase promotes pathogenic syndesmophyte formation in ankylosing spondylitis. *J Clin Invest.* 2019, **129**(12), pp.5357-5373.

455. Ding, J., Ghali, O., Lencel, P., Broux, O., Chauveau, C., Devedjian, J.C., Hardouin, P. and Magne, D. TNF-α and IL-1β inhibit RUNX2 and collagen expression but increase alkaline phosphatase activity and mineralization in human mesenchymal stem cells. *Life Sciences.* 2009, **84**(15), pp.499-504.

456. Murshed, M., Harmey, D., Millán, J.L., McKee, M.D. and Karsenty, G. Unique coexpression in osteoblasts of broadly expressed genes accounts for the spatial restriction of ECM mineralization to bone. *Genes Dev.* 2005, **19**(9), pp.1093-1104.

457. Gao, G., Chen, F.J., Zhou, L., Su, L., Xu, D., Xu, L. and Li, P. Control of lipid droplet fusion and growth by CIDE family proteins. *Biochim Biophys Acta Mol Cell Biol Lipids.* 2017, **1862**(10 Pt B), pp.1197-1204.

458. Hansen, J.S., de Mare, S., Jones, H.A., Goransson, O. and Lindkvist-Petersson, K. Visualization of lipid directed dynamics of perilipin 1 in human primary adipocytes. *Sci Rep.* 2017, **7**(1), p.15011.

459. Shaw, H.M., Santer, R.M., Watson, A.H.D. and Benjamin, M. Adipose tissue at entheses: the innervation and cell composition of the retromalleolar fat pad associated with the rat Achilles tendon. *J Anat.* 2007, **211**(4), pp.436-443.

460. Terashima, A. and Takayanagi, H. Overview of Osteoimmunology. *Calcif Tissue Int.* 2018, **102**(5), pp.503-511.

461. Yuan, Z.-C., Xu, W.-D., Liu, X.-Y., Liu, X.-Y., Huang, A.-F. and Su, L.-C. Biology of IL-36 Signaling and Its Role in

Systemic Inflammatory Diseases. *Frontiers in Immunology.* 2019, **10**(2532).

462. He, Q., Chen, H.-x., Li, W., Wu, Y., Chen, S.-j., Yue, Q., Xiao, M. and Li, J.-w. IL-36 cytokine expression and its relationship with p38 MAPK and NF-κB pathways in psoriasis vulgaris skin lesions. *Journal of Huazhong University of Science and Technology [Medical Sciences].* 2013, **33**(4), pp.594-599.

463. Croes, M., Oner, F.C., Kruyt, M.C., Blokhuis, T.J., Bastian, O., Dhert, W.J. and Alblas, J. Proinflammatory Mediators Enhance the Osteogenesis of Human Mesenchymal Stem Cells after Lineage Commitment. *PLoS One.* 2015, **10**(7), p.e0132781.

464. Sieper, J., Lenaerts, J., Wollenhaupt, J., Rudwaleit, M., Mazurov, V.I., Myasoutova, L., Park, S., Song, Y., Yao, R., Chitkara, D., Vastesaeger, N. and All, I.I. Efficacy and safety of infliximab plus naproxen versus naproxen alone in patients with early, active axial spondyloarthritis: results from the double-blind, placebo-controlled INFAST study, Part 1. *Ann Rheum Dis.* 2014, **73**(1), pp.101-107.

465. Wendling, D., Cedoz, J.P., Racadot, E. and Dumoulin, G. Serum IL-17, BMP-7, and bone turnover markers in patients with ankylosing spondylitis. *Joint Bone Spine.* 2007, **74**(3), pp.304-305.

466. Bal, A., Unlu, E., Bahar, G., Aydog, E., Eksioglu, E. and Yorgancioglu, R. Comparison of serum IL-1 beta, sIL-2R, IL-6, and TNF-alpha levels with disease activity parameters in ankylosing spondylitis. *Clin Rheumatol.* 2007, **26**(2), pp.211-215.

467. Benhamou, M., Gossec, L. and Dougados, M. Clinical relevance of C-reactive protein in ankylosing spondylitis and evaluation of the NSAIDs/coxibs' treatment effect on C-reactive protein. *Rheumatology (Oxford).* 2010, **49**(3), pp.536-541.

468. Pedersen, S.J., Sorensen, I.J., Lambert, R.G., Hermann, K.G., Garnero, P., Johansen, J.S., Madsen, O.R., Hansen, A., Hansen, M.S., Thamsborg, G., Andersen, L.S., Majgaard, O., Loft, A.G., Erlendsson, J., Asmussen, K.H., Jurik, A.G., Moller, J., Hasselquist, M., Mikkelsen, D. and Ostergaard, M. Radiographic progression is associated with resolution of systemic inflammation in patients with axial spondylarthritis treated with tumor necrosis factor alpha inhibitors: a study of radiographic progression, inflammation

on magnetic resonance imaging, and circulating biomarkers of inflammation, angiogenesis, and cartilage and bone turnover. *Arthritis Rheum.* 2011, **63**(12), pp.3789-3800.

469. Deodhar, A., Conaghan, P.G., Kvien, T.K., Strand, V., Sherif, B., Porter, B., Jugl, S.M., Gandhi, K.K. and group, M.s. Secukinumab provides rapid and persistent relief in pain and fatigue symptoms in patients with ankylosing spondylitis irrespective of baseline C-reactive protein levels or prior tumour necrosis factor inhibitor therapy: 2-year data from the MEASURE 2 study. *Clin Exp Rheumatol.* 2019, **37**(2), pp.260-269.

470. Hotamisligil, G.S., Shargill, N.S. and Spiegelman, B.M. Adipose expression of tumor necrosis factor-alpha: direct role in obesity-linked insulin resistance. *Science.* 1993, **259**(5091), pp.87-91.

471. Paroutoglou, K., Papadavid, E., Christodoulatos, G.S. and Dalamaga, M. Deciphering the Association Between Psoriasis and Obesity: Current Evidence and Treatment Considerations. *Curr Obes Rep.* 2020, **9**(3), pp.165-178.

472. Ahmed, M. and Gaffen, S.L. IL-17 in obesity and adipogenesis. *Cytokine Growth Factor Rev.* 2010, **21**(6), pp.449-453.

473. Koss, C.K., Wohnhaas, C.T., Baker, J.R., Tilp, C., Przibilla, M., Lerner, C., Frey, S., Keck, M., Williams, C.M.M., Peter, D., Ramanujam, M., Fine, J., Gantner, F., Thomas, M., Barnes, P.J., Donnelly, L.E. and El Kasmi, K.C. IL36 is a critical upstream amplifier of neutrophilic lung inflammation in mice. *Commun Biol.* 2021, **4**(1), p.172.

474. Hyvarinen, T., Hagman, S., Ristola, M., Sukki, L., Veijula, K., Kreutzer, J., Kallio, P. and Narkilahti, S. Co-stimulation with IL-1beta and TNF-alpha induces an inflammatory reactive astrocyte phenotype with neurosupportive characteristics in a human pluripotent stem cell model system. *Sci Rep.* 2019, **9**(1), p.16944.

475. Han, X., Yang, Q., Lin, L., Xu, C., Zheng, C., Chen, X., Han, Y., Li, M., Cao, W., Cao, K., Chen, Q., Xu, G., Zhang, Y., Zhang, J., Schneider, R.J., Qian, Y., Wang, Y., Brewer, G. and Shi, Y. Interleukin-17 enhances immunosuppression by mesenchymal stem cells. *Cell Death Differ.* 2014, **21**(11), pp.1758-1768.

476. Stal, R., van Gaalen, F., Sepriano, A., Braun, J., Reijnierse, M., van den Berg, R., van der Heijde, D. and Baraliakos, X. Facet joint ankylosis in r-axSpA: detection and 2-year

progression on whole spine low-dose CT and comparison with syndesmophyte progression. *Rheumatology (Oxford).* 2020, **59**(12), pp.3776-3783.

477. Kitaori, T., Ito, H., Schwarz, E.M., Tsutsumi, R., Yoshitomi, H., Oishi, S., Nakano, M., Fujii, N., Nagasawa, T. and Nakamura, T. Stromal cell-derived factor 1/CXCR4 signaling is critical for the recruitment of mesenchymal stem cells to the fracture site during skeletal repair in a mouse model. *Arthritis Rheum.* 2009, **60**(3), pp.813-823.

478. Sezer, U., Erciyas, K., Pehlivan, Y., Ustun, K., Tarakcioglu, M., Senyurt, S.Z. and Onat, A.M. Serum cytokine levels and periodontal parameters in ankylosing spondylitis. *J Periodontal Res.* 2012, **47**(3), pp.396-401.

479. Konkova, M., Abramova, M., Kalianov, A., Ershova, E., Dolgikh, O., Umriukhin, P., Izhevskaya, V., Kutsev, S., Veiko, N. and Kostyuk, S. Mesenchymal Stem Cells Early Response to Low-Dose Ionizing Radiation. *Frontiers in cell and developmental biology.* 2020, **8**, p.584497.

480. Liu, L., Yuan, Y., Zhang, S., Xu, J. and Zou, J. Osteoimmunological insights into the pathogenesis of ankylosing spondylitis. *J Cell Physiol.* 2021.

481. Ali, D., Hamam, R., Alfayez, M., Kassem, M., Aldahmash, A. and Alajez, N.M. Epigenetic Library Screen Identifies Abexinostat as Novel Regulator of Adipocytic and Osteoblastic Differentiation of Human Skeletal (Mesenchymal) Stem Cells. *Stem Cells Transl Med.* 2016, **5**(8), pp.1036-1047.

482. Heid, H., Rickelt, S., Zimbelmann, R., Winter, S., Schumacher, H., Dorflinger, Y., Kuhn, C. and Franke, W.W. On the formation of lipid droplets in human adipocytes: the organization of the perilipin-vimentin cortex. *PLoS One.* 2014, **9**(2), p.e90386.

483. Turner, N.A., Das, A., O'Regan, D.J., Ball, S.G. and Porter, K.E. Human cardiac fibroblasts express ICAM-1, E-selectin and CXC chemokines in response to proinflammatory cytokine stimulation. *Int J Biochem Cell Biol.* 2011, **43**(10), pp.1450-1458.

484. Schett, G., Lories, R.J., D'Agostino, M.-A., Elewaut, D., Kirkham, B., Soriano, E.R. and McGonagle, D. Enthesitis: from pathophysiology to treatment. *Nature Reviews Rheumatology.* 2017, **13**(12), pp.731-741.